ELECTROREFINING OF BASE METAL REFINERY RESIDUE COPPER ALLOY FOR PLATINUM GROUP METAL RECOVERY

Thesis submitted in partial fulfillment of the degree of Master of Science

Lizelle Kruyswijk
KRYLIZ001

_____

23 November, 2009

Abstract

Secondary leach concentrate (SLC) is an important bleed stream for minor elements from Anglo Platinum's Base Metal Refinery (BMR) which produces copper nickel and cobalt sulphate. It contains mainly sulphur, iron jarosites, un-leached base metals and platinum group metals (PGMs), which makes the treatment of SLC necessary. The SLC is currently toll-refined at Umicore's Hoboken smelter and refinery to recover revenue from entrapped valuable metals. This method of treatment results in excessively high costs due to high transport and toll refining expenses as well as penalties. Thus, an in-house method of treatment by Anglo Platinum itself would prove beneficial in that it would eliminate these excessive costs and also provide a method of treatment in the event of residues exporting becoming banned or strongly penalised in future. Therefore, a method for treating SLC in-house is investigated.

The first stage of the proposed treatment method involves a pyrometallurgical process where the removal of amphoterics by oxidative fuming, followed by reduction to recover base metals from the slag takes place. The PGMs are reported mainly to the metal alloy phase along with the base metals during this process. The project discussed in this report deals with the treatment of this furnace alloy which is referred to as Cu alloy. The Cu alloy is used to produce anodes to be applied to an electrorefining application for the recovery of Cu as a Cu cathode and PGMs in the form of anode slimes. Spent electrolyte from the BMR copper electrowinning section adjusted to specific pH and Cu concentration is used as electrolyte to which dissolvable metals (such as Ni and Fe) are recovered.

The purpose of the process is to recover PGMs to anode slimes with a composition suitable to be blended with the final concentrate that is sent to the Precious Metals Refinery (PMR). The performance of this process on the Cu alloy provided is investigated and the anode slimes produced are characterised in order to propose further methods of purification before blending with PMR feed. The typical energy consumption, cathodic current efficiency, anodic copper dissolution rate and deportment of elements (especially PGMs) are determined. The effects of various operating parameters on the performance are also investigated in order to propose operating conditions. The operating parameters that are investigated are current density, Cu and H_2SO_4 concentrations in electrolyte and the use of an additive. A preliminary process design based on knowledge and experience gained during the literature review and test work is given.

The major technical factors in electrorefining are the cathode purity, the production rate and the specific energy consumption. These factors are influenced primarily by anode quality, electrolyte conditions and cathode current density. Design considerations and typical design parameters for other industrial Cu electrorefining applications are studied as well as possible further treatment of anode slimes for the concentration of PGMs.

A total of eleven experiments were performed with a variety combinations of Cu concentration (30, 40 and 50 g/l), H_2SO_4 concentration (110, 130, 160 and 190 g/l) and current density (100, 125, 150, 250, 300 A/m^2). In each experiment only one parameter was changed while all others were kept constant at the base-case setting of 40 g/l Cu, 160 g/l H_2SO_4, and 125 A/m^2.

The testwork showed that electrolytic refining of the Cu alloy, produced by a two stage pyrometallurgical treatment of current SLC, produces a highly concentrated PGM residue at an overall SLC mass reduction of 99.3%, with excellent PGM recovery to the anode slimes material. The different operating parameters that were tested successfully, all showed very good repeatability and greater than 99% PGM recovery from the Cu alloy, which would result in an overall recovery of 98% from SLC. Very little or none of the base metals that were supplied by the anode or the electrolyte feed reported to the anode slimes. The typical operating conditions (cell potential, current efficiency, anodic Cu dissolution and element deportment) that were observed correlated well with literature and the theoretically calculated values.

The characteristics of the anode slimes produced stayed relatively similar throughout the different operating parameters and strong confidence can be placed in the production thereof and the recovery of the PGMs. The characteristics of the spent electrolyte and the Cu cathodes were also found to be suitable for integration in the BMR circuit.

The anode slimes composition was 20 to 30% PGMs, 20 to 30% base metals, 15 to 20% Ag, As, Te, Se, Pb and 2 to 5% Al, Si, Sb, Bi, Zn and Sn. The blending of these slimes with typical PMR feed will result in a new PMR feed where the Pt grade of the feed to PMR is reduced by 4 to 5.5%, the Cu grade increased by 2 to 4% and the Ni content reduced by ±4%. Other concerns are the increase of As, Te, and Pb by between 0.5 and 1%.

The PGM-rich (>60%) phase in the anode slimes is a mostly amorphous matrix phase containing mostly palladium and other PGMs, arsenic and tellurium [$Pd_{73}As_6Te_{21}$] with small amounts of Cu.

Anode slimes produced from electrorefining can either be subjected to an additional process step to remove Ag, Pb and base metals before it is blended with the final concentrate (FICO) as feed for PMR, or it can be sent to the metallics section in PMR which includes a roast and a leach stage. The treatment of the anode slimes depends on the nature of the slimes.

A preliminary process design was performed with proposed design parameters of electrolyte concentrations of 40 g/l Cu and 160 g/l H_2SO_4 at 65˚C and a current density of 200 A/m^2. The process consists out of seven cells in series with 55 anode cathode pairs in parallel per cell. The process has a maximum capacity of 127 t/m of anode material which allows 56 days of downtime per year if the current SLC produced (6600 t/a) is treated. The maximum capacity for Cu production is 1349 t/a and anode slimes 50.3 t/m. The power consumption per kg of anode dissolved will be 0.175 kWh/kg.

Disclaimer

I know the meaning of plagiarism and declare that all the work in the document, save for that which is properly acknowledged, is my own.

Date:_____

Signature:_____

ACKNOWLEDGEMENTS

I would like to acknowledge and thank the Mintek staff, Ephraim Mabusela, Calvin Mokwana, Johannes Maitse, Florence Jantjies, Alice Mukhabele, Mante Kgaria, Sifiso Khumalo and especially the Mintek metallurgist responsible for the project, Ndina Malaudzi, for their hard work and commitment throughout the project and getting quality results. Also, I would like to thank Thembi Thulare and Marthie Kotze, for allowing me to work in their department and giving me their support. The Mintek staff was always very helpful and cooperative in order to get the best possible solution to any questions that came up. I learnt a great deal during my time spent at Mintek and I would like to thank them for welcoming me into the company for the duration of the testwork.

Thanks also go to the Anglo Platinum Process Technology Department, Lloyd Nelson, Les Bryson and Debbie Erasmus for the initiation of the project and the provision of the required funds and resources. I was never left wanting for any kind of support, whether it was accommodation, provision of experimental requirements, technical support or just a word of motivation and inspiration.

I would also like to thank Jochen Peterson, Kathy Sole and Steve Woollam for their guidance during the write up of the thesis. They were there to bounce ideas off, get me into the right mode of thinking and also give their opinions of the meaning of the results. A special thank you also to Jochen and Kathy, for their efforts in the revision of the thesis.

Thank you to Petra Dinham from Anglo Research for her mineralogical analysis of the samples and discussions around the meaning of the results.

Lastly I would like to thank my family, partner and housemates for their support and motivation.

Table of Contents

1 INTRODUCTION ____ 15

1.1 Background ---- 16

1.2 Process Concept ---- 19

1.3 Problem Statement ---- 21

2 LITERATURE REVIEW ____ 22

2.1 Theory ---- 22

2.1.1 General Introduction ... 22

2.1.2 Redox Equilibria ... 23

2.1.3 Electrochemical Kinetics ... 25

2.1.4 Mass Transport ... 28

2.1.5 Cathode Morphology ... 30

2.1.6 Current Distribution ... 31

2.1.7 Anode Passivation ... 32

2.2 Operating Parameters ---- 33

2.2.1 Current Density ... 33

2.2.2 Electrolyte ... 34

2.2.3 Temperature ... 39

2.2.4 Anodes ... 41

2.2.5 Additives ... 43

2.2.6 Typical Operating Conditions ... 44

2.3 What to Expect During Electrorefining ---- 45

2.3.1 Behavior of Various Elements in Copper Electrorefining ... 45

2.4 Rustenburg Base Metal Refiners Internal Literature ---- 48

2.5 Process Design ---- 50

2.6 Further Processing of Anode Slimes ---- 52

3 RESEARCH OBJECTIVES & APPROACH ____ 54

3.1 Key Questions ---- 54

3.2 Objectives ----54
3.3 Approach ----55
4 EXPERIMENTAL 57
4.1 Parameters----57
4.2 Equipment----59
4.3 Procedures----62
4.3.1 Anode Casting 62
4.3.2 Electrorefining Testwork 63
4.4 Sample Analysis----66
4.4.1 Electrolyte Samples 66
4.4.2 Cathode Samples 66
4.4.3 Anode Slimes and Anode Samples 66
5 RESULTS AND DISCUSSION 67
5.1 Background ----67
5.2 Change in Anode Composition ----67
5.3 Typical Operating Conditions----70
5.3.1 Cell Potential 70
5.3.2 Current Efficiency 73
5.3.3 Anodic Cu Dissolution 74
5.3.4 Element Deportment 76
5.4 Product Characterisation ----90
5.4.1 Anode Slimes 90
5.4.2 Spent Electrolyte 100
5.4.3 Cathodes 101
5.4.4 Mass Reduction 103
5.5 Effect of Operating Parameters----105
5.5.1 Smoothing Agents 105
5.5.2 Current Density 107
5.5.3 Cu Concentration 113
5.5.4 H_2SO_4 Concentration 116

6 PROCESS DESIGN 119

6.1 Process Design Background 119

6.2 Process Design Parameters 120

7 CONCLUSIONS 123

8 RECOMMENDATIONS 127

9 REFERENCES 128

I. APPENDIX I 133

A. Background of BMR Expansion 133

B. Raw Material Composition 134

C. Comparison of Leaching vs. Electrorefining 135

D. Test Accuracy 136

E. Element Deportment Results 153

F. Product Characterisation Results 164

G. Effect of Blended Feed on PMR Feed Composition 166

H. Mineralogical Results for Initial Anodes 170

I. Mineralogical Results for Anode Slimes 172

J. Mineralogy Procedures 173

II. APPENDIX II 181

A. Anode Casting Report 182

List of Figures

Figure 1.1.a: Composition of Ausmelt TSL furnace alloy produced from treating SLC 18

Figure 1.2.a: Proposed flow sheet of Base Metals Refinery 20

Figure 2.1.a: Standard reduction potentials for metal ions (Nicol, 2008) 24

Figure 2.1.b: Schematic current potential curves for anodic and cathodic reactions (Nicol, 2008) 27

Figure 2.1.c: Calculated current-potential relationship 28

Figure 2.1.d: Rate-potential curve for an electrode reaction involving mass transport (Nicol, 2008) 30

Figure 2.2.a: The effect of copper concentration in the electrolyte on cell voltage during electrorefining (Hayes. 2003). 35

Figure 2.2.b: Effect of Cu Concentration on Cu^{2+} Diffusion Coefficient (Moats et al. 2000) 36

Figure 2.2.c: Effect of Acid Concentration on Cu2+ Diffusion Coefficient (Moats et al. 2000) 37

Figure 2.2.d: The effect of temperature on the cell voltage during electrorefining (Hayes, 2003) 39

Figure 2.2.e: The effect of temperature on diffusion coefficient (Moats et al. 2002) 40

Figure 2.2.f: Kinetic parameters for the Cu^{2+}/Cu^{0} reaction on a copper sheet cathode at various temperatures as determined by Cifuentes (2005) 41

Figure 2.2.g: Example of a typical anode casting 42

Figure 2.4.a: Deportment of PGMs (190 g/l H_2SO_4, 40 g/l Cu, 60ºC, 0.5 V) (Hanf, 1989) 49

Figure 2.5.a: Copper anode casting wheel 50

Figure 4.2.a: Expirimental set up 59

Figure 4.2.b: Polypropolene cell connected to thermocouple, heat exchanger, feed, spent and recyle lines 60

Figure 4.2.c: Impure Cu anode before test 60

Figure 4.2.d: Cu deposit on stainless steel cathode with one effective plating surface of 20 cm x 14 cm 60

Figure 4.2.e: Heat exchanger connected to hot water bath with PID controller 60

Figure 4.3.a: Original material (two-stage Ausmelt TSL alloy product) 62

Figure 4.3.b: Bottom half of silica sand mould for anodes 62

Figure 4.3.c: Molten metal transferred from furnace to casting ladle 63

Figure 4.3.d: Molten metal cast into closed top silica sand mould 63

Figure 4.3.e: Anode surface after dissolution in test 1 65

Figure 4.3.f: Anode slimes on filter paper produced from test 5 65

Figure 5.2.a: MLA backscattered electron image of anode cast from original material 68

Figure 5.2.b: MLA backscattered electron image of anode cast from altered material 68

Figure 5.2.c: Cell potential during test 8 with significant step change when anode passivation takes place. 69

Figure 5.3.a: Potential difference profiles between anode and cathodes and rectifier voltage 70

Figure 5.3.b: Theoretical and actual anode dissolution rate under various operating conditions 75

Figure 5.3.c: Concentration profiles of different elements during test 2 (base-case) 78

Figure 5.3.d: PGM deportment to anode slimes from anode and electrolyte 79

Figure 5.3.e: Base Metals deportment to anode slimes from anode and electrolyte 80

Figure 5.3.f: Impurity deportment to anode slimes from anode and electrolyte 80

Figure 5.3.g: Minor impurity deportment to anode slimes from anode and electrolyte 81

Figure 5.3.h: Recovery of PGMs from anode material to anode slimes 87

Figure 5.3.i: Recovery of base metals from anode to anode slimes 88

Figure 5.3.j: Recovery of impurities from anode to anode slimes 89

Figure 5.3.k: Recovery of minor impurities from anode to anode slimes 90

Figure 5.4.a: Composition of anode slimes compared with typical PMR feed composition 91

Figure 5.4.b: Deviation of blended feed composition from current PMR feed 93

Figure 5.4.c: Backscattered electron image of original anode material used in the base-case test with additives (Test 3) 94

Figure 5.4.d: Backscattered electron image of typical anode slime particle 95

Figure 5.4.e: XRD traces of anode slimes samples of test 1 – 7 showing amorphous phase 96

Figure 5.4.f: Comparison of bright white phases in anode and slimes 98

Figure 5.4.g: Comparison of grey bleb phases in anode and slimes 99

Figure 5.4.h: Comparison of the matrix phases in anodes and slimes 99

Figure 5.4.i: Nodular growth around edges first test cathode 103

Figure 5.4.j: Smooth surface of fourth test cathode. 103

Figure 5.4.k: Slimes and cathode production per kg of anode treated 104

Figure 5.5.a: Comparison of cell potential during tests with additives and without additives. 106

Figure 5.5.b: Increase in power consumption with an increase in current density 108

Figure 5.5.c: Increase in anode dissolution with an increase in current density 109

Figure 5.5.d: Deportment of Rh, Ru, Ir, Ag and Pg to slimes from anode and electrolyte 110

Figure 5.5.e: Deportment of As, Te, Sb, Bi, Se & S to slimes from anode and electrolyte 110

Figure 5.5.f: Comparison of cell potential at various current densities 111

Figure 5.5.g: Actual and calculated relationship between current density and cell potential 112

Figure 5.5.h: Comparison of cell potential at various Cu concentrations 115

Figure 5.5.i: Comparison of cell potential at different H_2SO_4 concentrations for altered anode material 116

Figure 5.5.j: Comparison of cell potential at different H_2SO_4 concentrations 118

Figure 6.1.a: Proposed flow sheet of Base Metals Refinery 119

List of Tables

Table 1.1.a: Content of trace elements and major elements in SLC 15

Table 2.1.a: Non –standard electrode potentials at electrorefining conditions 25

Table 2.2.a: Chemical specifications for copper cathode (Nicol, 2008) 38

Table 2.2.b: Typical operating conditions of a copper electrorefining process 45

Table 2.3.a: Recovery of elements to anode slimes and to electrolyte (Biswas, 2002) 47

Table 2.4.a: Results of electrorefining tests performed on BMR Cu bullion by Hanf et al. (1989) 50

Table 2.6.a: Typical composition of commercial Cu anodes and the slimes produced Chen (2004) 52

Table 4.1.a: Operating parameter combinations for different tests performed 57

Table 4.2.a: Experimental electrode dimensions and flow rate settings 61

Table 5.3.a: Power consumption for each test i.t.o kWh/kg Cu produced and anode dissolved 72

Table 5.3.b: Anode and cathode current efficiencies under various conditions 74

Table 5.3.c: Actual and theoretical dissolution rate under different conditions 76

Table 5.3.d: Recovery of elements from Anode to different product streams for Test 1 (110 g/l H_2SO_4) 83

Table 5.3.e: Recovery of elements from Anode to different product streams for Test 2 (Base-case) 83

Table 5.3.f: Recovery of elements from Anode to different product streams for Test 3 (Base-case With Additives) 84

Table 5.3.g: Recovery of elements from Anode to different product streams for Test 4 (100 A/m^2) 84

Table 5.3.h: Recovery of elements from Anode to different product streams for Test 5 (150 A/m^2) 85

Table 5.3.i: Recovery of elements from Anode to different product streams for Test 6 (30 g/l Cu) 85

Table 5.3.j: Recovery of elements from Anode to different product streams for Test 7 (50 g/l Cu) 86

Table 5.4.a: PGM grade of anode slimes 91

Table 5.4.b: Impurity grade in slimes produced by tests with original anode material 92

Table 5.4.c: Composition of phases present in initial anode used in base-case test with additives (Test 3) 94

Table 5.4.d: Composition of different phases in anode slimes 97

Table 5.4.e: Spent electrolyte concentrations after each test 100

Table 5.4.f: Impurities in cathodes 102

Table 5.5.a: Calculation of exchange current density (i_0) and the Tafel slope (b) 112

Glossary of Terms

BMR	–	Base Metals Refinery
SLC	–	Secondary Leach Concentrate
PGM	–	Platinum Group Metals (Pt, Pd, Rh, Ru, Ir, Os, Au)
BM	–	Base Metals (Ni, Cu, Fe & Co)
CPL	–	Copper Pressure Leach
PMR	–	Precious Metals Refinery
FICO	–	Final Concentrate
MC plant	–	Alloy Concentration Plant
SG	–	Specific Gravity
AMD	–	Advanced Materials Division
ASD	–	Analytical Services Division
SEM-EDX	–	Scanning Electron Microscope with Energy Dispersive X-ray
TSL	–	Top Submerged Lance
LME	–	London Metal Exchange
PID	–	Proportional–Integral–Derivative

Nomenclature

Symbol	*Description*	*Unit*
m	Mass	g or kg
M	Molecular Mass	g/mol or kg/kmol
n	Number of electrons per reaction (stoichiometrically)	Mol
W	Energy	Watt (W)
P	Power	kWh/kg
ŋ	Overpotential	Volts (V) or mV
ε	Current Efficiency	%
E	Electrode Potential	Volts (V)
E°	Standard Electrode Potential	Volts (V)
R	Universal Gas Constant	
T	Temperature	K
I	Applied Current	Ampere (A)
t	Time	Seconds (s)
A	Surface area	m^2
i	Current Density	A/m^2
i_0	Exchange Current Density	A/m^2
F	Faraday Constant	96 487 C/mol
V	Cell Voltage	Volts (V)
P	Power Consumption	kWh/kg
f_s	Fraction of slimes per unit anode	Fraction / %
t/m	Monthly capacity / throughput	Tonnes per month
t/a	annual capacity / throughput	Tonnes per annum
[Ox]	Activity (molarity) of oxidised species	mol/l
[Re]	Activity (molarity) of reduced species	mol/l
r	Rate of reaction	$mol/m^2.s$
r_m	Mass transfer limited rate	$mol/m^2.s$
k, h	Constants in rate equation	
a	Activity of reactants taking part in rate determining step	mol/l
∆G”	Free energy of activation	J
b	Tafel slope	mV/decade
k_L	Mass transfer coefficient	m/s
C_b	Bulk concentration	mol/l
D	Diffusion coefficient	m^2/s
δ	Diffusion layer thickness	mm

1 INTRODUCTION

The Base Metal Refinery (BMR) of Anglo Platinum currently produces nickel, copper, cobalt sulphate and sodium sulphate as saleable products, as well as a residue which serves as the main outlet for impurities from the refining processes. The residue generated from these processes is called the Secondary Leach Concentrate (SLC) and it contains mainly sulphur, iron jarosites, un-leached base metals and platinum group metals (PGMs), which makes the treatment of SLC attractive. The SLC is currently toll-refined at Umicore's Hoboken smelter and refinery. This treatment route results in high transport and refining costs as well as a long pipeline, which equate to a significant revenue loss. Also, it is projected that the export of residues will become a challenge in the near future due to new environmental laws being developed. It is thus beneficial and necessary for Anglo Platinum to develop an alternative treatment route which will result in significant mass reduction of the SLC or complete in-house treatment thereof. Thereby eliminating additional costs involved with toll refining and benefiting from the PGM values captured in the SLC.

BMR currently produces 550 t/m of SLC with the typical composition given in Table 1.1.a.

Table 1.1.a: Content of trace elements and major elements in SLC

Average Content in SLC					
g/t		**Wt %**		**Wt %**	
Pd	810	Fe	28.30	Se	0.399
Ag	700	S	26.00	Pb	0.318
Ru	550	SiO_2	25.00	Sb	0.256
Pt	170	Cu	16.62	Te	0.122
Rh	190	Ni	2.94	As	0.098
Au	100	Co	0.06	Bi	0.050
Ir	30			Zn	0.002

According to Hofirek (2001), the Cu and Ni are present predominantly as monosulfides and small quantities of unleached material. Iron is present either as a hematite or jarosite, depending on the secondary leach conditions. The formation of this precipitate is very important in the secondary leach because it is the only outlet for Fe from the process. It also collects non-metallic impurities from the liquor. Forming hematite is more preferable because it collects more impurities and is less soluble than jarosite; however, it is more difficult to filter. It is thought that the Ag, Pb, Zn, Mn and Cr present in the SLC are co-precipitates with or as jarosite analogues and Se and Te are presumed to be associated with the copper sulfides.

The PGMs that are present in the SLC is due to PGMs bypassing the Matte Concentration (MC) plant where the PGMs are separated from the base metals by magnetic separation and base metal leaching prior to being sent to the precious metals refinery (PMR). Some of the PGMs might not be captured with the magnetic fraction as it is supposed to (predominantly non-magnetic CuPdAu alloy and Ru pentlandite report to the base metal fraction) or it could be co-dissolved in the base metal leaching stages where the magnetic PGM fraction is concentrated (Ru and Rh are prone to dissolve under these conditions) (Hofirek, 2001).

If the economic climate allows, BMR is planned to undergo an expansion to increase the Ni production from 21 000t/a to 33 000t/a. This expansion involves a change in the process flow sheet which will include a Fe removal step. The Fe content in the new residue (similar to the old SLC) is said to be reduced by 80% (Dynatec, 2006). The residue will consist mainly of covelite (CuS) and elemental S. The other impurities and PGMs will still be exiting via this residue (Dinham, 2006). The background of the new flow sheet design is given in Appendix I, Section A. The implementation of this process is still indefinite so, in the interim, test work is done on the current SLC with the objective of either significantly minimising the mass or finding a process design that will treat the residue completely in-house. If the expansion continues, the residue treatment process should have the flexibility of treating the new residue economically as well. The criteria for such a residue treatment process are that all the products of the process can either be routed to the current process or produce saleable products or environmentally safe waste for disposal while maximising PGM recovery.

1.1 Background

Based on a review that was done on impurity removal from the secondary leach residue (Viljoen, 2007), two treatment processes were proposed: a pyrometallurgical and a hydrometallurgical process. SLC was successfully treated with a pyrometallurgical process at BMR from 1983 to 1989 where the PGMs were collected in a Cu bullion that was recycled to the smelter. This process was stopped due to operational problems with the furnace and the off-gas treatment. Experience gained in this process and an improvement in furnace designs could make a pyrometallurgical route once again attractive.

Hence, testing of a pyrometallurgical process was done in an Ausmelt Top Submerged Lance (TSL) furnace. The process concept was to fume off unwanted

minor elements (Pb, Bi, Sb, As, Se, Te) and then recover the valuable metals (PGMs, Cu, Ni, Co) to a small mass of alloy for further treatment while Fe, Si and other impurities are mostly rejected to the slag. The fuming was done under oxidative conditions to fume off selenides and tellurides. In order to get the valuable metals back into the matte phase the melt was subjected to reducing conditions with coal addition. This process offers an SLC mass reduction of ± 80% and an expected PGM recovery of 99%. The alloy obtained from this process would require further processing to separate the base metals and other impurities from the PGMs and ultimately obtain a product that is rich in PGMs and can be blended with the feed to Precious Metals Refinery (PMR). The process that was recommended by Viljoen (2007) made use of a subsequent oxidative pressure leach of the Cu alloy in H_2SO_4 to dissolve the base metals, leaching this residue with HNO_3 to dissolve the Ag. The PGM oxide residue can then be sent to PMR where it is subjected to the metallics process.

For the purpose of this project an alternative method of treating the Cu alloy is considered which involves the electrorefining of Cu. This process appeared attractive due to the production of Cu cathodes as a final product, a nickel-rich solution that can be recycled to BMR and a PGM-rich anode slime which might be suitable for treatment in the PMR metallics section. This would eliminate all the other complicated leaching steps. A comparison between a leaching process and electrolysis was done and is given in Appendix I, Section C.

The Cu content in the Ausmelt TSL furnace alloy is not as high as in the Cu bullion that was produced at BMR in 1983 to 1989 (which was ~90% Cu), but it would still be sufficient for the purpose of electrorefining. The composition of the Ausmelt TSL furnace alloy is shown in Figure 1.1.a. It can be seen that it contains mainly copper (80%) and also a significant amount of Ni (12%). The total PGM content in the alloy is ~1.1%. Impurities which might cause a problem in the further processing of the anode slimes / electrolyte are Ag, Pb, As, Te, Se and also Si. The complete analysis table can be viewed in Appendix I, Section B. It is thus necessary to investigate the deportment of the PGMs as well as the impurities to determine if such a process will be suitable, practical and beneficial to implement.

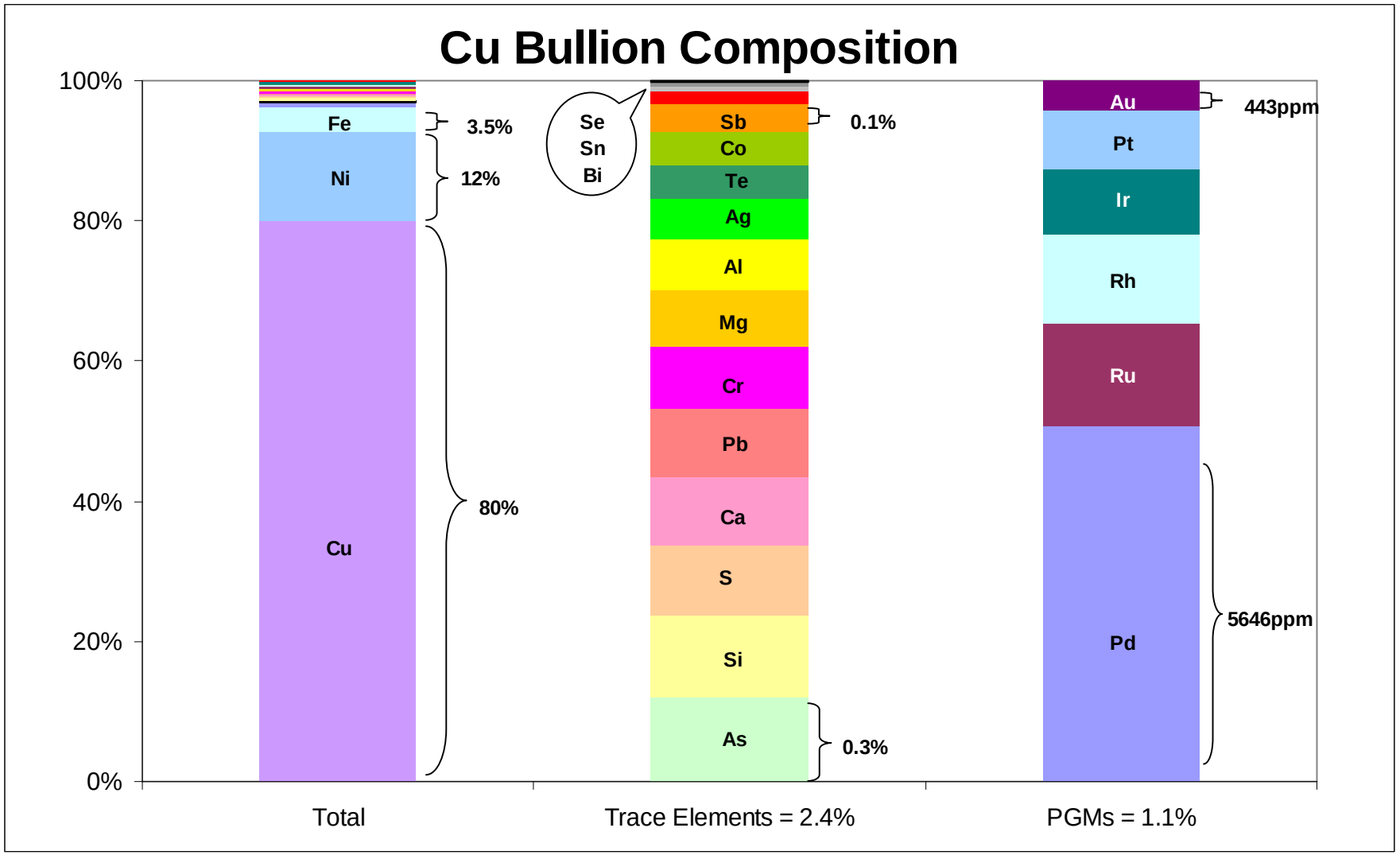

Figure 1.1.a: Composition of Ausmelt TSL furnace alloy produced from treating SLC

1.2 Process Concept

The proposed process uses the two-stage Ausmelt TSL furnace alloy to manufacture anodes which will be used in the electrorefining of Cu. Spent electrolyte from the BMR copper electrowinning can be used as electrolyte. The electrolyte after electrorefining will be rich in Ni and Fe and can subsequently be recycled to the primary leaching stages in BMR where the objective is to obtain a nickel-rich solution, or it can alternatively be sent directly to the Ni circuit where it will be blended with the Ni-rich primary leach solution and put through a number of purification steps in order to remove impurities prior to Ni electrowinning. The Fe and remaining Cu in this solution will be removed in the copper removal section which is the first step of purification. Anode slimes produced from electrorefining can either be subjected to an additional process step to remove Ag, Pb and base metals before being blended with the final concentrate (FICO) as feed for PMR, or can be sent to the metallics section in PMR which includes a roast and a leach stage. The treatment of the anode slimes depends on its nature. The pure copper cathodes that are produced will form part of the BMR final product, provided that they meet the specifications. This way, if it can be assumed that all the Cu and Ni currently present in the SLC will eventually be processed to a cathode, the total Cu production of BMR can be increased by 1056 t/a and the Ni production by 160 t/a. Recoveries will be close to 100% due to the preferential dissolution of these metals during electrorefining. Similarly, the PMR PGM throughput will increase by 14.5 t/a. Figure 1.2.a shows the proposed flow sheet for the SLC treatment.

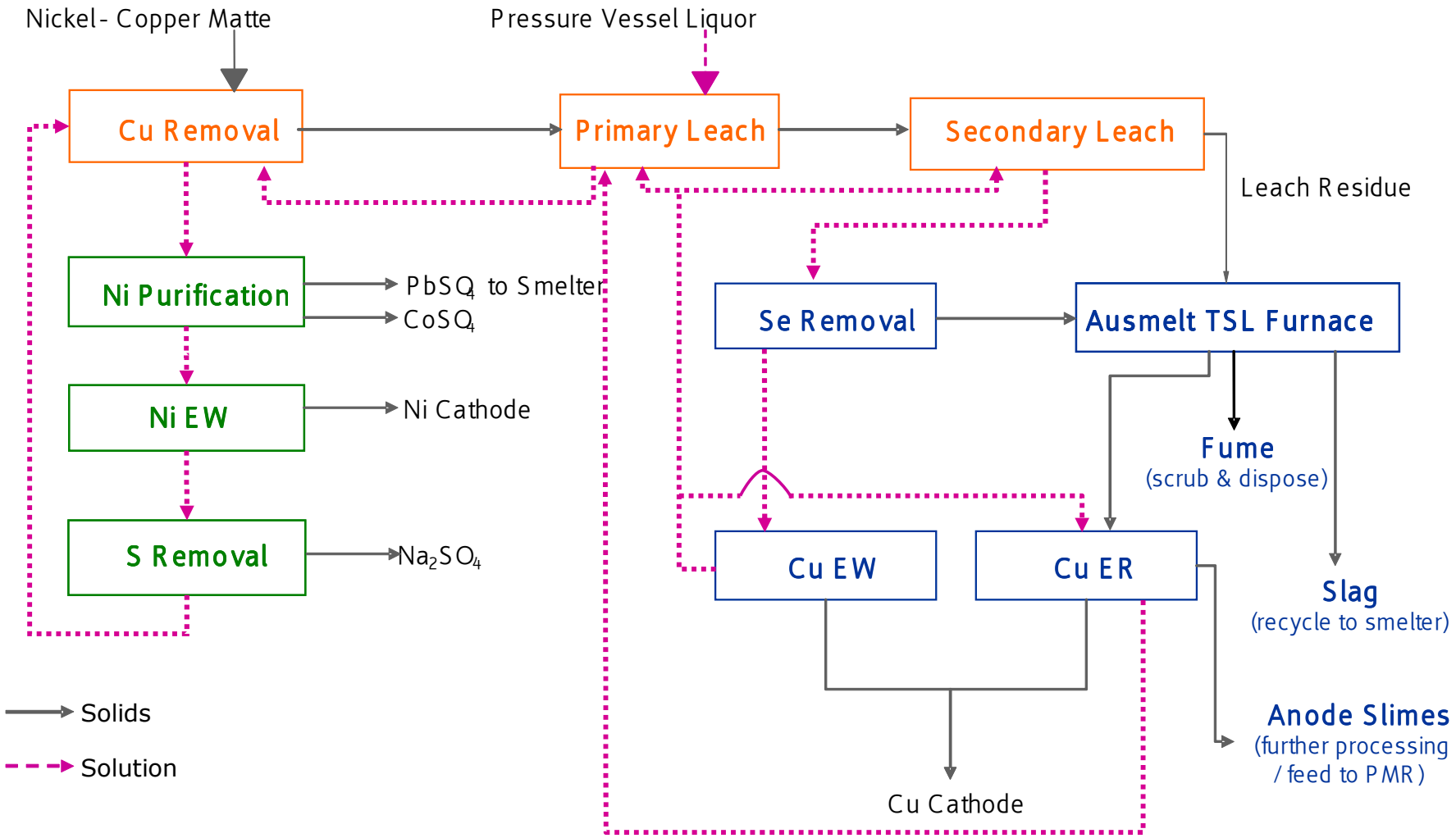

Figure 1.2.a: Proposed flow sheet of Base Metals Refinery

1.3 Problem Statement

The aim is to produce a suitable PGM concentrate in a form that can be easily processed to purify it and then be sent to PMR for final separation of PGMs, as well as recover Cu and Ni to BMR. The proposed process must be safe, cost efficient and economically feasible as well as practical and sustainable.

This project must thus investigate the performance of electrorefining of the Ausmelt TSL alloy provided. The anode slimes produced must be characterised in order to propose further methods of purification before final separation of PGMs.

During this project, the typical energy consumption, current efficiency, anodic copper dissolution rate and deportment of elements (especially PGMs) will be determined. The anode slimes will be characterised by mineralogical investigation and the effect of various operating parameters will be determined to propose optimal operating conditions. A preliminary process design will be performed using the knowledge and experience gained during the literature review and testwork.

2 LITERATURE REVIEW

2.1 Theory

2.1.1 General Introduction

Electrorefining is widely used for the purification and production of copper that is suitable for electrical applications. Such plants exist throughout the world on production scales between 1000 and 100 000 t/a.

In an electrorefining process, the anode is the impure metal and the impurities are lost during the passage of metal from the anode to the cathode during electrolysis. The electrode reactions in the case of Cu electrorefining are as follows.

- Anode reaction: $Cu \rightarrow Cu^{2+} + 2e^-$

  If Ni and Fe are also present in the impure anode, they will dissolve as follows:

  $$Ni \rightarrow Ni^{2+} + 2e^-$$

  $$Fe \rightarrow Fe^{2+} + 2e^-$$

- Cathode reaction: $Cu^{2+} + 2e^- \rightarrow Cu$

A suitable voltage is applied to the electrodes to cause oxidation of copper metal at the anode and reduction of Cu^{2+} to form copper metal at the cathode. This works efficiently because copper is both oxidized and reduced more readily than water. Metallic impurities with a lower reduction potential than copper are less noble and will readily dissolve at the anode but do not plate at the cathode. More noble metals with a higher reduction potential are not dissolved at the anode, instead they collect at the bottom of the cell as anode slimes. The anode slimes can be captured and processed to recover the valuable metals.

Cell voltage and current density are the two important parameters in copper electrorefining. The total voltage is determined by the equilibrium cell voltage, anodic and cathodic overpotential and Ohmic potential drop in electrolyte, hardware and power supply. It is generally accepted that copper production increases with an increase of current density at the cost of current efficiency. The electrolyte that serves as a carrier for the Cu^{2+} ions is sometimes in the form of a molten salt or non-aqueous electrolyte. These forms of electrolyte offer opportunities for increasing current densities and refining via lower oxidation states that are not stable in water. However, aqueous processes are the most widely used due to the ease of handling, more developed chemistry and

familiarity with aqueous process liquors and electrolytes. Cu electrorefining is typically conducted using a sulphate medium for the transport of Cu ions.

The theory behind the redox equilibria, electrochemical kinetics, mass transport, cathode morphology and current distribution for a Cu electrorefining operation are discussed in the following paragraphs (Nicol, 2008).

2.1.2 Redox Equilibria

As mentioned before, the two half reactions for the dissolution and deposition of Cu are equal but opposite, with a standard electrode potential of 0.34 V. The cell voltage can be considered to be composed of the difference between the potential of the cathode and that of the anode:

$$\Delta E = V = E_{cathode} - E_{anode}\ , \qquad \text{Thus, } \Delta \mathbf{E = 0\ V} \qquad \mathbf{(1)}$$

Thus, in the ideal case, the total cell voltage is only required to drive the current through the electrolyte.

The anode material in this case only consists of 80% Cu, 12% Ni, ~4% Fe and other impurities. To investigate what the behaviour of the impurities will be during the dissolution of Cu, the standard electrode potential of other elements are investigated.

Figure 2.1.a shows the standard reduction potentials for some metal ions. It can be observed that only the metals on the right-hand side of Cu will dissolve more readily than copper. Thus, some of the current that passes through the anode will be used to dissolve these metals (especially Ni and Fe). The remainder of the current will dissolve the Cu from the anode which is the major component. It can also be seen that the standard reduction potential for H_2O is on the left of Cu, meaning that Cu will be dissolved preferentially to the oxidation of H_2O to O_2, and O_2 evolution will not occur. At the cathode, Ag and Au (as well as other precious metals not shown in the figure) could be deposited more readily than Cu if in solution. This is not likely because they are on the left hand side of Cu and will not dissolve with the Cu from the anode. H_2O is also on the left-hand side of Cu which indicates that if there are any O_2 in solution at any time, it would be reduced to H_2O preferentially to the deposition of Cu. However, there would generally not be any O_2 in solution during the electrorefining of Cu and it does not play a significant role.

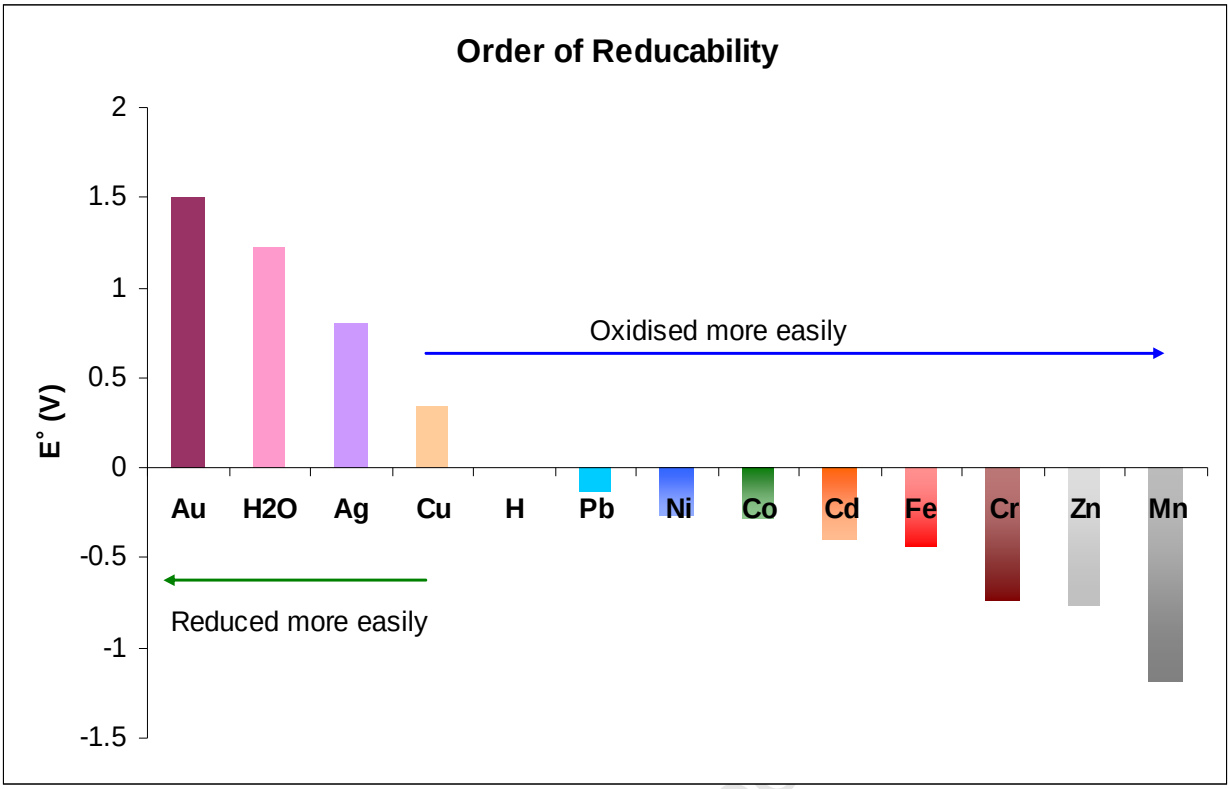

Figure 2.1.a: Standard reduction potentials for metal ions (Nicol, 2008)

In typical electrorefining, the reactions are not carried out under the standard conditions of unit activity. In order to quantitatively account for deviations from the standard states, the Nernst equation is applied to calculate the equilibrium potential for each half reaction under the specific conditions of electrorefining.

$$E = E^{\circ} - \frac{RT}{nF}.\ln\left(\frac{[\mathrm{Re}]}{[Ox]}\right) \qquad \textbf{(2)}$$

Where T: Temperature = 338 K (65˚C)

n: number of electrons transferred

F: Faraday's constant = 96 487 C/mol

[Ox] [Re]: activity of the oxidised or reduced species respectively

[Ox] + ne = [Re]

R: universal gas constant = 8.314 J/K mol

If it is assumed that the activity of the ions in solution is equal to the molar concentration and that the metals are only present as Me^{2+} ions and not complexed, the non-standard electrode potentials at typical BMR electrolyte conditions can be calculated to be the following:

Table 2.1.a: Non –standard electrode potentials at electrorefining conditions

Metal in Solution	Typical Concentration (M)	E° (V)	n	E
Cu	0.615	0.34	2	0.333
Ni	1	-0.25	2	-0.250
Fe	0.041	-0.44	2	-0.487
Ag	1.00E-06	0.8	1	0.398

It can be seen that at concentrations smaller than unity, the equilibrium potential decreases slightly, and the metals would dissolve more easily. The difference in equilibrium potential in the case of Ag is significant due to the very low concentration of Ag in solution. At even lower concentrations, the electrode potential might become lower than that of Cu and would start co-dissolving from the anode. However, a very small build-up of Ag in solution would increase the equilibrium potential again and it would stop dissolving.

2.1.3 Electrochemical Kinetics

The rate at which electrochemical reactions take place is dependent on the transfer of electrons across interfaces of anode/solution and solution/cathode more than just the reactant concentrations. This rate of transfer is governed mostly by the electrochemical potential difference across the interfaces or the and is described by Faraday's law:

$$m = \frac{M.I.t.\varepsilon}{n.F} \qquad \textbf{(3)}$$

where m: mass of metal deposited (g)

I: applied current (A)

t: time (s)

n: number of electrons per mole of metal oxidized or reduced

M: molecular mass of the metal (g/mol)

F: the Faraday constant (96 487 C/mol)

ε: current efficiency

Because the reaction across the surface is relatively heterogeneous, the use of current is often replaced with current density (i) which is the current passed through 1 m^2 of surface area (A):

$$i = \frac{I}{A} \text{ A/m}^2 \qquad \textbf{(4)}$$

From these equations it can be derived that the rate of reaction at the cathode (r) in moles/m^2.s is as follows:

$$r = \frac{i}{nF} \text{ mol/(m}^2\text{.s)} \qquad \textbf{(5)}$$

As proven earlier, if the current through an electrorefining cell is 0 A, the equilibrium cell potential is 0 V. If current is subsequently applied to the cell, the anodic potential will increase and the cathodic potential will decrease. This change in potential is defined as overpotential (η): $\eta = E - E_e$ with E_e: equilibrium potential of particular electrode.

It has been determined that the rate of reaction is related to the free energy of activation ($\Delta G^{\#}$) by:

$$r = \frac{k.T}{h}.\prod a.\exp\left(\frac{-\Delta G^{\#}}{RT}\right) \qquad \textbf{(6)}$$

where k and h are constants and $\prod$a is the product of activities of reactants taking part in the rate-determining step.

It is also known that for an electrode process the free energy is related to potential by:

$$\Delta G = -nFE \qquad \textbf{(7)}$$

If the potential of the electrodes, relative to a copper reference electrode, are measured at different current densities, the current can be plotted as a function of the potential as shown in the solid curve given in Figure 2.1.b. This curve is essentially the algebraic sum of the currents due to the reactions at the anode and at the cathode. At equilibrium where the applied current (i) = 0A and E_e = 0 V the opposite anodic and cathodic reactions are still taking place at equal and opposite rates. The current density due to each of these reactions is known as exchange current density (i_0) and is characteristic of a particular reaction. The exchange current density is a measure of the quantity of oxidation and reduction taking place at the equilibrium potential.

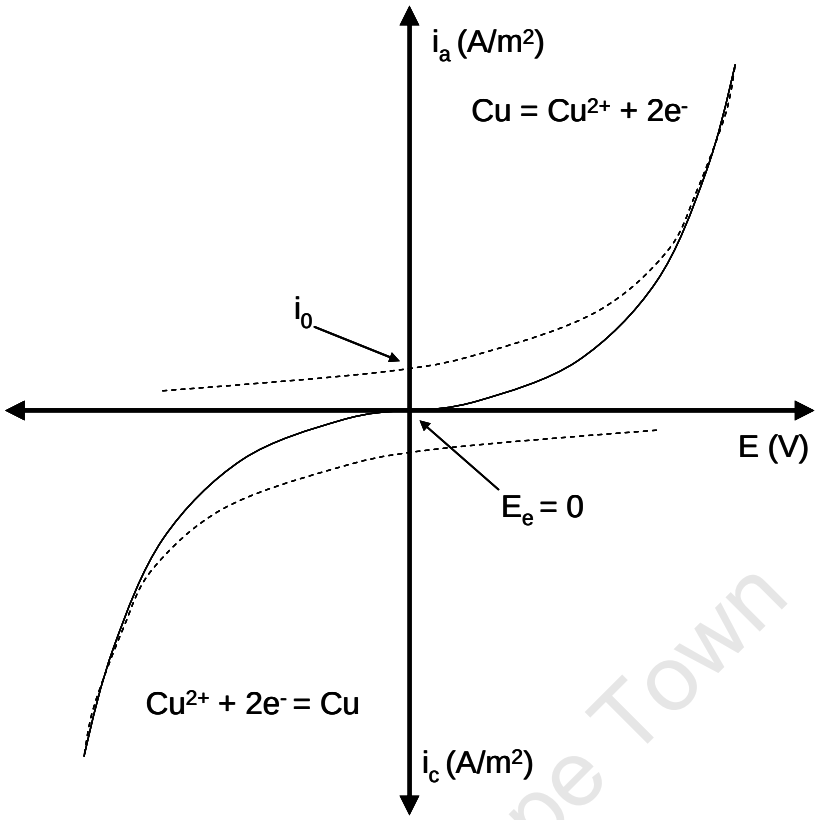

Figure 2.1.b: Schematic current potential curves for anodic and cathodic reactions (Nicol, 2008)

The anodic and cathodic overpotentials relationship with exchange current density and current (the dotted curves in Figure 2.1.b) is quantitatively well described by the Butler-Volmer reaction:

$$i = i_0.\left[\exp\left(\frac{\beta_a.F.\eta}{R.T}\right) - \exp\left(\frac{-\beta_b.F.\eta}{RT}\right)\right] \quad \textbf{(8)}$$

At high field regions where the reactions are not close to equilibrium, the anodic contribution to the cathodic reaction and vice versa can be neglected and the Butler Volmer equation can be simplified to describe the anodic and cathodic current density as follows:

Anodic: $\eta_a = b.\log\left(\frac{i_a}{i_0}\right)$ **(9)**

Cathodic: $\eta_c = b.\log\left(\frac{i_0}{i_c}\right)$ **(10)**

where b is the so-called Tafel slope and is given by $b = \frac{2.303.R.T}{(1-\beta)F}$ **(11)**

The exchange current density for Cu plating at the cathode at unit molarity and 25℃ is 0.2 A/m^2 and the Tafel slope is 40 mV/decade. The Butler-Volmer equations were used with these constants to draw up an approximate schematic of the current density vs. the overpotential applied to the electrodes up to a current density of 250 A/m^2. This relationship is shown in Figure 2.1.c.

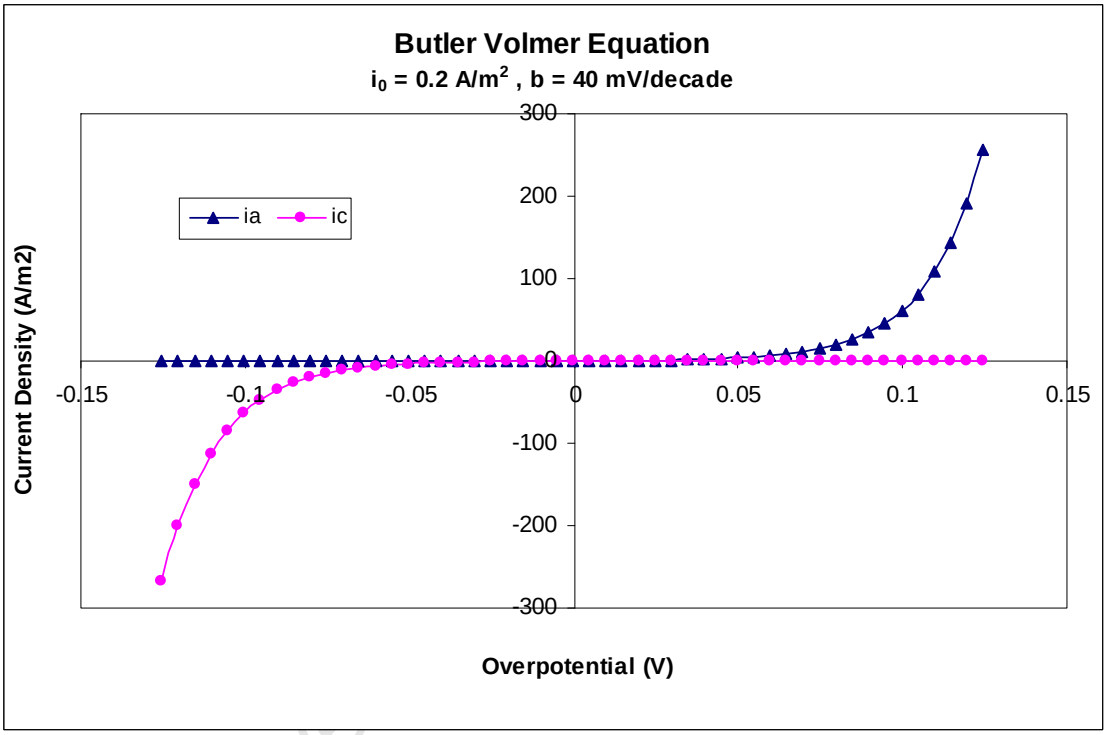

Figure 2.1.c: Calculated current-potential relationship

2.1.4 Mass Transport

If the rate of reaction due to current through the cell is faster than the electrons or ions can physically be transported to or from the electrode the reaction rate becomes mass-transport controlled. Mass transport of ions through the electrolyte is achieved by any of the following means.

Convection

This is due to hydrodynamic transport that is induced by stirring or pumping, air sparging, gas evolution at electrodes, density gradients or thermal gradients. It is often the most effective way of improving mass transport but is applied more in electrowinning practices than electrorefining.

Diffusion

Diffusion has to do with the transport of ions from high to low concentration regions. Due to Cu dissolving at the anode, the concentration in the anode regions will be high; in contrast, the concentration at the cathode will be low due to the transformation of Cu^{2+} ions to Cu metal. Thus, diffusion of Cu^{2+} ions is very relevant in electrorefining practices.

Migration

Migration is the movement of ions due to an electrical field. In acidic solutions such as the electrolyte used in Cu electrorefing, there is a good transport of current and the contribution of migration is relatively small and is often neglected.

In cases where the reaction is mass-transport controlled, the rate equation in terms of current density is no longer applicable. Instead, the rate is determined by the product of the bulk molar concentration (C_b) of the ion in solution and the mass transport coefficient (k_L).

Reaction rate controlled: $r = \frac{i}{nF}$ mol/(m^2.s) **(12)**

Maximum rate if mass transport controlled: $r_m = C_b.k_L$ mol/(m^2.s) **(13)**

The mass transport coefficient (k_L, m/s) is determined with the diffusion coefficient (D, m^2/s) of the ion moving through a diffusion layer which is a stationary film adjacent to the electrode surface and the physical thickness (δ, mm) of this film:

$k_L = \frac{D}{\delta}$ m/s **(14)**

The rate schematic for a mass-transport controlled system is illustrated in Figure 2.1.d:

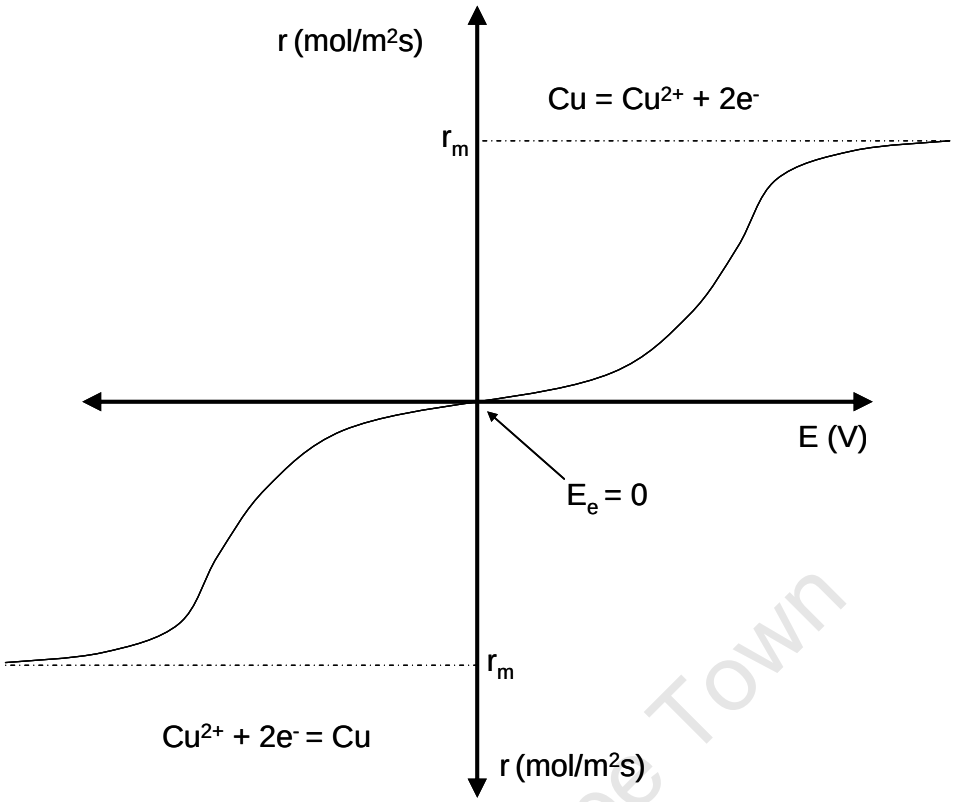

Figure 2.1.d: Rate-potential curve for an electrode reaction involving mass transport (Nicol, 2008)

2.1.5 Cathode Morphology

Cu electrorefining should produce cathodes that are uniformly thick and chemically pure that can be readily stripped, handled and processed. One of the most important factors that influences the morphology of the cathodes is the current density. As the current density increases, the mean size of crystallites that are deposited will decrease. Excessively high current densities can even produce very powdery deposits. Other factors that will result in finer crystal growths are:

- Decrease in metal ion concentration
- Decrease in temperature
- Reduction in mass transport
- Increase in smoothing agents.

An increased grain size or roughness in cathode promotes occlusion of anode residues and electrolyte, resulting in contamination of the cathodes and is thus not preferred. It is aimed to obtain a fine-grained cathode surface with lateral crystal growth. The maximum

current density that is generally applied in industrial operations is 30-40% of the limiting current density.

Developments in improving cathode quality have been reusable cathodes, electrolyte purification, monitoring of additives, periodic current reversal and anode preparation machines (Hiskey, 1999).

2.1.6 Current Distribution

The distribution and extent of reactions taking place on the electrode surfaces are dependent on the current distribution over an electrode surface or throughout a cell. It has been proven that current is not uniform and is mainly dependent on the following factors:

- Size and geometry of cell
- Current density
- Conductivity of solution
- Kinetics of the electrode reactions
- Mass transport to the electrode

Distinctions are made between three different types of current distribution:

1) *Primary current distribution* – Assumed that overpotentials do not play a role in current distribution but only the geometrical distances between the electrodes.

2) *Secondary current distribution* – Takes activation overpotentials (i.e., conductivity of electrolyte) and geometrical distances into account but assumes that there is no concentration variation near the electrode.

3) *Tertiary current distribution* – Assumes that the reactions are mass-transport controlled, thus takes into account geometry, conductivity as well as mass transport.

It should be aimed to maintain as uniform as possible current distribution throughout the tankhouse to prevent poor cathode quality, decreased current efficiency, non-uniform cathode growths (dendrites), short-circuiting, loss of production, and local anode passivation. There are a number of precautions that can be taken to ensure uniform current distribution:

- Uniform electrode spacing
- Vertical hanging of anodes and cathodes

- Flat cathodes and anodes
- Good electrolyte composition
- Avoidance of passivation.

Good contacts of anodes and cathodes to the bus bars (current distributor bars) also minimises energy loss and contributes to uniform current distribution among all electrodes (Biswas et al., 2002).

2.1.7 Anode Passivation

Anode passivation is the build-up of non-porous layers on anode surface. This tends to block mass transport of dissolved ions to the electrolyte. Current density, temperature, additives and anode or electrolyte compositions are some of the influencing factors on anode passivation. All of these mainly relate to the solubility of various ions in the electrolyte.

Radhakrishnamurthy et al. (1980) described anode passivation as follows:

> "The concentration of copper ions at both the cathode and the anode change with time; a decrease occurs at the cathode and an increase occurs at the anode. As the concentration of copper ions increases at the anode, a point is reached when the copper salt precipitates on the anode and acts as a mechanical barrier for the copper ion transfer."

Anode passivation, caused primarily by copper sulphate precipitation on the anode and the slime layer present on the anode surface, was demonstrated to depend on electrolyte composition, temperature, anode composition and parameters affecting the mass transport of copper ions, as well as $CuSO_4$ solubility (Gu et al. 1994)

From the work of Gu et al. (1994) it is evident that the higher the silver content in the anodes, the larger the amount of suspended slime and this reduces the time it takes for anode passivation to take place as it obstructs the transfer of ions through the slimes layer at very high current densities.

As mentioned before, the passivation time and periodic passivation phenomena were found to be closely associated with thiourea concentration and degradation (Hiskey and Cheng, 1998).

2.2 Operating Parameters

The major technical factors in electrorefining practice are specific energy consumption, the production rate and the cathode purity. The operating parameters that influence these factors the most are the anode quality, electrolyte conditions and cathode current density. A literature review was done on these operating parameters in detail to summarise the effect each of these has on the technical factors as well as the typical operating conditions that are currently applied in electrorefining applications.

The operating parameters must be selected such that both the anodic dissolution and the deposition of the Cu occur efficiently while none of the impurity metals transfer from the anode to the cathode and passivation of the anode is minimal. The objective is to recover all the precious metals with as little as possible base metals and other impurities to the anode slimes and produce a good quality, highly crystalline deposit at the cathode.

2.2.1 Current Density

The current density and voltage required to produce such a current are important factors in the capital and working cost of a plant. The theory presented in the previous section showed that current density is in direct relationship with the rate of reaction, as long as mass transport is not the limiting factor. Thus, in order to achieve high production rates, high current densities are required. Unfortunately, current density can not be increased indefinitely due to a number of limiting factors. Pletcher and Walsh (1990) described the effects of excessive current density as the following:

1) Increased impurity levels in the cathode deposit due to increased roughness of cathodes caused by high current density. Cathode roughness promotes occlusion of anode residues and electrolyte in the cathode.

2) Anode passivation occurs at high current density (>280 A/m^2) which limits or suspends production rates.

Another limiting factor mentioned by Nicol (2008) is the cost implication of high voltage drop across electrolyte due to high current density.

Radhakrishnamurthy et al. (1980) investigated the problems associated with operating at increased current densities and came to similar conclusions:

1) Anode passivation occurs, resulting in increased cell voltage (energy waste)

2) Production of rough and powdery deposits

3) Deterioration of cathode quality and purity

4) Decrease in current efficiency.

A model for the diffusion coefficient of Cu^{2+} ions in simulated electrorefining electrolytes, applied by Moats et al., (2000), indicates that rapid precipitation of $CuSO_4$ occurs at the high current densities used in accelerated passivation experiments.

At some refineries, periodic current reversal is applied which allows operation at higher current densities. The current reversal of short periods at a specific interval serves as a de-passivation mechanism, where the anode acts as a cathode and vice versa, thereby depleting the built up copper concentration within the anodic boundary layer and preventing the precipitation of $CuSO_4$. The limited use of this technology, however is the significant increase in energy consumption (Biswas et al., 2002).

2.2.2 Electrolyte

The electrolyte used for copper electrorefining typically consists of $CuSO_4$ and H_2SO_4. The effect of the concentrations of these substances on the performance of the electrorefining process has been thoroughly investigated in previous research.

The importance of H_2SO_4 in solution is highlighted by Hayes (2003) and a number of reasons why electrolytes should contain sulphuric acid are given:

1) The inspection of the E_h-pH diagram for the Cu-S-H_2O system suggests that formation of cupric oxide or hydroxide will occur more easily if an acidic solution is not maintained.

2) Better conductivity can be achieved with an increased acid content, thereby lowering electrical resistance.

3) Sulphuric acid is generally relatively cheap.

This was confirmed with the work of Casas et al. (2000) who used the Pitzer and Davie ion-interaction model to simulate the distribution and concentration of chemical species in sulphuric acid – cupric sulphate solutions. The simulations showed that the concentrations of the different species are very dependent on pH. It was found that the conductivity of the aqueous solution increases with acidity.

The electrolyte acid and copper concentration not only affect the solubility of copper sulphate and electrical conductivity but also affect the equilibrium electrode potential as illustrated by the Nernst relationship (equation 2) in Section 2.1.2.

The presence of Cu^{2+} in the electrolyte is mainly to reduce cell voltage and anode / cathode polarisation which is the accumulation of ions around an electrode, causing the accumulation of a charge. The effect of Cu concentration on these factors is shown in Figure 2.2.a (Hayes, 2003). However, the solubility of copper at high current densities is limited and precipitation of $CuSO_4$ will take place if concentrations are too high, resulting in anode passivation.

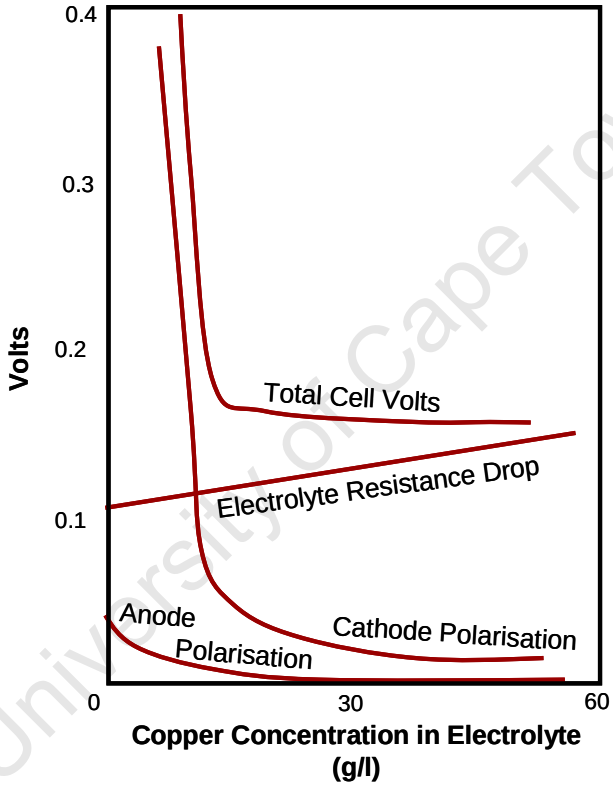

Figure 2.2.a: The effect of copper concentration in the electrolyte on cell voltage during electrorefining (Hayes. 2003).

The concentration of Cu in the electrolyte also plays a large role in the purity of the cathodes that are produced. If the Cu concentration across a cell is typically in the range of 45 g/l to 15 g/l, good commercial purity cathodes are produced but at lower concentrations (15 g/l to 8 g/l) the cathodes will be impure and will need to be re-melted. At extremely low concentrations (8 g/l to 0.2 g/l), the cathode will be very impure and will need purification before being re-melted in the anode furnace (Pletcher and Walsh, 1990).

It is generally known that the deposition and dissolution processes are significantly affected by the diffusion coefficient (mass transport) of copper within electrolyte. The effects of copper, acid, and temperature on copper diffusivity were measured for simulated industrial electrolytes by Moats et al. (2000) and are shown in Figure 2.2.b and Figure 2.2.c. It was found that an increase in copper concentrations slightly decreased the diffusivity of Cu^{2+} ions in the electrolyte. Mass transport at high concentrations would thus be poorer and could play a significant role on the rate of reaction.

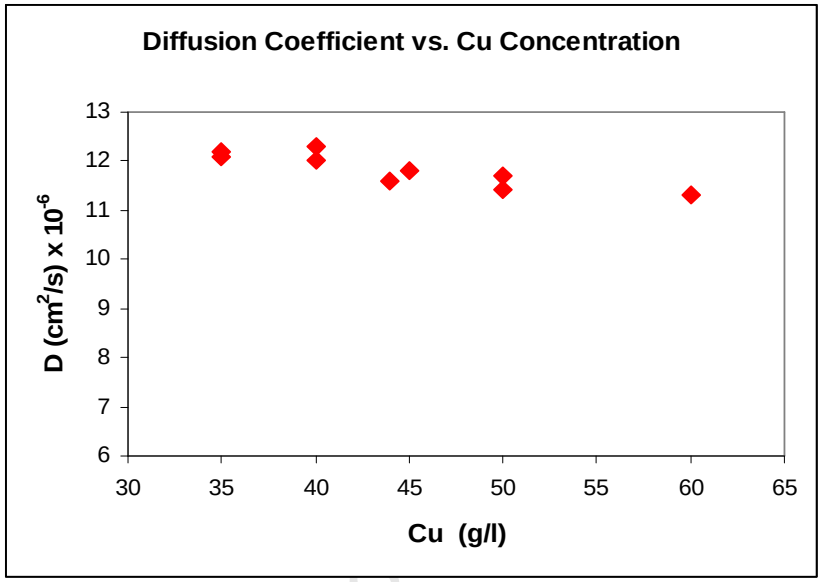

Figure 2.2.b: Effect of Cu Concentration on Cu^{2+} Diffusion Coefficient (Moats et al. 2000)

An increase in acid concentration also showed a decrease in the diffusivity of cupric ions (Figure 2.2.c). Electrorefining operations typically use acid concentrations of 160 g/l to 200 g/l in order to decrease the electrolyte resistance thereby minimising the power loss to ohmic resistance. At very high acid concentrations the decrease in diffusivity of the cupric ion might start playing a significant role and aggravate anode passivation by increasing the chances of $CuSO_4$ precipitation.

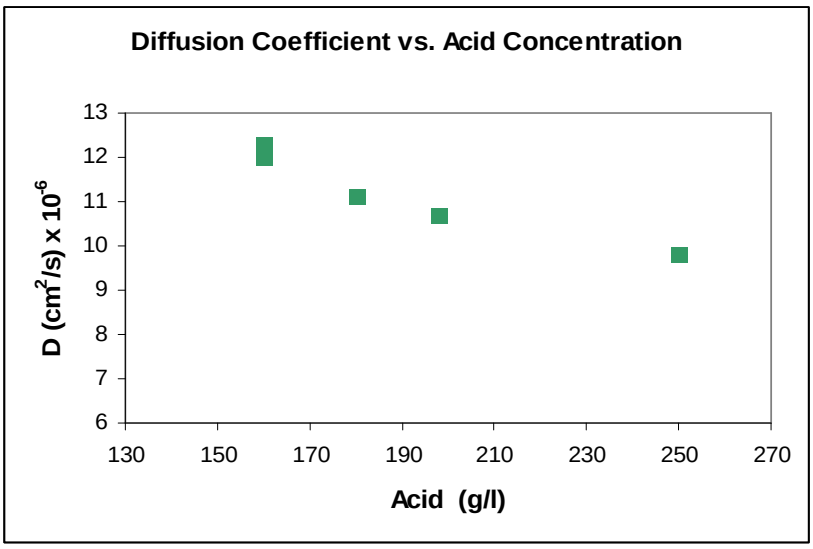

Figure 2.2.c: Effect of Acid Concentration on Cu2+ Diffusion Coefficient (Moats et al. 2000)

Electrolyte can be occluded in copper cathodes by entrapment, resulting in impure cathodes. This can be minimised by:

- Producing smooth and dense copper cathodes
- Controlling impurity levels in electrolyte, by bleeding electrolyte to remove the build-up of impurities (Biswas et al., 2002).

Suspension of solids in the electrolyte can also lead to co-deposition of impurities in the cathodes.

A study of cathode nodulation was done by Anderson et al. (1982) and it was found that an increasing Cu^{2+} concentration nominally decreased nodulation and subsequent occlusion of impurities in the cathode.

The continuous build-up of impurities int the electrolyte is due to impurities dissolving from the anode and recycled with the electrolyte. Excessive impurity build-up will influence the cathode purity and can thus not be sustained. The build-up is removed from the electrolyte by a bleed stream that can subsequently be subjected to the following processes in order to purify and recycle the electrolyte:

1) Cu electrowinning

2) Electrowinning As, Bi and Sb into an impure cathode deposit

3) Evaporation of water and precipitation of $NiSO_4$ crystals

4) Recycling remaining concentrated acid to electrolyte (Biswas et al., 2002)

An example of impurity build-up in electrolyte leading to cathode impurity was experienced by a Zambian copper smelter at Mufulira (Nyirenda and Phiri, 1997). It was found that an increase in Ni content in the anodes (0.1% Ni content) led to an increase of Ni content in the electrolyte (10 g/l) as well as in the final Cu cathode (1.2 ppm). Although the London Metal Exchange (LME) Grade A specification is a maximum of 10 ppm Ni in cathode, the copper smelter had a target of only 1 ppm Ni in cathode. A large bleed stream was required to maintain good cathode quality. The bleed stream was subsequently evaporated to precipitate $NiSO_4$ crystals and recycle the concentrated acid to the electrolyte. The LME Grade A specifications for impurities in Cu cathode production are given in Table 2.2.a (Nicol, 2008):

Table 2.2.a: Chemical specifications for copper cathode (Nicol, 2008)

Element	LME Grade A (ppm)
Se	2
Te	2
Bi	2
Sb	4
As	5
Pb	5
S	15
Sn	5
Ni	10
Fe	10
Ag	25

The electrolyte is circulated through the electrorefining cells at a steady slow flow with one inlet (near the bottom of the cell) on the one side and an overflow outlet at the other. The importance of this kind of circulation is given by Pletcher and Walsh (1990), it is stated that a steady slow flow of electrolyte cell is necessary for the following reasons:

- Good temperature control
- Gentle increase in mass transport
- Minimum compositional gradients throughout the cell
- Replenishing of organic additives
- Settling of anode slimes at the bottom of the cell so as not to come into contact with the cathodes.
- Removal (bleed stream) of element build-up in solution such as Ni, Fe etc.

2.2.3 Temperature

Temperature plays an important role in the solubility of the elements in the electrolyte as well as the solution conductivity. Generally, better operation is experienced at high temperature, but excessively high temperatures will result in significant evaporation and a reduction in energy efficiency (Biswas et al., 2002). The boiling point of the solution might also be reached which could result in unwanted gas emissions.

The effect of temperature on the cell voltage and anode / cathode polarisation is shown in Figure 2.2.d (Hayes, 2003). It can be seen that increased temperature significantly reduces the electrolyte resistance and cell voltage.

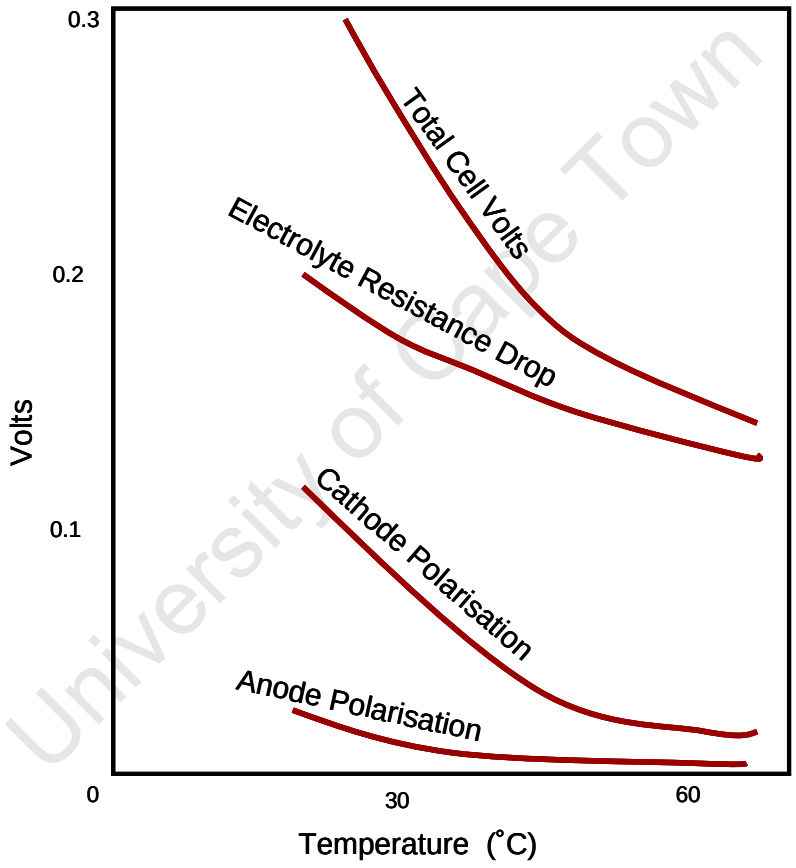

Figure 2.2.d: The effect of temperature on the cell voltage during electrorefining (Hayes, 2003)

In a model developed by Moats et al. (2000) for the diffusion coefficient, it was also shown that an increase in temperature increases the diffusion coefficient of Cu^{2+} ions, thereby improving mass transport and allowing higher current densities before the precipitation of $CuSO_4$ occurs. The effect of temperature on the diffusion coefficient as determined by Moats et al. (2002) is shown in Figure 2.2.e.

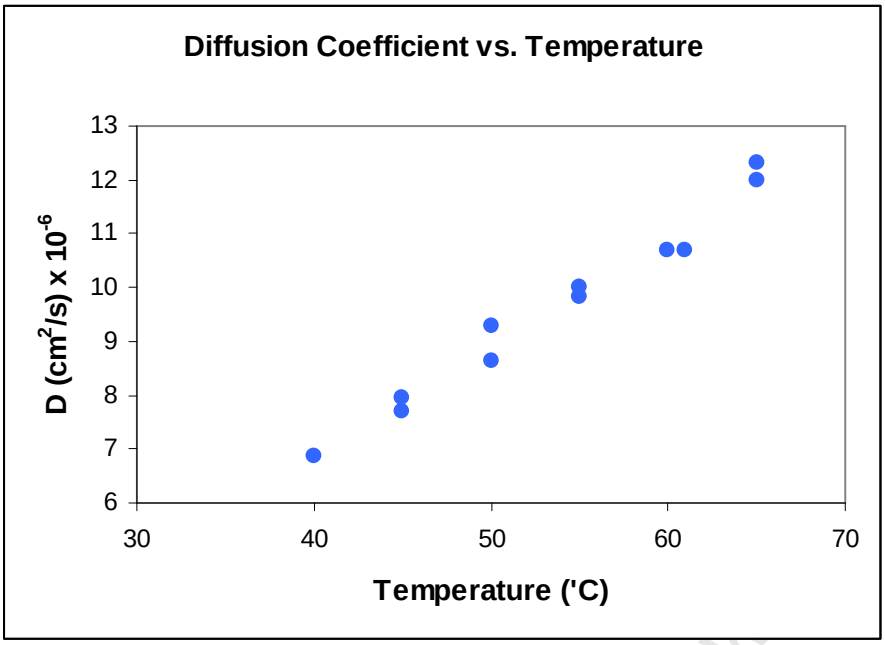

Figure 2.2.e: The effect of temperature on diffusion coefficient (Moats et al. 2002)

In confirmation of this, Cifuentes et al. (2007) developed a model for the operation of a laboratory-scale copper electrowinning cell. The model determined that an increase in temperature decreases the cell voltage and the specific energy consumption, while increasing the copper production rate slightly.

Biswas (2002) stated that an increase in temperature:

1) Increases the solubility of $CuSO_4.5H_2O$ thereby preventing it from precipitating on the anode and causing anode passivation;

2) Lowers electrolyte density and viscosity and can thus allow anode slimes to settle to the bottom more easily, thus minimising slimes reporting to the cathode;

3) Increases the rate of reaction of Cu dissolving from the anode.

It was found that nodulation is more substantial at temperatures lower than 50˚C and that it decreased markedly with an increase in temperature to between 50˚C and 70˚C (Anderson et al. 1982).

Cifuentes and Simpson (2005) investigated the temperature dependence of various kinetic parameters for the copper electrodeposition reaction. Numerical relationships between temperature and exchange current density, as well as temperature and limiting current density were determined experimentally. These relationships are illustrated in the Figure 2.2.f:

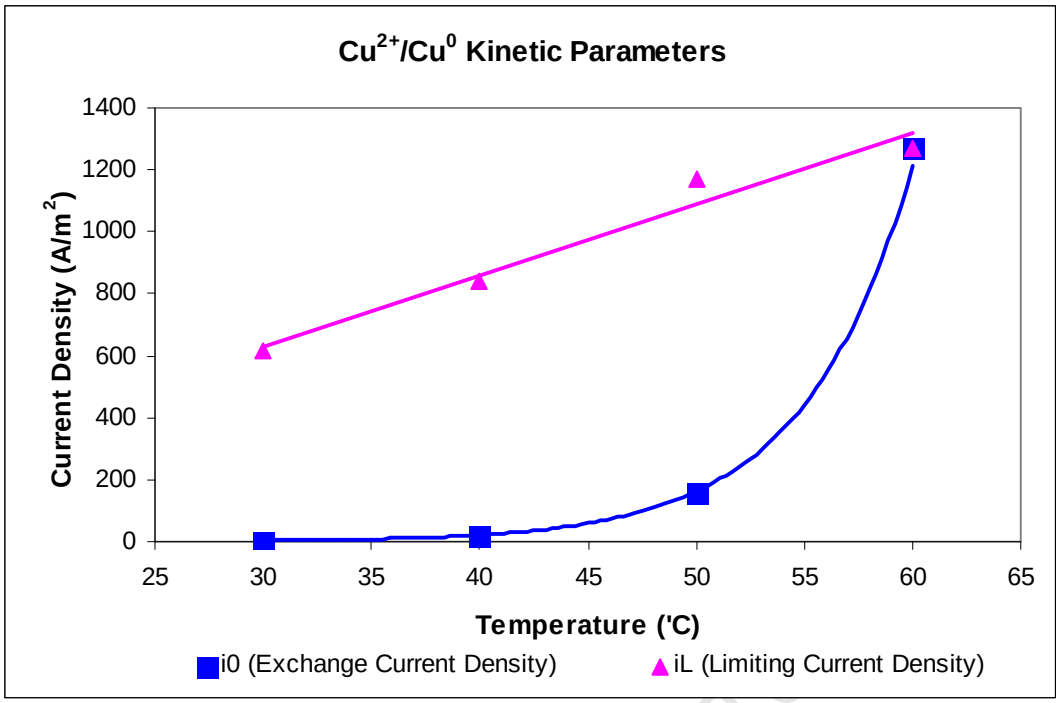

Figure 2.2.f: Kinetic parameters for the Cu^{2+}/Cu^{0} reaction on a copper sheet cathode at various temperatures as determined by Cifuentes (2005)

The above finding simply shows the importance of increased temperature during electrorefining.

Cifuentes et al. (2006) also investigated the relationships of species concentration as a function of temperature in aqueous Cu^{2+}-H_2SO_4 solutions and found that the species concentrations are linearly dependent on the operating temperature and that the prevalent species at high temperatures are $[Cu^{2+}]$ and $[HSO_4^-]$.

2.2.4 Anodes

In order to cast anodes suitable for electrorefining, blister copper produced from Cu ore normally needs to be fire refined to remove the excess amounts of S and O. If S and O concentrations are relatively high in Cu blister, SO_2 bubbles (blisters) will form in newly cast anodes which will make them weak and bumpy. Fire refining takes place in two steps (Biswas et al., 2002):

1) *Step 1* – Selective oxidation by means of injecting air through the molten metal for the removal of SO_2 and other impurities. The S content is reduced to 0.002%.

2) *Step 2* – Deoxidation by hydrocarbon (typically propane) reductions for the removal of oxygen as CO and H_2O. Oxygen content is reduced to 0.15% O.

This process is similar to the two-stage process that the SLC material of the present study was subjected to in the Ausmelt TSL furnace.

Most copper anodes are cast in open anode-shaped impressions on top of flat copper moulds. Newly pored anodes are cooled by spraying water on the tops and bottoms of the moulds. An example of a typical Cu anode is shown in Figure 2.2.g

Figure 2.2.g: Example of a typical anode casting

(Asarco, Mineral Discovery Centre, 17 July 2009, image at: www.asarco.com/AMDC/smelting.html)

Anodes suitable for electrorefining need to have flat surfaces and uniform thickness. This is to make sure that all the anodes in an electrorefining cell reach the end of their useful life at the same time and also contributes to obtaining uniform current distribution over the surface area and throughout the cell. Vertical and flat anodes essentially improve cathode purity and increase current efficiency.

One electrorefining cycle generally returns 15-20% of the anode as anode scrap to be thoroughly washed and remelted. It takes typically 21 days for an anode to dissolve before it has to be re-melted (Biswas et al., 2002).

The anodes should be manufactured in such a way that as little as possible oxidation takes place (to minimise passivation) and also to obtain an anode with finely and homogeneously distributed copper throughout the anode to ensure uniform dissolution of the anode, subsequently preventing anode disintegration.

The Ni concentration in the Cu alloy material used for the anodes of this project is relatively high (12%) compared to traditional Cu anodes used in electrorefining (0.3%) and it is thus necessary to investigate the forms in which Ni will present itself in both the anode and the anode slimes. A study of nickel-bearing copper anodes and anode slimes were performed by Chen and Dutrizac, b, (1989). It was found that in anodes containing > 0.3% Ni, NiO crystals, Cu-Ni-Sb oxides, Cu-Ni silicates, $NiFe_2O_4$ and other Ni-bearing iron oxide phases are present along with Ni in solid solution within the copper matrix. It was shown that all of the oxide nickel phases remain largely undissolved during electrorefining.

McKay and Peters (1991) suggested that a suitable way to increase copper extractions by up to 50% is to use a packed particulate anode, thereby increasing the surface area for dissolution. It was shown that high-grade copper alloy can be successfully electrorefined using particulate anodes, provided there is no obstruction to convection in the anode compartment and that the particles sizes are about $1/10^{th}$ of the thickness (eg. 2 mm for 20 mm anode thickness) of the anode bag.

This work also established that the presence of Fe and Pb in the copper alloy leads to a reduction of total copper extraction. It was found that Fe in the form of bornite (Cu_5FeS_4) stopped dissolving after losing no more than 25% of its Cu content. .

2.2.5 Additives

Additives, such as chloride, thiourea and glue are used in electrorefining as grain refiners and levelling agents for deposition. They allow the production of smooth dense cathodes which will not entrap impurities from the electrolyte or suspended particulates.

In order to minimise entrapment of electrolyte or anode slimes, smooth dense cathodes are required. The addition of levelling and grain-refining agents (guar gum and thiourea amongst others respectively) encourages this kind of cathode deposition (Biswas et al., 2002).

Biswas et al. (2002) stated that the levelling action of glue is caused by the deposition of the large protein molecules on the tips of protruding copper grains. These protein molecules create an electrically resistant barrier at the tips of these protrusions and then forces sideways growth, ultimately creating a dense and level surface.

Chloride ions are a common addition to enhance the dissolution and the use of guar gum has typically been used as a brightening additive for electrowinning. The drawback in using guar is that it is hard to dissolve into solution and tends to readily break down. The

electroplating in such conditions will be very erratic. Another additive that is often used is thiourea; however, the use of this results in sulphur co-deposition from the plating residues in the solution. Sulphur then co-deposits as an undesirable impurity in the copper deposit (Janik 2001).

Jin and Gali, (2001) also investigated the effect of thiourea on cathode polarisation and found that at thiourea concentrations of 1, 2 and 4 g/l polarisation of the Cu cathode occurred at low overpotentials and a depolarisation occurred at high overpotentials. Between these two occurences there was a transition current density, which increased with thiourea concentration. This transition current density decreased with time after thiourea was added due to its apparent decomposition. However, it was stated that at current densities lower than 350 A/m^2, as is currently applied in the industry, concentrations of thiourea higher than 1 g/l still only produced a polarizing effect on the copper cathode through the formation of a sulphide film on the cathode.

The effect of additives on anode passivation in electrorefining of copper was investigated by Ilkhchi et al. (2006). Passivation of industrial copper anodes under high current densities were reported with the additions of thiourea, glue and chloride ions as additives. It was found that the addition of glue and thiourea prolongs the time before passivation at low concentrations but reduces it at higher concentration and that chloride addition prolongs the passivation time at concentrations higher than 40 ppm.

The addition of most additives increases the polarization of the cathode and results in an inhibition of Cu deposition (Muresan et al. 1999)

Very good automised additive additions are available for careful monitoring of additives.

The principal levelling agents used in copper electrorefineries are bone glues, and the principal grain-refining agents are thiourea and chloride ions (added as HCl or NaCl). The typical glue, thiourea and Cl ion addition in grams per tonne of cathode are 40-90 g/t, 10-60 g/t and 35-65 g/t respectively (Biswas et al, 2002).

2.2.6 Typical Operating Conditions

Typical operating conditions for commercial electrorefining operations were given by various sources and are shown in Table 2.2.b.

Table 2.2.b: Typical operating conditions of a copper electrorefining process

Source	Current Density A/m^2	Cell Voltage V	Cu g/l	Acid g/l	Temperature ˚C	Additives Y/N
Biswas et al. (2002)	250 – 290	0.3 - 0.4	40-50	170-200	60 – 70 Steam Heated	Yes, 0.02 - 0.05 g/l Cl 1 – 10 ppm levelling agents & grain refining organics
Pletcher & Walsh (1990)	100 – 200	0.15 - 0.3	40 – 55	180 – 250	60 – 65	Yes, Levellers, brighteners and surfactants
Moskalyk & Alfantazi (2003)	180 – 280		35 – 45	150 – 220	55 – 65	
McKay & Peters (1991)	200		40	200	55	
Jin & Gali (2001)	150 – 350		42	160	65	Yes, 4 mg/l thiourea
Chen & Dutrizac (2004)	180 - 300		40 - 45	160 - 280	60 – 66	Yes

2.3 What to Expect During Electrorefining

2.3.1 Behavior of Various Elements in Copper Electrorefining

Ni

As stated before, Ni requires a lower applied potential than Cu and will dissolve from the anode rapidly. However, it was found that Ni that occurs as $NiFe_2O_4$, Cu-Ni-Sb oxides and other oxidate nickel phases will remain largely undissolved during electrorefining (Chen and Dutrizac, b, 1989).

Ag, Se and Te

Chen and Dutrizac, a (1989) studied the mineralogical deportment and reaction of Ag during electrorefining and found that the silver in the copper matrix dissolved, but was then rapidly precipitated from the electrolyte by a variety of reactions. Part of it is reduced to its elemental form by the Cu^+ ion but can subsequently redissolve. Some precipitates as a complex Cu-Ag-Pb-As-Se oxidate and some reacts with $Cu_2(Se,Te)$ particulates liberated from the anode and forms copper-bearing silver selenide or silver-bearing copper selenides. It is important to note that if there is Ag in solution in the

vicinity of the cathode at any time, it will electroplate preferentially to Cu because it requires a smaller applied potential. However, the reaction of Ag precipitation is sufficiently fast that the Ag/Se ratio in the bulk anode is an approximate indication of the Ag/Se ratio of the selenides in the slimes layer.

Au and PGMs

Biswas et al. (2002) stated that Au and PGMs do not dissolve in sulphate electrolyte but simply drop from the anode surface, as they are liberated, and report to anode slimes.

Au (and possibly other PGMs) that are in solid solution within the copper matrix are liberated in the elemental form in spike-like particles of <1 μm. Some Au is also detected in complex Cu-Ag-As-Se oxidate precipitates in the anode slimes (Chen and Durtizac, a, 1988).

Pb, Sn, As, Bi, Co, Sb and S

These elements will essentially dissolve rapidly from the Cu anode and stay mostly in solution which would cause a build-up in electrolyte, and therefore need to be removed via a bleed stream to prevent cathode contamination (Biswas et al., 2002). They could be entrapped in the copper cathode by occlusion.

However, some Pb and Sn re-precipitate as $PbSO_4$ and SnO_2 respectively (Biswas et al., 2002)

Sb and As dissolve electrochemically from copper anodes as trivalent ions but can oxidises again to a valency of 5 by O_2, if there were any dissolved in electrolyte, which is unlikely. Sb(V) has a lower solubility in electrolytes than As(V), and forms a floating slime, which is a ragged residue of amorphous structure (Petkova, 1997). During electrorefining, these floating slime particulates can be included electrochemically in growing cathode copper deposits.

According to Chen and Dutrizac (2005), Pb, As and Sb would re-precipitate to $PbSO_4$, $SbAsO_4$, Sb-As oxide, Sb-As-Bi oxide, $Pb_5(AsO_4)_3(OH,Cl)$ and an oxide phase of mainly Cu-Ag-AsO_4-SO_4. It was also stated that a high As content facilitates the precipitation of Sb and Bi from the electrolyte and would cause them to report to the anode slimes. At some refineries, the concentrations of Sb and Bi in the electrolyte are controlled by adding Pb and As to the anodes in order to promote precipitation of these impurities.

Xiao et al. (2007) also showed that Bi and Sb precipitate as copper arsenite if As is present in the electrolyte. It was proved that these Bi-Sb-As precipitates reports to the anode slimes with the undissolved PGMs.

Co and Fe

Like Ni, these base metals will also mostly dissolve in the electrolyte unless they are in an oxide form which would not dissolve under specific conditions (Biswas, 2002).

The behaviour of different impurities depends on the specific element and the form in which it is present in the anode and electrolyte. A closer investigation into the mineralogy of the anode will explain some of the behaviours.

Biswas et al. (2002) presents a table of fractions of anode elements that typically enter the slimes and the electrolyte (see Table 2.3.a).

Table 2.3.a: Recovery of elements to anode slimes and to electrolyte (Biswas, 2002)

Element	% to Slimes	% to Electrolyte
Cu	<0.2	>99.8
Au	100	0
Ag	>99	<1
Se	98	2
Te	98	2
Pb	98	2
Bi	60	40
Sb	60	40
As	25	75
S	1	99
Ni	1	99
Co	1	99
Fe	0	100
Zn	0	100

Cathode Purity

Sedzimir et al. (1985) found that in Cu electrorefining with an ammonium electrolyte, an increase in current density had the following effect on copper cathode impurities:

- Ag content decreases sharply
- Ni increases slightly

- As increases significantly
- Sb decreases sharply

and with an increase in electrolyte temperature:

- Ag increases
- Ni increases
- As decreases
- Sb increases slightly.

It was also found that the ammonia concentration does not have an effect on the impurity deportment to the copper cathodes.

It is likely that the behaviour of these elements will be similar in a sulphate electrolyte.

2.4 Rustenburg Base Metal Refiners Internal Literature

SLC was successfully treated with a pyrometallurgical process at BMR from 1983 to 1989 where the PGMs were collected in a Cu bullion that was recycled to the smelter. This mode of operation led to lock-up of PGMs over extended periods, increased overall PGM losses, and a build-up of process impurities in the process. Thus, in order to treat the Cu bullion, a process was established whereby the PGMs could be collected in a high grade alloy. The proposed process involved electrorefining, pressure leaching of anode slimes and reduction and volatilisation of the lead contained in the anode slimes leach residue (Hanf et al., 1989). Unfortunately, the Cu bullion production process was stopped due to operational problems with the furnace and the off-gas treatment.

Some electrorefining experiments were performed and reported by Hanf et al. (1989). A number of tests with different operating parameters were performed to determine the optimal conditions. An additional test was done, combining all the optimal operating conditions and it was found that the PGMs can be separated very efficiently from copper and other base metals. Figure 2.4.a illustrates the deportment of PGMs after electrolysis of this copper bullion.

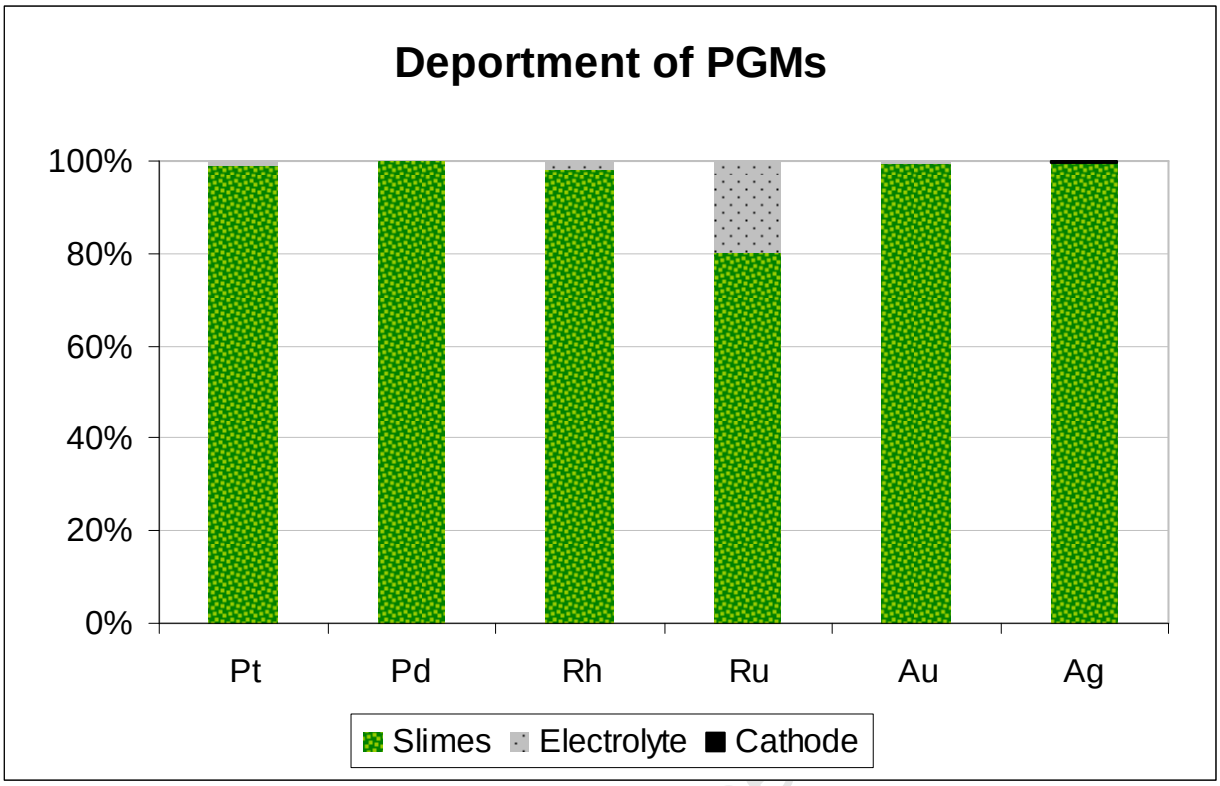

Figure 2.4.a: Deportment of PGMs (190 g/l H_2SO_4, 40 g/l Cu, 60ºC, 0.5 V) (Hanf, 1989)

It can be observed that almost all of the PGMs that were present in the anode reported to the anode slimes with the exception of some of the ruthenium and rhodium, which were dissolved in the electrolyte. The copper bullion that these tests were performed on consisted of 90% copper and had very little nickel and iron present. The optimal operating conditions obtained from this test work were as follows:

- H_2SO_4 : 190 g/l
- Cu^{2+} : 40 g/l
- Current density : 200 A/m^2
- Voltage : 0.5 V
- Temperature : 60ºC

The mass reduction obtained was 91.3% and the anode slimes still contained ±47% Cu.

Tests were performed at different operating parameters. The deportment results at each setting are given in Table 2.4.a:

Table 2.4.a: Results of electrorefining tests performed on BMR Cu bullion by Hanf et al. (1989)

H_2SO_4	Cu	Temperature	Current Density	Results
g/l	g/l	˚C	A/m^2	
80	60	35	≈200	7% Pt, 60% Rh and 70% Ru lost to electrolyte
180	60	65	≈200	7% Rh and 60% Ru lost to electrolyte
80	80	60	200	14% Rh and 40% Ru lost to electrolyte
190	40	60	200	1.7% Rh and 20% Ru lost to electrolyte

2.5 Process Design

Anodes can be cast either continuously with a Hazelett twin-belt type caster or a mould-on-wheel type (Biswas et al., 2002). Anodes are cast with thin tops where the anode is not submerged to minimise the amount of undissolved anode scrap to be remelted (see Figure 2.2.g). There are numerous casting methods available, Figure 2.5.a shows an example of an anode casting wheel. Molten copper is poured into a mould and the wheel is turned for the next mould. The mass of the copper being cast is sensed and controlled by load cells at each mould.

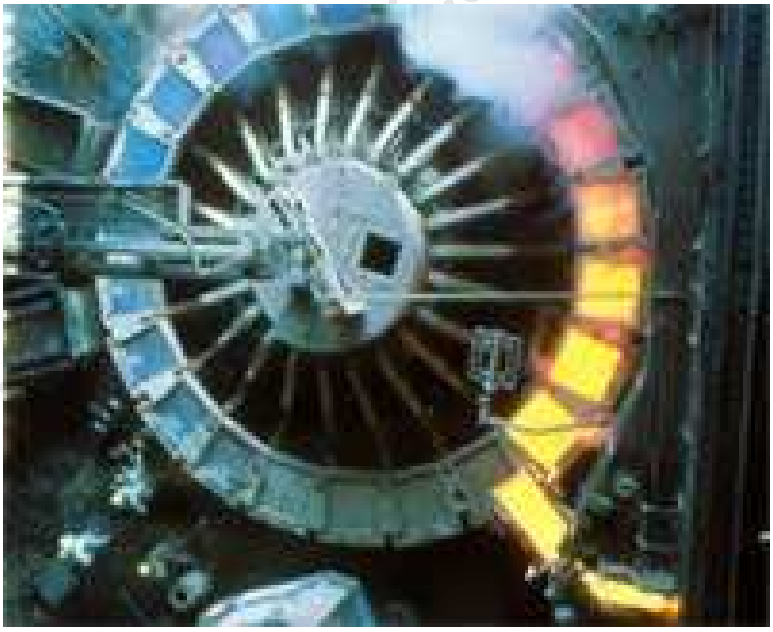

Figure 2.5.a: Copper anode casting wheel

(Schoolscience.co.uk, 17 July 2009, image at: http://resources.schoolscience.co.uk/CDA/14-16/cumining)

In order to ensure flat and vertical anodes, refineries generally treat their anodes in an automated anode preparation machine which performs the following tasks Biswas et al. (2002):

1) Weighs the anodes, and redirects under- or overweight anodes back to melting furnace.

2) Straightens the lugs, and machines a knife edge on each lug (on which the anode hangs)

3) Flattens anodes with pressure

4) Loads anodes into a spaced rack which will be dropped into an electrorefining cell.

Electrorefining is generally done with typical anode castings of 360 – 400 kg which have the dimensions of 1 m x 1 m and a thickness of 4 cm – 5 cm. These are stacked between cathode blanks at a distance of 5 cm. Cathode starter blanks can be either titanium or stainless steel at a thickness of 1 mm – 3 mm welded to copper support bars. One electrorefining cycle generally returns 15-20% of the anode as anode scrap to be thoroughly washed and remelted. It takes typically 21 days for an anode to dissolve before it has to be re-melted (Biswas et al.,2002).

The process is continuous, with purified electrolyte entering on one end of the cell and overflowing at the other end of the cell into an electrolyte collection system. Cathodes are allowed to plate for 7 to 10 days before they are removed from the cell, washed and stripped from the blanks (cathodes cannot be allowed to grow too thick or too close to the slime-covered anode surface). The mass of one Cu plate is generally 50–80 kg.

The vertical edges of the cathode blanks are covered with long tight-fitting polymer edge strips to prevent Cu from plating around the edges of the cathodes. This would make it very difficult to strip the cathodes. In practice, the sizes of the anodes are generally slightly longer than the cathodes sheets in the cell. This is to minimise heavy edge deposits at the bottom edge of the cathode (edge strips will eliminate growth on vertical edges) (Pletcher and Walsh, 1990).

Industrial cells are 3 m – 6 m long and 1.1 m – 1.3 m deep, leaving a space of 0.1 m – 0.2 m underneath the electrodes. Each cell contains 60 – 70 anode cathode pairs and is made of pre-cast polymer concrete or made with concrete and lined with a flexible polyvinyl chloride lining (older applications).

Cells are connected electrically in series to form sections of 20 – 40 cells. Cathodes of one cell are connected to the anodes of the next cell by placing them all on one bus bar. Each cell should be able to be isolated for removing anodes and cathodes as well as for cleaning and maintenance (Biswas et al., 2002).

Inco's copper refinery in Copper Cliff uses anodes of 272 kg that dissolve for 28 days and plates cathodes for 14 days. Each cell contains 38 anode-cathode pairs and runs at a current density of 177 A/m^2 (Moskalyk and Alfantazi cited Davenport, 2003)

In some applications the anode slimes are recovered from the cell by woven cloth or polymer bags with controlled porosity that surrounds the anodes and catches the slimes (Pletcher, 1990). In other cases, the cells are cleaned periodically in order to collect the slimes.

2.6 Further Processing of Anode Slimes

It has been concluded from the behaviour of various elements in copper that the anode slimes likely to result from the current Cu alloy will consist mainly of undissolved PGMs and Ni-bearing iron oxides, re-precipitated Pb and Sn, complex Cu-Ag-Pb-As-Se oxides and some precipitated Sb-As-Bi oxides. The typical composition of slimes produced from commercial copper anodes was given by Chen and Dutrizac (2004) and is shown in Table 2.6.a.

Table 2.6.a: Typical composition of commercial Cu anodes and the slimes produced Chen (2004)

	Anode (%)	Slimes (%)
Cu	99	16-24
Au	0.01	0.1-2
Ag	0.1	4-25
Se	0.07	4-15
Te	0.02	0.2-3.5
As	0.04	0.5-2
Sb	0.02	0.3-2
Bi	0.0075	0.1-0.8
Pb	0.1	4-22
Ni	0.55	0.4-26
O	0.14	-

The PGMs present in the anode will behave similarly to Au and report to the slimes. It can be seen that the base metals, Pb, Ag, Se and Te content in the anode slimes is significant, and in order to recover the PGMs from the slimes, further processing is required to remove these impurities. The first step in the typical flowsheet to recover the PGMs entails a decopperizing step. Many operations apply an air-H_2SO_4 atmospheric leach at 80˚C, but in order to reduce processing time and improve copper extraction, pressure leaching with O_2-H_2SO_4 at elevated pressures and temperatures has also been considered (Chen and Dutrizac, 2004). Decopperising the anode slimes specified in

Table 2.6.a produces a residue with Au concentrated as metallic Au, an Ag-Au-Se phase and as a solid solution in the Ag-Se phase. It was found (Beauchemin et al., 2007) that the Sb and Bi mostly dissolve in the decopperizing process but will re-precipitate partly as $BiAsO_4$, Sb-As-O and Sb-As-Bi-O.

After decopperising, the anode slimes, Ag can be leached from the residue with thiourea and Fe^{3+} as oxidant at 60˚C (Amer, 2003).

Au and possibly other PGMs can selectively be leached from impurities such as Pb, Ag, Sb, Zn, Cu and Sn with chlorination optimisation (Dönmez et al., 1999).

It was also proposed by Hanf et al. (1989) to subject the anode slimes produced from the BMR Cu bullion to pressure leaching with sulphuric acid and subsequent reduction and volatilisation of the lead contained in the anode slimes leach residue.

3 RESEARCH OBJECTIVES & APPROACH

3.1 Key Questions

Gathered from the given literature review, the major technical factors in successful electrorefining are the cathode purity, the production rate and the specific energy consumption. These factors are influenced primarily by anode quality, electrolyte conditions and cathode current density.

The electrolyte conditions, current density, temperature, additive addition, circulation rate and anode composition must be selected in such a way that anodic dissolution and the deposition of the metal occur with optimum efficiency while none of the impurity metals can transfer from the anode to the cathode. Good recovery of PGMs to the anode slimes must be achieved and the slimes must be in a form that can be easily processed to be purified and sent to PMR for final separation of PGMs. To do this efficiently, passivation of the anode must be avoided and the anode slimes must be able to settle to the bottom of the cell fast enough to prevent co-deposition of PGMs or other impurities in the cathode product.

This project will therefore investigate electrorefining as an option for recovering a PGM rich stream as well as achieving the separation and recovery of Ni in solution and Cu as saleable Cu cathodes. The anode slimes produced will be characterised by their composition and mineralogy in order to foresee further processing requirements. The proposed process must be safe, cost efficient as well as practical and sustainable.

3.2 Objectives

The objectives of this project are to:

1) Determine the typical total cell potential, cathodic current efficiency, anodic copper dissolution rate and deportment of elements (especially PGMs) during electrorefining of Cu from the alloy produced from the two-stage Ausmelt testwork on SLC.

2) Characterise the anode slimes formed to determine the behaviour of the PGMs and other impurities during electrorefining and also to recommend possible process steps necessary for the purification of the PGM concentrate.

3) Evaluate the effect of current density, copper and acid concentration on electrorefining products and subsequently propose optimal conditions.

4) Perform a preliminary process design, based on experimental results and knowledge gained from literature study.

3.3 Approach

Anglo Platinum has approached Mintek to conduct the casting of anodes and the electrorefining tests. The project was planned, supervised and managed by the MSc candidate at Mintek in conjunction with the Mintek metallurgist responsible for the project, Ndina Malaudzi throughout the duration of the testwork.

The following approach was followed throughout the duration of the testwork:

1) *Identification of key parameters and test matrix.*

   As can be observed from the literature review, Cu electrorefining is generally conducted at 160 g/l Sulphuric Acid, 40 g/l Cu, 100-300 A/m^2 and 65˚C. Therefore the test parameters were designed around these industrial operating conditions. One of the tests was designed to use fresh spent electrolyte from the Cu electrowinning section at BMR.

2) *Development of suitable test cell*

   The anode dimensions and test duration were selected in such a way that the amount of slimes produced from one test was sufficient (minimum 20 g) for mineralogical and chemical analysis thereof. A suitable cell for the selected anode dimensions was chosen. The heating of the circulated electrolyte was carried out in a heat exchanger using Proportional–Integral–Derivative (PID) control with a valve controlling the flow of hot water from a hot water bath into the heat exchanger.

3) *Collect sufficient electrolyte from BMR Cu spent solution and transport to Mintek*

4) *Determine required electrolyte feed flow rate, recirculation rate as well as operating period*

   In order to minimise the time required for performing one test, the anode dimensions were made as large as possible to obtain a large surface area and

subsequent increased rate of dissolution; however, the anode size was limited by the amount of raw material available.

The feedrate of fresh electrolyte required for a minimum change in Cu concentration was determined by taking into account the difference between the rate of Cu deposition and the rate of Cu dissolution. A circulation of electrolyte was required for temperature control as well as to provide better mass transport. The circulation rate was chosen to deliver 2.5 electrolyte volume replacements per hour.

5) *Outline and plan experimental methodology, sampling intervals, variables to be recorded.*

6) *Production of anodes and dealing with problems encountered during the casting thereof.*

The anodes were cast by the Advanced Materials Division (AMD) of Mintek. The casting technology of the Cu alloy material has been investigated and discussed by AMD due to difficulties encountered during the casting process. The report submitted by AMD is attached in Appendix II for reference.

7) *Schedule tests and manpower for continuous ±3 day test runs (continuous sampling and analysis)*

8) *Conducting of testwork in Mintek laboratories.*

9) *Analysis of solution samples by Mintek and solid samples by Anglo Platinum.*

4 EXPERIMENTAL

4.1 Parameters

Eleven experiments were performed with variety combinations of Cu concentration, H_2SO_4 concentration and current density combinations (see Table 4.1.a). In each experiment only one parameter was changed, while all others were kept constant at the base-case setting of 40 g/l Cu, 160 g/l H_2SO_4, and 125 A/m^2. The Cu and H_2SO_4 concentrations for the base-case were chosen based on the typical concentrations of electrorefining, determined during the literature review. The current density for the base-case setting was chosen to be much lower than what was mentioned in the literature for two reasons. Firstly, the Cu alloy that is used during this test work has a much lower Cu content (~80%) than typical anodes in the industry (~99%) and it is expected that the optimal current density for this material would be lower due to passivation effects resulting from the high impurity content. Secondly, a conservative current density might allow us to see the effects of Cu and H_2SO_4 concentrations more easily by not being dominated by the effect of high current density. An additional experiment, with BMR Cu electrowinning spent electrolyte was also performed to determine the viability of implementing electrorefining without adjusting the electrolyte within the current operation.

Table 4.1.a: Operating parameter combinations for different tests performed

Experiment	Current Density (A/m²)	Cu Concentration (g/l)	Acid Concentration (g/l)	Special Condition
1	Typical Cu Spent Condition			
	125	40	***110***	***Lowest Acid & 55˚C***
2	125	40	160	Base-case
3	125	40	160	***With Additives***
4	***100***	40	160	***Low CD***
5	***150***	40	160	***High CD***
6	125	***30***	160	***Low Cu***
7	125	***50***	160	***High Cu***
8	125	40	***130***	***Low Acid***
9	125	40	***190***	***High Acid***
10	***250***	40	160	***Higher CD***
11	***300***	40	160	***Highest CD***

During experiments 2 to 11, the temperature was kept constant at 65ºC. Test 2 and test 3 were carried out under similar conditions with the only difference being the addition of smoothing additives to test 3 in order to verify the improvement on the

surface morphology of the copper deposit. It was found that the surface morphology improves significantly with the use of additives and it was decided to continue its addition for the remainder of the tests.

The concentration of additives added was calculated based on a 10 times reduction of typical additive addition in the industry (investigated in the literature review). It was decided to reduce the amount of additive in this way due to the small scale of the test. The amount of chloride ions, guar gum and thiourea added was calculated to be ± 3.5, 4 and 1 respectively in mg per kg of cathode produced. This related to additive concentrations in the electrolyte of:

- Chloride: 18 mg/l
- Guar Gum: 6 mg/l
- Thiourea: 3 mg/l

The electrolyte feed and circulating flow rates for each test were 1.5 l/h and 20 l/h respectively and the anode-cathode spacing was maintained at 3 cm.

The feedrate of fresh electrolyte required for minimum change in Cu concentration was determined by taking into account the difference between the rate of Cu deposition and the rate of Cu dissolution. A circulation of electrolyte was required for temperature control as well as to provide better mass transport. The circulation rate was chosen to deliver 2.5 electrolyte volume replacements per hour. The anode-cathode spacing was chosen to mimic typical electrorefining design.

4.2 Equipment

The experimental set up of the equipment used is illustrated in Figure 4.2.a.

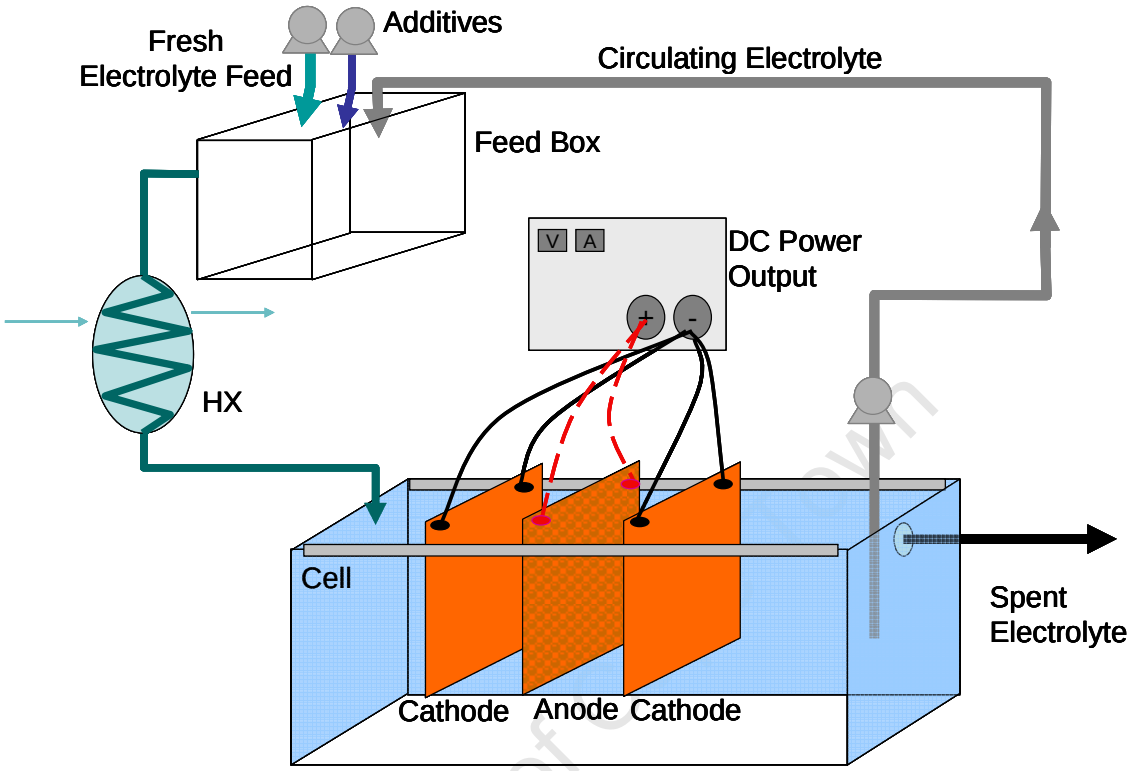

Figure 4.2.a: Expirimental set up

An undivided poly propylene cell (Figure 4.2.b) with a working solution volume of ± 8 l was used for each test. One impure Cu anode (see Figure 4.2.c) was placed into the cell between two stainless steel cathode blanks with a spacing of 30 mm between the surfaces of the electrodes. The effective anode and cathode areas were controlled using electroplating tape to cover the anode area that should not be electrolytically active (the active anode height was kept at 195mm, everything above that was covered). Each cathode had only one effective plating surface facing the anode (See Figure 4.2.d).

The feed solution, recirculating flow and the smoothing additives were mixed in the feed box prior to feeding into the cell. The electrolyte temperature was controlled by circulating the cell electrolyte through a heat exchanger. The electrolyte was heated by the flow of hot water from a hot water bath through an inlet valve to the heat exchanger which uses PID control. The heat exchanger used is shown in Figure 4.2.e.

Figure 4.2.b: Polypropolene cell connected to thermocouple, heat exchanger, feed, spent and recyle lines

Figure 4.2.c: Impure Cu anode before test

Figure 4.2.d: Cu deposit on stainless steel cathode with one effective plating surface of 20 cm x 14 cm

Figure 4.2.e: Heat exchanger connected to hot water bath with PID controller

The experiments were conducted by feeding a constant current through a rectifier. Each electrode (anode and both cathode) were connected to the rectifier with two wires on each side of the electrode for better current distribution. The cell potential was monitored throughout the test with a multimeter by taking measurements on the hanger bars of a cathode and the anode for each cathode.

The cell feed electrolyte was made up in a 170 l feed drum to the required concentrations and was mixed continuously to prevent any crystallisation or inhomogeneous feed to the cell

The spent electrolyte was taken at the opposite end of the cell feed by overflowing into a line at a specific overflow heigth, collecting the spent electrolyte into a single drum by gravity. The spent electrolyte flow rate would be the same as the flow of the combined feed to the cell.

Other equipment that was used during the experiment was:

1) Balance to measure starting and finishing masses of anodes and cathodes
2) Buchner filters and filter paper for filtering anode slimes collected from the cell after each electrorefining test
3) Drying oven for drying slimes samples
4) Hot plates and magnetic stirrers to make up organics
5) Wash water bottles
6) Titration setup for the monitoring of Cu and H_2SO_4 concentrations
7) Drill for drilling parts out of the anode and cathode after electrolysis to send for analysis

The electrode dimensions and flow rate settings that were decided on are shown in Table 4.2.a. These dimensions would produce enough anode slimes over a period of 2 – 3 days. The fresh feed flow rate would ensure that Cu and H_2SO_4 concentrations did not change significantly throughout the test and the recirculation rate would improve mass transport while administering temperature control.

Table 4.2.a: Experimental electrode dimensions and flow rate settings

Anode Dimensions (h x w x t)	19.5 x 14 x 2	cm
Cathode Dimensions (h x w)	20 x 14	cm
Anode Cathode Spacing	3	cm
Fresh Feed Flow rate	1.5	l/h
Circulating Rate	20	l/h
Cell Volume	± 8	l

4.3 Procedures

4.3.1 Anode Casting

The anode material was cast into silica sand moulds. Figure 4.3.a is a picture of the cross section of the original material. Figure 4.3.b shows the bottom half of the closed top mould that was used for most of the anodes. A number of different variations of this mould were used in an attempt to produce anodes with as little as possible shrinkage and gas captured so that it can have a smooth surface. A number of the moulds that were produce did not satisfy the desire for a smooth surface and were recycled to the original material to be remelted. These anodes are referred to as *failed anodes*. The casting procedure and technology for producing anodes, as well as the challenges that were encountered were discussed by AMD in a report provided to Anglo Platinum. This report is attached as Appendix II. The furnace that was used for the melting of the material is shown in Figure 4.3.c where the molten material is being transferred from the furnace to the casting ladle. The casting ladle was then used to poor the molten metal into the mould in a controlled fashion. This is shown in Figure 4.3.d.

Figure 4.3.a: Original material (two-stage Ausmelt TSL alloy product)

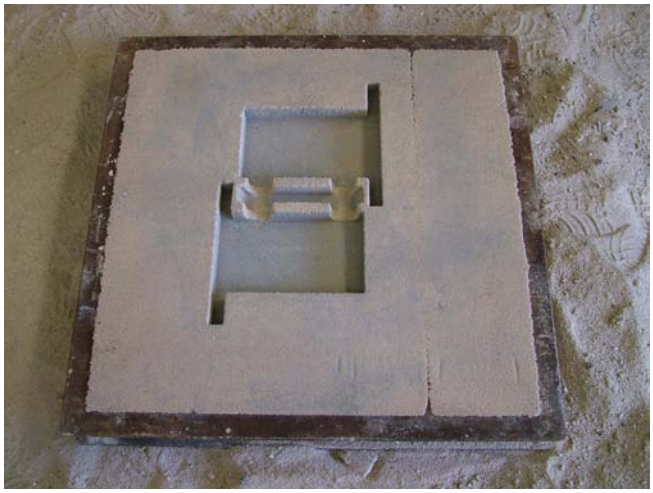

Figure 4.3.b: Bottom half of silica sand mould for anodes

Figure 4.3.c: Molten metal transferred from furnace to casting ladle

Figure 4.3.d: Molten metal cast into closed top silica sand mould

Due to a limited amount of raw material, the failed anodes and remaining anode scrap from previous tests were re-melted to cast more anodes. This could have lead to a slight change in anode composition due to silica contamination from the moulds or other forms of contamination. Between test 7 and test 8 a significant change occurred in the composition of the anode material, possibly due to contamination of the molten material. Hence, the initial anodes for tests 8 to 11 were inconsistent with the rest of the anodes and cannot be compared to the rest of the tests.

4.3.2 Electrorefining Testwork

All the input and output solid products and solution volumes were weighed and recorded as accurately as possible for mass-balancing purposes.

The procedures that were followed during the conducting of a test are described in detail.

Feed Solution Preparation

150 *l* of feed solution was measured into a calibrated drum and the Cu and H_2SO_4 concentrations were adjusted to the required test settings by diluting or spiking with $CuSO_4.5H_2O$ and 98% H_2SO_4 respectively. Chloride ions were added by adding a specific amount of NaCl that would result in 18 mg/l Cl^- ions.

The guar and thiourea was made up in solutions with concentration of 300 mg/l and 150 mg/l respectively. These solution mixtures would be added to the cell at a controlled rate of 0.5 ml/min throughout the test which would result in the additive concentration in the electrolyte of 6 mg/l and 3 mg/l.

Cathode and Anode Preparation:

The cathode surface was prepared by buffing with 180 grit sandpaper and then taping off to the required cathode area with electroplating tape. The cathode was then dipped in a 1:1 (v/v) nitric acid-water solution for 30 minutes and allowed to drip dry prior to inserting it into the cell. The anode surface was washed under running water to ensure that the surface was clean.

Filling Up the Cell

After ensuring that the cell was clean and free from any solids or solutions, the cathodes and anode were inserted in the cell and positioned to be exactly 3 cm apart. The cell was then filled with fresh electrolyte until there was an overflow of solution into the spent electrolyte line. Guar and Thiourea was added to the cell fill electrolyte to obtain concentrations of 6 mg/l and 3 mg/l respectively. The recirculation pump was then switched on to allow the heat exchanger to fill up before topping the cell up again. The recirculation pump was subsequently calibrated, as well as the feed pump and organic pump. The recirculation pump was then started to warm up the solution to the required temperature before the test could start. A sample was taken of the electrolyte when the test was started.

The negative terminal of the power source was then connected to both cathodes at two places on each cathode and the positive terminal of the power source was connected to the anode at two places.

Once all of the above procedures were completed, the test was started.

During the Test:

At the start of the test, the fresh feed and organic pumps were started and the power source was switched on by setting the current according to the required current density and surface area.

Throughout the test, the following readings were monitored:

- Solution temperature
- Current
- Voltage readings between the anode and both cathodes
- Feed flow rate
- Cu and H_2SO_4 concentration (by titration).

Samples were also taken throughout the test of the spent electrolyte in order to monitor the concentration profiles of different elements.

After the Test:

After the test the electrolyte in the cell was drained and filtered to separate the anode slimes from the electrolyte. The anodes and cathodes were taken out of the cell, scraped clean and rinsed with filtered electrolyte to recover slimes attached to them. The slimes were washed twice with 800 ml of 100 g/l H_2SO_4, before being weighed and placed in a drying oven overnight at 60˚C. The cathodes were stripped from the stainless steel blanks and weighed before being drilled for sampling. A sample of all the spent electrolyte collected was taken after agitating it for a period of time to ensure homogenous composition. Examples of an anode after being dissolved and anode slimes are shown in Figure 4.3.e and Figure 4.3.f, respectively.

Figure 4.3.e: Anode surface after dissolution in test 1

Figure 4.3.f: Anode slimes on filter paper produced from test 5

4.4 Sample Analysis

4.4.1 Electrolyte Samples

The copper and acid concentrations were monitored by titration. The acid was titrated with 0.51 M sodium bicarbonate using a mixed indicator. The copper was titrated using potassium iodide and sodium thiosulphate using starch as the indicator. The rest of the chemical analyses were carried out by the Mintek Analytical Services Division (ASD) using ICP-OES and ICP-MS.

4.4.2 Cathode Samples

The cathode analysis was also conducted by ASD. The anode and copper deposits were drilled at the top, middle and bottom along the width of each anode and copper deposit. 15 g of the solid sample were dissolved in 70 g of nitric acid (65%). The dissolved metal was then diluted with deionised water in a 250 ml flask before sending the samples for analysis. The only element analysed using solid samples was sulphur for both the anode and cathode samples.

4.4.3 Anode Slimes and Anode Samples

The anode slimes and anodes were analysed at Anglo Research Laboratories using mass spectrometry for PGM analysis. The elements that were analysed for were as follows:

1. Pt	2. Pb
3. Pd	4. As
5. Rh	6. Al
7. Ru	8. S
9. Ir	10. Cr
11. Os	12. Mg
13. Au	14. Si
15. Ag	16. Te
17. Cu	18. Sb
19. Ni	20. Bi
21. Fe	22. Sn
23. Co	24. Se
25. Ca	26. Zn

The mineralogical analyses were performed with the Scanning Electron Microscope with Energy Dispersive X-ray analysis (SEM-EDX) technique. The analysis is standardless and normalised. The detection limit for elements is 0.5 mass percent within a phase. It was set to detect oxide or element/alloy. The SEM-EDX analysis cannot determine OH / H_2O compositions.

5 RESULTS AND DISCUSSION

5.1 Background

The testwork showed that electrolytic refining of the Cu alloy, produced by a two stage pyrometallurgical treatment of current SLC, produces a highly concentrated PGM residue at an overall SLC mass reduction of 99.3%, with excellent PGM recovery to the anode slimes material. The different operating parameters that were tested successfully all showed very good repeatability and greater than 99% PGM recovery. An unfortunate contamination of the original material occurred before high current densities and different H_2SO_4 concentrations could be tested; however, the data collected proved to be useful and sufficient for the objectives of this project. The typical operating conditions that were observed correlated well with literature and the theoretically calculated values. The characteristics of anode slimes stayed relatively similar throughout the different operating parameters and strong confidence can be placed in the production thereof and the recovery of the PGMs. The characteristics of the spent electrolyte and the Cu cathodes were also found to be suitable for integration in the BMR circuit. The results obtained during this testwork are discussed in detail in this section.

5.2 Change in Anode Composition

Due to difficulties encountered during the casting of the anodes (see Appendix II), a significant contamination of the original material occurred after the 7th test. Due to a limited amount of raw material, there was no fresh material without the contamination to continue the remainder of the tests. Although the rest of the tests were performed with the altered material, it was found that the change in behaviour during the tests was significant and the results of tests 8 to 11 could not be compared to the rest of the earlier tests. Although the actual chemical composition of the anode material only changed slightly with the amount of silicon captured in the material, the phases that occurred in the anode changed from a Cu, Ni metal matrix to an alloy of the Cu, Ni, Fe and Si as a silicide in the anode. The clear differences between the original material and altered material can be seen in Figure 5.2.a and Figure 5.2.b.

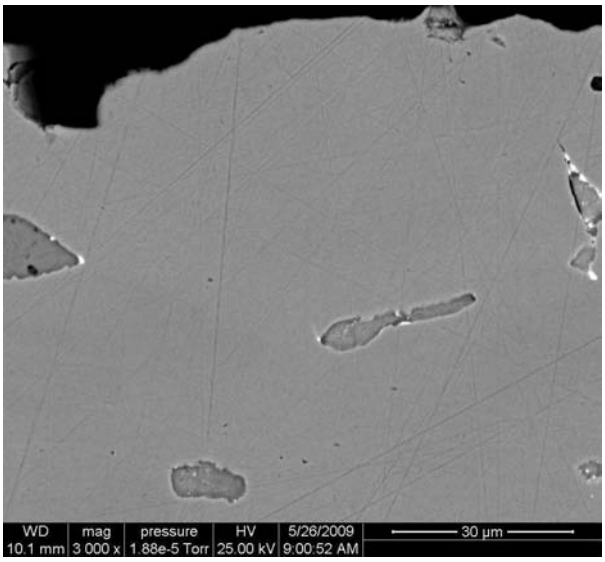

Figure 5.2.a: MLA backscattered electron image of anode cast from original material

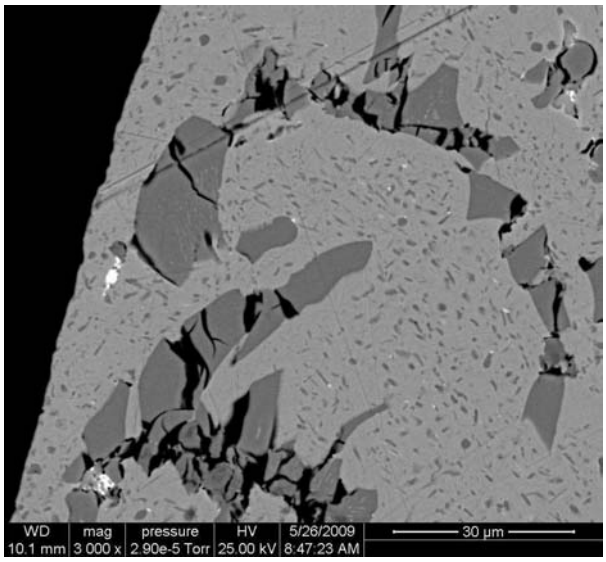

Figure 5.2.b: MLA backscattered electron image of anode cast from altered material

In Figure 5.2.a, it can be seen that the metal matrix is clean and simple. It consists mainly of three phases:

1) Light grey – the metal matrix containing mainly Cu, Ni and Fe in metal form.

2) Dark grey – a CuS alloy containing mainly Cu, S and also Te.

3) Bright white – An alloy containing mostly Pb, Bi, Ag, and also some Pd.

In Figure 5.2.b of the altered material, the above phases still existed but it was found that the light grey Cu-Ni-Fe phase contained much less Ni and Fe and was more concentrated in Cu. The Ni and Fe were present in a fourth phase (the darker grey needles embedded in the metal matrix). This phase also contained Si which points to an alloy of a Ni, Fe silicide which also contains Cu to a certain extent.

This change in the mineralogical composition of the material led to dramatic influences on the behaviour of the anodes during dissolution. Some of the major changes in behaviour were the following:

1) The colour of the anode changed significantly from a brassy silver colour to a reddish copper colour.

2) Significant passivation of anodes occurred within a short period of time. This was indicated by the step change in cell potential that can be observed in Figure 5.2.c. The rest of the tests that were performed with the altered material showed similar trends and can be seen in Appendix I, Section D.

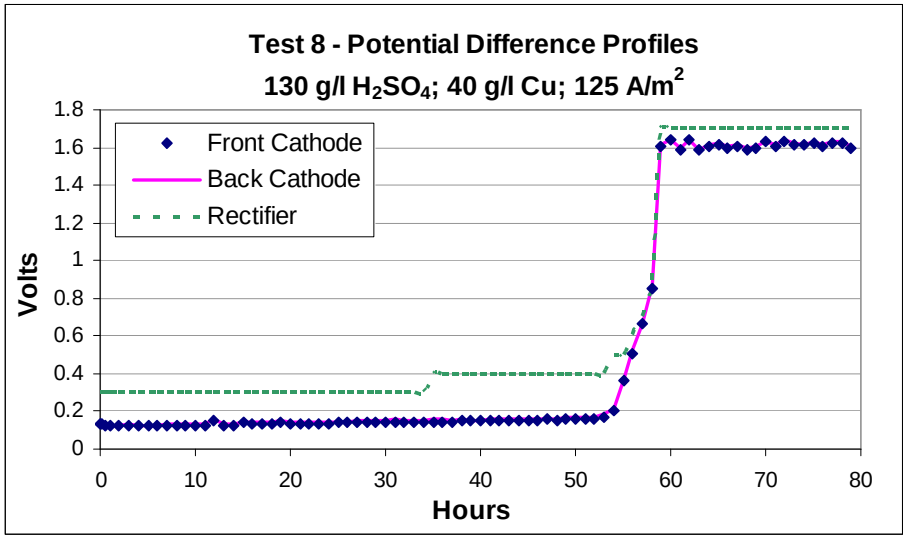

Figure 5.2.c: Cell potential during test 8 with significant step change when anode passivation takes place.

3) The amount of suspended solids in the electrolyte increased and could be observed in the heat exchanger. The slimes adhered to the heat exchanger during and after the test. This is an indication that the physical properties of the anode slimes had changed.

4) The electrolyte was foaming at the anode-electrolyte surface. This was an indication of oxygen evolution which was possibly caused by the high cell potential and the absence of Cu dissolution. Oxygen evolution was confirmed by the increase in acid concentration with time at the high current density.

5) The chemical composition and characterisation of the anode slimes changed drastically. Due to the fact that the Cu, Ni, Fe metal matrix phase was transformed to a Ni,Fe Silicide alloy in the altered material, the Cu, Ni and Fe no longer dissolved during electrorefining and also reported directly to the anode slimes which resulted in very impure anode slimes.

This comparison with the original material with the contaminated material gives background to the results that are observed throughout the tests. The behaviour of the results during the last four tests which are observed to be very different from the earlier tests can be attributed to anode contamination and not to the operating parameters. Therefore, for the investigation of operating conditions, element deportment and anode slimes characterisation, these tests will not be discussed in detail, as the investigation thereof will be of no value for the development of a Cu alloy treatment route.

5.3 Typical Operating Conditions

5.3.1 Cell Potential

In order to investigate the cell potential during the electrorefining of the Cu alloy provided, the anode-cathode potential difference was monitored on an hourly basis throughout each test. The potential profile of each test is given in Appendix I, Section D. It can be noted that the potential difference profiles between the anode and cathodes are very similar for each test (with the exception of the last four tests where the original material was altered). The potential profile for the base-case scenario (160 g/l H_2SO_4, 40 g/l Cu, 125 A/m^2 with no additives) is given in Figure 5.3.a. It can be seen that the cell potential starts at ± 0.13 V and then slowly increases as time progresses. After 86 hours of operation, this potential difference has increased to ± 0.15 V. Therefore, if it is estimated or assumed that the cell potential increase is linear over the period of the test, the linear increase in cell voltage will be ± 0.23 mV/h. The rectifier voltage was only measured in units of 0.1 V, which explains the sudden jump from 0.2 to 0.3 V. In reality, the rectifier voltage was rounded up or down, and would show a much smoother, flatter curve if it were measured at 0.01 V units. The discrepancy between the rectifier voltage and the cell voltage is possibly due to resistance of the equipment or connections that were used.

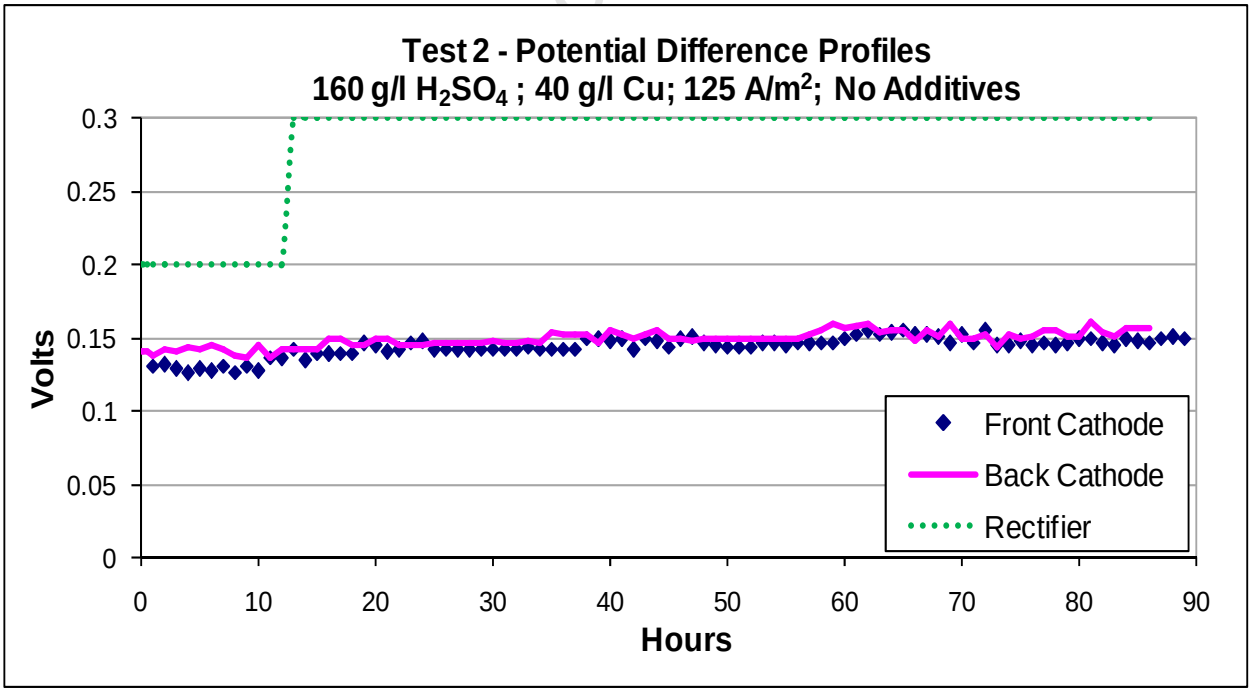

Figure 5.3.a: Potential difference profiles between anode and cathodes and rectifier voltage

The reason for the increase in cell potential could be a function of the following factors:

1) The resistance to current flow will increase with an increase in suspended solids due to anode dissolution. In this case, it could be anticipated that the amount of solids in suspension in the electrolyte could reach equilibrium when the amount of solids released from the anode into electrolyte is equal to the amount of solids settling at the bottom of the cell per unit of time. When this equilibrium occurs, the cell potential due to suspended solids would stay constant. However, given the low solids density, the effect of suspended solids is unlikely to be a measurable effect.

2) Decrease of chemically active surface area resulting in anode passivation. Cell potential will increase if there is an increase in anode passivation. Slight anode passivation could occur as a larger fraction of the anode is being dissolved. Some of the particles around the easily dissolved species that do not dissolve will drop from the anodes, but some will stay attached to the anode surface, thereby forming a slimes layer on the anode and reducing the chemically active surface area available for dissolution. Decreased dissolution results in lower current through the cell and increased cell potential.

3) Increase in anode or cathode polarization over time as a function of metal concentration in the vicinity. As the metal ion dissolves from the anode, the metal concentration will increase in the vicinity of the anode surface area. If the metal concentration becomes too high it might precipitate slightly as $CuSO_4$ and prevent further dissolution of the anode and resistance to current flow will increase. Similarly, if the metal concentration in the vicinity of the cathode surface is too low due to lack of mass transport or excessive current density, there will be less ions available for depositing on the cathode and resistance will be increased.

If it is assumed that the cell potential increases linearly at a rate of 0.23 mV/h over the entire time of electrorefining and that the typical dissolution time is 21 days (as stated in the literature review, Section 2.5), the total increase in cell potential will be ± 0.177 V, resulting in a terminal voltage of 0.25 V. The total power consumption for dissolving 147.29 g/m^2.h (as it is in the base-case) is calculated with the following equation:

$$P = \frac{VIt}{m} \text{ kWh/kg} \qquad \textbf{(15)}$$

where V : Average cell voltage (V)

I : Applied current (A)

t : Time of dissolution or plating (s)

m : Mass of anode dissolved or Cu plated (g)

P : Power consumption (kWh/kg)

(In this case current and mass were used per 1 m^2 area which cancels out in the equation).

$$\text{Thus, } P = \frac{\left(\frac{0.25+0.13}{2}\right)V \times 125A/m^2 \times 21days \times 24hrs}{147.29g/m^2.hr \times 24hrs \times 21days} \quad \textbf{(16)}$$

$$= 0.16kWh/kg$$

The same equation was used to determine the power consumption per kg of anode dissolved and kg of Cu cathode produced for each test and the results are shown in Table 5.3.a. The last four tests show a significant increase in power consumption (in grey italic) due to the passivation that occurred during the test as a result of the different composition of the anode relative to the original material (the passivation can be observed in the potential difference profiles given in Appendix I, Section D).

Table 5.3.a: Power consumption for each test i.t.o kWh/kg Cu produced and anode dissolved

Test	Special Condition	kWh/kg Cu Produced	kWh/kg Anode Dissolved
Test 1	110 g/l H_2SO_4	0.225	0.217
Test 2	Base-case*	0.125	0.118
Test 3	With Additives	0.121	0.115
Test 4	100 A/m^2	0.111	0.104
Test 5	150 A/m^2	0.140	0.131
Test 6	30 g/l Cu	0.126	0.121
Test 7	50 g/l Cu	0.128	0.123
Test 8	*130 g/l H_2SO_4*	*0.475*	*0.460*
Test 9	*190 g/l H_2SO_4*	*0.850*	*0.961*
Test 10	*250 A/m^2*	*1.135*	*1.506*
Test 11	*300 A/m^2*	*1.344*	*2.220*

*160 g/l H_2SO_4, 40 g/l Cu, 125 A/m^2

5.3.2 Current Efficiency

Current efficiency is a measure of how efficiently the current is being used to perform only the desired tasks. With regards to cathode current efficiency, it will be the fraction of the current that is utilised to plate Cu and with regards to anode current efficiency, it will be the fraction of the current that is used to dissolve the targeted metal (Cu) from the anode. In typical industrial electrorefineries, the impure anodes are composed of ±99% Cu; however, the anode material used in the present experiments is composed of a large amount of Ni and Fe as well. Thus, the current will not only be used to dissolve Cu but also Ni and Fe and these have to be taken into account when calculating the anode current efficiencies. If it is assumed that the impure anodes contain on average 12% Ni and 4% Fe and the remainder of the dissolvable metal is Cu, the equations for calculating anode and cathode current densities are as follows:

Anode: $$\xi_a = \left(\frac{(m_{loss} - m_s).n.F}{(0.12.M_{Ni} + 0.04.M_{Fe} + (1-0.16).M_{Cu}).I.t} \right) x100 \quad \textbf{(17)}$$

Cathode: $$\xi_c = \left(\frac{m_{Cu}.n.F}{I.M_{cu}.t} \right) x100 \quad \textbf{(18)}$$

Where ξ : the current efficiency for the anode (a) or cathode (c), (%)

m_{Cu} : mass of copper plated on cathode, (g)

$M_{Cu/Ni/Fe}$: molecular mass of Cu or Ni or Fe, (g/mol)

n : number of electrons transferred/mole Cu plated or anode dissolved

F : Faraday constant, (96 487 C/mol)

I : applied current, (A)

t : duration of deposition or dissolution, (s)

m_{loss} : mass of anode lost during period of dissolution, (g)

m_s : mass of slimes produced during period of dissolution, (g)

These calculations assume that each metal dissolves in proportion to its composition in the alloy, which would be most likely if the metals were all in their metallic form in the alloy. The mineralogy and composition of the anodes are discussed in more detail in section 5.4. The current efficiencies achieved are shown in Table 5.3.b. An interesting observation is the high anode current efficiencies (>100%) in cases where the H_2SO_4 concentration was higher than 110 g/l. This is an indication that current is

not the only contributor to the dissolution of anodes. It is well known that direct acid leaching of base metals is possible in strong acidic solutions. Thus, it is possible that some copper dissolution took place purely due to leaching. This suspicion gains further confidence during the characterisation of the anode slimes in Section 5.4.1. It was considered that an inaccuracy of the mass of slimes produced due to loss of solids to filter paper and attachment to the anode or cathode after electrorefining could have played a roll in the calculation of the current efficiency. The sensitivity of the calculation to the slimes mass was tested and it was found to be considerably insensitive. Thus, there is a high confidence in the calculation of the anode current efficiency.

Table 5.3.b: Anode and cathode current efficiencies under various conditions

Test	Special Condition	Anode ξ (%)	Cathode ξ (%)
Test 1	110 g/l H_2SO_4	94.1	98.8
Test 2	Base-case*	102.4	98.6
Test 3	With Additives	100.8	97.5
Test 4	100 A/m^2	101.5	96.7
Test 5	150 A/m^2	103.4	98.4
Test 6	30 g/l Cu	99.9	98.4
Test 7	50 g/l Cu	99.8	98.5
Test 8	*130 g/l H_2SO_4*	*86.8*	*96.5*
Test 9	*190 g/l H_2SO_4*	*69.2*	*97.4*
Test 10	*250 A/m^2*	*60.0*	*97.4*
Test 11	*300 A/m^2*	*50.7*	*96.7*

*160 g/l H_2SO_4, 40 g/l Cu, 125 A/m^2

It can be observed that current efficiencies of >***98%*** for the deposition of Cu can be easily obtained. In cases where the original material was different (Tests 8 – 11), the cathode current efficiencies were lower. This is most likely due to the fact that the reactions that were taking place were more of an electrowinning nature than electrorefining. This can be assumed due to the high cell potential after a certain period of time, the oxygen evolution that took place (see Section 5.1) and the low anode current efficiencies.

5.3.3 Anodic Cu Dissolution

Figure 5.3.b shows the actual dissolution rate compared to the theoretical dissolution rate of the Cu, Ni, Fe alloy (84%, 12%, 4%, respectively) at the different operating conditions. During the initial tests, the dissolution rate followed the theoretical dissolution closely, but is slightly higher. This is due to the possible leaching of

anode material due to high acid concentrations. In the last four tests the actual dissolution was significantly less than the theoretical as discussed earlier. The dissolution at 30 g/l and 50 g/l was also slightly lower than the theoretical prediction; it could be due to slight contamination of anodes that already took place during the production these anodes (when investigating the content of these anodes, slight increases in Si content was observed, Appendix I, Section E). Figure 5.3.b and Table 5.3.c shows that the main contributor to anode dissolution is current density, and the electrolyte concentrations play only a minor role.

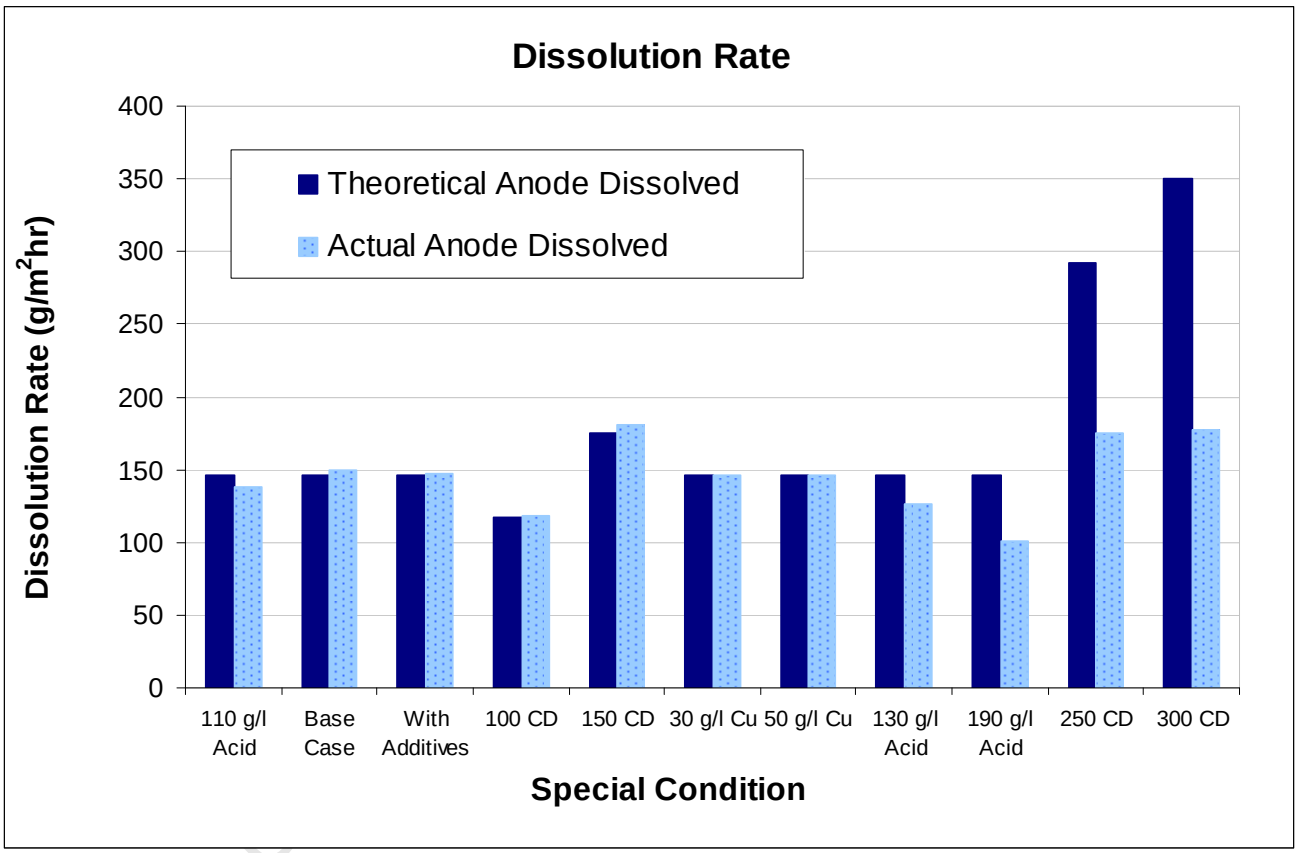

Figure 5.3.b: Theoretical and actual anode dissolution rate under various operating conditions

Table 5.3.c: Actual and theoretical dissolution rate under different conditions

Test	Special Condition	Anode Dissolution (%/m^2.h)	Actual Dissolution (g/m^2.h)	Theoretical Dissolution (g/m^2.h)
Test 1	110 g/l H_2SO_4	1.8	137.6	146.1
Test 2	Base-case*	3.0	149.5	146.1
Test 3	With Additives	2.6	147.3	146.1
Test 4	100 A/m^2	2.1	118.7	116.9
Test 5	150 A/m^2	3.2	181.3	175.3
Test 6	30 g/l Cu	2.6	145.9	146.1
Test 7	50 g/l Cu	2.5	145.8	146.1
Test 8	*130 g/l H_2SO_4*	*3.1*	*126.8*	*146.1*
Test 9	*190 g/l H_2SO_4*	*4.7*	*101.0*	*146.1*
Test 10	*250 A/m^2*	*2.8*	*175.4*	*292.2*
Test 11	*300 A/m^2*	*3.5*	*177.7*	*350.7*

*160 g/l H_2SO_4, 40 g/l Cu, 125 A/m^2

If operating at a current density of 150 A/m^2 with a typical industrial anode design (360 kg, 1 m x 1 m, and 20% scrap rate) the dissolution cycle period for an anode will be 34 days. This period can be reduced by increasing current density to increase dissolution while not sacrificing efficiency, but this could not be confirmed in the current test work.

With application to the BMR, the Cu anode production will be ±1320 t/a. Thus, 428 anode/cathode pairs will be required for the treatment of all the Cu alloy produced per year with a cycle time of 34 days at 150 A/m^2.

5.3.4 Element Deportment

Overall Mass Balance

In order to perform a mass balance the input and output streams were identified as the following:

In:

1) Mass of element removed from the surface of the anode = grade in initial anode x (mass of initial anode – mass of final anode)

2) Mass of element in electrolyte feed = concentration in electrolyte feed x total volume fed during the test (flow rate x time)

Out:

1) Mass of element in slimes = grade in slimes x mass of slimes

2) Mass of element in cathode = (grade in front cathode x mass of front cathode) + (grade in back cathode x mass of back cathode)

3) Mass of element in spent electrolyte = concentration in spent electrolyte x total volume out (recorded)

It should be noted that concentrations of a specific element that were reported to be below detection limit were assumed to be 0 g/l for mass-balance purposes. This is not necessarily accurate but the effects are assumed to be negligible. The input and output streams' grades, concentrations and mass or volume flows for each test are given in Appendix I, Section E.

The accountability for each element was determined by dividing the sum of the output streams by the sum of the input streams. Accountability was generally good with a few exceptions, such as a large over-accountability for Os and Si and under-accountability for Ag. It should be noted that large volumes of electrolyte were used during the test in order to maintain stable Cu and H_2SO_4 concentrations, thus a significant change in element concentration will not be observed. The exact changes in concentrations can thus not be detected with confidence, due to the variability of solution analysis.

The overall deportment of each element to a different product stream was performed by dividing the amount of element in the product stream by the amount of element in the total input (anode + electrolyte feed). Due to the large volume of electrolyte that was used, the amount of an element fed via the electrolyte could, in some cases, be larger than the amount supplied by the anode. This would play a large role in the deportment of the specific element because not all of the element present in the electrolyte will precipitate to the slimes or deposit at the cathode but will remain in the electrolyte due to the minimal changes in element concentrations in the electrolyte throughout the tests.

The concentration profiles of various elements in the electrolyte during electrorefining were monitored by sampling and analyses at specified intervals. It was proven that minimal changes in concentrations occurred during the test work for all the tests due to the constant fresh feed flow rate. With the added effect of analysis variance and bias, the concentration change throughout the test should be almost negligible. An

example of this is given in Figure 5.3.c where the concentration profiles of a number of elements during the base-case test (test 2) are shown.

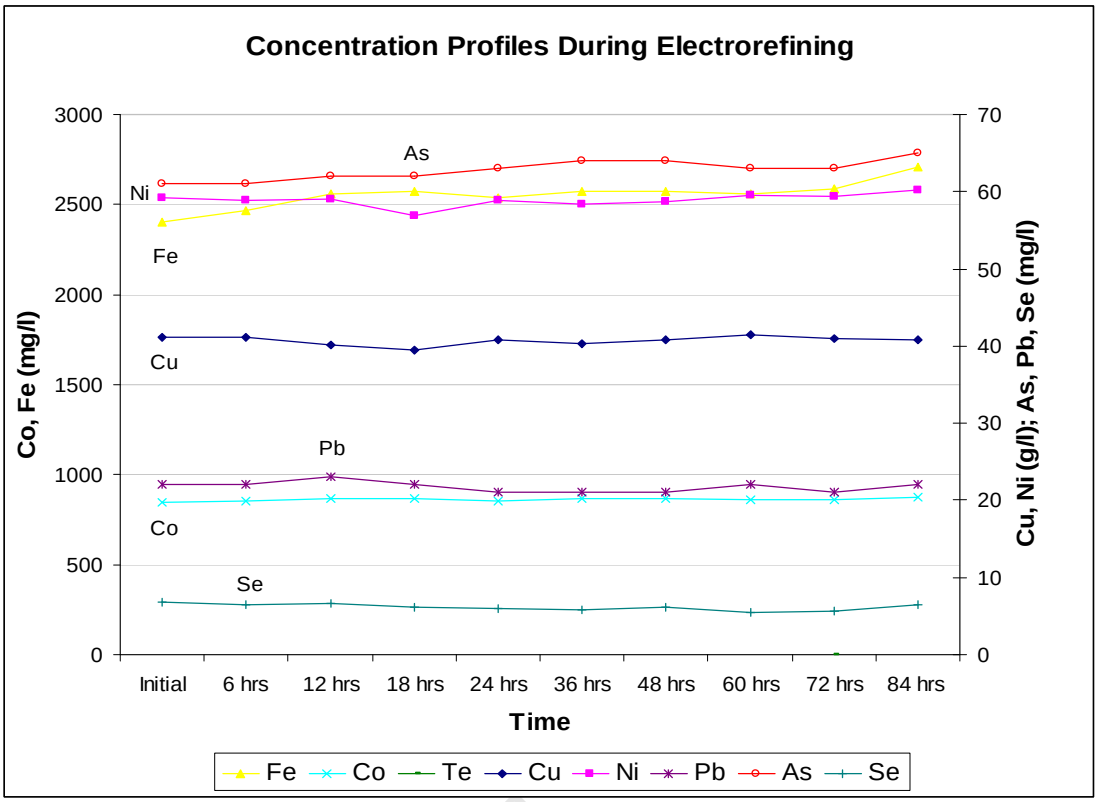

Figure 5.3.c: Concentration profiles of different elements during test 2 (base-case)

In order to calculate comparable deportment of elements regardless of the accountability, the deportment of the element was normalised to 100% by dividing it by the accountability for the specific element.

Tables of the calculated accountability and deportments from the total input (anode +electrolyte) are given in Appendix I, Section E. These tables have shown that the deportment of all the PGMs from the anode *and* electrolyte is not only to the anode slimes. Rh, Ru and Ir especially show some deportment to the electrolyte. This could be due to the fact that some of the PGMs that were originally in solution do not precipitate with the slimes but stay in the electrolyte. However, as mentioned earlier, confidence in the electrolyte analysis is relatively low and no definite conclusions can be drawn from this. In order to get a clearer comparison between the behaviour of different elements at the different operating parameters that were tested with the original material, the deportment of the elements are illustrated in the following column charts:

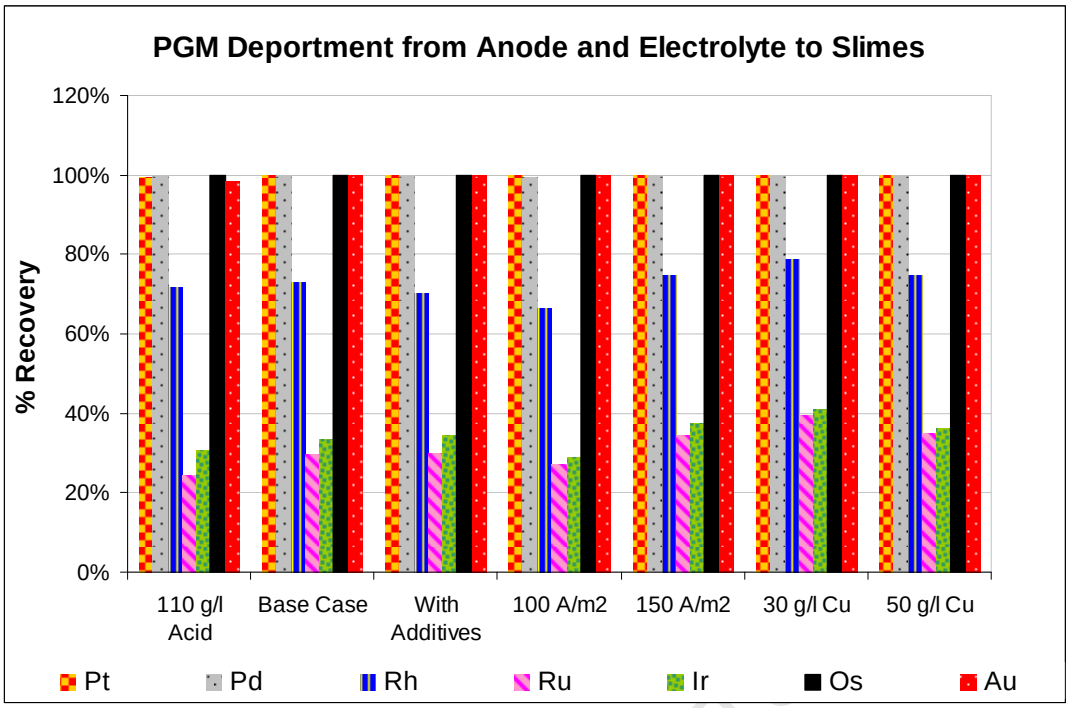

Figure 5.3.d: PGM deportment to anode slimes from anode and electrolyte

Figure 5.3.d shows the overall deportment of PGMs to the anode slimes throughout the different operating parameters that were tested successfully. Due to the detectable concentrations of Rh, Ru and Ir in the electrolyte feed and the spent electrolyte, the deportments of these PGMs are not 100% to the anode slimes as they are for Pt, Pd, Os and Au which were below detection limit (assumed to be 0). However, it can be noted from the electrolyte analysis given in Appendix I, Section E that the concentrations of the Rh, Ru and Ir do not change significantly (2.6 to 2.9 mg/l, 15 to 17 mg/l and 0.3 to 0.4 mg/l respectively), indicating that the dissolution of the anode does not result in an increase in concentration in the electrolyte. If the expected 99% recovery from SLC to Cu alloy is achieved and a PGM recovery from Cu alloy to anode slimes of 99% is obtained, the overall PGM from SLC will be 98%.

As expected, Figure 5.3.e shows that very little or none of the base metals that were supplied by the anode and the electrolyte feed deported to the anode slimes. With a Cu deportment of less than 0.1%, this means that more than 99.9% of the Cu has reported to the electrolyte or deposited on the cathode. In the same way, ~0% of Ni and 0.05 to 0.3% of Fe reported to the slimes. Figure 5.3.c shows that the concentration of Cu was maintained at ± 40 g/l throughout the test, which means that a large fraction of the overall deportment of Cu will be to the electrolyte due to the large volume of spent electrolyte compared to the mass of copper deposited on the cathode.

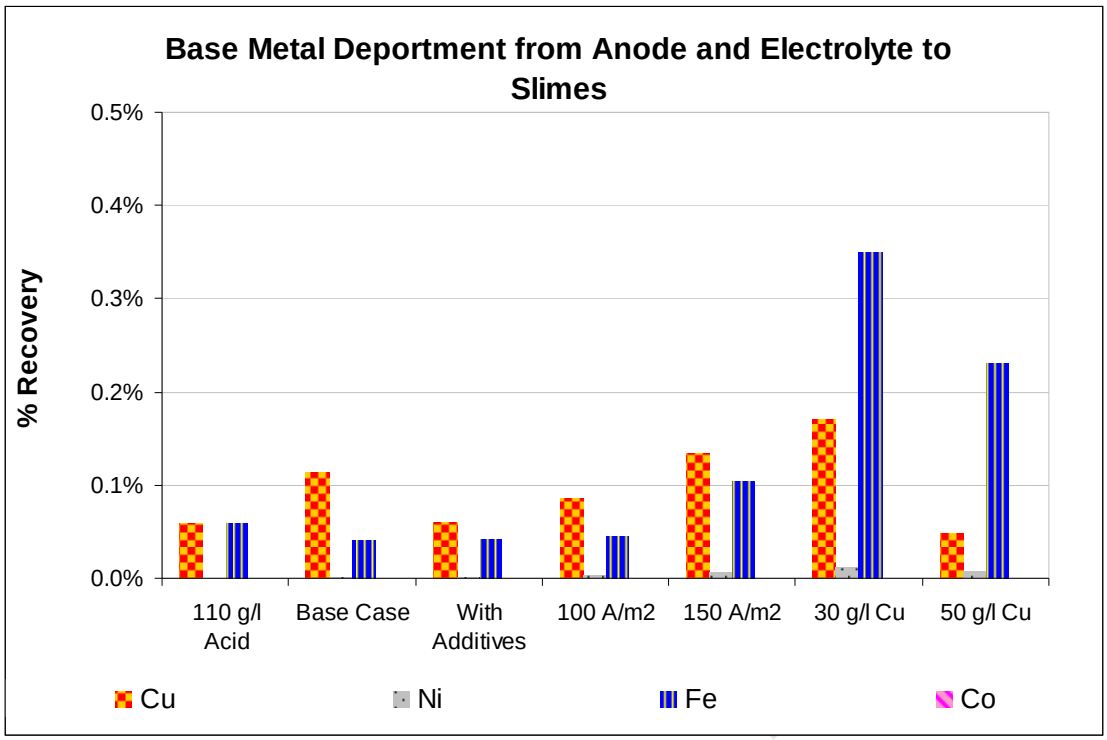

Figure 5.3.e: Base Metals deportment to anode slimes from anode and electrolyte

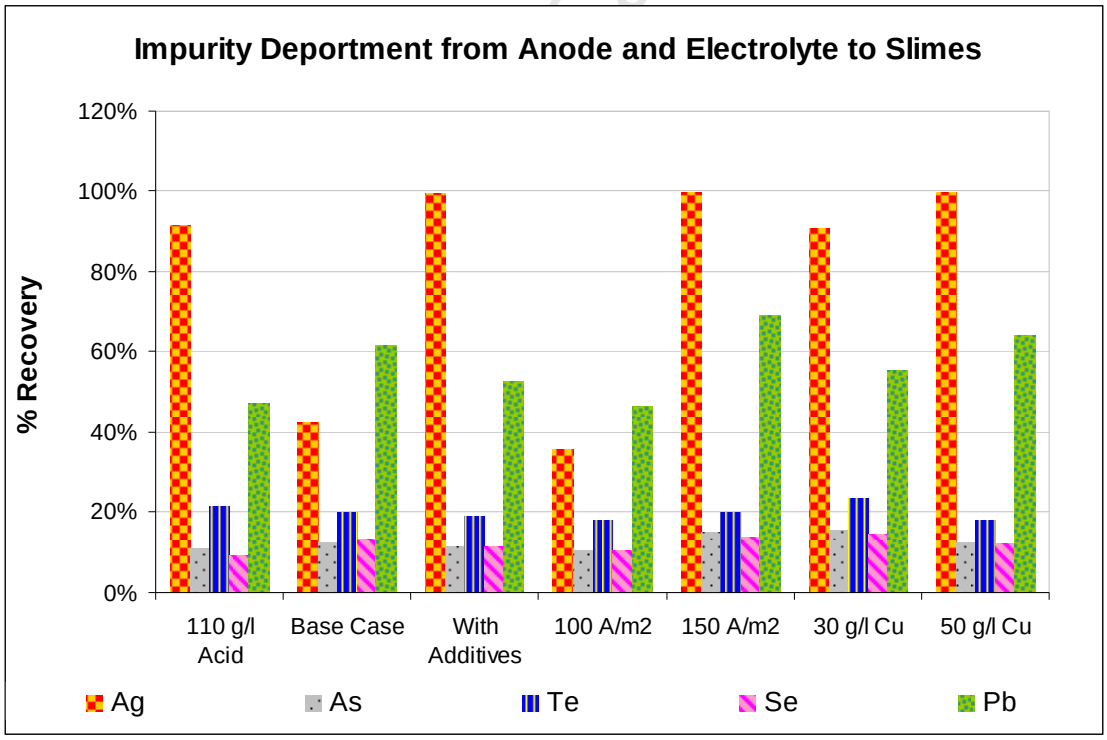

Figure 5.3.f: Impurity deportment to anode slimes from anode and electrolyte

When investigating the main anticipated impurities as shown in Figure 5.3.f, Se and Te deportment from the electrolyte and the anode to the slimes is between 10 – 20%. It should be noted that the amount of these elements entering and exiting via the

electrolyte is significant relative to the amount provided by the anode. Thus, even though the overall deportment of it to the slimes may be low, the recovery of it from the anode only to the anode slimes might still be high. In the case of Pb, it is seen that its recovery is between 50 and 70%. This is expected as it was found in the literature review that Pb will precipitate as a $PbSO_4$. Arsenic showed a low recovery from the total feed but this could also be simply due to significant amounts of this present in electrolyte streams. Ag showed high recovery to the anode slimes as was expected from the literature review in Section 2.3.1. However, the accountability of Ag was as low as 15% at times and this is most likely due to inaccuracy of electrolyte analysis.

In Figure 5.3.g the same investigation was done for some of the minor impurities such as Zn, which showed almost no deportment to the anode slimes. It was found that Sn behaves similarly to Zn in these circumstances and that some of the Sb and Bi (10 – 30%) reports to the slimes. The deportment of Si to the anode slimes is also generally below 10%.

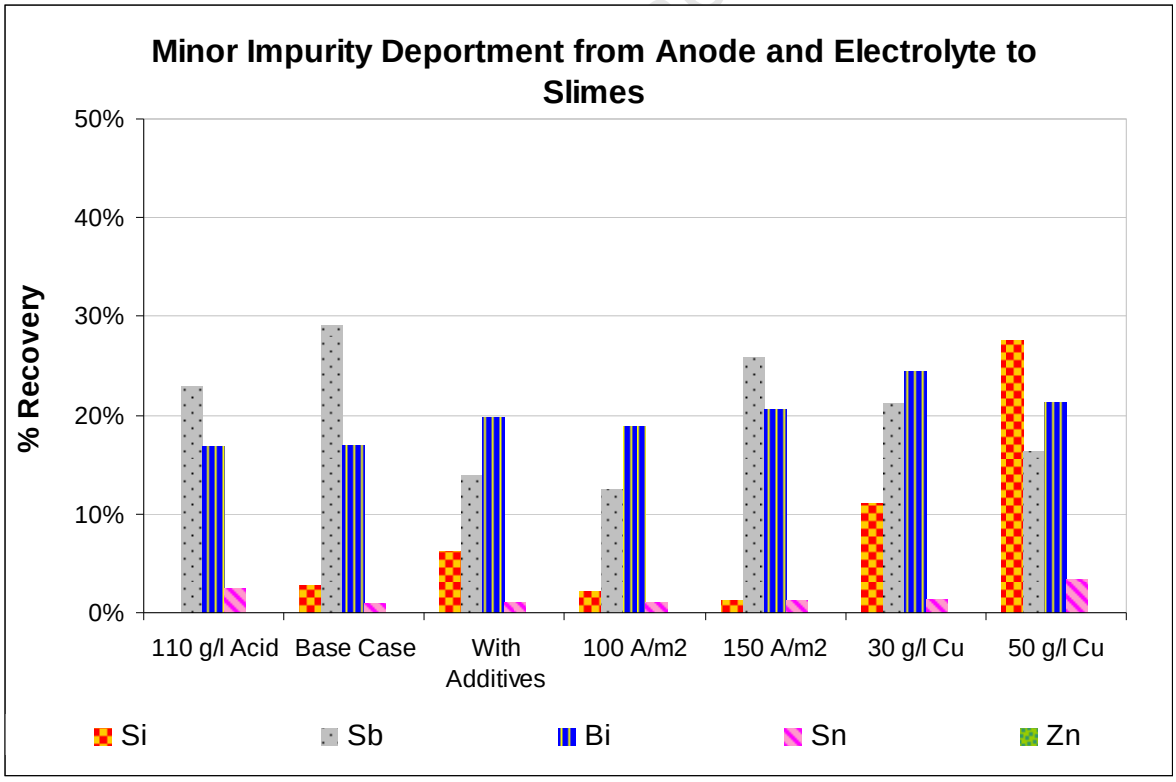

Figure 5.3.g: Minor impurity deportment to anode slimes from anode and electrolyte

Recovery from Anodes

Unfortunately, the overall deportment of elements from the electrolyte and the anode to the slimes does not reveal much of what happens to the elements that are released only from the anode during electrorefining. This is due to the large volume of electrolyte that was used, resulting in electrolyte concentrations staying relatively constant throughout these tests. Therefore, it is needed to perform a new mass balance, defining new input and output streams that will depict the deportment of elements provided by the anodes only. The new input and output streams for this mass balance are defined as follows:

In:

1) Mass of element removed from the surface of the anode = grade in initial anode x (mass of initial anode – mass of final anode)

Out:

1) Mass of element in slimes = grade in slimes x mass of slimes

2) Mass of element in cathode = (grade in front cathode x mass of front cathode) + (grade in back cathode x mass of back cathode)

3) Mass of element in spent electrolyte – Mass of element in electrolyte feed = (concentration in spent electrolyte x total volume out (recorded)) – (concentration in electrolyte feed x total volume fed during the test (flow rate x time))

The recovery of each element to a certain product stream is once again calculated by dividing the mass in the specific output stream by the mass in the input stream and the accountability. The recoveries of the elements from the anode to the different products are shown in Table 5.3.d to Table 5.3.j.

Table 5.3.d: Recovery of elements from Anode to different product streams for Test 1 (110 g/l H_2SO_4)

Element	% Accountability	% Recovery from Anode		
		To Slimes	To Electrolyte	To Cathode
Pt	105.7	99.6	0.0	0.4
Pd	95.0	99.9	0.0	0.1
Rh	114.7	100.4	-0.6	0.2
Ru	89.0	105.3	-5.3	0.0
Ir	105.9	103.7	-3.7	0.0
Os	130.9	100.0	0.0	0.0
Au	92.8	98.3	0.0	1.7
Ag	13.4	101.6	-1.6	0.0
Cu	140.0	0.5	8.1	91.4
Ni	167.3	0.0	100.0	0.0
Fe	68.5	1.0	98.7	0.4
Co	673.8	0.0	100.0	0.0
Pb	63.0	84.5	15.0	0.5
As	85.1	101.5	-1.8	0.3
S	16552.6	0.9	99.1	0.0
Si	730.2	0.0	98.6	1.4
Te	42.0	609.7	-512.6	2.9
Sb	70.5	79.7	20.3	0.0
Bi	90.9	25.4	74.6	0.0
Sn	107.5	2.5	97.5	0.0
Se	29.9	956.4	-1074.4	17.9
Zn	611.1	0.2	97.0	2.8

Table 5.3.e: Recovery of elements from Anode to different product streams for Test 2 (Base-case)

Element	% Accountability	% Recovery from Anode		
		To Slimes	To Electrolyte	To Cathode
Pt	84.0	100.0	0.0	0.0
Pd	86.8	99.9	0.0	0.1
Rh	89.4	102.9	-3.5	0.6
Ru	106.4	89.6	9.4	1.0
Ir	82.7	103.2	-3.2	0.0
Os	90.9	100.0	0.0	0.0
Au	84.1	100.0	0.0	0.0
Ag	18.5	42.5	57.4	0.1
Cu	100.3	1.1	-19.7	118.6
Ni	461.3	0.0	100.0	0.0
Fe	127.5	0.3	99.5	0.2
Co	686.2	0.0	100.0	0.0
Pb	44.7	140.2	-40.2	0.0
As	94.0	100.9	-1.3	0.3
S	48359.6	0.3	99.7	0.0
Si	172.2	17.4	-125.7	8.3
Te	16.0	1520.9	-1541.5	120.5
Sb	76.5	85.6	13.9	0.5
Bi	96.5	25.1	74.6	0.3
Sn	113.3	1.0	99.0	0.0
Se	137.2	277.7	-380.3	2.6
Zn	1571.8	0.1	99.9	0.0

Table 5.3.f: Recovery of elements from Anode to different product streams for Test 3 (Base-case With Additives)

Element	% Accountability	% Recovery from Anode		
		To Slimes	To Electrolyte	To Cathode
Pt	102.6	99.8	0.2	0.0
Pd	92.5	99.7	0.2	0.0
Rh	106.3	101.4	-1.5	0.1
Ru	133.6	85.6	14.3	0.1
Ir	135.2	88.1	11.9	0.0
Os	149.5	100.0	0.0	0.0
Au	88.4	100.0	0.0	0.0
Ag	18.1	99.6	0.0	0.4
Cu	191.5	0.3	39.7	60.0
Ni	587.7	0.0	100.0	0.0
Fe	224.7	0.3	99.6	0.1
Co	1028.3	0.1	99.8	0.0
Pb	74.4	79.2	20.8	0.0
As	74.8	93.7	6.3	0.0
S	60032.1	0.3	99.7	0.0
Si	28.6	59.3	-160.9	1.6
Te	21.4	811.5	-716.4	4.9
Sb	87.3	34.9	65.0	0.1
Bi	101.2	24.8	75.1	0.0
Sn	101.9	1.2	98.8	0.1
Se	51.3	535.5	-447.9	12.5
Zn	834.6	0.0	98.2	1.8

Table 5.3.g: Recovery of elements from Anode to different product streams for Test 4 (100 A/m^2)

Element	% Accountability	% Recovery from Anode		
		To Slimes	To Electrolyte	To Cathode
Pt	92.1	99.7	0.3	0.0
Pd	90.9	99.6	0.3	0.0
Rh	79.2	126.3	-26.5	0.2
Ru	100.2	109.7	-9.7	0.1
Ir	113.1	92.9	7.1	0.0
Os	139.3	100.0	0.0	0.0
Au	81.3	100.0	0.0	0.0
Ag	46.0	35.7	64.2	0.1
Cu	76.8	1.3	-48.6	147.3
Ni	409.9	-0.1	100.1	0.0
Fe	114.3	0.7	99.3	0.0
Co	580.2	0.3	99.7	0.0
Pb	78.7	74.5	25.5	0.0
As	43.5	168.5	-68.5	0.1
S	191167.1	0.1	-100.1	0.0
Si	180.2	5.0	94.4	0.5
Te	117.7	174.5	-275.3	0.8
Sb	62.6	49.2	50.7	0.1
Bi	87.2	30.1	69.9	0.0
Sn	88.2	1.3	98.7	0.0
Se	144.3	224.0	-328.0	4.0
Zn	274.2	0.2	-104.3	4.0

Table 5.3.h: Recovery of elements from Anode to different product streams for Test 5 (150 A/m^2)

Element	% Accountability	% Recovery from Anode		
		To Slimes	To Electrolyte	To Cathode
Pt	93.2	100.0	0.0	0.0
Pd	91.7	99.9	0.0	0.1
Rh	99.3	101.2	-1.6	0.5
Ru	109.1	93.8	5.1	1.0
Ir	109.6	95.4	4.6	0.0
Os	140.5	100.0	0.0	0.0
Au	85.8	100.0	0.0	0.0
Ag	20.1	99.7	0.0	0.3
Cu	148.9	0.7	23.3	76.0
Ni	37.4	1.1	98.7	0.2
Fe	122.0	1.0	99.0	0.0
Co	233.3	0.5	99.3	0.2
Pb	42.7	125.5	-25.5	0.1
As	81.1	106.5	-6.5	0.0
S	3796.6	4.0	96.0	0.0
Si	212.7	11.9	84.6	3.5
Te	34.9	524.8	-477.2	52.4
Sb	79.8	65.3	34.6	0.1
Bi	89.4	29.1	70.9	0.0
Sn	110.4	1.2	98.8	0.0
Se	37.6	796.1	-925.2	29.0
Zn	20.9	2.1	47.8	50.1

Table 5.3.i: Recovery of elements from Anode to different product streams for Test 6 (30 g/l Cu)

Element	% Accountability	% Recovery from Anode		
		To Slimes	To Electrolyte	To Cathode
Pt	101.3	100.0	0.0	0.0
Pd	90.2	100.1	-0.1	0.0
Rh	101.7	101.6	-2.4	0.7
Ru	115.8	95.4	3.6	1.0
Ir	124.7	84.9	15.1	0.0
Os	132.7	100.0	0.0	0.0
Au	86.0	100.0	0.0	0.0
Ag	45.8	93.3	6.4	0.2
Cu	131.9	1.0	9.3	89.7
Ni	306.8	0.2	99.7	0.0
Fe	124.7	2.5	97.5	0.0
Co	304.1	1.1	98.8	0.1
Pb	68.8	85.0	14.9	0.1
As	169.9	45.2	54.8	0.0
S	91878.0	0.1	99.9	0.0
Si	90.7	40.7	57.7	1.6
Te	13.4	1259.6	-1311.6	152.0
Sb	84.2	50.1	49.6	0.2
Bi	80.8	33.7	66.3	0.0
Sn	104.5	1.4	98.5	0.1
Se	180.9	161.2	-268.5	7.3
Zn	351.8	0.3	78.2	21.5

Table 5.3.j: Recovery of elements from Anode to different product streams for Test 7 (50 g/l Cu)

Element	% Accountability	% Recovery from Anode		
		To Slimes	To Electrolyte	To Cathode
Pt	97.4	100.0	0.0	0.0
Pd	93.6	100.0	0.0	0.0
Rh	108.5	100.0	-0.1	0.1
Ru	115.8	93.6	6.4	0.1
Ir	109.5	94.0	6.0	0.0
Os	146.6	100.0	0.0	0.0
Au	87.5	100.0	0.0	0.0
Ag	45.6	99.8	0.0	0.2
Cu	202.0	0.2	41.9	57.8
Ni	28.4	1.8	98.2	0.0
Fe	123.3	1.9	97.8	0.4
Co	333.9	0.7	99.3	0.0
Pb	50.4	124.8	-31.3	6.4
As	74.0	94.0	6.0	0.0
S	30559.1	0.7	99.3	0.0
Si	78.4	99.0	-2.5	3.5
Te	20.8	765.7	-668.5	2.8
Sb	77.1	43.2	56.7	0.0
Bi	80.6	31.1	68.9	0.0
Sn	218.0	3.4	96.3	0.3
Se	157.5	171.7	-281.1	9.4
Zn	316.1	0.3	-102.9	2.7

It can be seen from these tables that some of the recoveries to electrolyte results seem confusing. At times it shows a very large recovery to the anode slimes and a negative recovery to the electrolyte. The reasons for this are, firstly, that the analysis variability of the electrolyte might be very large compared to the amount of element provided by the anode, (due the large volumes of electrolyte that were used), and secondly, the concentration in the spent electrolyte might be lower than the concentration in the electrolyte feed resulting in a negative recovery to electrolyte (this is observed in the cases of Pb, Te and Se). These concentration differences could be due to the precipitation of these elements or the variability of the analysis.

Most importantly, it can be seen from these tables that the ratio of PGM mass in the slimes to the mass removed from the anode is almost always close to 100%. This is desirable because it indicates that minimal PGM loss occurred during the transformation of the anode to the anode slimes. In cases where there was over-accountability for the element, the recovery of the PGM to the anode slimes were lower (i.e. Ru and Ir), which is most likely a result of the variability of electrolyte analyses.

It can be seen that ~99-100% of the Ni and Fe reports to the electrolyte as is expected. The Cu that is removed from the anode is all plated at the cathode. The actual mass of Cu plated is higher than the mass of Cu removed from the anode and this is due to Cu from the feed electrolyte also plating at the cathode. This explains why the recovery of Cu from the anode to the electrolyte is very low, and from the anode to the cathode is high and sometimes > 100%.

In order to get an indication of the mass of different elements in the slimes relative to the mass of the same element removed from the anode throughout the change in operating parameters, the recoveries of some elements from the anode to the anode slimes are illustrated in Figure 5.3.h to Figure 5.3.k.

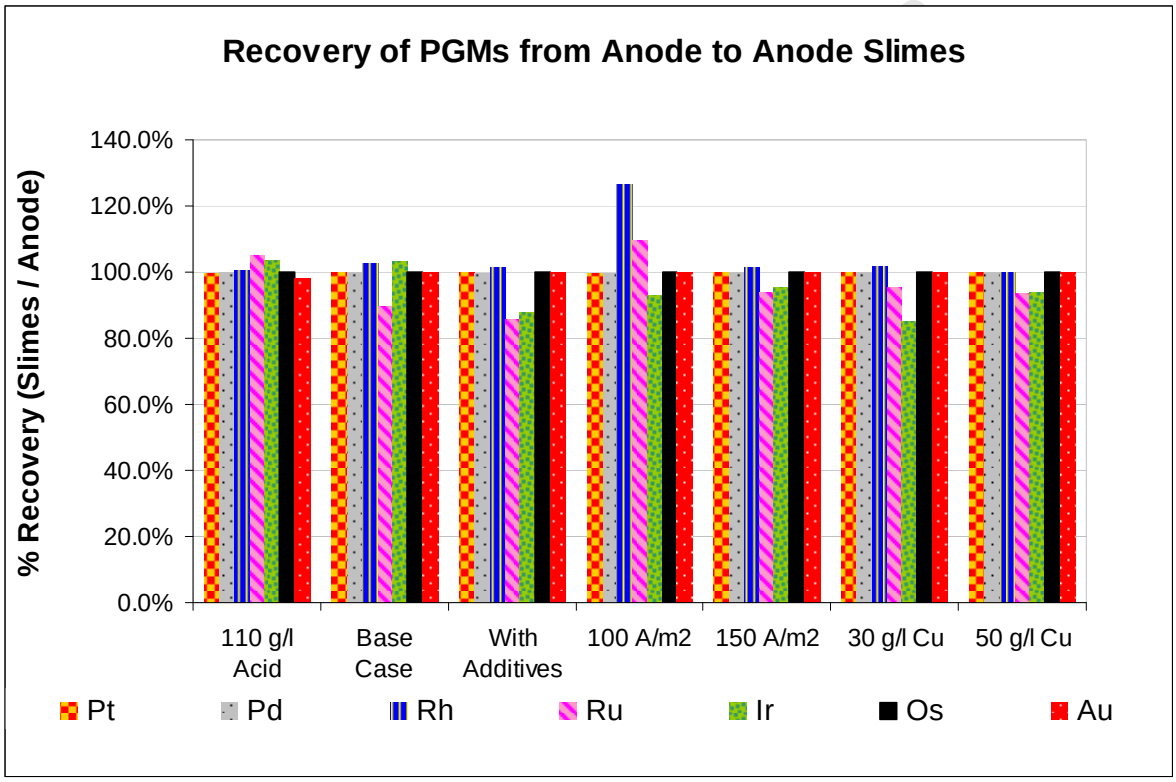

Figure 5.3.h: Recovery of PGMs from anode material to anode slimes

Figure 5.3.h shows that the recovery of PGMs stayed close to 100% throughout the change in operating conditions. The recovery of Ru and Ir was the lowest in some cases however, after investigating the actual analyses and masses in Appendix I, Section E; it was suspected that this could be due to over-accountability for these metals in the electrolyte analyses. (The recovery is calculated by dividing the mass of the element in anode slimes by the mass of it supplied by the anode and then dividing by the accountability)

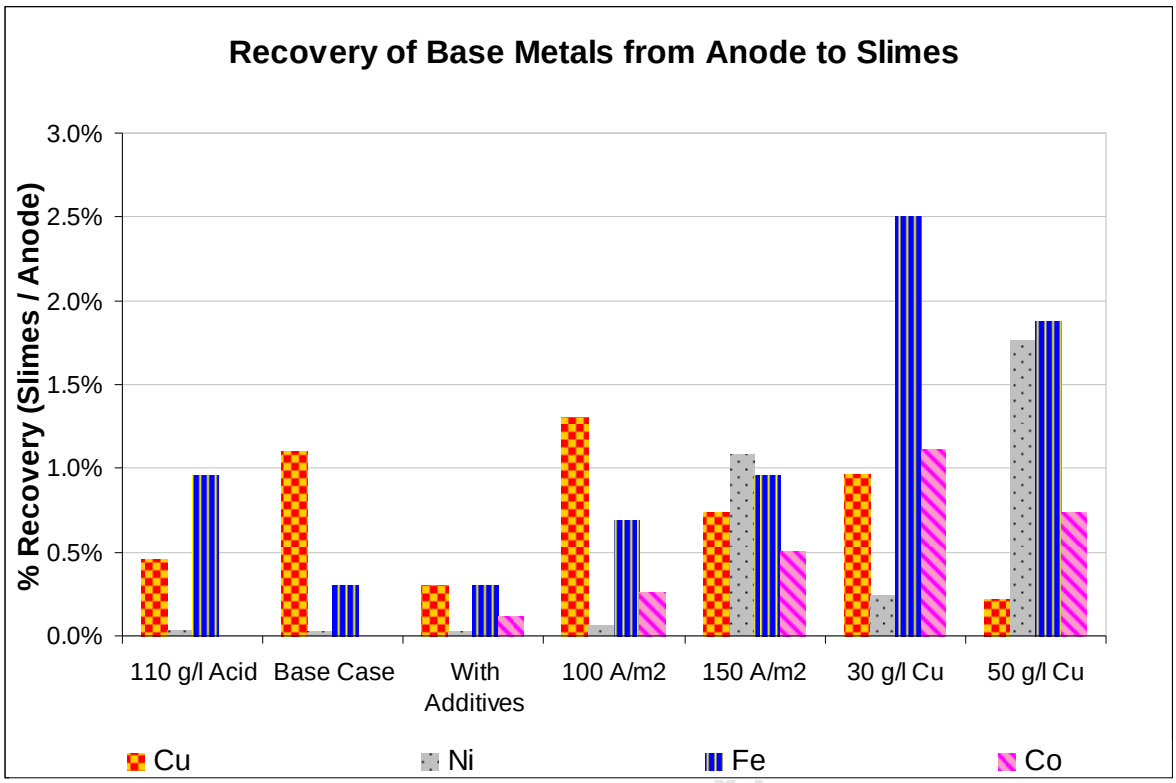

Figure 5.3.i: Recovery of base metals from anode to anode slimes

Figure 5.3.i shows the base metal recovery from the anode to the anode slimes. This figure confirms that the majority of the base metals are dissolved from the anode and reports to either the electrolyte or the cathode. In most cases, less than 1.5% of the all base metals supplied by the anode stays in the solid form and reports to the anode slimes which are desirable effects. This is a very good indication that electrorefining is an excellent method for concentrating PGMs.

The recovery of Pb, As and Ag to the anode slimes were all close to 100% indicating that these elements either does not dissolve, or re-precipitates after dissolution and report to the anode slimes.

A very interesting phenomenon is found when investigating the mass of Se and Te in the slimes compared to the mass provided by the anode as shown in Figure 5.3.j. It was found that there were two to twelve times higher Se and Te in the slimes than was supplied by the anode. This indicates that some of the Se and Te provided by the electrolyte feed have precipitated to the slimes. The reason that there is still a low overall deportment of these elements is the fact that the mass in the electrolyte was high compared to the mass in the anode and that the majority of it still remained in solution in the spent electrolyte. It should be noted that the accountability for

these elements were variable and often very low (especially where the very high recoveries are observed) and is thus very subject to solution analysis.

The recovery of Pb is in a high range of 70 – 100%. The reason that this fraction is not higher than 1 (like the Se and Te) might be because of the very small amount of Pb in the electrolyte feed. The recovery of Arsenic showed that only 10 – 30% of the As was dissolved from the anode and reported to the electrolyte. Ag also showed high recovery to the anode slimes, as was expected from the literature review, as the amount of Ag in the slimes was generally ±90% of that supplied by the anode. Due to the low concentrations of these elements and the variability of the analysis, accurate conclusions regarding the behaviour of these elements cannot be made.

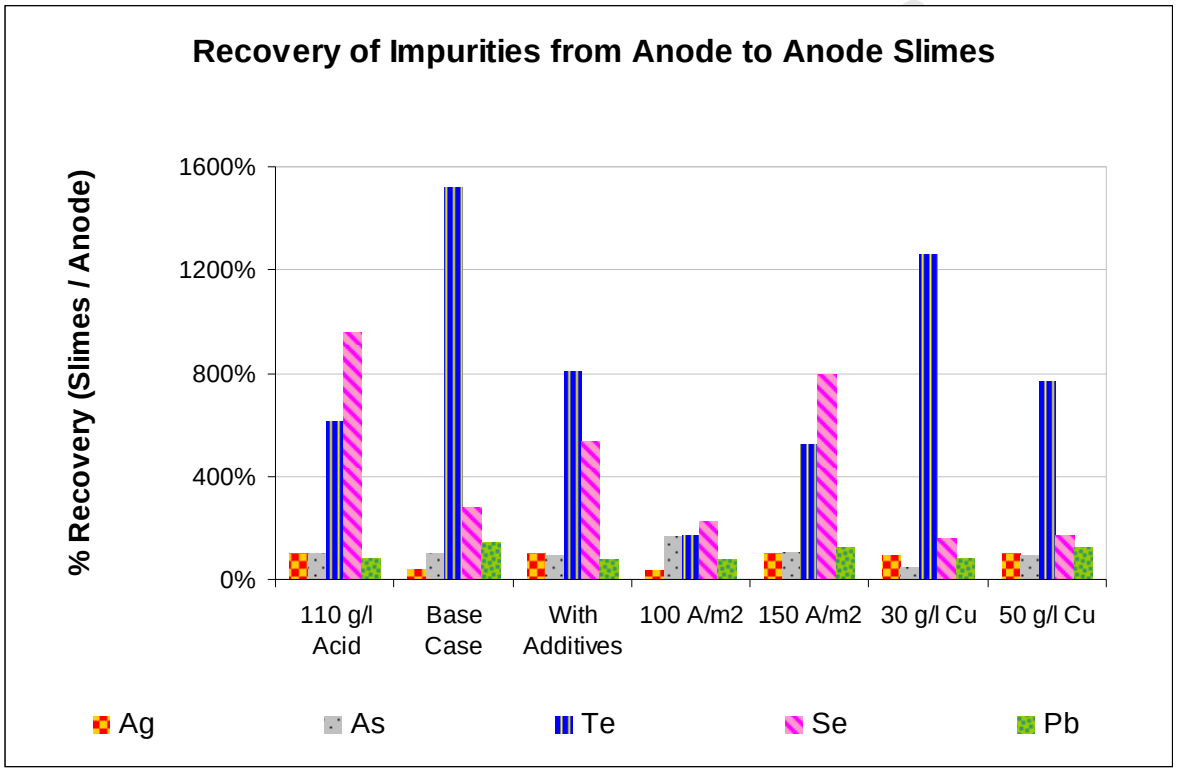

Figure 5.3.j: Recovery of impurities from anode to anode slimes

Figure 5.3.k shows the recovery of the remaining minor impurities from the initial anode. It can be seen that almost all Zn and Sn goes into solution, 20 – 30% of Bi remains in the anode slimes, and 40 – 80% of Sb remains in the anode slimes. The recovery of Si to the anode slimes seems to be very variable and it could be that this is a function of anode composition rather than operating condition (when the analysis of the original anodes are investigated) due to the difficulties that were encountered during anode casting regarding Si contamination.

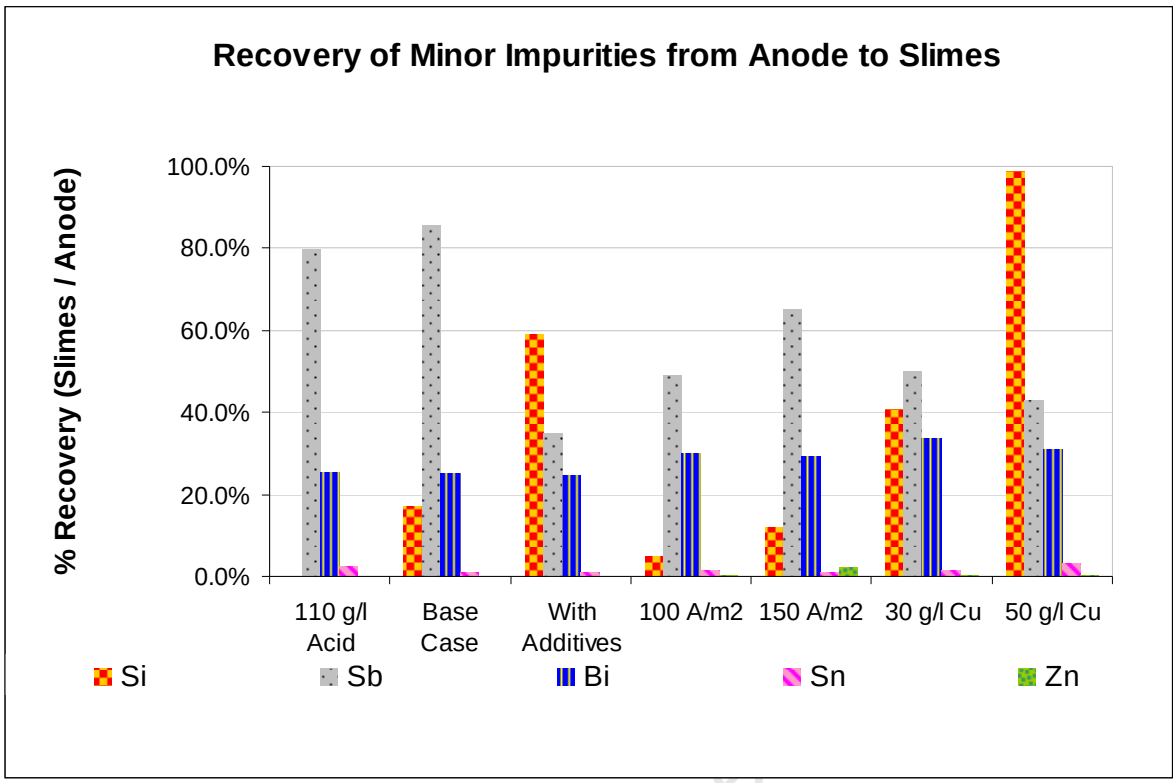

Figure 5.3.k: Recovery of minor impurities from anode to anode slimes

5.4 Product Characterisation

5.4.1 Anode Slimes

Composition

It is important to know the composition of the anode slimes in order to decide whether integration with the current PMR feed is viable, or if further processing will be required.

Figure 5.4.a shows the summarised mass composition of the slimes for every test, as well as the typical mass composition of the PMR feed from the MC plant. None of the slimes that were produced had PGM content as high as the PMR feed and the impurities in the anode slimes were significantly higher than in the PMR feed. The elemental composition of the anode slimes is given in Table 5.4.a and b.

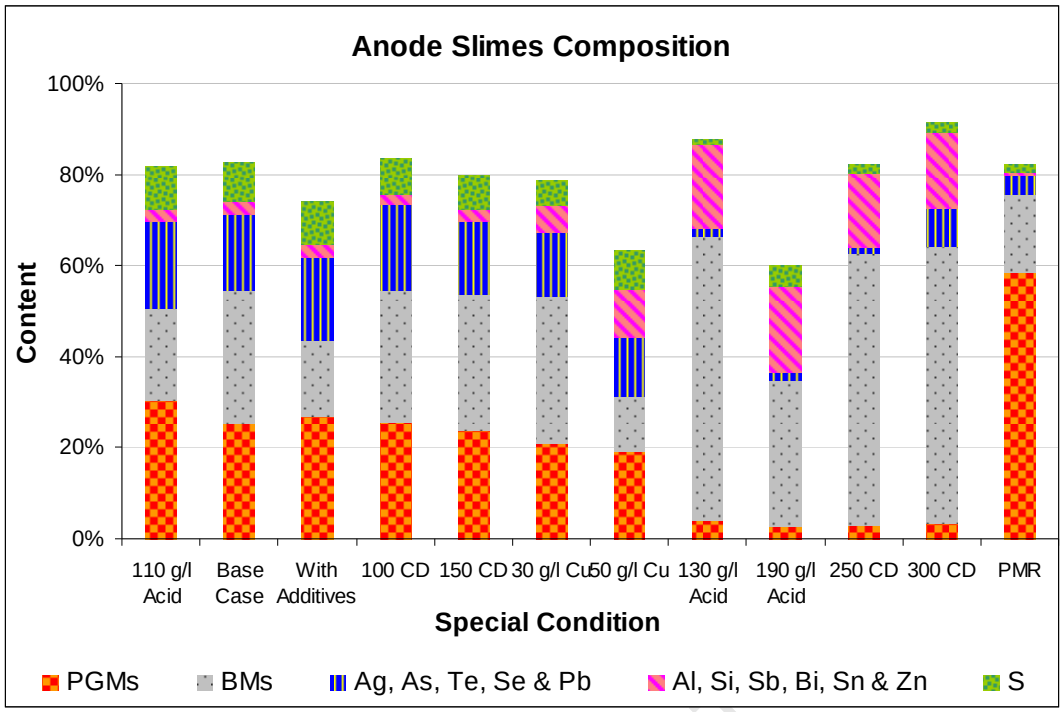

Figure 5.4.a: Composition of anode slimes compared with typical PMR feed composition

It can be observed that the major impurities in the anode slimes are the base metals and amphoterics like As, Te, Se and Pb as well as silver. It can also be seen that the total accountability for the slimes mass was ±80%; it is suspected that the remainder of the slimes mass consist of mainly hydrogen or oxygen in precipitated sulphates or hydroxides or oxides. Table 5.4.a shows the elemental concentrations of the PGMs in the anode slimes and the typical PMR feed concentrations. It can be seen that only Pt and Ir occur in lower levels in the anode slimes than in the typical PMR feed. This is because very low levels of Pt and Ir actually bypass the MC plant to ultimately report to the SLC.

Table 5.4.a: PGM grade of anode slimes

Special Condition	Pt (%)	Pd (%)	Rh (%)	Ru (%)	Ir (%)	Os (%)	Au (%)
110 g/l H_2SO_4	3.35	17.43	4.77	3.45	0.12	0.02	1.38
Base-case	2.57	13.76	3.87	3.88	0.11	0.02	1.09
With Additives	2.73	14.62	3.78	4.21	0.13	0.03	1.19
100 A/m^2	2.51	14.01	3.62	4.15	0.12	0.02	1.13
150 A/m^2	2.41	13.04	3.43	3.63	0.11	0.02	1.04
30 g/l Cu	2.22	11.42	3.02	3.35	0.10	0.02	0.89
50 g/l Cu	1.95	10.66	2.81	3.00	0.09	0.02	0.83
130 g/l H_2SO_4	0.43	2.17	0.52	0.58	0.01	0.00	0.21
190 g/l H_2SO_4	0.30	1.75	0.29	0.30	0.01	0.00	0.15
250 A/m^2	0.33	1.88	0.38	0.40	0.01	0.00	0.17
300 A/m^2	0.35	2.04	0.39	0.40	0.01	0.00	0.18
PMR	30.00	17.00	3.50	4.60	1.40	0.67	1.30

The remainders of the elements in anode slimes are considered impurities and the grade of it is given in Table 5.4.b. These anode slimes were produced by the original uncontaminated anode material. A breakdown of the slimes produced by the altered material is given in Appendix I, Section F.

Table 5.4.b: Impurity grade in slimes produced by tests with original anode material

Element	110 g/l H_2SO_4	Base-case	With Additives	100 A/m^2	150 A/m^2	30 g/l Cu	50 g/l Cu
Ag (g/t)	7330	3420	10 400	9080	9600	177 00	17 000
Cu (g/t)	187 500	28 1600	155 200	27 0600	272 400	266 500	84 700
Ni (g/t)	2800	6400	6000	10 800	15 500	23 800	14 400
Fe (g/t)	10 500	6100	6700	8100	12 300	32 200	21 800
Co (g/t)	<500	<500	630	770	600	1400	930
Pb (g/t)	52 600	49 800	57 700	53 400	45 100	37 800	37 600
As (g/t)	63 000	57 900	59 300	63 400	60 000	46 300	38 300
Al (g/t)	2000	1800	<1000	<1000	<1000	<1000	<1000
S (g/t)	95 500	86 500	93 700	78 700	78 300	56 100	84 700
Cr (g/t)	<1000	<1000	1100	<1000	1500	<1000	<1000
Mg (g/t)	<1000	<1000	<1000	<1000	<1000	<1000	<1000
Si (g/t)	<3000	4800	14 200	8000	3800	42 800	96 800
Te (g/t)	61 200	46 300	48 300	53 900	39 100	32 400	27 800
Sb (g/t)	20 000	19 300	10 900	10 500	15 900	11 100	8020
Bi (g/t)	3400	2900	3950	3910	3440	2870	2430
Sn (g/t)	155	53	69	67	65	63	291
Se (g/t)	7050	7820	7460	7820	6610	5260	4580
Zn (g/t)	9	12	9	16	11	37	24

Elements such as Ag, As, Te, Se and Pb may be of concern due to high concentrations in the anode slimes. The important thing to consider, however, is the mass input of the deleterious elements, relative to current inputs to PMR and how these will impact on the downstream processing. The effect of blending the projected amounts of slimes with the PMR feed was investigated to determine whether these concentrations could be problematic. Figure 5.4.b shows what the deviation of composition will be from current PMR feed if the typical slimes produced per annum (based on slimes production of test, 3-3.5 t/m) were blended with the typical annual PMR feed (±22 t/m). It can be seen that the Pt concentration of the feed to PMR will reduce by 4 to 5.5%, the Cu composition will increase by 2 to 4% and Ni content will reduce by ±4%. The typical and projected mass throughput is given in Appendix I, Section G.

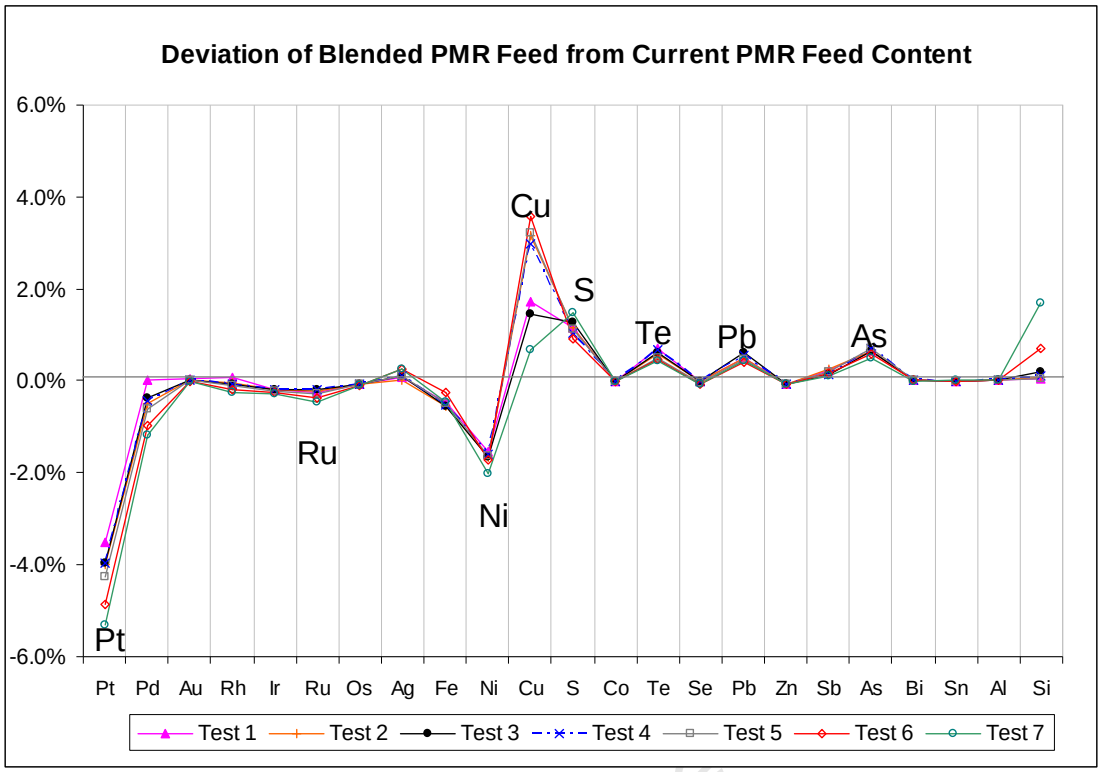

Figure 5.4.b: Deviation of blended feed composition from current PMR feed

Mineralogy

In order to investigate the formation of anode slimes, the original anodes were also investigated. The phases present in the anode give insight into the formation of anode slimes with respect to where the different slimes phases come from and how the anode phases change during electrorefining.

A backscattered-electron image of the initial anode used in the base-case test is shown in Figure 5.4.c and the composition of each phase is given in Table 5.4.c.

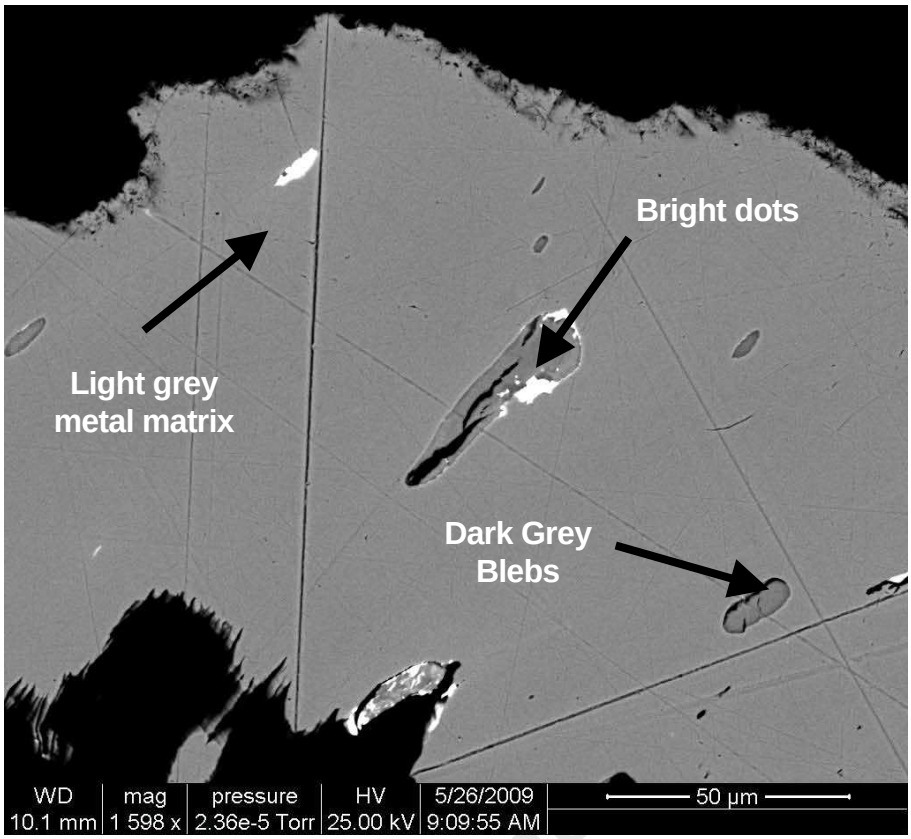

Figure 5.4.c: Backscattered electron image of original anode material used in the base-case test with additives (Test 3)

The phases and their compositions were very similar for all the anodes used during the first seven tests. The backscattered-electron images and analyses of all anodes are given in Appendix I, Section H.

Table 5.4.c: Composition of phases present in initial anode used in base-case test with additives (Test 3)

Light Grey Matrix	Cu	84.54
	Ni	11.83
	Fe	2.67
	Pd	0.56
	Si	0.28
Dark Grey Blebs	Cu	68.83
	S	20.11
	Te	5.78
	Fe	4.68
	Ni	0.36
	Se	0.22
Bright Dots	Pb	42.71
	Bi	23.65
	Ag	18.91
	Cu	7.96
	Ni	7.47

It can be seen from Figure 5.4.c that the major phase in the original anode is the light grey Cu-Ni-Fe alloy with a composition very similar to the overall composition of the Cu alloy. It is possible that the PGMs are distributed in this phase at very low levels and are therefore undetected. The dark grey bleb-like phase consists mostly of Cu, S and Te which points to the presence of copper sulphides and copper tellurides. The small very bright phase normally occurs around the edges of such copper sulphide phases but is also observed as small little dots within the Cu-Ni-Fe matrix. The bright phase is mainly a Pb-Bi-Ag phase with a small amount of Cu and Ni dispersed in it.

The same investigation was done on the anode slimes and, based on the composition of the samples, two distinct populations were identified. The first population included Tests 1 to 7 and the second comprised Tests 8 to 11. Thus, the phases present were similar for Tests 1 to 7 (see Appendix I, Section I). An MLA backscattered-electron image of a typical anode slime particle is shown in Figure 5.4.d. Reflected light images and more backscattered-electron images of the rest of the anode slimes can be seen in Appendix I, Section I.

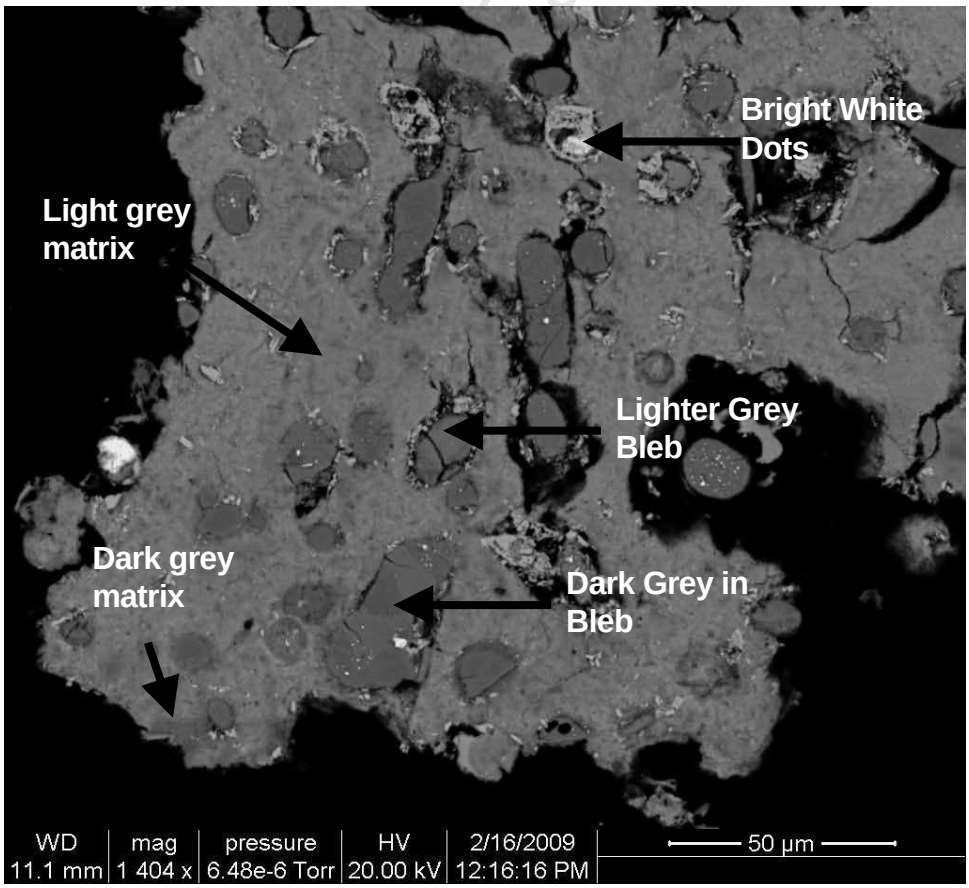

Figure 5.4.d: Backscattered electron image of typical anode slime particle

It was observed that there are mainly four phases in all anode slimes. The phases are described as follows:

1) *Light grey matrix* – Rich in PGMs, palladium arsenic telluride [$Pd_{73}As_6Te_{21}$] phase with small amounts of Cu

2) *Dark grey matrix* – More amorphous PGM-rich phase with higher O content

3) *Dark grey in blebs* – A copper sulphate hydrate [$CuSO_4.5H_2O$] phase also containing Cu telluride and Fe.

4) *Lighter grey blebs* – Digenite [Cu_9S_5] with tellurides and large amounts of Pb

5) *Small bright white spots* - A lead sulphate [$PbSO_4$] phase, containing mostly Pb, Bi, Ag.

The distinct amorphous component, observed as a hump in each of the traces, is present in Tests 1 to 7 (see Figure 5.4.e). Other XRD traces are given in Appendix I, Section J). The amorphous component ranges between 60 and 80 mass percent in Tests 1 to 7, as calculated by the Rietveld refinement method.

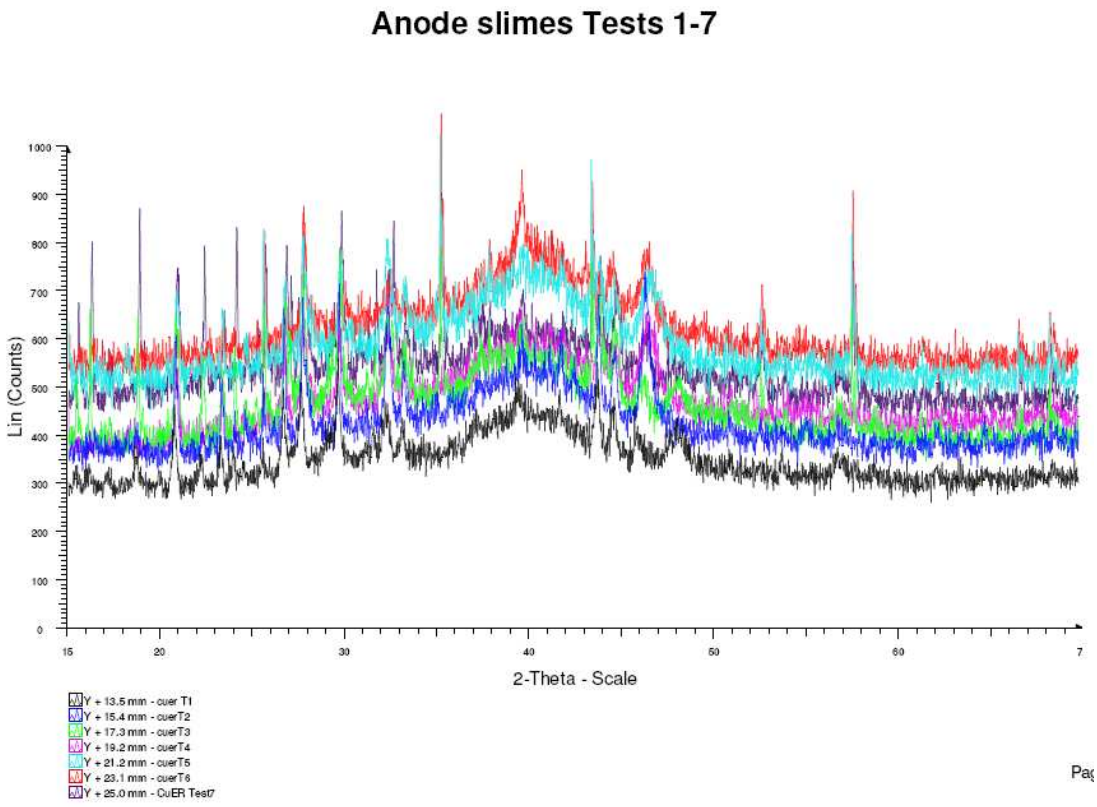

Figure 5.4.e: XRD traces of anode slimes samples of test 1 – 7 showing amorphous phase

SEM-EDX analysis was performed on the anode slimes to determine the composition of these phases. Although the phases in the slimes are similar for all test products, the element concentrations varied slightly. The phase compositions for slimes phases produced during the first test are shown in Table 5.4.d.

Table 5.4.d: Composition of different phases in anode slimes

Element	Light Grey Matrix	Darker Grey Matrix*	Dark Grey in Blebs	Lighter Grey Blebs	Bright White Dots
Pd	38.3	21.6			
As	11.5	11.9	1.1		
Rh	8.1	10.9			
Ag	7.4	4.5	2.5	3.0	18.91
Pt	6.6	6.3			
Te	6.4	6.9	8.2	7.0	
Sb	6.0	4.5			
Cu	5.3	5.5	52.3	47.4	7.96
Ru	4.2	9.4			
Au	4.1	2.6			
O		13.2			
S	1.9	2.0	29.2	23.3	
Se	0.5	0.7	0.4	1.4	
Fe			6.4	7.7	
Pb				10.2	42.7
Bi					23.7
Ni					7.47

*Amorphous phase (dark grey matrix), not analysed accurately

When comparing the phases in the anode slimes with the phases in the anodes, it was found that the composition of the bright white particles in the original anodes is similar to those in the anode slimes (Figure 5.4.f). Thus, it is suspected that this phase does not take part in reactions during electrorefining and reports directly to the anode slimes.

The Cu sulphide (digenite) or telluride phase (dark grey blebs) also has a similar content as the bleb phase in the original anode (Figure 5.4.g). This also indicates that this phase is not influenced extensively by electrorefining but reports to the anode slimes. The main difference is the reduction of Cu content by ±10%. This suggests that dissolution of Cu from the sulphide or telluride takes place, possibly through leaching in the acidic electrolyte after dropping from the anode surface. An increase in S is also evident which suggests the precipitation of sulphates, as expected from the literature review in Section 2.3.1. The Pb concentration increases with the sulphur content in the lighter bleb phase (which is much more prominent) which suggests the precipitation of $PbSO_4$.

The light grey matrix phase and amorphous phase in the anode slimes contains most of the PGMs and are completely new phases (Figure 5.4.h). Due to the fact that there is no Cu-Ni-Fe metal phase (the matrix phase in the original anode) remaining in the slimes, it can be suggested that this new phase is formed during the dissolution of the metallic Cu, Ni and Fe from the matrix phase. It is likely that these PGMs were distributed in the Cu, Ni metal matrix at very low levels that were not detected (detection limit = 0.5%). A small percentage of Cu remains in this phase together with As, Te and Sb. This Cu is possibly complexed with some of the PGMs or Ag as tellurides or arsenides. The PGM-bearing phase is thus a PGM-As-Te phase with > 60% PGMs.

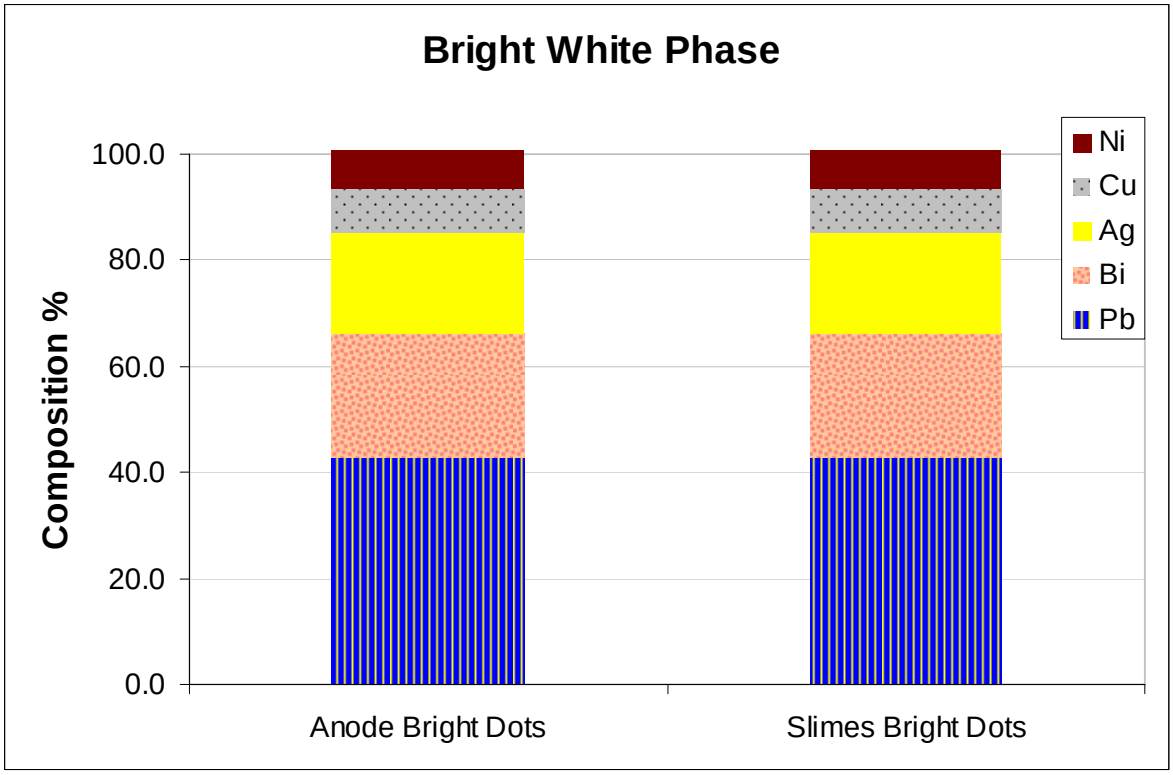

Figure 5.4.f: Comparison of bright white phases in anode and slimes

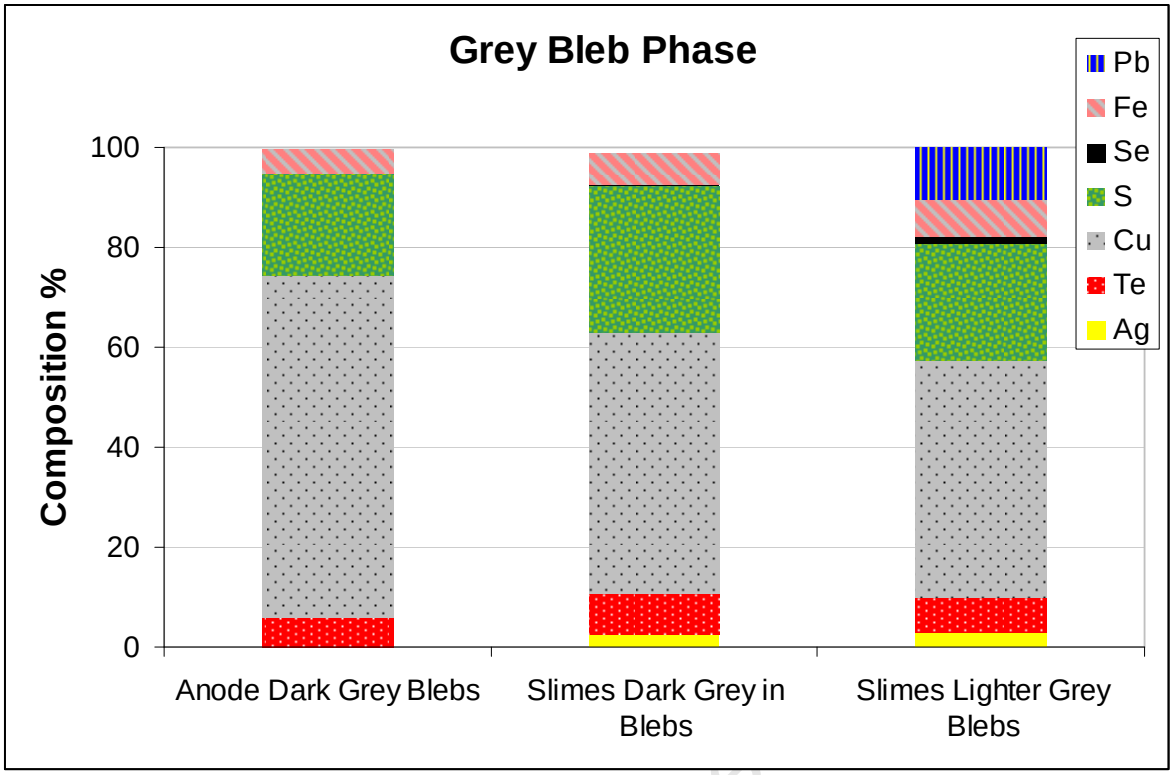

Figure 5.4.g: Comparison of grey bleb phases in anode and slimes

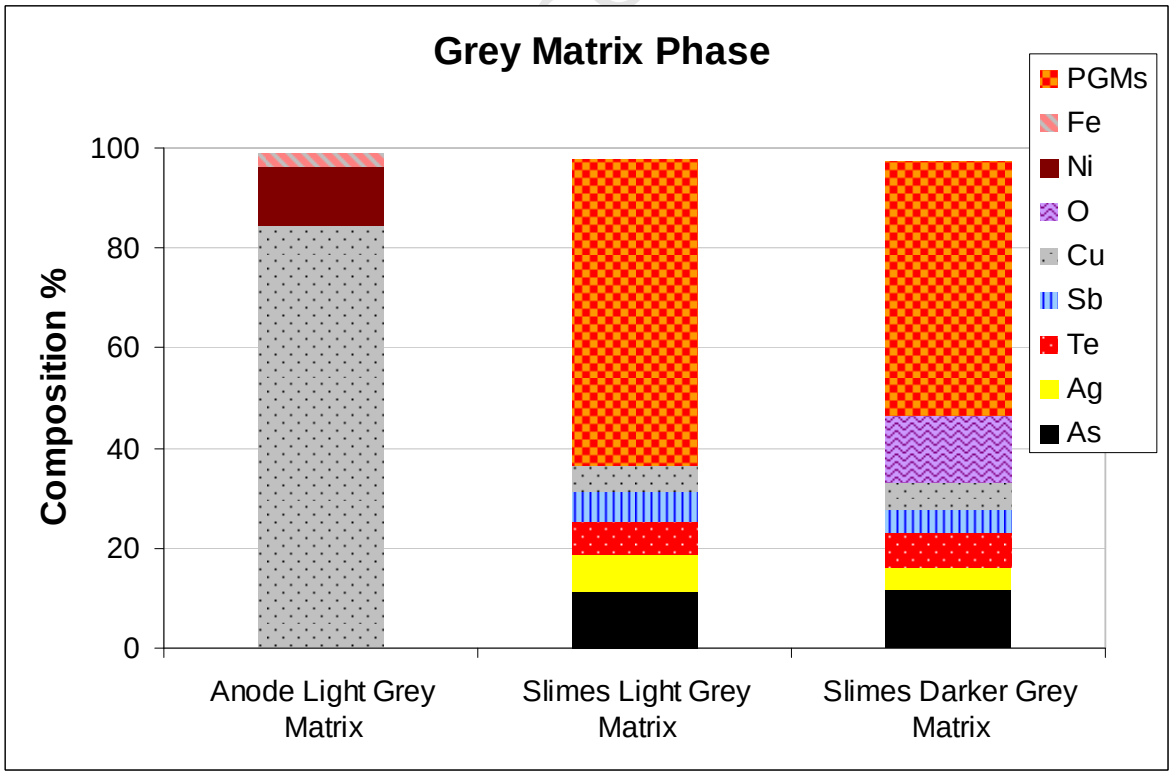

Figure 5.4.h: Comparison of the matrix phases in anodes and slimes

5.4.2 Spent Electrolyte

The spent electrolyte produced during electrorefining will need to be recycled to the process in order to bleed some of the impurities, and recover the Ni to the Ni electrowinning and the Co to the Co solvent extraction circuits. In order to determine the optimal position in the process flow sheet to integrate the spent electrolyte, the concentrations need to be investigated. The final spent electrolyte concentrations that were obtained after each test performed with the original material are given in Table 5.4.e.

Table 5.4.e: Spent electrolyte concentrations after each test

Element		110 g/l Acid	Base-case	With Additives	100 A/m^2	150 A/m^2	30 g/l Cu	50 g/l Cu
Pt	mg/l	<0.2	<0.2	0.01	0.01	<0.2	<0.2	<0.2
Pd	mg/l	<0.2	<0.2	0.055	0.06	<0.2	<0.2	<0.2
Rh	mg/l	2.8	2.6	2.6	2.5	2.5	1.7	2.5
Ru	mg/l	16	17	16	15	15	11	15
Ir	mg/l	0.4	0.4	0.4	0.4	0.4	0.3	0.4
Os	mg/l	<0.2	<0.2	<0.2	<0.2	<0.2	<0.2	<0.2
Au	mg/l	<0.2	<0.2	<0.01	<0.2	<0.2	<0.2	<0.2
Ag	mg/l	0.1	0.85	<0.2	2.22	<0.2	0.37	<0.2
Cu	g/l	41.23	40.1	36.9	38.4	38.2	28.2	40.5
Ni	g/l	56.4	58.28	55.86	52.82	55.06	40.95	52.39
Fe	g/l	2.65	2.73	2.56	2.45	2.58	1.972	2.52
Co	mg/l	944	931	877	868	898	644	838
Ca	mg/l	51.43	52.44	49.02	48.78	49.22	41.27	48.83
Pb	mg/l	8.7	5.7	8.4	8.3	4.4	6.5	5.1
As	mg/l	74	74	74	74	73	54	71
Al	mg/l	43.44	45.71	45.76	42.4	41.72	32.29	43.49
S	g/l	98.34	118.8	114.4	110.3	111.6	98.95	113.2
Cr	mg/l	3.06	2.87	2.56	2.51	2.58	4.78	6.17
Mg	mg/l	33.21	33.54	32.71	30.93	31.12	23.69	31.54
Si	mg/l	112	30.86	34.83	48.44	66.6	74	66.69
Te	mg/l	33	33	33	33	33	22	34
Sb	mg/l	10	8.6	11	10	10	8.9	11
Bi	mg/l	2.5	2.6	2.6	2.3	2.9	1.9	2.4
Sn	mg/l	0.9	1	1	0.8	1.2	1	2.2
Se	mg/l	10	9.2	9.2	9.1	9	6.6	8.6
Zn	mg/l	26.1	27.62	27.73	26	25.69	21.93	25.08

The Ni concentration is relatively high, between 50 and 60 g/l. This is slightly lower than typical Ni electrowinning feed concentration of 70 g/l and it is possible to blend it with Ni electrowinning feed to obtain a higher concentration. However, the impurities like Cu, Pb, Co, Fe, Zn, etc, will result in significant contamination of the Ni cathodes. The typical concentrations in the current Ni feed are:

- Ni: 72.93 g/l

- Co: 7.80 mg/l
- Cu: 101.93 mg/l
- Fe: 10.55 mg/l
- Pb: 0.70 mg/l
- Zn: 1.51 mg/l

These are much lower than the concentrations in the spent electrolyte produced by electrorefining. Thus, the electrolyte stream will have to be subjected to purification before the Ni can be recovered. However, if it is subjected straight to the purification circuit, the high acid content will have to be neutralised and will incur extra costs. Therefore it would make sense to send the acidic Ni-rich spent electrolyte from electrorefining to the primary leaching stage where acid is required and the objective is to leach Ni from the BMR feed material. The acid will be used for leaching of Ni and the Ni from electrorefining will report to the Ni purification circuit together with the newly leached Ni after the primary leach stage. Most of the other impurities will also have an opportunity to be removed from the stream in the purification circuit and will also be diluted significantly with the Ni-rich leach liquor. The Ni purification circuit consists of:

1) Cu and Fe Removal

2) Pb Removal

3) Co Removal

Some other impurities like Zn will also be removed in some of the above stages to a certain extent.

5.4.3 Cathodes

The impurities in the Cu cathodes produced are given in Table 5.4.f. These impurities should be compared with the chemical specifications given in Table 2.2.a on page 38.

Generally, only Se, Te, Ni and Fe in the cathodes produced are higher than the target specified by the LME grade A specifications. This could be due to the high concentrations in the electrolyte or cathode porosity resulting in high entrainment of electrolyte. Analytical bias could also play a role in some of the results.

Table 5.4.f: Impurities in cathodes

Element		110 g/l Acid		Base-case		With Additives		100 A/m^2		150 A/m^2		30 g/l Cu		50 g/l Cu	
		Front	Back	Front	Back	Front	Back	Front	Back	Front	Back	Front	Back	Front	Back
Pt	ppm	4.0	3.8	0.2	<0.167	<0.167	<0.167	<0.167	<0.167	<0.167	<0.167	<0.167	<0.167	<0.167	<0.167
Pd	ppm	5.7	3.3	6.8	6.3	1.3	2.3	1.7	2.8	2.8	2.0	1.7	1.0	<0.167	<0.167
Rh	ppm	2.8	1.5	7.7	8.2	1.3	1.7	1.3	1.5	3.5	7.3	9.7	8.2	1.0	0.8
Ru	ppm			13.0	14.3	1.0	0.8	1.0	1.2	14.5	14.2	15.5	13.5	1.2	0.8
Ir	ppm			<0.167	<0.167	<0.167	<0.167	<0.167	<0.167	<0.167	<0.167	<0.167	<0.167	<0.167	<0.167
Os	ppm			<0.167	<0.167	<0.167	<0.167	<0.167	<0.167	<0.167	<0.167	<0.167	<0.167	<0.167	<0.167
Au	ppm	7.5	2.2	0.2	<0.167	0.2	0.2	<0.167	0.2	<0.167	<0.167	<0.167	0.2	<0.167	<0.167
Ag	ppm			0.3	<0.167	1.2	1.8	1.0	1.3	1.0	1.2	1.5	2.2	1.8	1.3
Ni	ppm			85.2	83.5	24.0	24.3	28.3	33.5	101.7	112.7	88.5	86.3	14.7	8.3
Fe	ppm	126.7	51.7	266.7	50.0	111.7	10.8	6.3	7.5	6.5	4.2	6.8	3.8	416.7	<0.833
Co	ppm			5.3	5.8	13.7	1.5	2.8	3.2	7.3	7.0	6.2	2.7	0.5	0.3
Ca	ppm	150.0	88.3	41.7	13.8	10.8	5.3	23.3	66.7	16.7	36.7	0.8	0.8	20.0	4.7
Pb	ppm	8.3	8.3	<0.167	<0.167	1.0	0.7	<0.167	0.8	1.0	0.3	2.0	0.5	74.3	95.0
As	ppm	6.7	2.5	7.8	5.0	0.8	0.8	0.8	0.8	0.8	0.8	0.8	0.8	<0.167	<0.167
Al	ppm	<0.833	<0.833	<0.833	<0.833	25.0	20.0	25.0	18.3	18.3	20.0	20.0	20.0	<0.833	5.8
Cr	ppm			2.2	2.5	1.5	0.8	0.8	1.2	1.0	1.2	1.2	0.7	2.0	0.7
Mg	ppm	<0.833	<0.833	<0.833	<0.833	<0.833	<0.833	<0.833	<0.833	<0.833	<0.833	<0.833	<0.833	<0.833	<0.833
Si	ppm	63.3	<0.833	65.0	85.0	8.0	16.7	43.3	10.8	41.7	38.3	66.7	68.3	45.0	233.3
Te	ppm	7.8	7.8	123.3	118.8	11.8	7.3	7.5	9.2	138.7	139.8	148.5	168.3	5.7	3.7
Sb	ppm			4.3	2.7	0.3	0.8	0.8	0.7	1.0	0.8	1.8	2.3	0.5	0.3
Bi	ppm			2.3	0.2	0.5	<0.167	<0.167	<0.167	<0.167	<0.167	<0.167	<0.167	<0.167	<0.167
Sn	ppm			<0.167	<0.167	0.3	<0.167	<0.167	<0.167	<0.167	<0.167	<0.167	0.3	1.3	1.2
Se	ppm	4.0	1.8	1.7	3.0	5.8	5.5	4.3	4.8	8.2	9.0	9.5	9.8	9.2	12.7
Ti	ppm			<0.167	0.7									<0.167	<0.167
Mn	ppm			5.7	5.2	<0.167	<0.167	<0.167	<0.167	<0.167	<0.167	<0.167	<0.167	<0.167	<0.167
Cd	ppm			<0.167	<0.167	<0.167	<0.167	<0.167	<0.167	<0.167	<0.167	<0.167	<0.167	<0.167	<0.167
Zn	ppm	4.2	4.8	<0.167	<0.167	8.2	14.7	8.2	9.2	9.2	8.8	92.5	96.3	6.8	12.5

The cathode morphology is shown in Figure 5.4.i. It can be seen that the morphology is much rougher around the edges of the cathode. Figure 5.4.j shows the surface of a cathode produced during test 4 (100 A/m^2). It can be seen that the colour of the cathode is darker around the edges of the cathode which could indicate some entrainment of electrolyte or slimes due to higher porosity around the edges. The thickness of the cathodes was relatively uniform throughout the length and width of the cathode which indicates that the current distribution was good through the depth of the cell. The weight of the front cathode was also very similar to the back cathode after each test, showing that the current distribution was relatively equal between the back and the front of the anode.

Figure 5.4.i: Nodular growth around edges first test cathode

Figure 5.4.j: Smooth surface of fourth test cathode.

5.4.4 Mass Reduction

Figure 5.4.k shows the mass of slimes and cathode produced per kg of anode for the tests that were performed with the original composition material. It can be seen that the amount of slimes produced stays relatively constant over the range of operating conditions (27 – 42 g/kg). The slight increase in slimes produced during the last two tests at special copper concentration is most probably a function of the silica content in the initial anode material that was used (the increase in Si content in anodes can be seen in Appendix I, Section E.). The cathode production also stayed relatively constant at slightly less than 1 kg of Cu plated per kg of anode dissolved.

Considering that 20% less copper dissolved than were plated, it is safe to say that ± 20% of the Cu cathode is plated from the electrolyte feed. This gives an indication as to how large the Cu concentration drop will be across a cell at a given fresh feed rate.

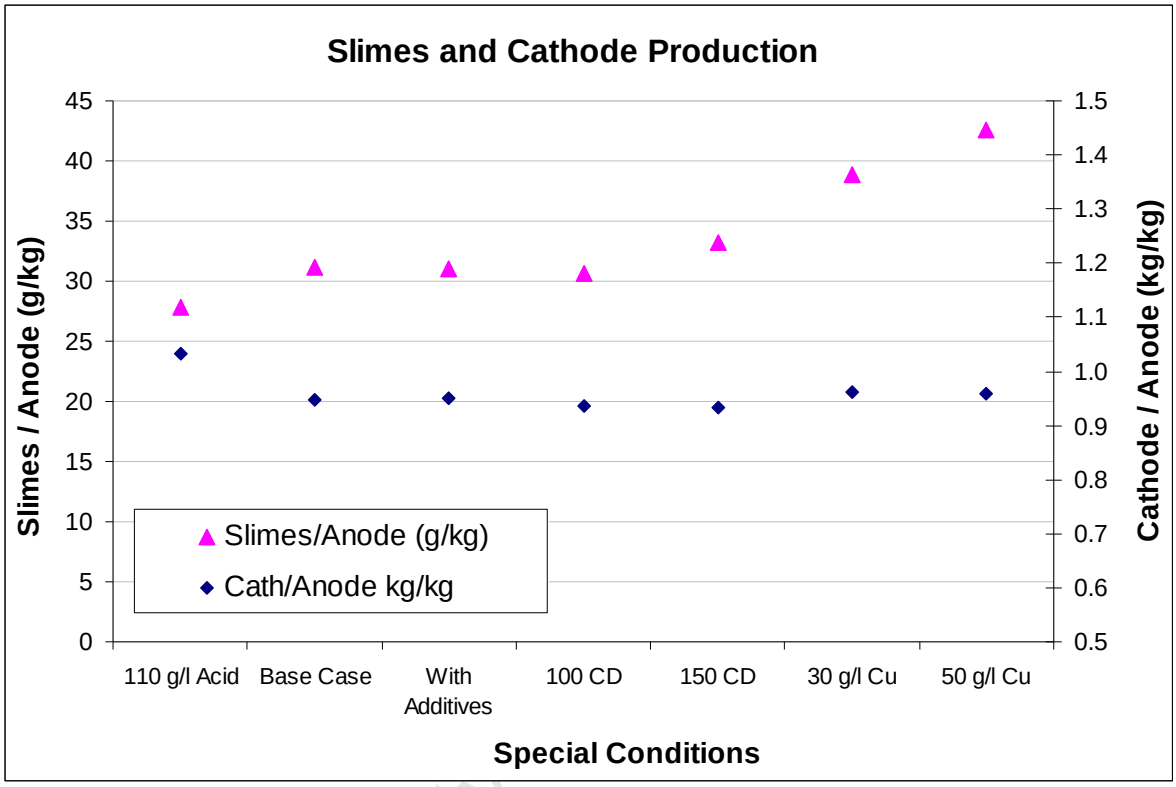

Figure 5.4.k: Slimes and cathode production per kg of anode treated

Given these results of an average slimes production of 33 g and cathode production of 1 kg per kg of anode, the typical BMR SLC of 550 t/m can be converted into:

- Anode slimes: 3.63 t/m or 43.56 t/a
- Copper cathode: 110 t/m or 1320 t/a
  - 1056 t/a produced from BMR SLC
  - 264 t/a produced from BMR leach liquor

(These calculations assume an 80% mass reduction by pyrometallurgical treatment of SLC prior to electrorefining.)

At an average of 33 g/kg slimes production, the Cu alloy mass is reduced by 96.7%, and an overall SLC mass reduction of 99.3% is achieved.

5.5 Effect of Operating Parameters

The effects of Cu and H_2SO_4 concentrations, current density as well as the addition of smoothing agents were investigated. The combination of parameter settings that were used are shown in Table 4.1.a. It was aimed to maintain a constant voltage, Cu and H_2SO_4 concentration throughout the tests and these parameters were monitored on an hourly basis throughout the tests. It should be noted that the concentrations did vary from the original set point at times. This could have been due to titration bias by different operators or actual change in concentration due to the effect of current density. In Test 7, the Cu concentration was set to be 50 g/l. Due to low ambient temperatures and the high concentration in the electrolyte, $CuSO_4$ started to crystallise in the feed box during the test. Thus, a significant drop in Cu concentration occurred. The average concentration (45 g/l) was, however, still higher than the base-case setting (40 g/l) and can thus still be compared to the base-case to a certain extent. The stabilities of all these parameters are shown in Appendix I, Section D.

5.5.1 Smoothing Agents

The second and third tests were to determine whether smoothing additives would improve the morphology of the copper deposit. The copper and acid concentrations were 40 g/l and 160 g/l, respectively, the current density was 125 A/m^2 and temperature was 65°C. The additives added in Test 3 were guar gum, thiourea and sodium chloride. The measured cell potential for the two tests is shown in Figure 5.5.a.

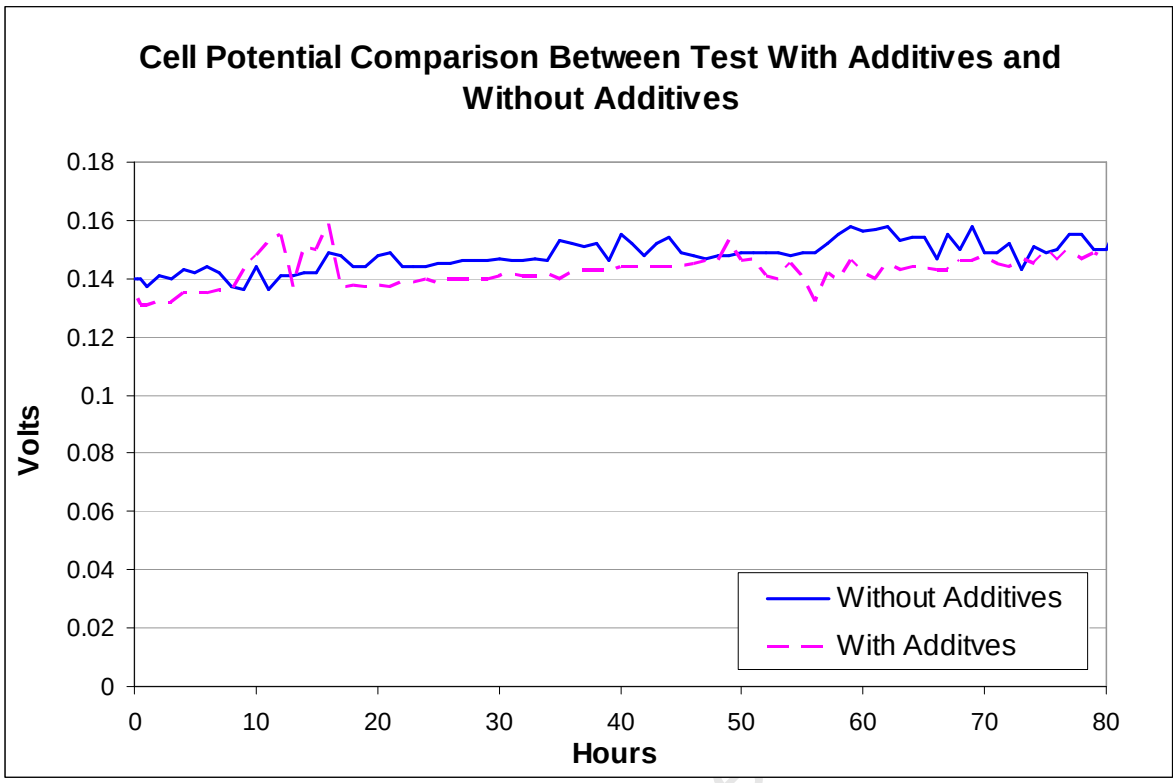

Figure 5.5.a: Comparison of cell potential during tests with additives and without additives.

As discussed before, the cell potential increased slightly throughout the test. The cell potential without additives was slightly higher than it was with additives for the larger part of the test. However, this difference may not be significant enough to draw any conclusions. The following differences between the two tests were noticed:

1) Power consumption

- Without Additives: 0.125 kWh/kg anode; 0.118 kWh/kg cathode
- With Additives: 0.121 kWh/kg anode; 0.115 kWh/kg cathode

2) Current Efficiency

- Without Additives: Anodic = 102.4%; Cathodic = 98.57%
- With Additives: Anodic = 100.8%; Cathodic = 97.5%

3) Anodic dissolution

- Without Additives: 149.5 $g/m^2.h$
- With Additives: 147.3 $g/m^2.h$

The power consumption with additives was slightly lower due to the lower cell voltage. The anodic and cathodic current efficiencies also decreased slightly with the use of additives, as well as the anodic dissolution. An explanation for this could be slight passivation of the electrode surfaces due to the absorption of the organics to the surface, resulting in less Cu being dissolved or plated. However, the drop in cell voltage is counter-intuitive in this regards as the presence of organics is expected to pose some resistance to current flow thereby rather increasing the cell voltage.

The main observation made was that the test without the smoothing agent had an irregular deposit surface. This area was covered in anode sludge which was lodged between the copper deposit grains. The smoothing additives resulted in an improved cathode surface morphology and less anode slimes were lodged between the copper deposit grains. This was confirmed by the cathode analysis shown in Table 5.4.f where almost all of the impurity concentrations were reduced significantly with the use of additives. The smoothing additives were subsequently added to all the succeeding tests in order to minimise entrainment.

5.5.2 Current Density

The effects of the change in current density on the power consumption, current efficiency, dissolution rate and product mass are as follows:

1) Power consumption

- 100 A/m^2: 0.104 kWh/kg anode; 0.111 kWh/kg cathode
- 125 A/m^2: 0.115 kWh/kg anode; 0.121 kWh/kg cathode
- 150 A/m^2: 0.131 kWh/kg anode; 0.140 kWh/kg cathode

2) Current Efficiency

- 100 A/m^2: Anodic = 101.5%; Cathodic = 96.7%
- 125 A/m^2: Anodic = 100.8%; Cathodic = 97.5%
- 150 A/m2: Anodic = 103.4%; Cathodic = 98.4%

3) Anodic dissolution

- 100 A/m^2: 118.3 g/m^2.h
- 125 A/m^2: 147.3 g/m^2.h
- 150 A/m^2: 181.3 g/m^2.h

4) Product mass

- 100 A/m^2: Slimes: 30.64 g/kg anode; Cathode: 0.94 g/kg anode
- 125 A/m^2: Slimes: 31.05 g/kg anode; Cathode: 0.95 g/kg anode
- 150 A/m^2: Slimes: 33.26 g/kg anode; Cathode: 0.93 g/kg anode

The power consumption at each current density is plotted in Figure 5.5.b. The power consumption will continue increasing at a similar rate as shown below with a further increase in current density. Thus, the power consumption will increase even more as less copper is produced per unit of energy. If it is assumed that the increase in power consumption is at least linear with an increase in current density, it can be calculated that the power consumption at 250 A/m^2 and 300 A/m^2 will be at the very least 0.18 and 0.20 kWh per kg of anode dissolved, respectively.

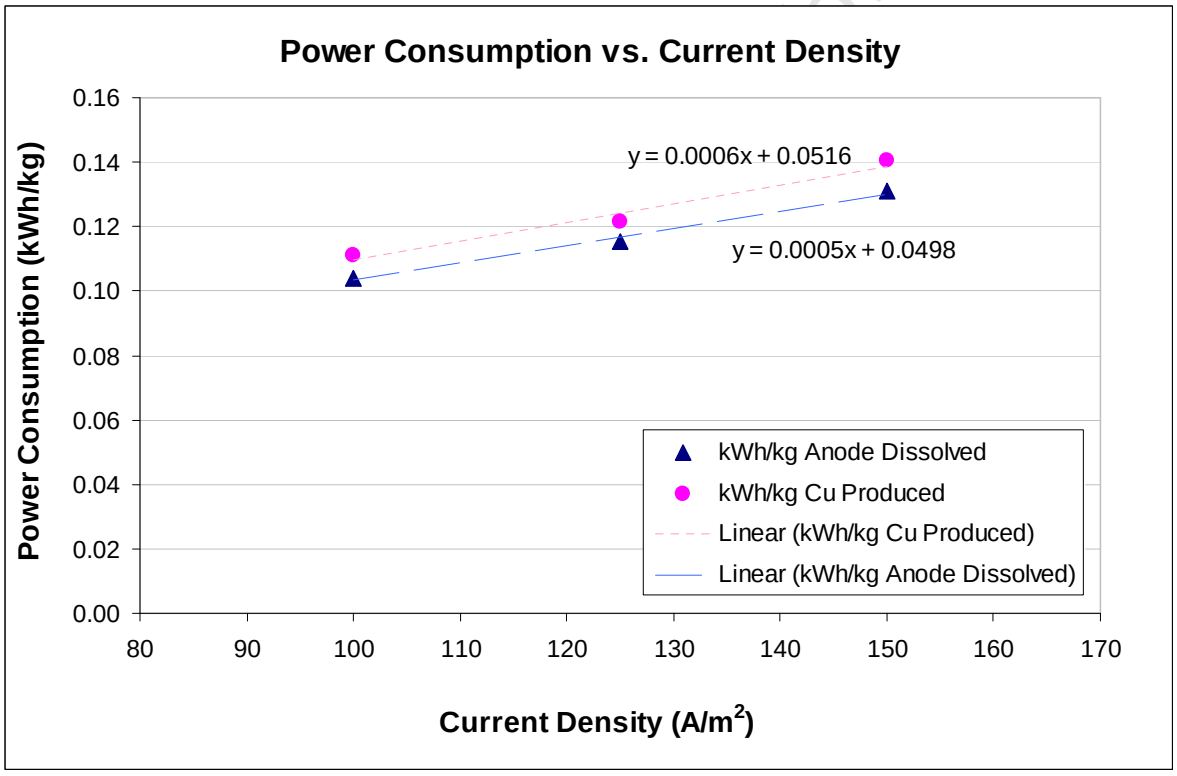

Figure 5.5.b: Increase in power consumption with an increase in current density

The cathodic current efficiency increased with an increase in current density. This is counter-intuitive as it is expected that current efficiency will decrease. It could thus be assumed that the increase in the calculated current efficiency is not real. However, it still shows that the current efficiency was not adversely affected by the increase in current density and current densities higher than 150 A/m^2 could still be beneficial without sacrificing current efficiency excessively.

As expected, the dissolution rate increased with current density as shown in Figure 5.5.c. The anode dissolution rate will stop increasing with current density as soon as mass transport becomes the rate-limiting factor and the current efficiency reduces. Thus, the linear relationships given in Figure 5.5.c represent the best case scenario if no anode passivation, mass transport limiting or drop in current efficiency occur. Thus, the anode dissolution rates at 250 A/m^2 and 300 A/m^2 would be, at most, 292 g/m^2.h and 351 g/m^2.h, respectively.

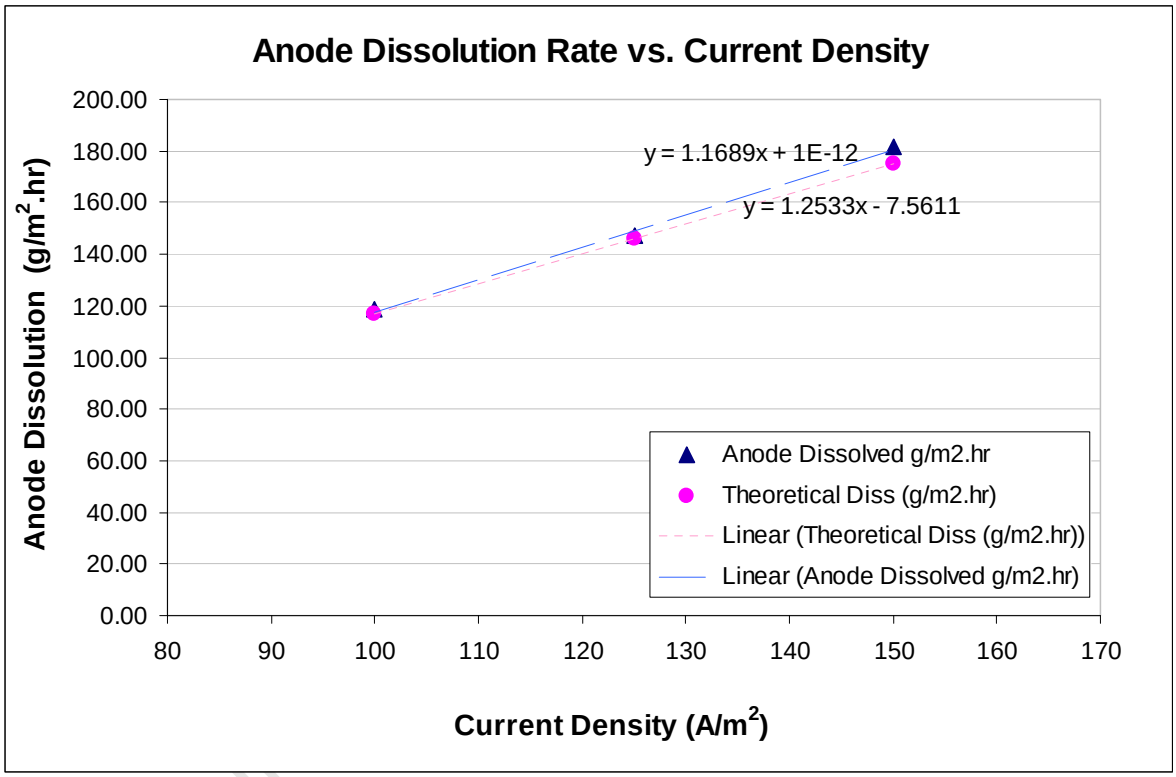

Figure 5.5.c: Increase in anode dissolution with an increase in current density

The mass of slimes produced per kg of anode increased with an increase in current density. This could be due to the fact that not enough time was allowed for all the elements to dissolve from a particle before it became detached from the anode. It could also be that the change in slimes mass production could simply be a function of original anode content or bias occurring during the filtration and drying of the slimes.

When investigating the recovery of elements from the anode to the anode slimes in Figure 5.3.h to Figure 5.3.k to no evidence was found of any element that was retained in the anode slimes more preferentially as a function of current density. However, when investigating the element deportment from the anode and the

electrolyte to the slimes, a number of elements showed an increased deportment to the anode slimes. These elements are shown in Figure 5.5.d and Figure 5.5.e.

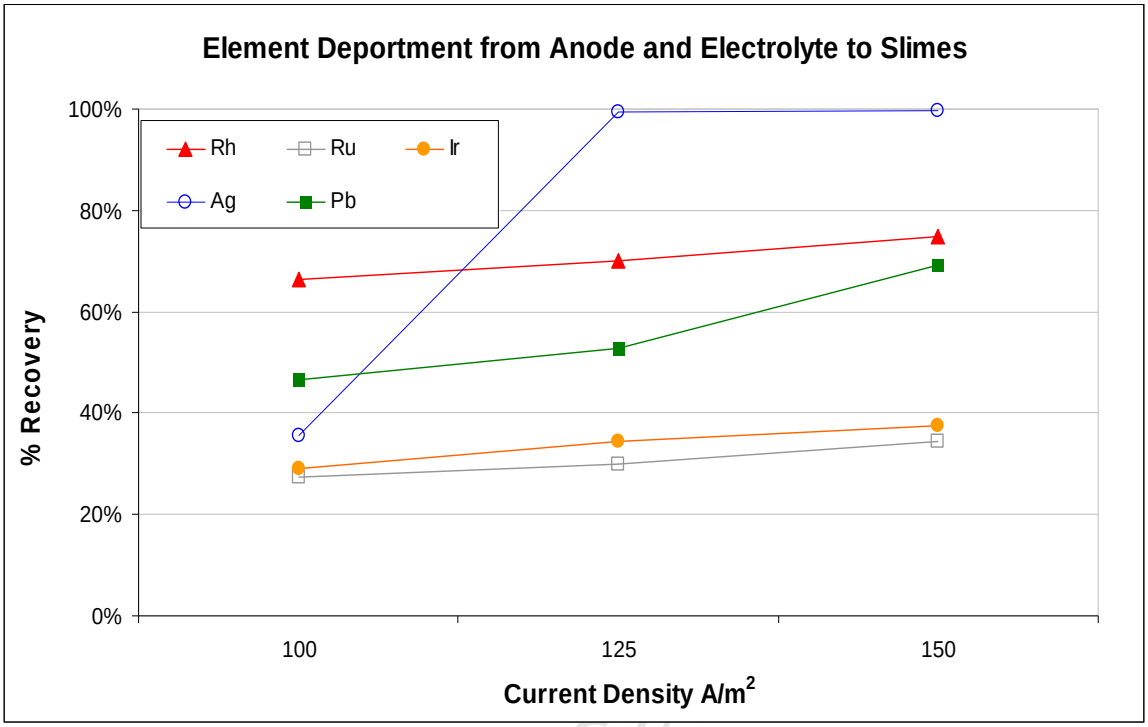

Figure 5.5.d: Deportment of Rh, Ru, Ir, Ag and Pg to slimes from anode and electrolyte

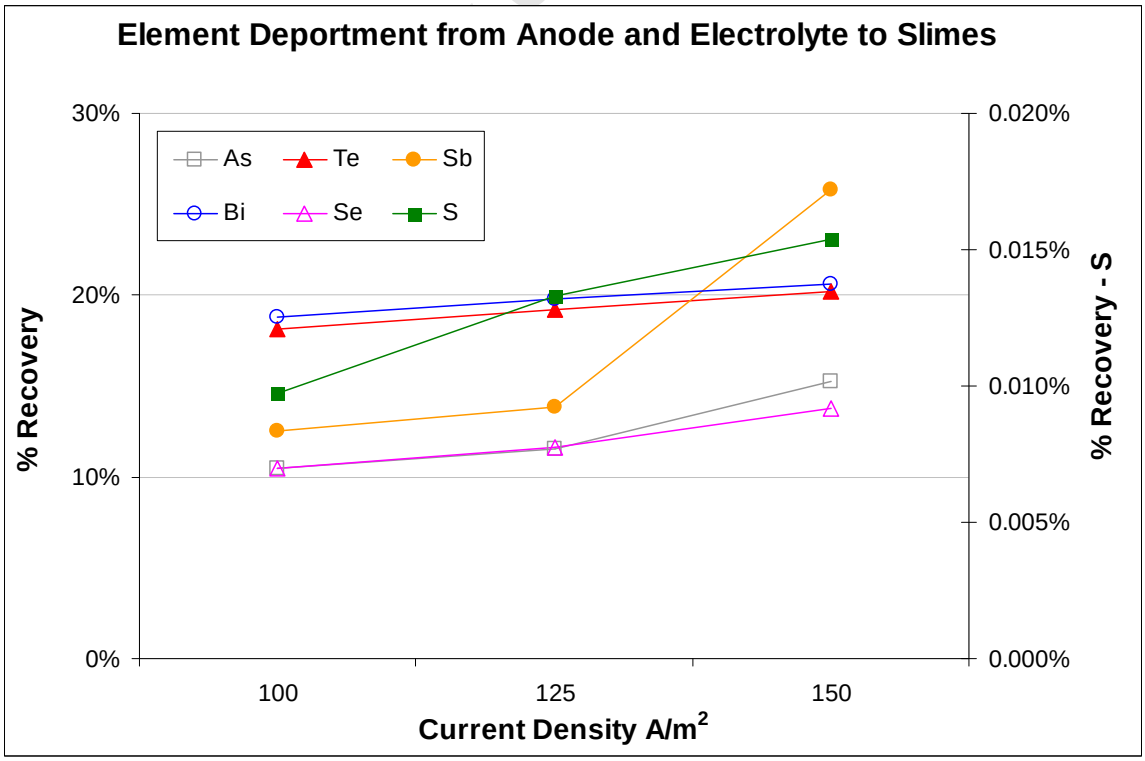

Figure 5.5.e: Deportment of As, Te, Sb, Bi, Se & S to slimes from anode and electrolyte

An increase in recovery of Rh, Ir and Ru from the electrolyte was observed at the points that had increased current density. If this is a true representation of the PGM behaviour it would be the desired effect. However, the deportment of these elements was calculated with electrolyte analysis which was very variable and cannot be assumed to be accurate.

Figure 5.5.f shows the cell potential at different current densities. As expected, a higher current density resulted in a higher cell voltage:

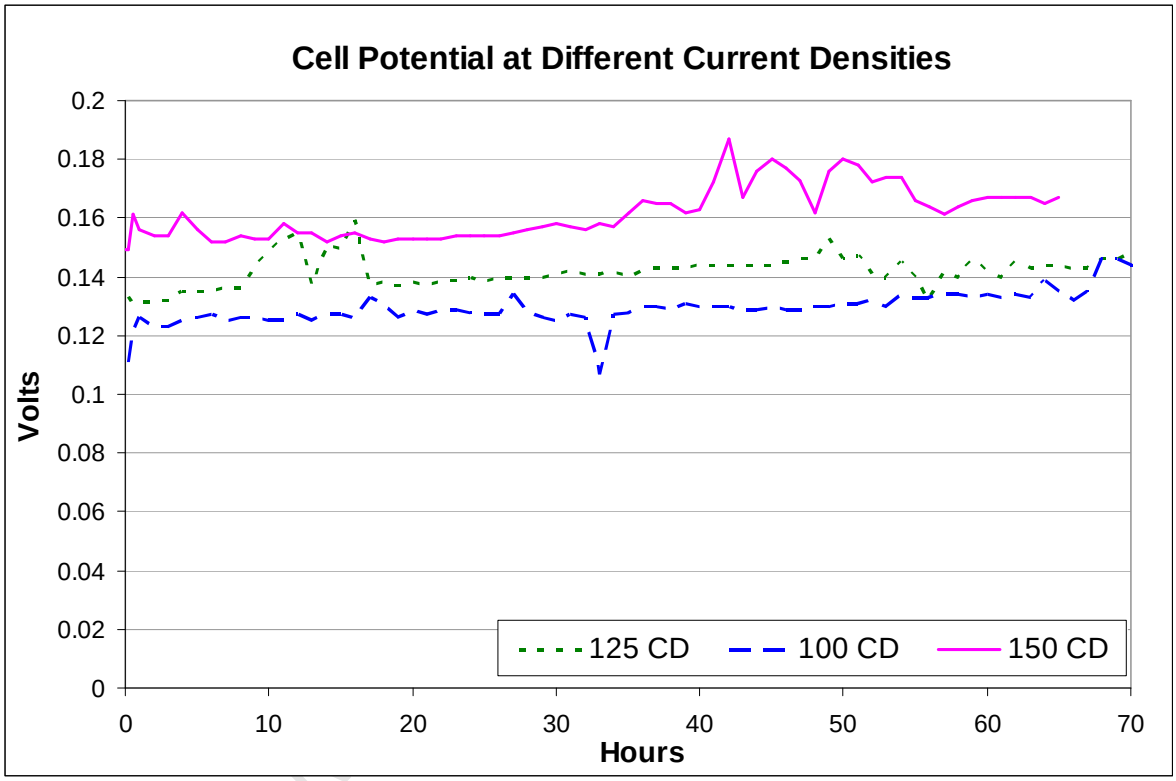

Figure 5.5.f: Comparison of cell potential at various current densities

It is known from the literature review (Section 2.1.3) that the relationship between the anodic current density and the anodic overpotential is given by the following high field approximations of the Butler Volmer relationship:

Anodic: $\eta_a = b.\log\left(\frac{i_a}{i_0}\right)$;

Where η_a is the overpotential of $E - E_a$

It was also calculated in the literature review that the equilibrium potential for Cu electrorefining is $E_e = 0$ V. Thus $\eta_a = E - 0$ V

The experimental data were used in combination with the Butler-Volmer relationship to determine values for i_0 and b by iteration. The error between the actual overpotential obtained during the testwork and the calculated overpotential was minimised by iterating the values of i_0 and b.

The solution that was obtained from this procedure is given in Table 5.5.a.

Table 5.5.a: Calculation of exchange current density (i_0) and the Tafel slope (b)

E (mV)	i_a (A/m^2)	E-E_a (mV)	η_a (mV)	Squared Errors	b(mV)	i_0 (A/m^2)	E_e
127.47	100.00	127.5	125.3	4.6	**202.9**	**24.1**	0
140.27	125.00	140.3	145.0	22.5			
163.70	150.00	163.7	161.1	6.8			
			SSE:	33.89			

These constants were used to determine the current density over a range of cell potentials. This relationship, together with the actual results that were obtained, is shown in Figure 5.5.g.

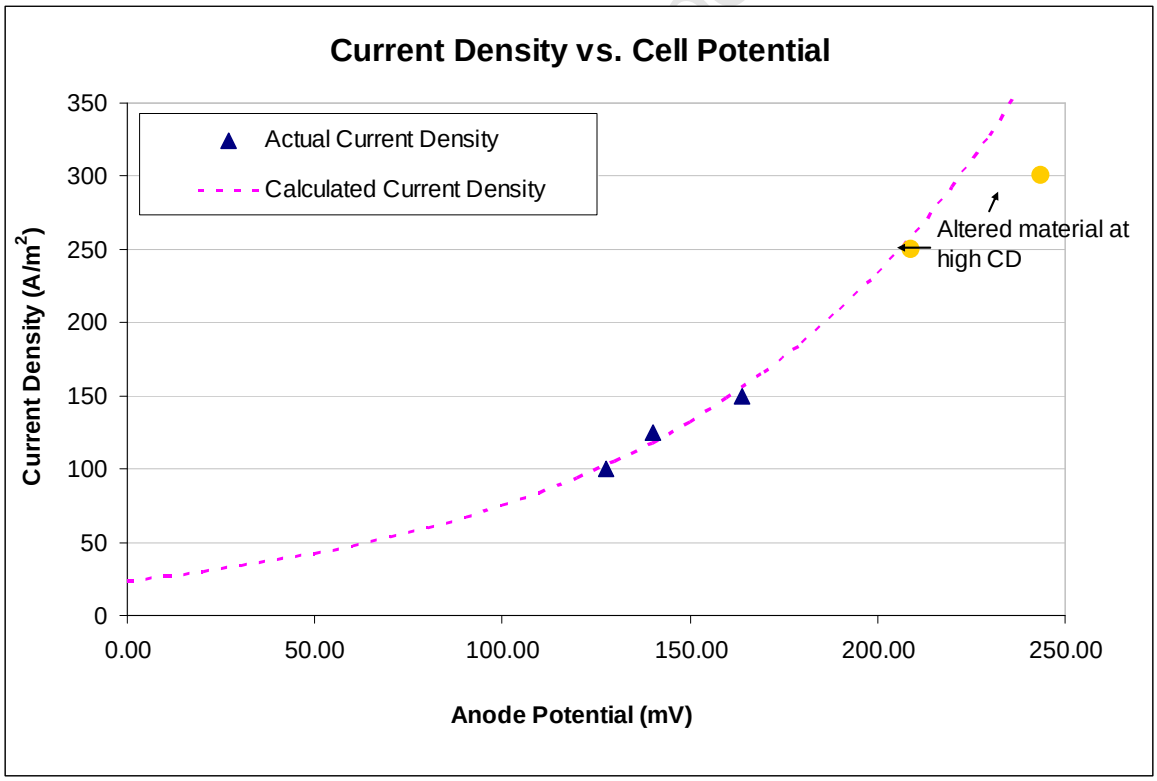

Figure 5.5.g: Actual and calculated relationship between current density and cell potential

An additional two tests were performed at higher current densities of 250 A/m^2 and 300 A/m^2 to determine what the highest viable current density will be for optimal operation. However, these tests were performed last and therefore on the altered

material. Caution is thus taken to compare these results with the rest of the results. It can be seen from the last two tests (Appendix I, Section D) that the cell potential increased significantly during the test due to anode passivation (as discussed earlier). However, the initial voltages of these tests might be useful to compare with the cell voltages of the rest of the tests. The initial cell voltages at these current densities were:

- 250 A/m^2: 0.209 V
- 300 A/m^2: 0.2435 V

These points are indicated with the yellow dots on Figure 5.5.g. It can be seen that the cell voltage of the 250 A/m^2 test also correlated well with the calculated relationship, but that at 300 A/m^2 the cell voltage started to deviate. This could be due to mass transport becoming the limiting factor, and that a current density of 300 A/m^2 exceeds the maximum mass-transport rate or it could simply be due to the anode composition. However, both of the last tests were performed with exactly the same material, as it was the same anode that was machined clean for the last test. There should thus be no difference in performance due to material composition; it is thus more likely that mass transport started to play a significant role.

5.5.3 Cu Concentration

In Test 7, the Cu concentration was set to be 50 g/l. Due to low ambient temperatures and the high concentration in the electrolyte, $CuSO_4$ started to crystallise in the feed box during the test. Thus, a significant drop in Cu concentration occurred. The average concentration (45 g/l) was, however, still higher than the base-case setting (40 g/l) and can thus still be compared to the base-case to a certain extent.

The effects of the change in Cu concentration on the power consumption, current efficiency, dissolution rate and product mass are as follows:

1) Power consumption

- 30 g/l: 0.121 kWh/kg anode; 0.126 kWh/kg cathode
- 40 g/l: 0.115 kWh/kg anode; 0.121 kWh/kg cathode
- 45 g/l: 0.122 kWh/kg anode; 0.128 kWh/kg cathode

2) Current Efficiency

- 30 g/l: Anodic = 99.9%; Cathodic = 98.4%

- 40 g/l: Anodic = 100.8%; Cathodic = 97.5%
- 45 g/l: Anodic = 99.8%; Cathodic = 98.5%

3) Anodic dissolution

- 30 g/l: 145.9 g/m^2.h
- 40 g/l: 147.3 g/m^2.h
- 45 g/l: 145.8 g/m^2.h

4) Product mass

- 30 g/l: Slimes: 38.82 g/kg anode; Cathode: 0.96 g/kg anode
- 40 g/l: Slimes: 31.05 g/kg anode; Cathode: 0.95 g/kg anode
- 45 g/l: Slimes: 42.51 g/kg anode; Cathode: 0.96 g/kg anode

It can be observed from all these variables, that the values for the 30 g/l and 45 g/l tests correlate closely with each other but not with the 40 g/l test. This is because the original material has changed slightly already since the 40 g/l test was performed. A number of re-castings had taken place before the Cu concentration tests were performed (test 6 and test 7). Thus, it might make more sense to only compare these two tests with each other.

The power consumption increased and the current efficiency and anodic dissolution rate decreased slightly with increasing copper concentration in the electrolyte. This is as expected as these parameters are inversely related to each other. However, the changes are very small and no real conclusions can be drawn.

The mass of slimes that were produced per kg of anode increased slightly with an increase in Cu concentration (see Figure 5.4.k), but this could also be attributed to the higher silica content in the original anode material (see Appendix I, Section E).

The cell potential measured for the three copper concentrations is shown in Figure 5.5.h. The general trend was an increase in cell potential with time, but no real differentiation can be made between the cell potentials at different Cu concentrations that were tested.

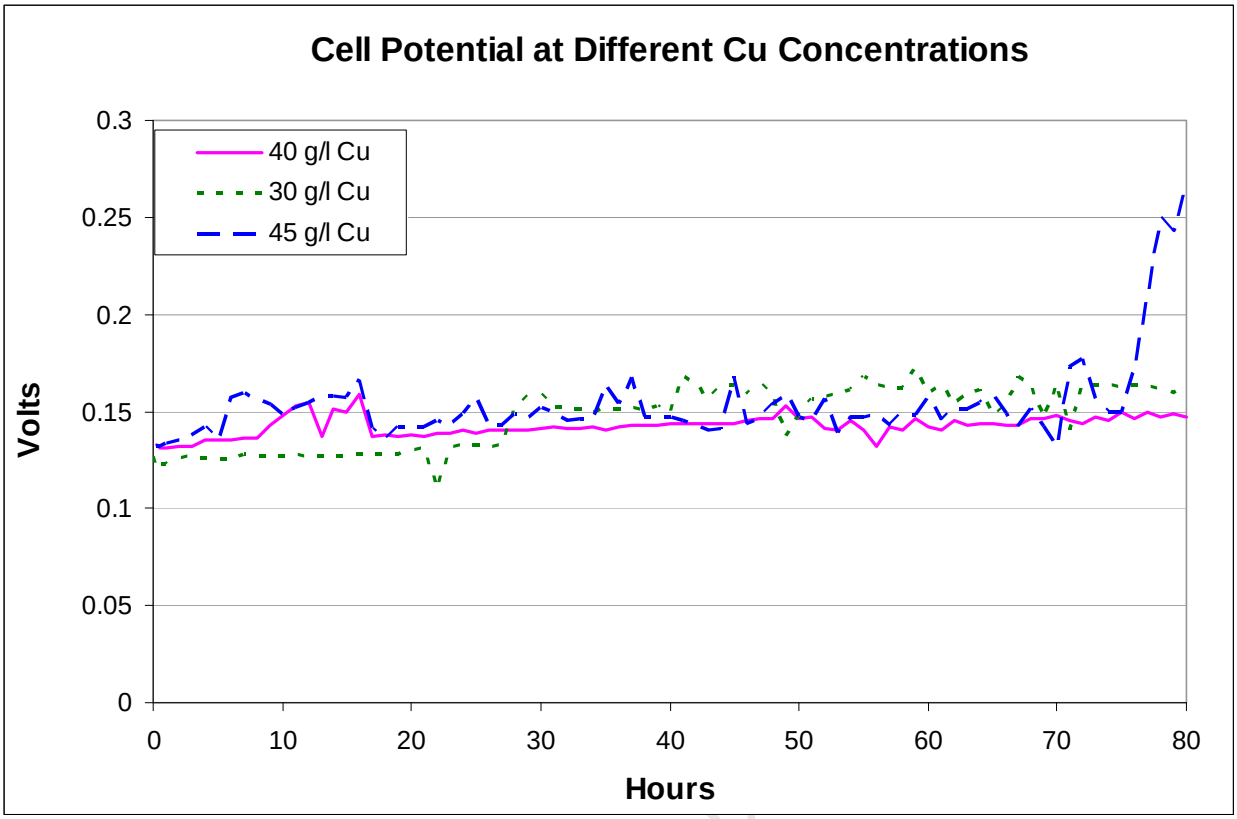

Figure 5.5.h: Comparison of cell potential at various Cu concentrations

When investigating the slimes/anode ratio of element masses, it is observed that the amount of the following elements in the slimes compared to the amount removed from the anode is higher at increased Cu concentrations:

- Lead
- Arsenic
- Silver
- Zinc
- Silicon

These observations also correspond with the deportment from the electrolyte and the anode to the slimes. Thus, it might be suggesting that an increase in Cu concentration resulted in a higher recovery of these elements. This might be due to a reduction of solubility of these elements at high metal concentrations in the electrolyte.

5.5.4 H_2SO_4 Concentration

The effect of acid was tested at the base conditions of 40 g/l copper, 125 A/m^2 and 65˚C. The 130 g/l and 190 g/l sulphuric acid tests, Test 8 and Test 9, were conducted after the anode composition had changed. It is therefore difficult to evaluate the effect of acid concentration on the process. However, the cell potential during these two tests can give some information regarding the effect of H_2SO_4 concentration on electrorefining (see Figure 5.5.i).

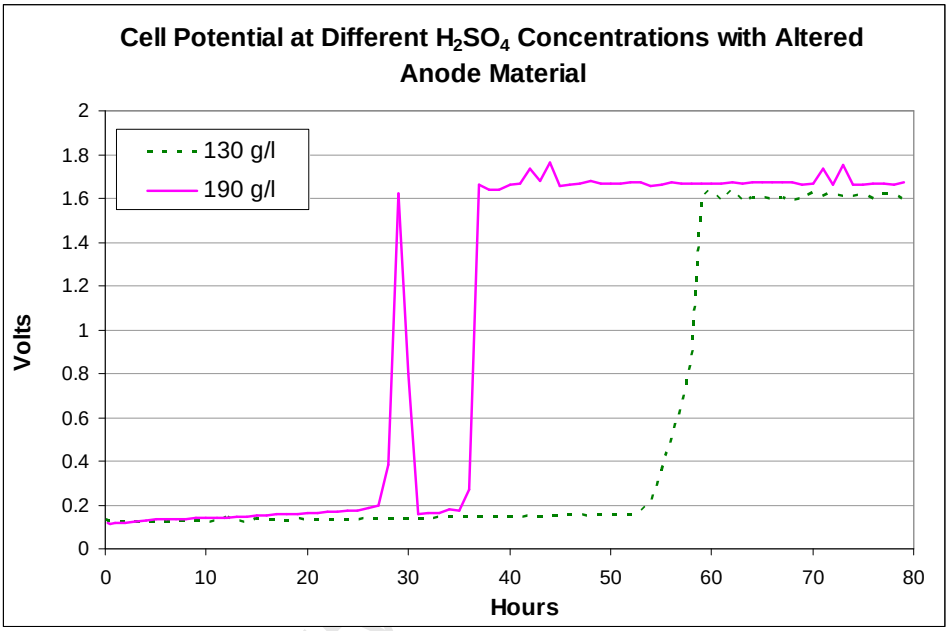

Figure 5.5.i: Comparison of cell potential at different H_2SO_4 concentrations for altered anode material

The cell potential measured for the 130 and 190 g/l tests increased abruptly after 58 hours and 36 hours, respectively, indicating anode passivation. The absence of anode passivation at 160 g/l acid as compared to the passivation observed at 130 g/l acid, shows that the passivation was linked to the anode composition and not to H_2SO_4 concentration. It is most likely that the composition and/or physical properties of the anode are the primary cause of passivation. No passivation of the anode took place at 160 g/l acid but this would be because the anode had more Cu available for dissolution than the altered material used for the tests shown in Figure 5.5.j. The acid concentration, however, did affect the time before passivation for these anodes. The shortening of time before passivation at higher concentrations indicated that high acid concentration exacerbates anode passivation. It is likely that the shortening of time before passivation at higher acid concentrations is due to the normally dissolving Cu being dissolved faster at higher acidities similar to the following reaction: $Cu+2H^+ \rightarrow Cu^{2+}+H_2$. After all the dissolvable Cu is removed from the anode,

only the contaminated alloy remains which does not dissolve and subsequently result in a higher cell potential which indicates anode passivation.

For the purpose of investigating the effect of H_2SO_4 concentration on the actual power consumption, current efficiency, dissolution rate and product mass, only test 1 at 110 g/l and test 2 at 160 g/l H_2SO_4 without additives were compared.

1) Power consumption

- 110 g/l: 0.225 kWh/kg anode; 0.217 kWh/kg cathode
- 160 g/l: 0.118 kWh/kg anode; 0.124 kWh/kg cathode

2) Current Efficiency

- 110 g/l: Anodic = 94.2%; Cathodic = 98.8%
- 160 g/l: Anodic = 102.4%; Cathodic = 98.6%

3) Anodic dissolution

- 110 g/l: 137.6 $g/m^2.h$
- 160 g/l: 149.5 $g/m^2.h$

4) Product mass

- 110 g/l: Slimes: 27.83 g/kg anode; Cathode: 1.03 g/kg anode
- 160 g/l: Slimes: 31.18 g/kg anode; Cathode: 0.95 g/kg anode

The power consumption was significantly higher at low acid concentrations. This is as expected as H_2SO_4 increases the conductivity of the electrolyte (see literature review Section 2.2.2). This also explains the lower anodic current efficiency and anodic dissolution at low H_2SO_4 concentrations. However a current efficiency of >100% experienced at high H_2SO_4 concentration indicates added dissolution of the anode purely due to leaching of Cu in the highly acidic solution. All consequent tests at similar concentrations indicated the same results (Table 5.3.b).

An increase in slimes product mass is also observed at higher H_2SO_4 concentrations. This could be due to a change in anode composition or a reduction of solubility of a number of elements due to high acidic concentration. Especially Cu seemed to be recovered to the slimes to a greater extent at higher acid concentration (see Figure 5.3.e and Figure 5.3.i). Thus, the most PGM-concentrated residue was produced at low acid concentration (Figure 5.4.a).

The cell potentials at 110 g/l and 160 g/l H_2SO_4 are shown in Figure 5.5.j. It can be seen that the cell potential at 110 g/l was very high for the first 45 hours of the test. Upon inspecting the cell connections during this test, it was discovered that the wires in the cables connecting the power supply and the back cathode were detached from the connector. It was therefore assumed that there was no current flow in the back cathode for the first 45 hours. Consequently, the mass of copper deposited on the front cathode was four times more than that on the back cathode. This is an indication that the operating current density on the front cathode was double the set point (250 A/m^2) for the first 45 hours before it was reduced to 125 A/m^2 when the cables were properly connected.

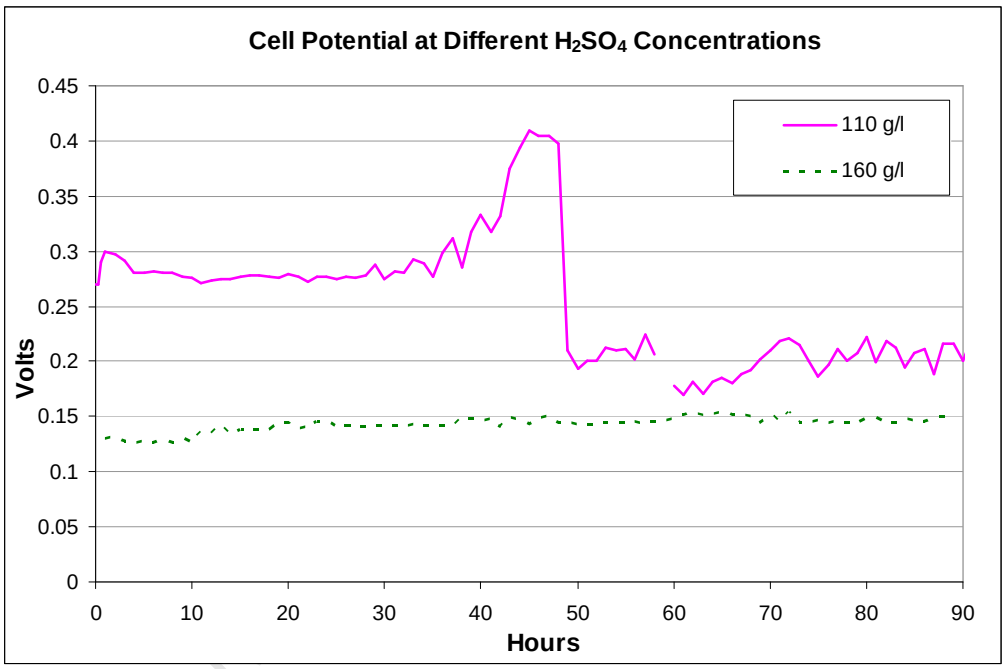

Figure 5.5.j: Comparison of cell potential at different H_2SO_4 concentrations

The cause for the increase in voltage measured on the front cathode between 40 to 45 hours for the 110 g/l test was not confirmed, but it could have been caused by anode sludge accumulation on the anode surface, resulting in increased resistance which caused the voltage to increase. The anode sludge accumulation could have been a result of the high rate of anode dissolution on the surface facing the front anode at the high current density (~250 A/m^2).

After the current density was restored to 125 A/m^2, the cell potential was still higher than the cell potential at 160 g/l H_2SO_4 which indicates lower electrolyte conductivity, as expected.

6.1 Process Design Background

A preliminary process design was performed based on the current production of SLC (550 t/m) and estimated mass reduction (80%) by the proposed pyrometallurgical treatment of SLC. A design factor of 15% is incorporated in the design to allow for down time due to cell cleaning and maintenance as well as the possibility of increases in capacity requirement. The proposed process design will fit in to the current BMR process flow as indicated by Figure 6.1.a.

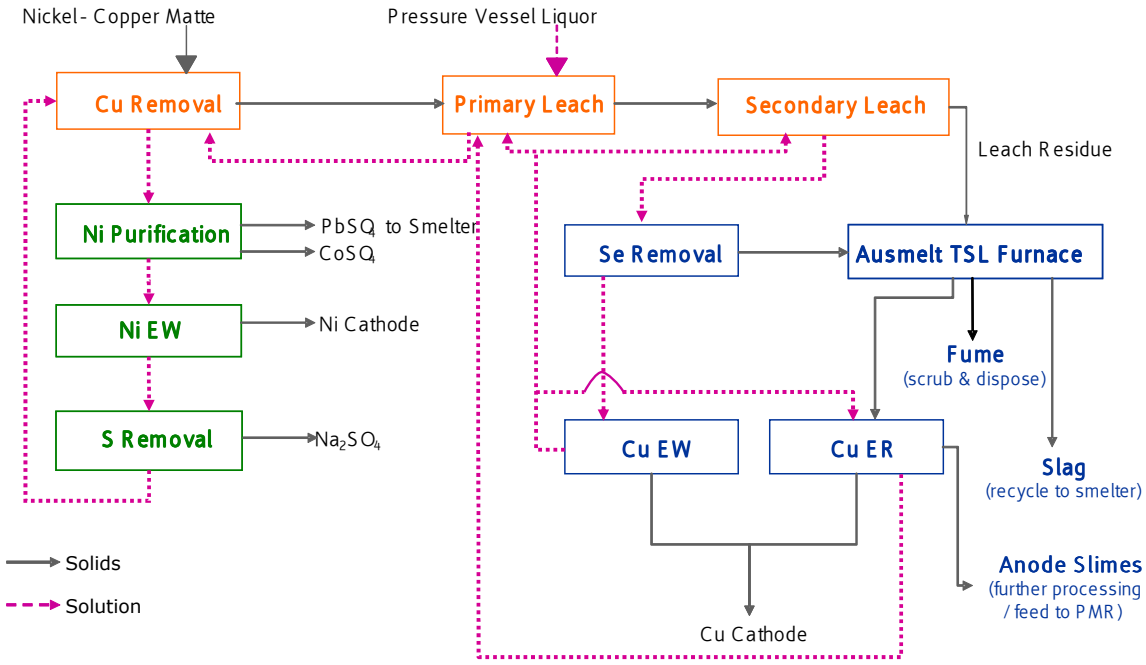

Figure 6.1.a: Proposed flow sheet of Base Metals Refinery

The optimal electrolyte concentrations of 40 g/l Cu and 160 g/l H_2SO_4 at 65˚C and a current density of 200 A/m^2 are proposed for the process design. Even though no valid testwork at this current density was performed on the given material, it is suggested to be a suitable current density due to the fact that current efficiency was still very high at 150 A/m^2 and no passivation took place. However, due to the nature of the anode material (not high Cu purity) it is expected that very high current densities, as applied by other electrorefining operations, might result in problems in terms of anode passivation and low current efficiencies. Thus 200 A/m^2 and anodic and cathodic current efficiencies of 98% and 95%, respectively, are chosen as a worst case scenario for production. It is possible to optimise the process or prove that higher current densities can be used without excessive power consumption.

Design anode, cathode and cell dimensions were chosen according to typical plant designs as obtained during the literature review. The number of anodes, cathodes and cells are calculated based on the amount of anode material that needs to be treated per month. The fresh electrolyte feed required to maintain Cu and H_2SO_4 concentrations and power consumption of the entire tank house (given that all cells operate in series and electrodes in a cell operate in parallel) are calculated as well. The total voltage required is the sum of the cell voltages for 6 cells in parallel (6 x 0.2 V). A small number of large cells are chosen as opposed to a larger number of smaller cells in order to minimize the voltage required from the rectifier.

6.2 Process Design Parameters

The assumptions, design parameters, calculated variables and final production figures and energy consumption are given below:

Feed:				
Current SLC Residue:	550	t/m	6600	t/a
Pyrometallurgical treatment reduces SLC mass by	80%			
Cu Alloy tonnage	110	t/m	1320	t/a
Minimum extra capacity to design for	15%			
Minimum design capacity	127	t/m	1518	t/a
Constant Variables & Assumptions:				
Molar mass (Cu)	63.55	g/mol		
Molar mass (Ni)	58.69	g/mol		
Molar mass (Fe)	55.85	g/mol		
Anode composition:				
% Cu	84%			
% Ni	12%			
% Fe	4%			
n (moles of electrons transferred)	2			
Faraday constant	96488	C/mol		
Density of Cu Alloy	8200	kg/m^3		
Anodic current efficiency	98%			
Cathodic current efficiency	95%			
Design Parameters:				
Current density	200	A/m^2		

Cu concentration	40	g/l
Acid concentration	160	g/l
Temperature	65˚C	
No of cells	6	cells
Anodes		
Length of anode	1	m
Witdth of anode	1	m
Anode starting thickness	0.04	m
% Anode un-dissolved	20%	
No. Anodes per Cell	64	anodes/cell
Total no. of anodes	384	anodes
Time required for 1 anode cycle	24	days/anode cycle
Cathodes		
Length of cathode blank sheet	0.9	m
Width of cathode blank sheet	1	m
Thickness of cathode blank sheet	0.01	m
No. of cathodes blank sheets per cell	65	cathodes blanks
Total no. of cathodes blank sheets	390	cathodes blanks
Total no. of Cu deposit sheets	768	Cu deposit sheets
Time required for 1 cathode cycle	12	days/cathode cycle
Cell		
Cell voltage	0.2	V
Cell height	1.2	m
Anode-cathode spacing	0.05	m
Cell length	9.6	m
Cell width	1.1	m
Cell volume	12.7	m^3
Calculated variables:		
Anodes		
Anode surface area	1	m^2
Anode surface area per cell	128	m^2/cell
Starting mass of anode	328	kg
Mass anode dissolved	262.4	kg
Mass anode remaining	65.6	kg
Anode volume remaining	0.008	m^3
Anode final width	0.8	cm
Anode dissolution	229.1	$g/m^2.h$

Mass to dissolve per cell per anode cycle	16 794	kg/cell/anode cycle		
Anode dissolved per cell per month	21 114	kg/cell/m		
Cu dissolved from anode per cell per month	17 736	kg Cu/cell/m		
Anode cycles/month	1.3	anode cycles		
Cathodes				
Cathode surface area per cathode	1.8	m^2		
Cathode surface per cell	115	m^2/cell		
Cu deposit sheet weight	58.4	kg/cathode		
Cathode deposition	225.3	$g/m^2.h$		
Mass cathode to plate per cell per cathode cycle	7473	kg/cell/cathode cycle		
Cu plated per cell per month	18 683	kg/cell/m		
Cathode cycles per month	2.5	cathode cycles		
Electrolyte				
Cu plated from fresh electrolyte per cell per month	947	kg/cell/m		
Fresh electrolyte feed rate required per cell	33	l/h/cell		
Total electrolyte feed required	197	l/h		
Total electrolyte inventory	76	m^3		
Current required for specified design current density	23 040	A/cell		
Cells required to dissolve design capacity	5.99	cells		
Products:				
Anode feed capacity	127	t/m	1 520	t/a
Cu production capacity	112	t/m	1 345	t/a
Slimes production capacity	4.2	t/m	50.3	t/a
kg Cu Produced per kg Anode dissolved	0.88	kg/kg anode		
Downtime available (if only 110 t/m processed)	4.6	days/month	55.4	days/annum
% over design	15.2%			
Energy Consumption:				
Current	23040	A		
Total voltage	1.2	V		
Power	27.6	kW		
Power consumption/kg anode treated	0.175	kWh/kg		
Power consumption/kg cathode produced	0.178	kWh/kg		

7 CONCLUSIONS

The testwork showed that electrolytic refining of the Cu alloy, produced by a two stage pyrometallurgical treatment of current SLC, produces a highly concentrated PGM residue at an overall SLC mass reduction of 99.3%, with excellent PGM recovery to the anode slimes material. The different operating parameters that were tested successfully all showed very good repeatability and greater than 99% PGM recovery, which would result in an overall recovery of 98% from SLC. An unfortunate contamination of the original material occurred before high current densities and different H_2SO_4 concentrations could be tested. The phases present in the anodes used for these tests were alloys of the Cu, Ni, Fe and Si as a silicide instead of the Cu, Ni metal matrix found in the original material that was used for the initial tests. The results obtained from these tests were very different from the initial tests and it is acknowledged that these differences are not a function of the operating parameters that were tested but of the change in anode composition.

The typical operating conditions that were observed correlated well with literature and the theoretically calculated values. The characteristics of anode slimes stayed relatively similar throughout the different operating parameters and strong confidence can be placed in the production thereof and the recovery of the PGMs. The characteristics of the spent electrolyte and the Cu cathodes were also found to be suitable for integration in the BMR circuit. The results obtained during this testwork are discussed in detail in this section.

Cell Voltage and Power Consumption

The cell potential measured between the anode and the cathode was generally between 0.13 and 0.2 V. The lowest cell voltage obtained was at low current density (100 A/m^2), and the highest at high current density (150 A/m^2). Cu concentration did not have a significant effect on cell voltage but low H_2SO_4 concentration contributed to an increased cell voltage. The cell potential increased slowly as time progresses during electrorefining. It is suspected that a build-up of slimes on the anode surface and an increase in suspended solids are the main contributors to this potential increase. The power consumption varied between 0.104 – 0.217 kWh/kg cathode produced and 0.111 – 0.225 kWh/kg anode dissolved. The power consumption was lower at low current densities but a low acid concentration resulted in an increase in power consumption due to the reduction of the solution conductivity.

The high field approximation to the Butler-Volmer equation and the experimental results were used to determine the exchange current density and the Tafel slope. The best fitted values for these were 24.13 A/m^2 and 202.99 mV, respectively. The test performed at 250 A/m^2 current density also correlated well with the calculated relationship, but at 300 A/m^2 the cell voltage started to deviate. This could be due to mass transport becoming the limiting factor at such high current densities or simply due to the change in anode composition.

Current Efficiency and Anode Dissolution

In most cases where the initial anode material was original and the acid concentration was high, the anode current efficiency was higher than 100%. It is concluded that current is not the only contributor to the dissolution of anodes but that base metal leaching from the anode also occurs due to the acidity of the electrolyte. It was also observed that current efficiencies of >98% for the deposition of Cu can be obtained and that the addition of smoothing additives adversely affects the current efficiency. Current efficiency did not decrease with increased current density.. It is therefore suspected that a higher operating current density than the tested 150 A/m^2 might be optimal for production without excessively compromising efficiency.

Anode dissolution for the current densities tested ranged from 118.68 g/m^2.h at 100 A/m^2 and 181.3 g/m^2.h at 150 A/m^2. These masses are 1.5 x of each other which is what is to be expected from Faraday's law. It can be concluded that current density is the main determining factor for anode dissolution rates and not Cu and H_2SO_4 concentrations.

Element Deportment

It was found that the recovery of PGMs from the anode to the anode slimes is very close to 100% in most cases. This is desirable because it indicates that no PGM loss occurs during the transformation of the anode to the anode slimes. In cases where PGMs were in solution prior to electrorefining, the deportment of all the PGMs from the anode and electrolyte is not 100% to anode slimes. Rh, Ru and Ir especially show some deportment to the electrolyte. This could however be due to a variability in electrolyte analysis.

Very little or none of the base metals that were supplied by the anode or the electrolyte feed reported to the anode slimes. With a Cu recovery of less than 0.1% to anode slimes, more than 99.9% of the Cu from the anode stayed in solution and/or

deposited on the cathode. In the same way, ~100% of Ni reported to electrolyte as well as ~99.7 – 99.95% of the Fe.

The mass of Se and Te in the anode slimes is two to twelve times more than was supplied by the anode. This indicates that some of the Se and Te in solution reacted with other elements and precipitated to the slimes. The slimes/anode ratio for Pb is in a high range of 0.7 – 1. Only 10 – 30% of the As was removed to the electrolyte, and the majority of the Ag reported to the anode slimes. It was found that Zn and Sn are almost completely dissolved in the electrolyte. The mass of Sb and Bi present in the slimes is up to 80% less than it was in the anode.

Product Characterisation

The anode slimes composition was generally 20-30% PGMs, 20-30% base metals, 15-20% Ag, As, Te, Se, Pb and 2-5% Al, Si, Sb, Bi, Zn and Sn. This leaves ± 20% unaccounted for, which is suspected to be composed mainly of oxygen in the form of oxides. If these typical anode slimes material is to be blended with the annual PMR feed, the increased mass of feed material to PMR will have a Pt grade of 4 to 5.5% lower, Cu grade of 2 to 4% higher and Ni grade of ±4% lower than the current PMR feed. Other concerns are the increase of As, Te, and Pb by between 0.5 and 1%. The most PGM-concentrated residue was produced at low H_2SO_4 concentration at the cost of low current efficiency and high power consumption.

The major phase in the original anode is a light grey Cu-Ni-Fe alloy with a composition very similar to the overall composition of the Cu alloy, possibly with a distribution of PGMs at low levels. There is also a dark grey bleb-like phase consisting mostly out of Cu, S and Te which points to the presence of copper sulphides and copper tellurides and, lastly, a small very bright phase containing mainly Pb-Bi-Ag and some Pd with a small amount of Cu and Ni dispersed in it. Similar phases were found in the anode slimes. The light grey matrix phase composition has, however, changed to a phase rich in PGMs, palladium, arsenic and tellurium [$Pd_{73}As_6Te_{21}$], with small amounts of Cu. An amorphous phase amounting to 60-80% of the mass composition was also present within this matrix. These two phases contain most of the PGMs in the slimes (up to 60% PGM).

The Ni concentration in the spent electrolyte is between 50 and 60 g/l and slightly lower than a typical Ni electrowinning feed concentration of 70 g/l. It also contains impurities like Cu, Pb, Co, Fe, Zn which will result in significant contamination of the Ni cathodes. Thus, the electrolyte stream will have to be subjected to purification

before the Ni can be recovered. Due to the high acidity of this solution, it would be most suitable to use it as a lixiviant in the pressure leaching of Ni stage. Thereby, the Ni concentration would be increased and the acidity would be reduced by the leaching reactions. Only Se, Te, Ni and Fe in the Cu cathodes produced during the testwork showed content higher than the target specified by the LME grade A specifications.

The average slimes and cathode production are 33 g and 1 kg per kg of anode, respectively. This equates to an SLC mass reduction of 99.3%, an additional Cu production of 1320 t/a, and slimes production of 43.5 t/a.

Process Design

A preliminary process design was performed with proposed design parameters of electrolyte concentrations of 40 g/l Cu and 160 g/l H_2SO_4 at 65˚C and a current density of 200 A/m^2. The process was designed to treat 110 t/m of anode material with a design factor of 15%, at anodic and cathodic current efficiencies of 98% and 95%, respectively.

The process consists of seven electrolytic cells in series with 55 anode cathode pairs in parallel per cell. The anode dimensions are 1 m x 1 m x 4 cm and the cathodes 1 m x 0.9 m. The process has a maximum capacity of 127 t/m of anode material which allows 56 days of downtime per year if only 110 t/m is treated. The maximum capacity for Cu production is 112 t/m and anode slimes, 4.2 t/m. The power consumption per kg of anode dissolved will be 0.175 kWh/kg. It is possible to optimise the process to increase current efficiencies or prove that higher current densities can be used without excessive power consumption.

8 RECOMMENDATIONS

Following the above investigations, there are a number of consequent issues that need to be considered or investigated before proceeding with the selection of an SLC process route. Some of these are listed below.

1) The influence of acid concentration and high current density on the original copper alloy material could not be clearly observed due to the change in anode composition. It would prove worthwhile to investigate higher current densities in order to determine the optimal current density before mass transport and anode passivation becomes limiting. This way, maximum production can be obtained, while reducing both capital and operating costs. It is possible that different acidity might also lead to better operation.

2) The procedure and design of the anode casting stage should be investigated and tested in order to produce suitable anodes for electrorefining cost efficiently.

3) The downstream effects of reduced Pt and increased Cu, Te, Pb and As in the PMR feed should be investigated to determine the viability of integrating the anode slimes with the PMR feed directly or to the metallics section in PMR, The maximum capacity for these elements in PMR and the possible bleed locations from the process to prevent impurity build-up also should be determined.

4) If it is found that the slimes composition is not suitable to blend with PMR feed, further processing steps, like decopperising, should be tested on anode slimes in order to produce an upgraded residue for treatment in PMR.

5) A cumulative cost analysis in terms of capital and production costs should be performed on the pyrometallurgical anode casting as well as electrorefining stages to show the feasibility of the proposed process. The current toll-refining contract should be investigated in detail in order to accurately specify the magnitude of the saving based on the projected capital and operating costs of the new proposed process.

6) The availability of existing equipment that can be re-used for the construction of the new plant should be investigated to reduce capital cost. There is a possibility of modifying the previously used Anglo Platinum Converting Process pilot plant for the two-stage Ausmelt process and also using existing tankhouse equipment from BMR to compose the cells required for electrorefining.

9 REFERENCES

Amer, A.M. (2003) *"Processing of copper anodic-slimes for extraction of valuable metals",* Waste Management, Vol 23, pp 763-770

Andrews, L. (2008) *"Mineralogy of trial Ausmelt samples"*, Mineralogy Report No: M/08/31, Mineralogical Research Department, Anglo American.

Andersen, T.N. Pitt, C.H. Livingston, L.S. (1982) *"Nodulation of electrodeposited copper due to suspended particulate",* Journal of Applied Electrochemistry, Vol 13 Number 4, pp 429-438

Asarco, Mineral Discovery Centre, 17 July 2009, image at: www.asarco.com/AMDC/smelting.html

Beauchemin, S. Chen, T.T. Dutrizac, J.E. (2007) *"Behaviour of antimony and bismuth in copper electrorefining circuits"*, Canadian Metallurgical Quarterly, Vol 47, Number 1, pp 9-25

Biswas, A. K. Davenport, W.G. King, M. Schlesinger, M. (2002) *"Extractive Metallurgy of Copper"*, Fourth Edition, Pergamon Press, Elsevier Science, pp 247 - 283

Casas, J.M. Alvarez, F. Cifuentes, L. (2000) *"Aqueous speciation of sulfuric acid-cupric sulfate solutions"*, Chemical Engineering Science, Vol 55, pp 6223-6234

Chen, T.T. Dutrizac, J.E. (1988) "*The behaviour of gold and silver during copper electrorefining*", BMR Technical library, ID 9668

Chen, T.T. Dutrizac, J.E., a (1989) *"A mineralogical study of the deportment and reaction of silver during copper electrorefining",* Metallurgical and Materials Transactions B, Vol 20, Number 3, pp 345-361

Chen, T.T. Dutrizac, J.E., b (1989) *"A mineralogical overview of the behaviour of Nickel during copper elctrorefining"*, Metallurgical and Materials Transactions B, Vol 21, Number 2, pp 229-238

Chen, T.T. Dutrizac, J.E. (2004) *"Gold in the electrorefining of copper and the decopperizing of copper anode slimes"*, Gold Process Mineralogy Part II, pp 48-52

Chen, T.T. Dutrizac, J.E. (2005) *"Mineralogical characterization of a copper anode and the anode slimes from the La Caridad copper refinery of Mexicana de Cobre"*, Metallurgical and Materials Transactions B, Vol 36B, pp 229-240

Cifuentes, L. Casas, J.M. Simpson, J. (2007) *"Modelling the effect of temperature and time on the performance of a copper electrowinning cell based on reactive electrodialysis"*, Chemical Engineering Science, Vol 63, pp 117-1130

Cifuentes, L. Simpson, J. (2005) *"Temperature dependence of the cathodic and anodic kinetics in a copper electrowinning cell based on reactive electrodialysis"*, Chemical Engineering Science, Vol 60, pp 4915-4923

Cifuentes, L. Casas, J.M. Simpson, J. (2006) *"Temperature dependence of the speciation of copper and iron in acidic electrolytes"*, Chemical Engineering Research and Design, Vol 84(A10), pp 965-969

Dinham, P. (2006) *"Mineralogical study of leach residues from the Dynatec pilot plant trial",* Anglo Research Report, M/06/11

Dönmez, B. Ekinci, Z. Çelik, C. Çolak, S. (1999) *"Optimisation of the chlorination of gold in decopperised anode slime in aqueous medium"*, Hydrometallurgy, Vol 52, pp 81-90

Dynatec. (2006) *"Rustenburg BMR Expansion. Hydrometallurgical Testwork"*, Dynatec Corporation, Job 260, Vol 1 & 2

Gu, Z.H. Chen, J. Fahidy, T.Z. (1994) "*A study of anodic slime behaviour in the electrorefining of copper*", Hydrometallurgy, Vol 37, pp149-167

Hanf, N.W. Frampton, G.L. Farrell, L.J. (1989) "*Copper bullion treatment for the recovery of precious metals*", BMR Technical library, Vol ID 0-1436, ID 1772; Project ref. No 500.3039P88P/P89/1

Hayes, P. (2003) "*Electrorefining of Copper*", Process Principles in Mineral and Materials Production, Third Edition, pp 352 – 360

Hiskey, J.B. Cheng, X. (1998) *"Fundamental studies of copper anode passivation during electrorefining Part III. The effect of thiourea",* Metallurgical and Materials Transactions B, Vol 29B, pp53-58

Hiskey, J.B. (1999) "*Principles and practical considerations of copper electrorefining and electrowinning*", Copper Leaching Solvent Extraction, and Electrowinning Technology, pp 169 – 172

Hofirek, Z. (2001) *"Secondary leach residue (SLR) production, characterisation and treatment",* Anglo Platinum Technical Report, ref: RBMR-108

Ilkhchi, M.O. Yoozbshizadeh, H. Safarzadeh, S.M. (2000) "*The effect of additives on anode passivation in electrorefining of copper*", Chemical Engineering and Processing, Vol 46, pp 757 – 763

Janik, R. (2001) "*Ductility additives for electrorefining and electrowinning*", United States Patent 6183622, Plymouth, MI, Primary class: 205/585

Jin, S. Gali, E. (2001) *"Effect of thiourea on the copper cathode polarization behaviour in acidic copper sulphate at 65˚C"*, Metallurgical and Materials Transactions B, Vol 32B, pp 887-893

McKay, D.J. Peters, E. (1991) "*The electrorefining of copper-rich alloys using particulate anodes*", BMR Technical library, Report No15 0-6362

Moats, M.S. Hiskey, J.B. Collins, D.W. (2000) *"The effect of copper, acid, and temperature on the diffusion coefficient of cupric ions in simulated electrorefining electrolytes."* Hydrometallurgy, Vol 56, pp 255-268

Moskalyk, R.R. Alfantazi, A.M. (2003) *"Review of copper pyrometallurgical practice: today and tomorrow"*, Minerals Engineering, Vol 16, pp 893-919

Muresan, L. Varvara, S. Maurin, G. Dorneanu, S. (1999) *"The effect of some organic additives upon copper electrowinning from sulphate electrolytes"*, Hydrometallurgy, Vol 54, pp 161-169

Nicol, M. (2008) "*Hydrometallurgy Theory and Practice Study Guide 2008*", Module 8, University of Cape Town, pp 55 – 58

Nyirenda, R.L. Phiri, W.S. (1997) *"The removal of nickel from copper electrorefining bleed-off electrolyte"*, Minerals Engineering, Vol 11, Number 1, pp 23-37

Petkova, E.N. (1997) *"Mechanisms of floating slime formation and its removal with help of sulphur dioxide during the electrorefining of anode copper"*, Hydrometallurgy, Vol 46, pp 277 – 286

Pletcher D. Walsh F.C. (1990) *"Industrial Electrochemistry"* Second Edition, Kluwer, pp 231 - 237

Radhakrshnamurthy, P. Srinivasan, G.N. Srinivasan, R. (1980) "*Scope of periodic current reversal in electrorefining of copper*", Electrochem. Soc. India, Vol 29, Number 4, pp 280-282

Schoolscience.co.uk , 17 July 2009, image at: http://resources.schoolscience.co.uk/CDA/14-16/cumining

Sedzimir, J. Gumowska, W. Haranczyhk, I. Kustowska, B. Jasinska, B. Pasierb, H. (1985) *"Silver, nickel, arsenic and antimony behaviour in the process of electrorefining of copper in the copper ammine electrolyte"*, BMR Technical library, Report No 2733

Verotnikov, M. Borbat, V. Kuzmichev, G. (1969) "*Behaviour of iridium and ruthenium in electrorefining of copper*", BMR Technical library, Report No 2 0-653

Viljoen, K. (2007) *"Removal of impurities from the secondary leach residue at Anglo Platinum Base Metal Refiners. Part 1: Literature Review"*, Anglo Research, Project No. P200701632, Report No. 1

Xiao, F. Zheng, Y. Wang Y. Xu, W. Li, C. Jian, H. (2007) *"Novel technology of purification of copper electrolyte"*, Trans.Nonferrous Met. Soc. China, Vol 17, pp 1069-1074

APPENDIX I

I. APPENDIX I

A. Background of BMR Expansion

The BMR nickel production will be increased from 21 000 to 33 000 t/a. In addition to this, a pressure iron removal circuit will be implemented. The aim is to dissolve all the Fe that would normally report to the SLC, and re-precipitate it elsewhere in the circuit to separate Fe effectively recycle it to the Waterval Smelter. The BMR flow sheet after the expansion will be as follows:

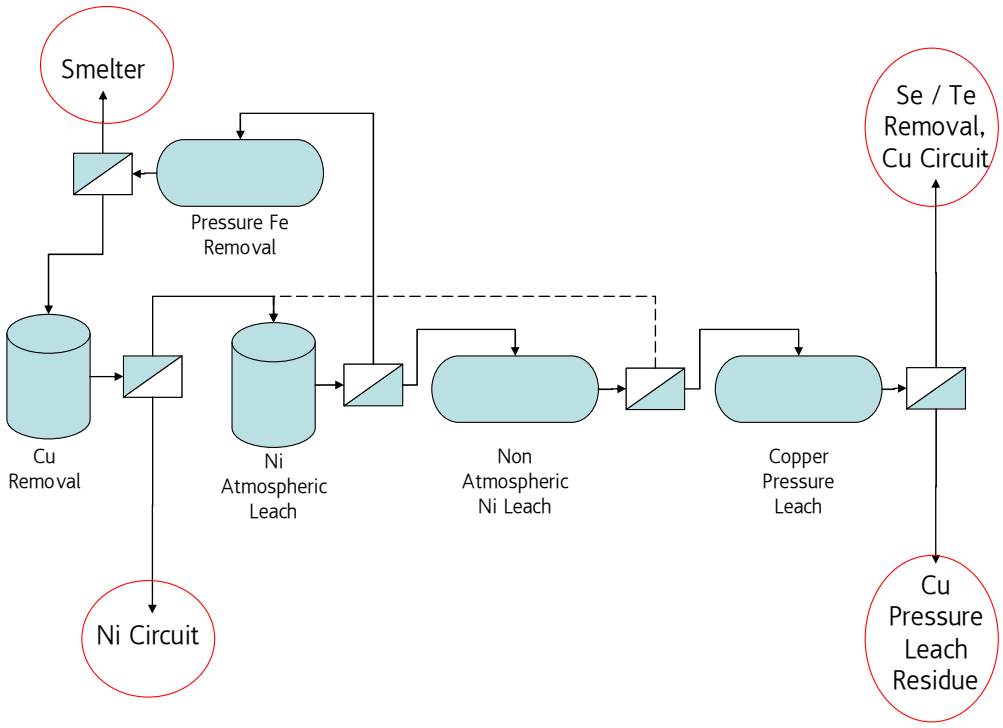

Figure A.1: Future process flow of base metals refinery, Anglo Platinum

SLC will undergo a ±70% mass reduction after most of the iron is removed in this new process. This has significant effects on transport and refining costs for toll refining. The new residue will be referred to as Copper Pressure Leach (CPL) residue. Figure shows the projected composition of the CPL (Dynatec, 2006).

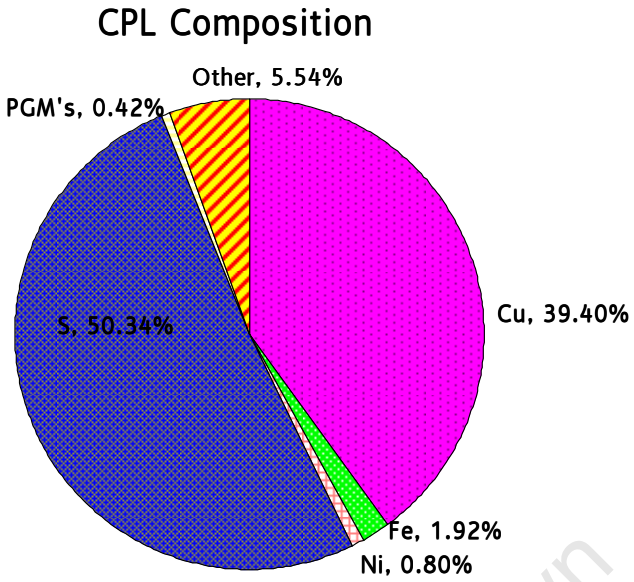

Figure A.2: Predicted composition of the CPL residue after expansion of BMR

B. Raw Material Composition

Table B.1: Composition of Ausmelt TSL furnace product – Cu alloy (electrorefining raw material)

Pt	ppm	735.67	Si	%	<0.1
Pd	%	0.39	Te	ppm	891.67
Rh	ppm	1038.67	Sb	ppm	791.67
Ru	ppm	1387.33	Bi	ppm	420.00
Ir	ppm	40.33	Sn	ppm	108.33
Os	ppm	5.67	Se	ppm	61.33
Au	ppm	351.67	Ti	ppm	<20
Ag	ppm	918.33	Mn	ppm	14.73
Cu	%	82.39	Cd	ppm	<2
Ni	%	11.97	Pb	%	0.284
Fe	%	3.97	As	%	0.250
Co	%	0.147	Al	%	<0.1
Ca	%	<0.1	S	%	0.160
Mg	%	<0.1	Cr	%	<0.1

C. Comparison of Leaching vs. Electrorefining

Table C.2: Advantages and disadvantages of pressure leaching vs. electrorefining

	Advantages	Disadvantage
Pressure Leaching	• BMR already experienced in pressure leaching of base metals. • H_2SO_4 available on site • Recovery of Ni and Cu in solution.	• Have to dissolve 97% of residue – energy intensive. • Will require capital projects for installation of setup. • Need graining operation for plant setup as well as test work. • Not necessarily 100% removal of base metals. • Possible dissolution of some PGMs with base metals.
Electrorefining	• Simultaneous production of Cu as cathode – cuts out significant pipeline. • Recovery of Ni in solution • Existing tank house facilities • BMR also experienced in tank house operation	• High value PGM slimes handling in Cu tank house – security issue. • Possible co-deposition of impurities with copper. • Possible losses of PGMs to electrolyte. (Buildup)

D. Test Accuracy

Test 1

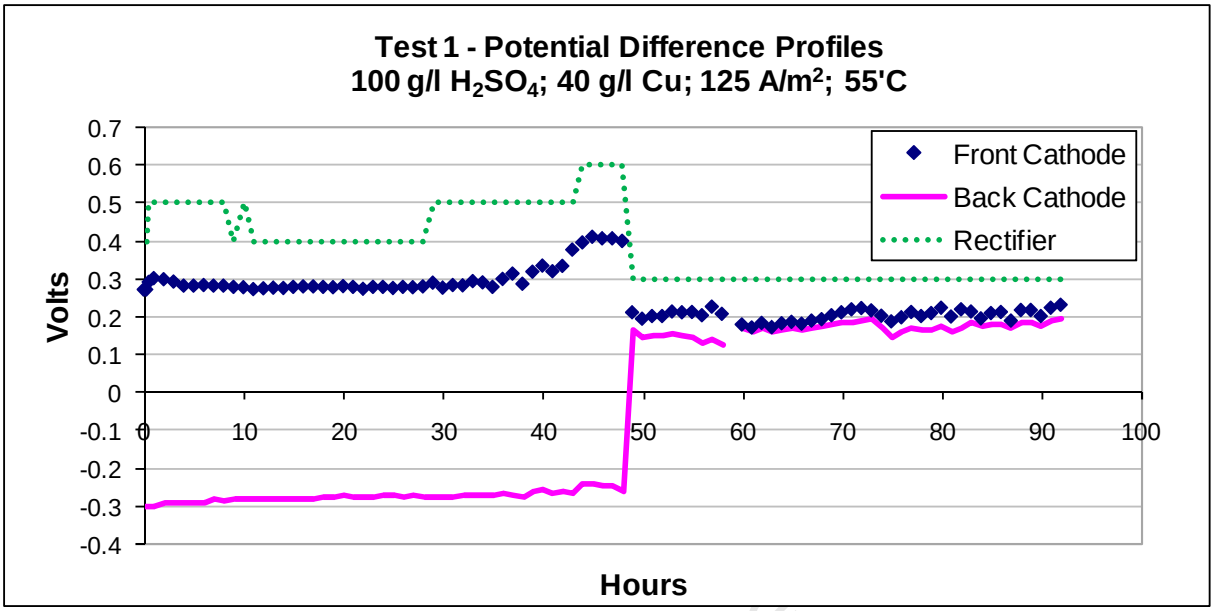

Figure D.1: Potential difference between back cathode and anode, front cathode and anode and the rectifier potential for test 1

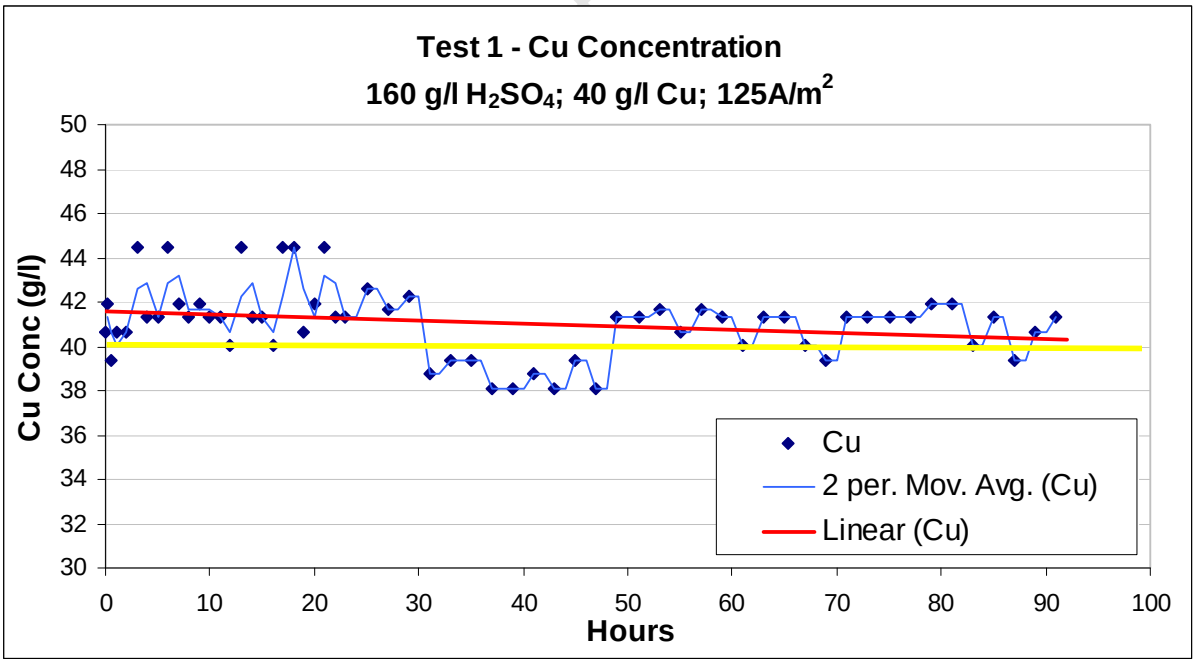

Figure D.2: Copper concentration monitored during test 1 (110 g/l H_2SO_4)

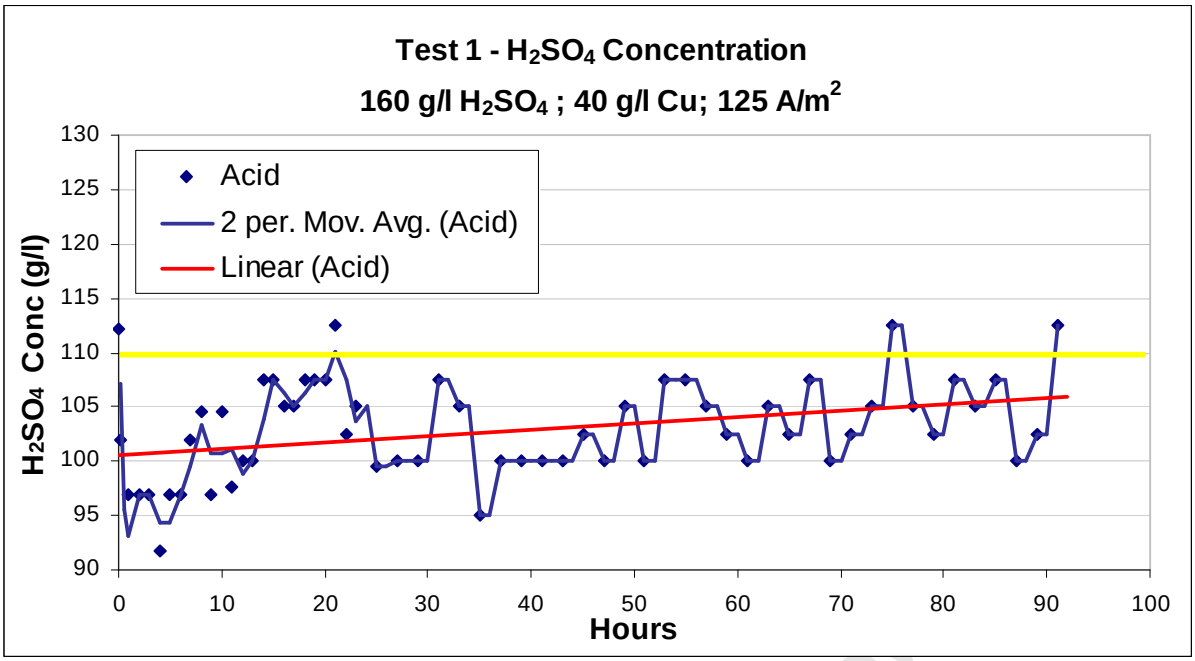

Figure D.3: H_2SO_4 Concentration profile during test 1 (110 g/l H_2SO_4)

Test 2

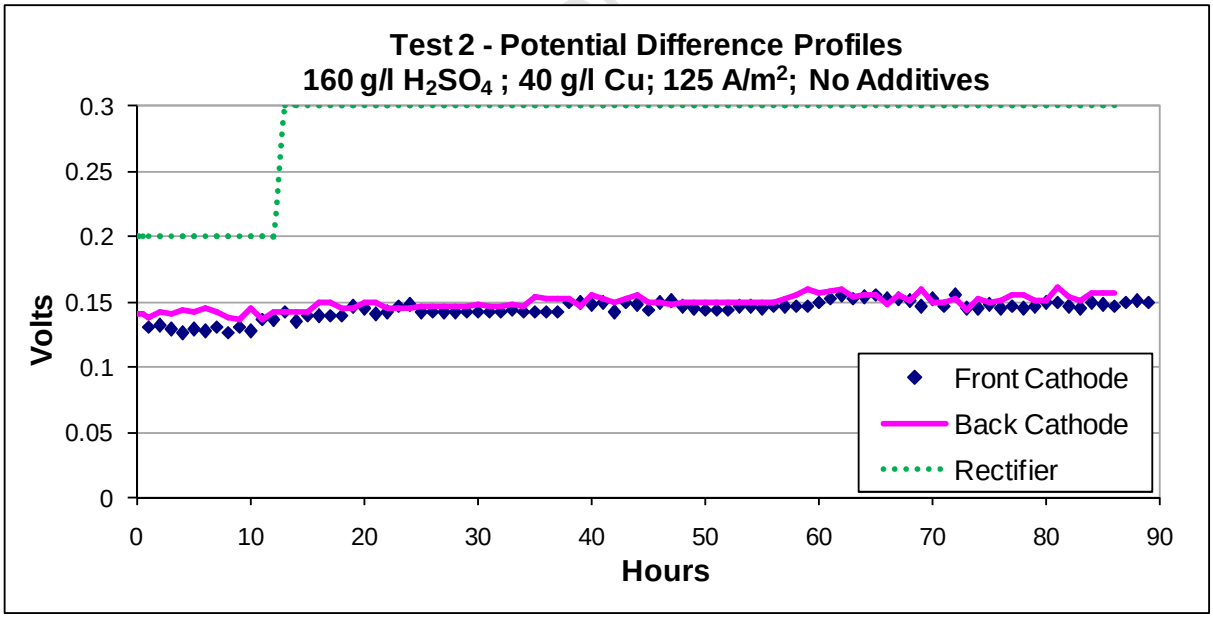

Figure D.4: Potential difference between back cathode and anode, front cathode and anode and the rectifier potential for test 2

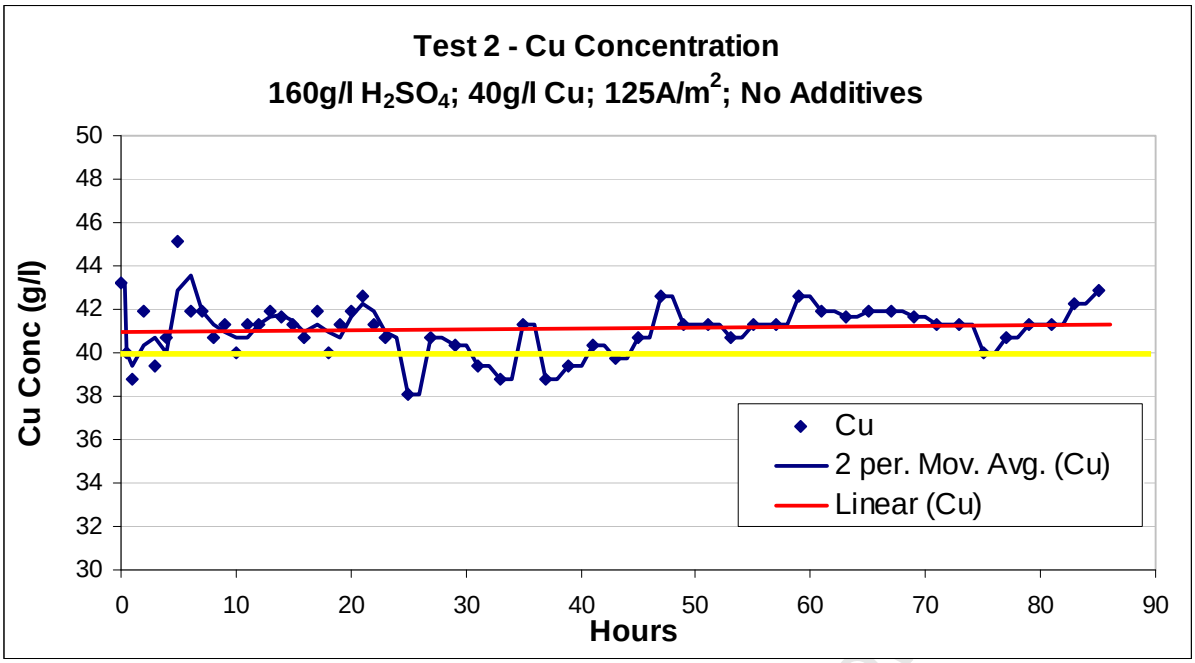

Figure D.5: Cu concentration profile during test 2 (Base-case)

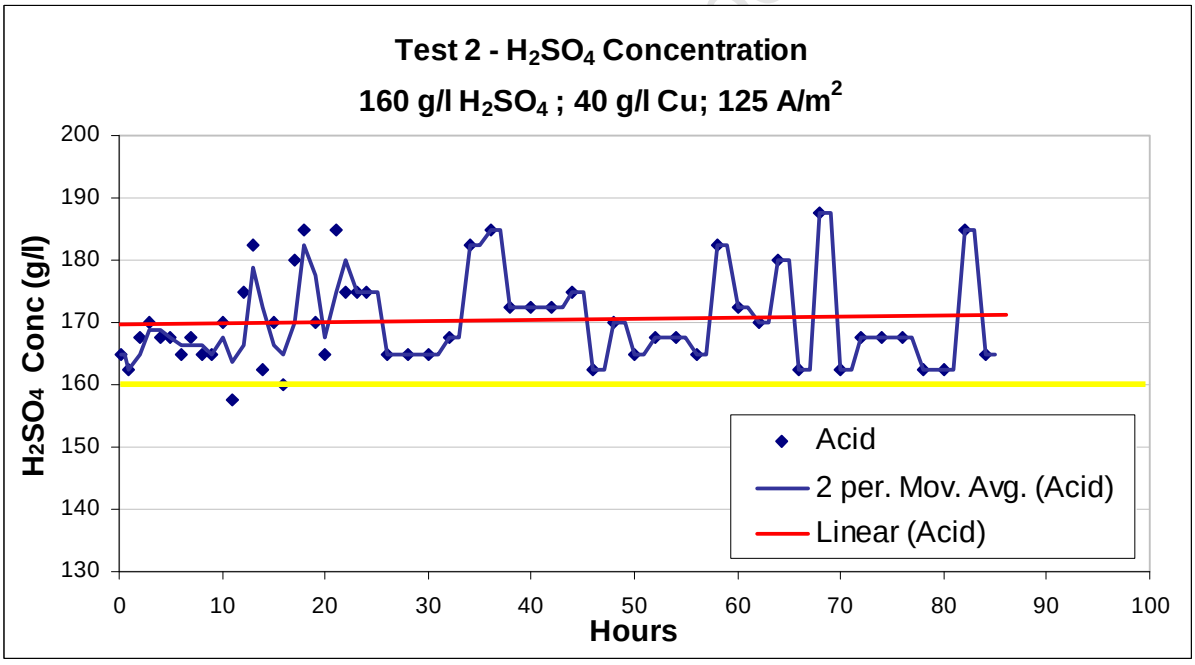

Figure D.6: H_2SO_4 Concentration profile during test 2 (Base-case)

Test 3

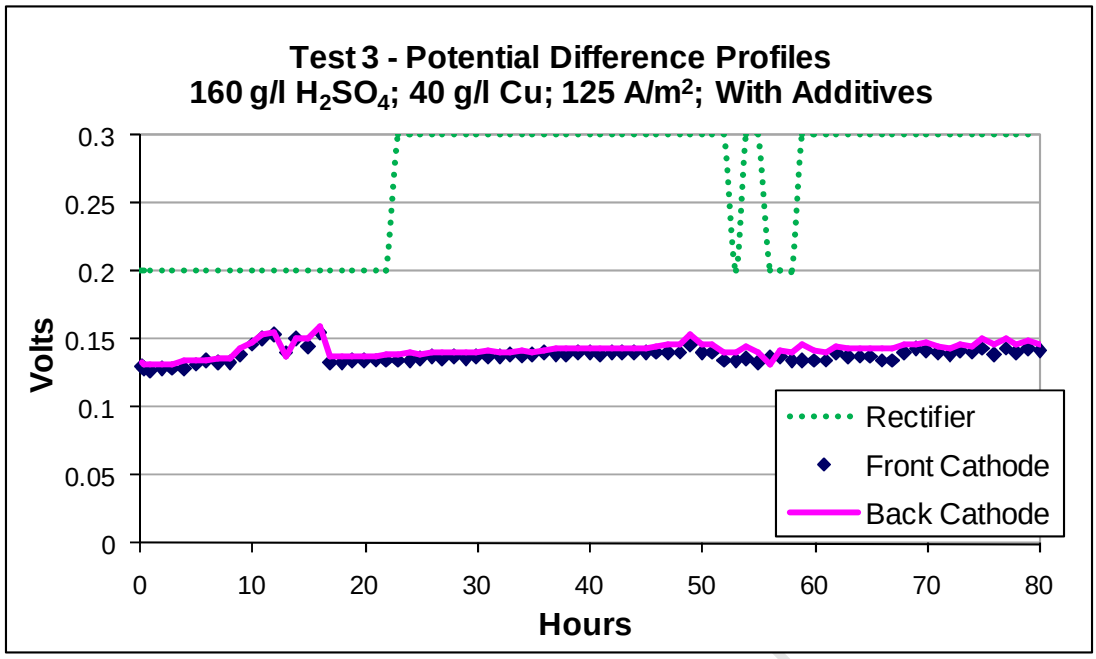

Figure D.7: Potential difference between back cathode and anode, front cathode and anode and the rectifier potential for test 3

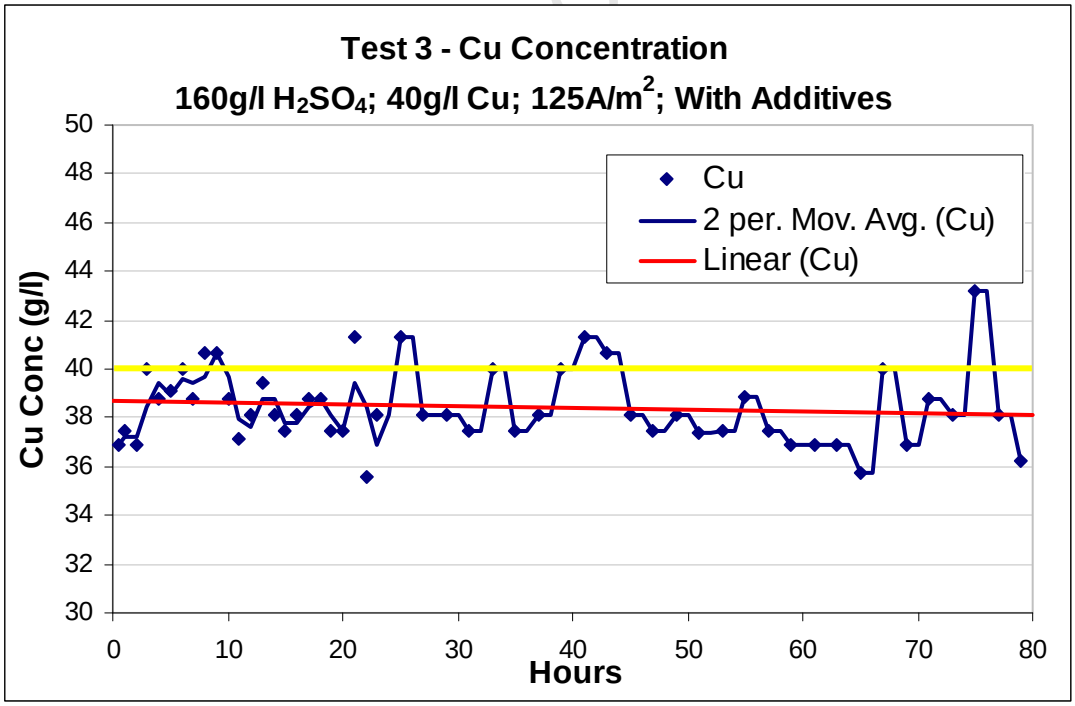

Figure D.8: Cu concentration profile during test 3 (Base-case with additives)

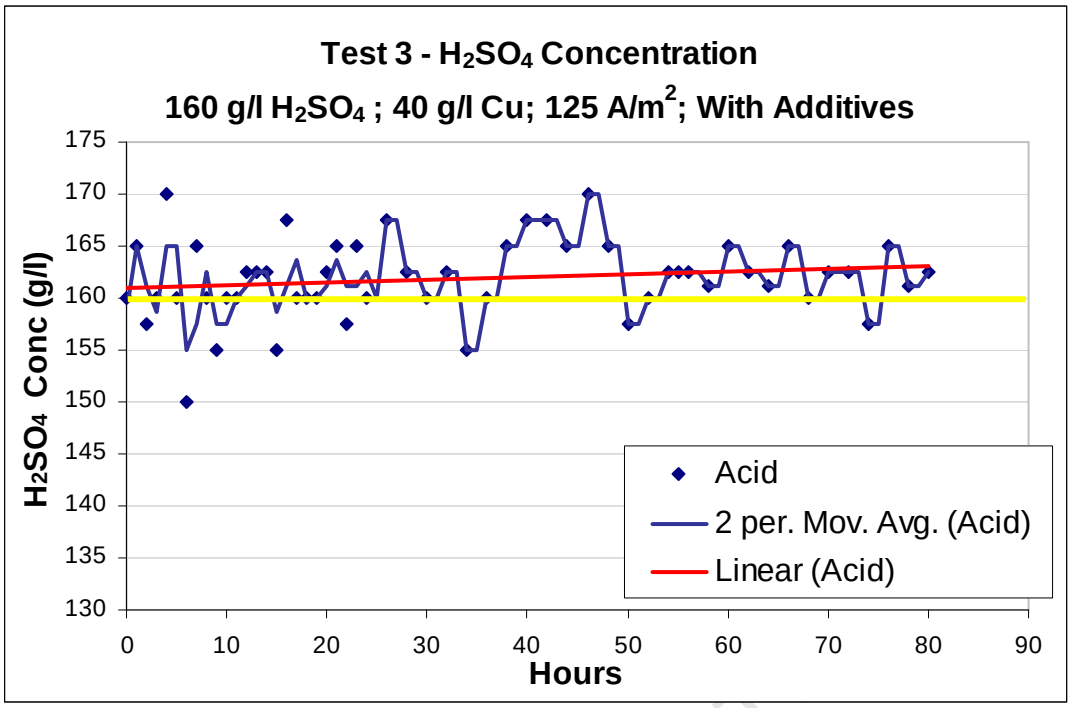

Figure D.9: H_2SO_4 Concentration profile during test 3 (Base-case with additives)

Test 4

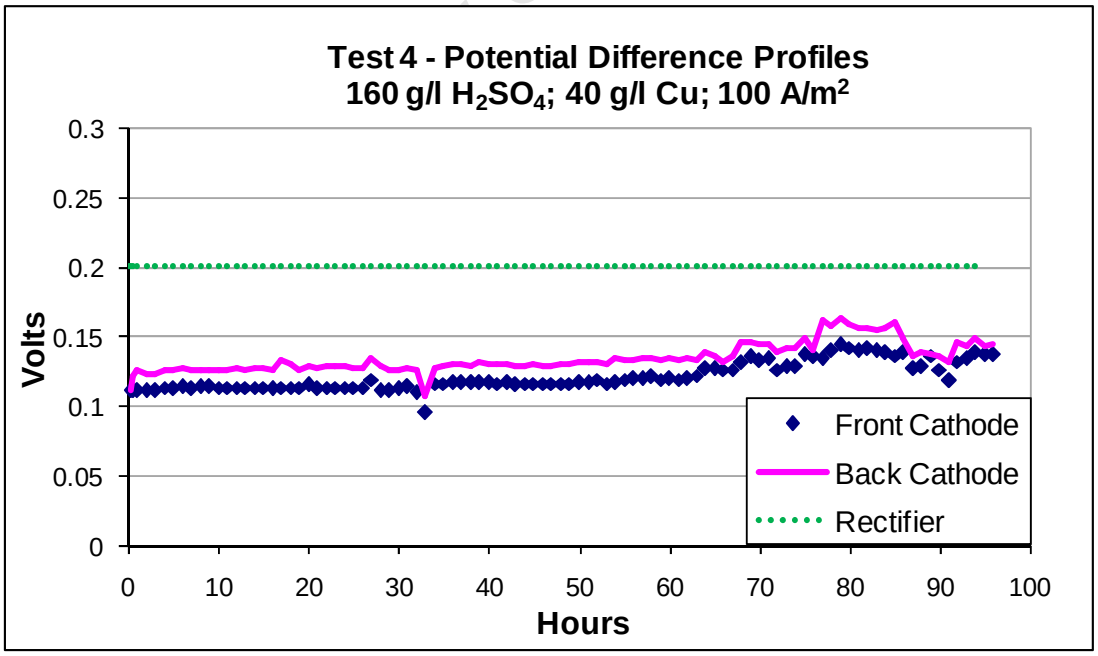

Figure D.10: Potential difference between back cathode and anode, front cathode and anode and the rectifier potential for test 4

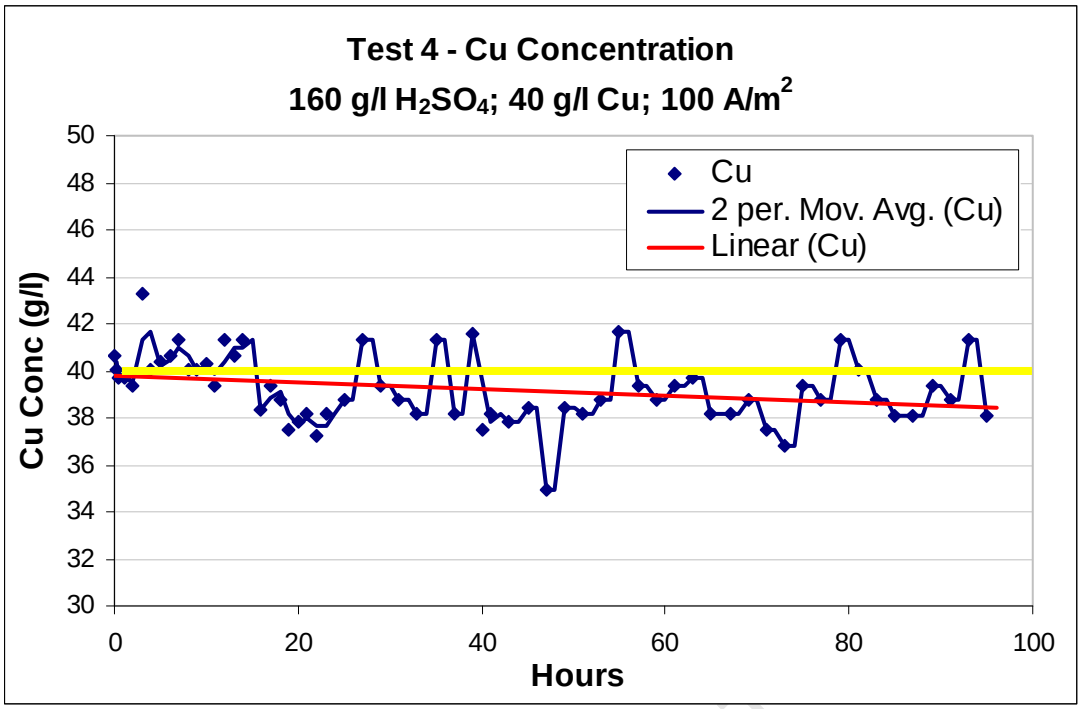

Figure D.11: Cu concentration profile during test 4 (100 A/m^2)

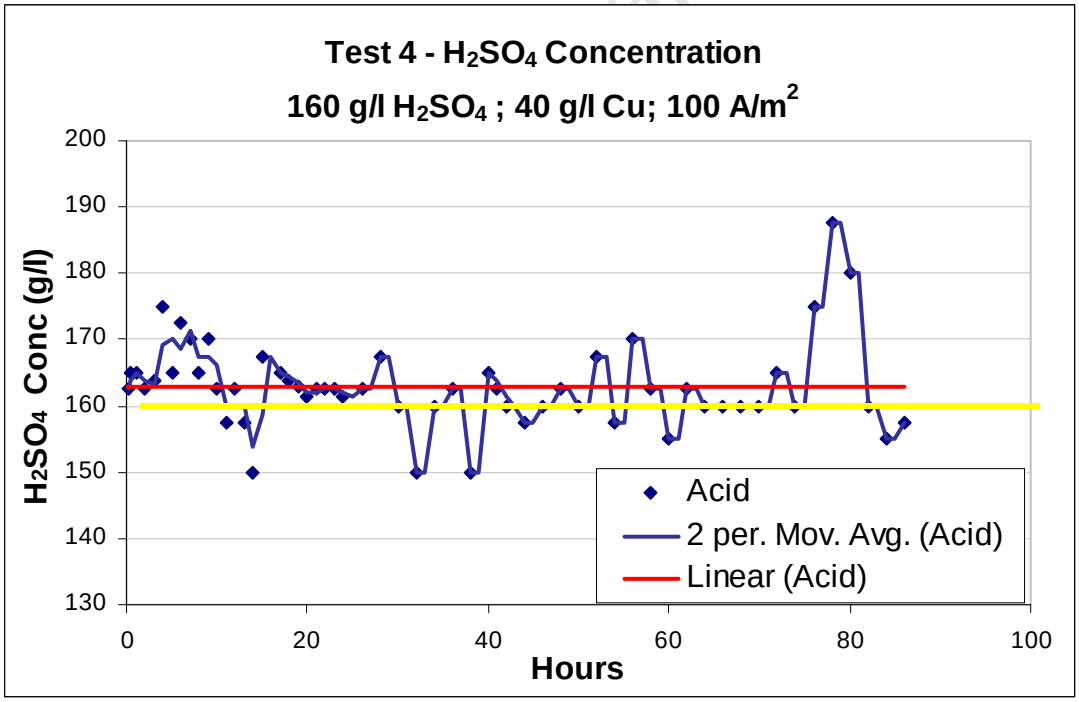

FigureD.12: H_2SO_4 Concentration profile during test 4 (100 A/m^2)

Test 5

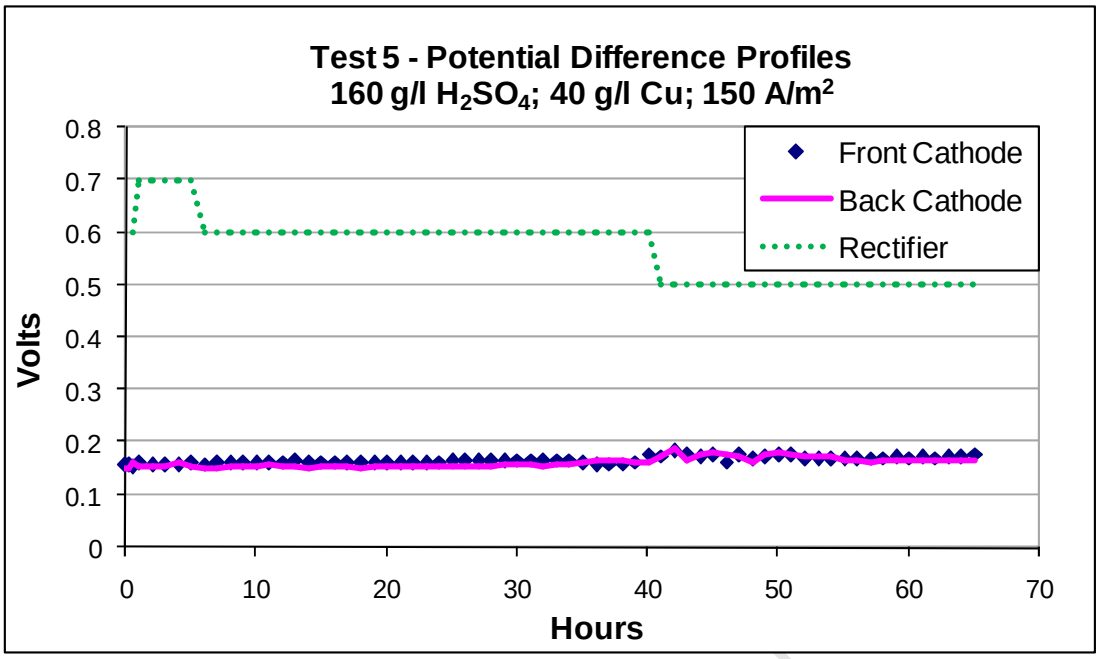

Figure D.13: Potential difference between back cathode and anode, front cathode and anode and the rectifier potential for test 5

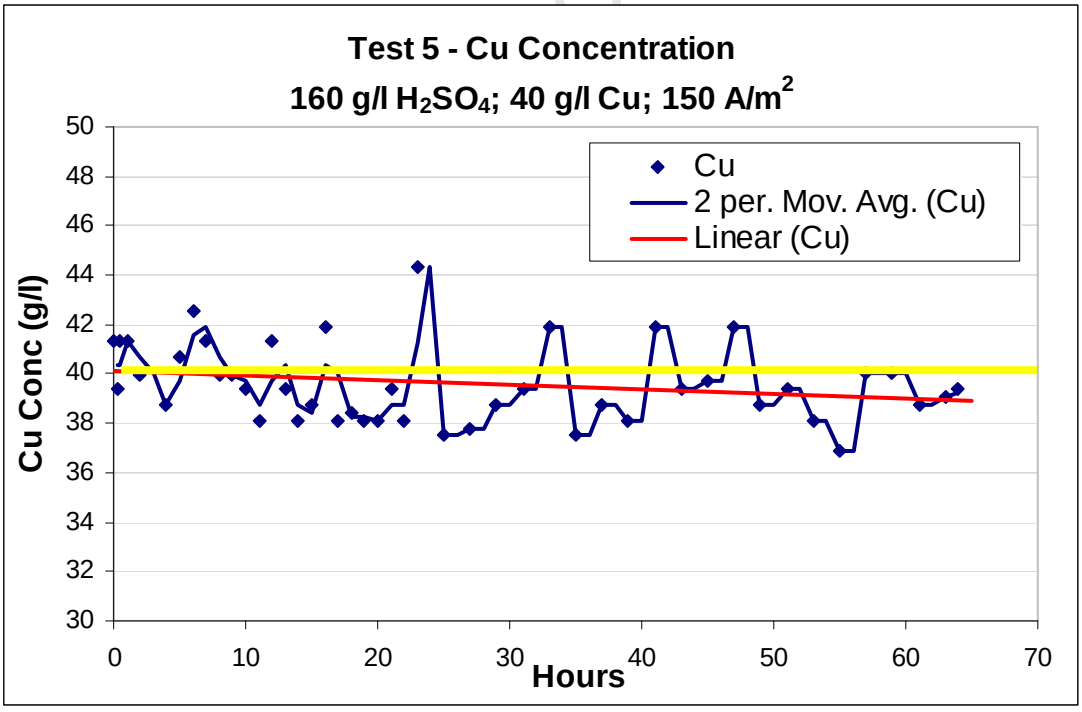

Figure D.14: Cu concentration profile during test 5 (150 A/m^2)

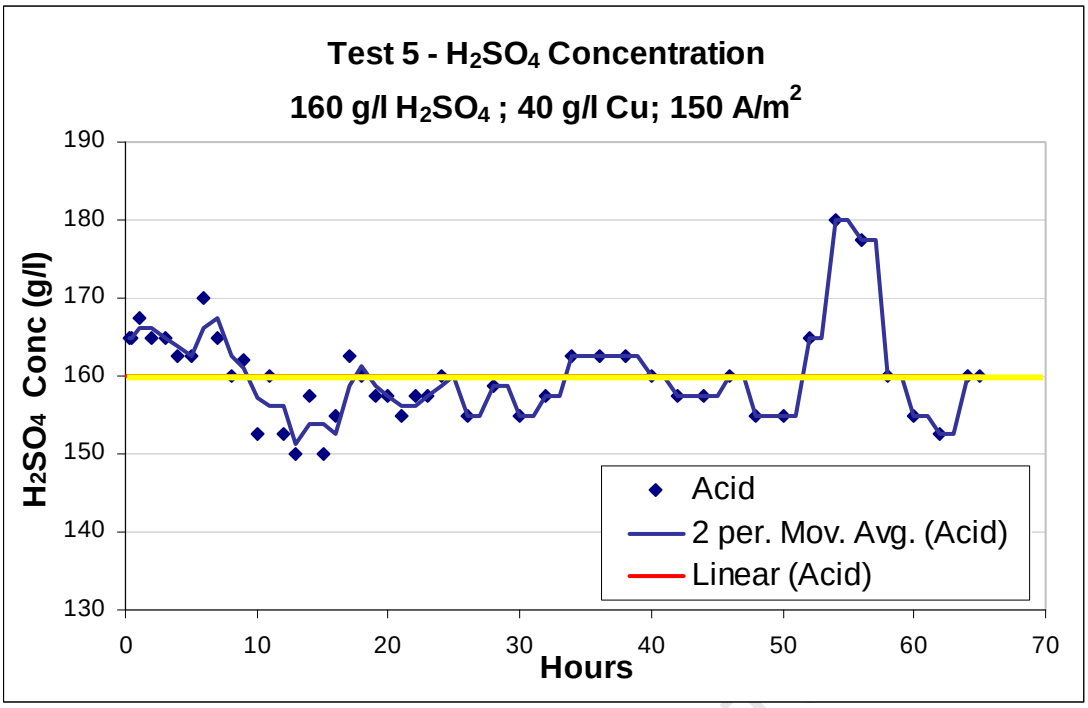

Figure D.15: H_2SO_4 Concentration profile during test 5 (150 A/m^2)

Test 6

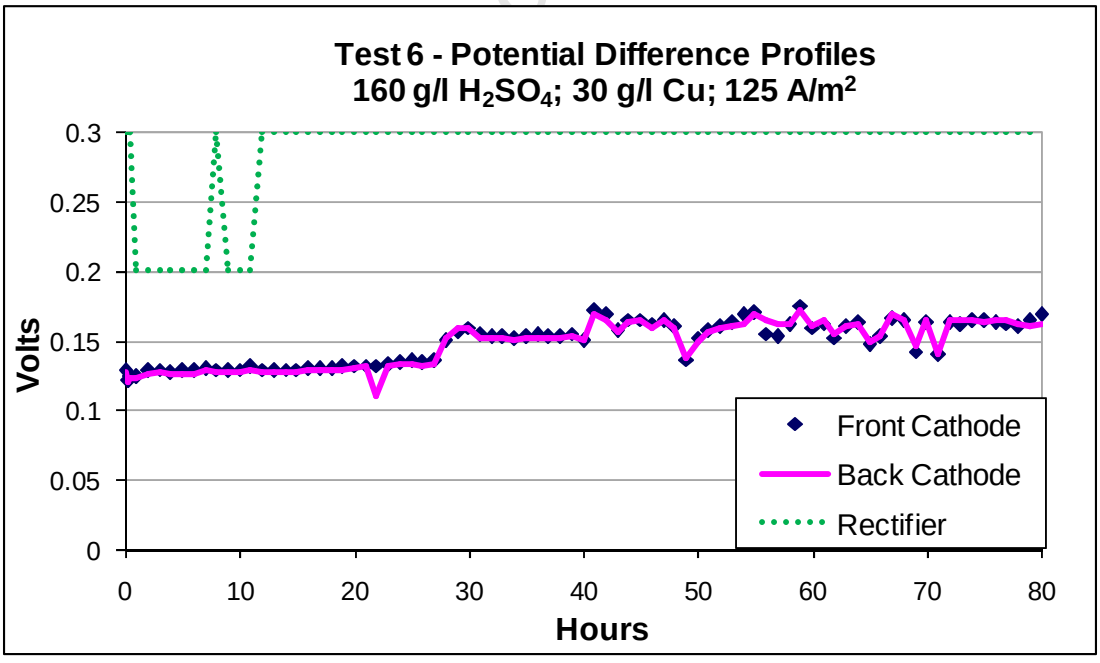

Figure D.16: Potential difference between back cathode and anode, front cathode and anode and the rectifier potential for test 6

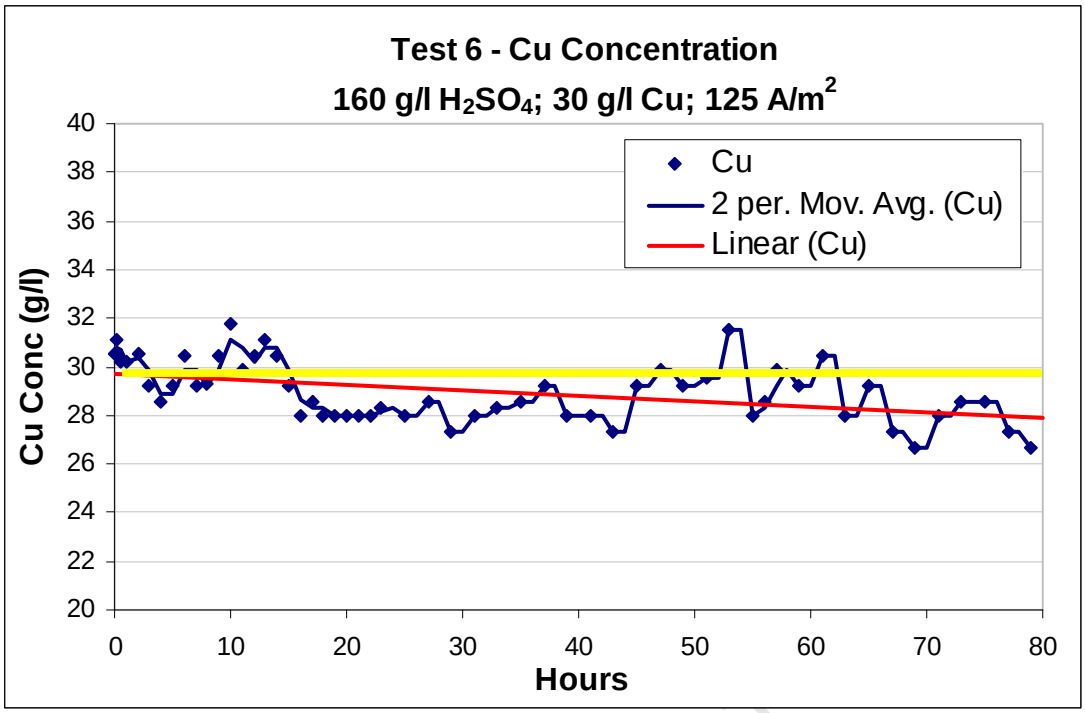

Figure D.17: Cu concentration profile during test 6 (30 g/l Cu)

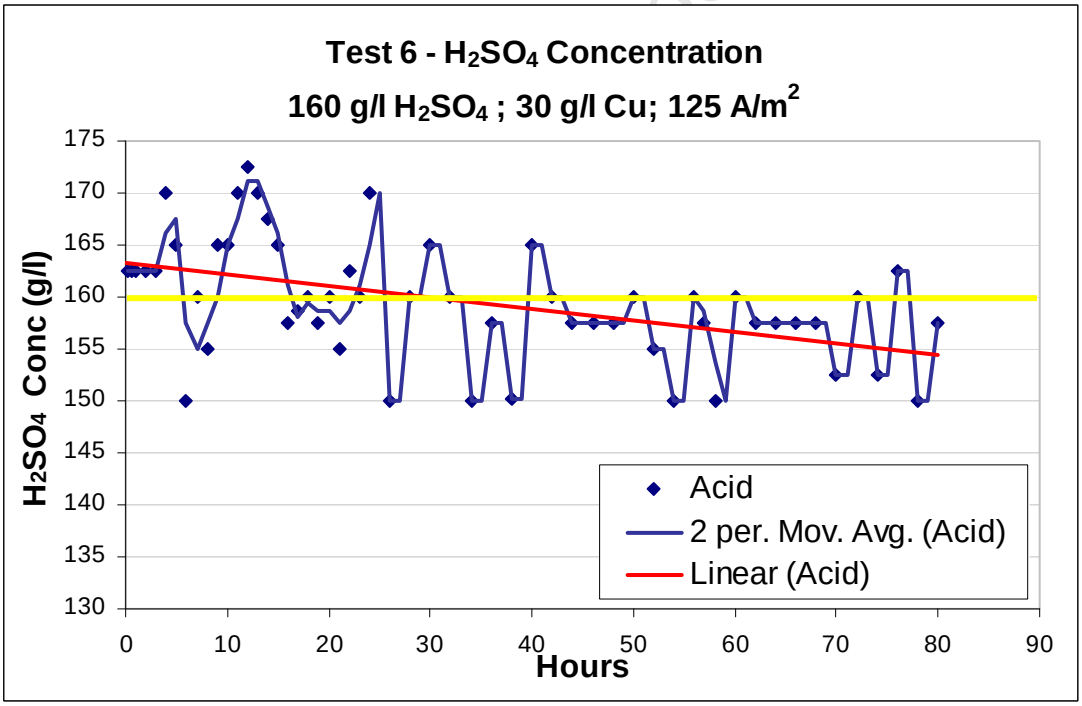

Figure D.18: H_2SO_4 Concentration profile during test 6 (30 g/l Cu)

Test 7

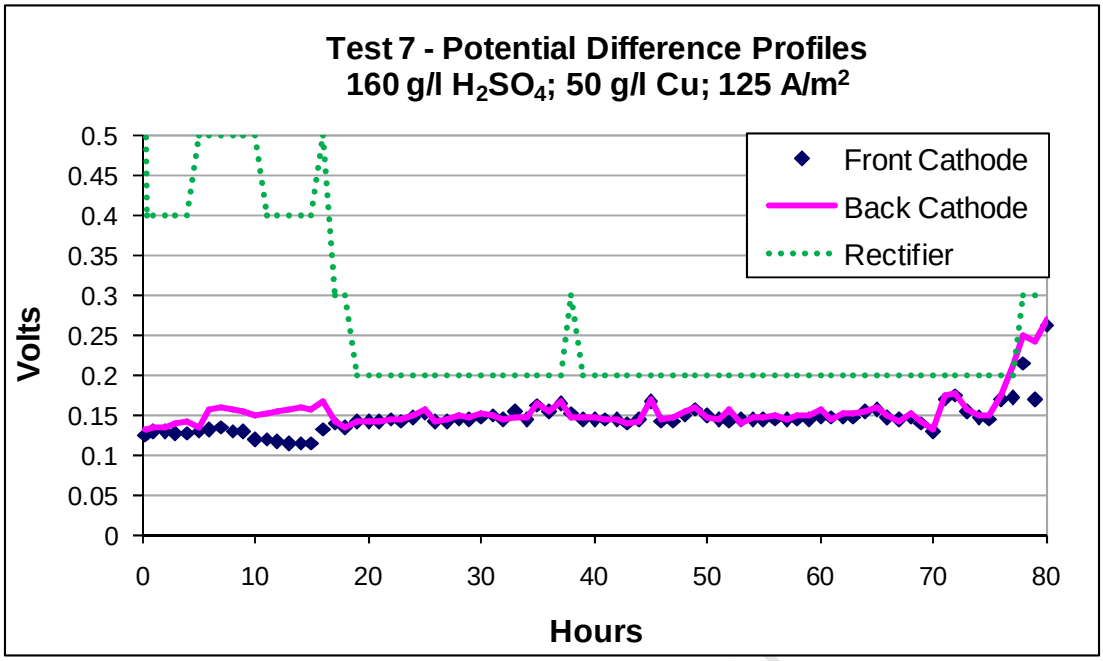

Figure D.19: Potential difference between back cathode and anode, front cathode and anode and the rectifier potential for test 7

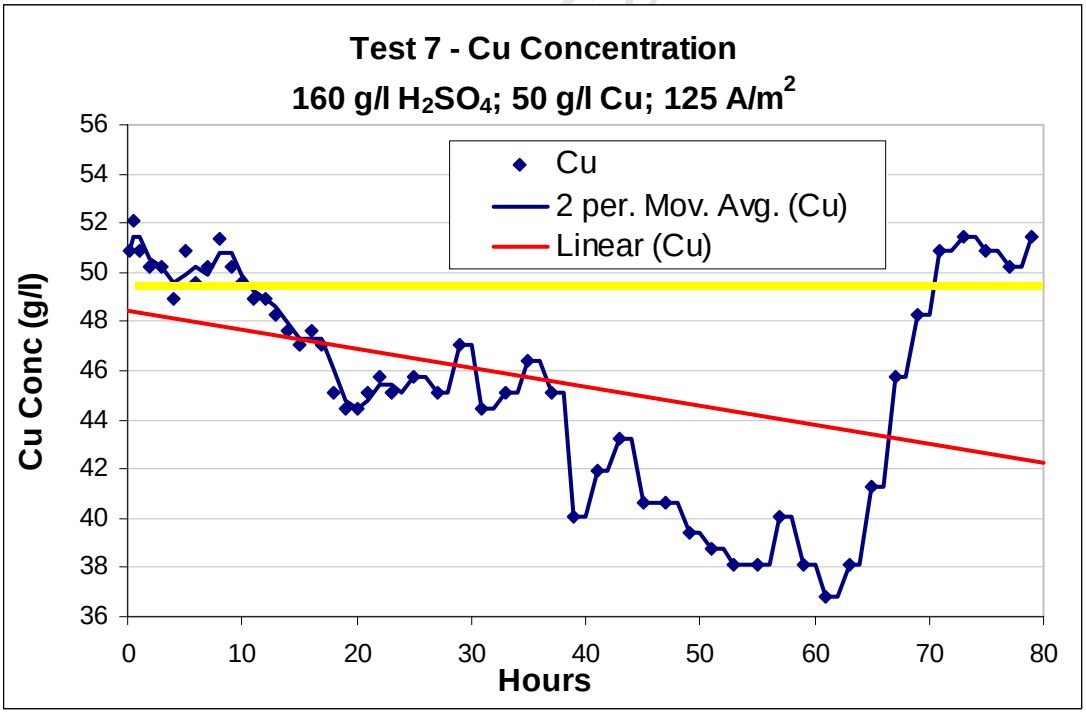

FigureD.20: Cu concentration profile during test 7 (50 g/l Cu)

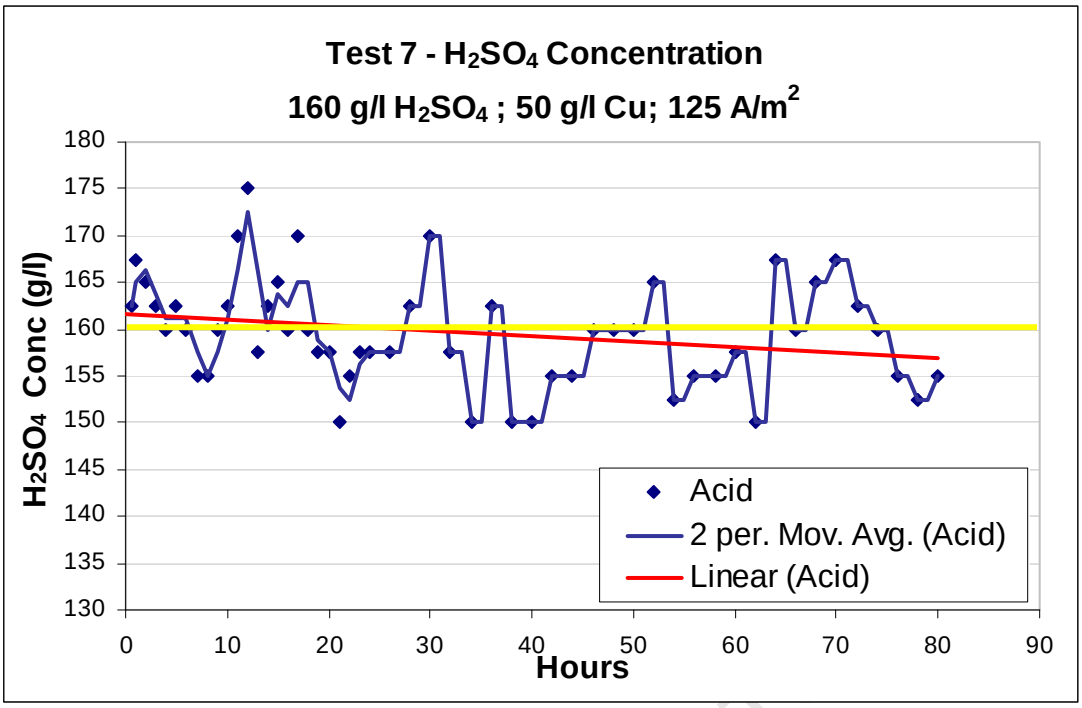

Figure D.21: H_2SO_4 Concentration profile during test 7 (50 g/l Cu)

Test 8

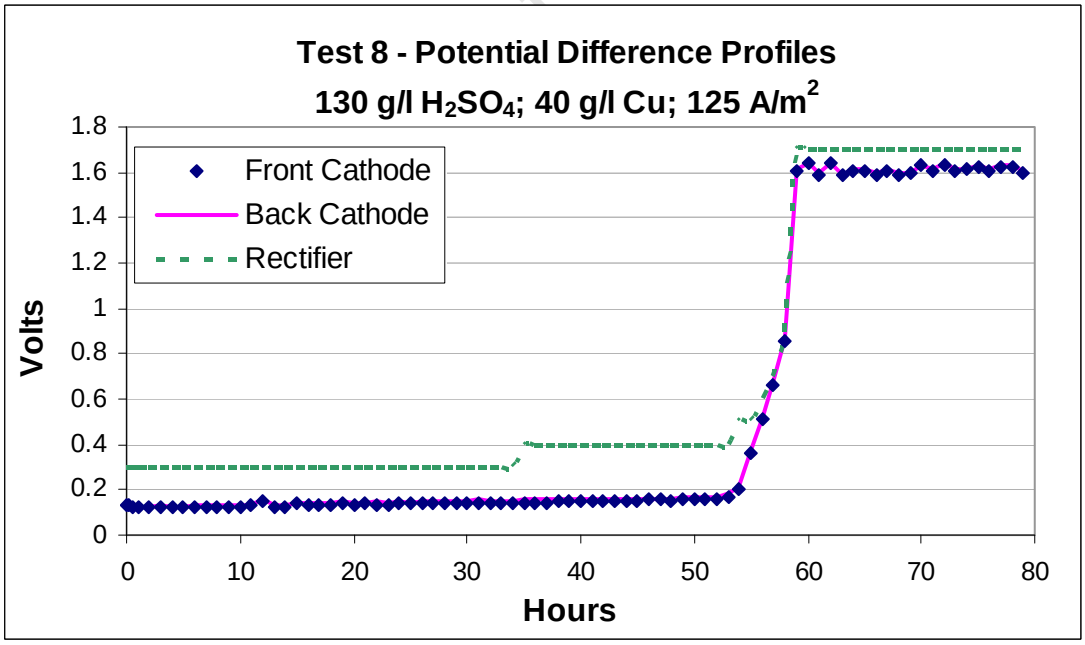

Figure D.22: Potential difference between back cathode and anode, front cathode and anode and the rectifier potential for test 8

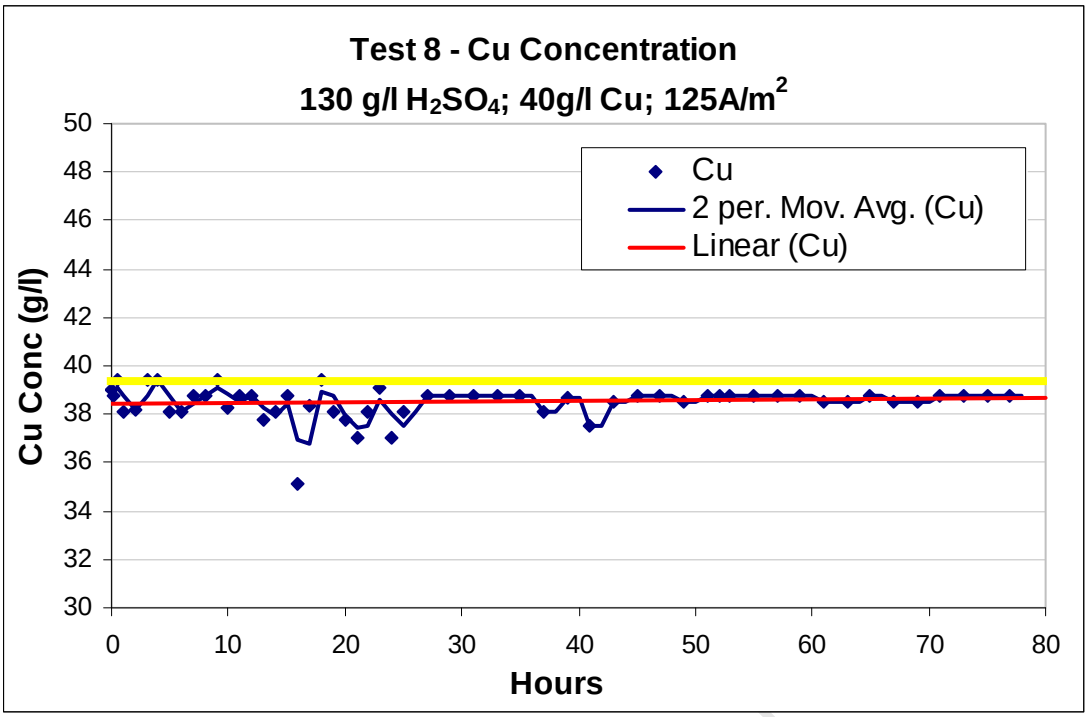

Figure D.23: Cu concentration profile during test 8 (130 g/l H_2SO_4)

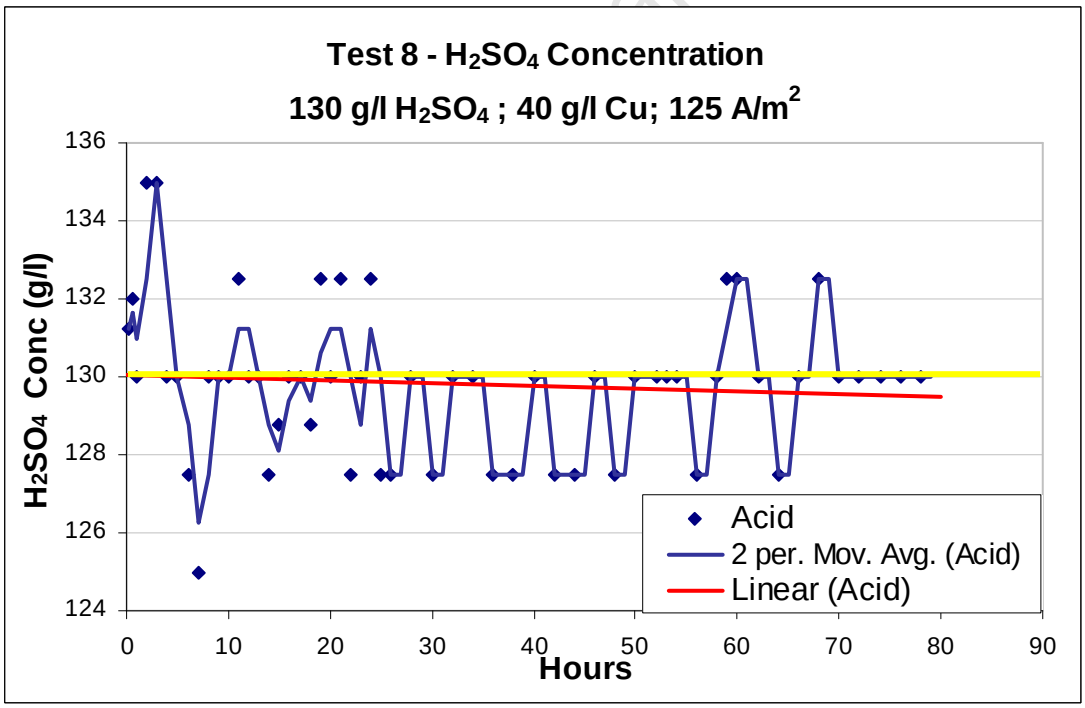

Figure D.24: H_2SO_4 Concentration profile during test 8 (130 g/l H_2SO_4)

Test 9

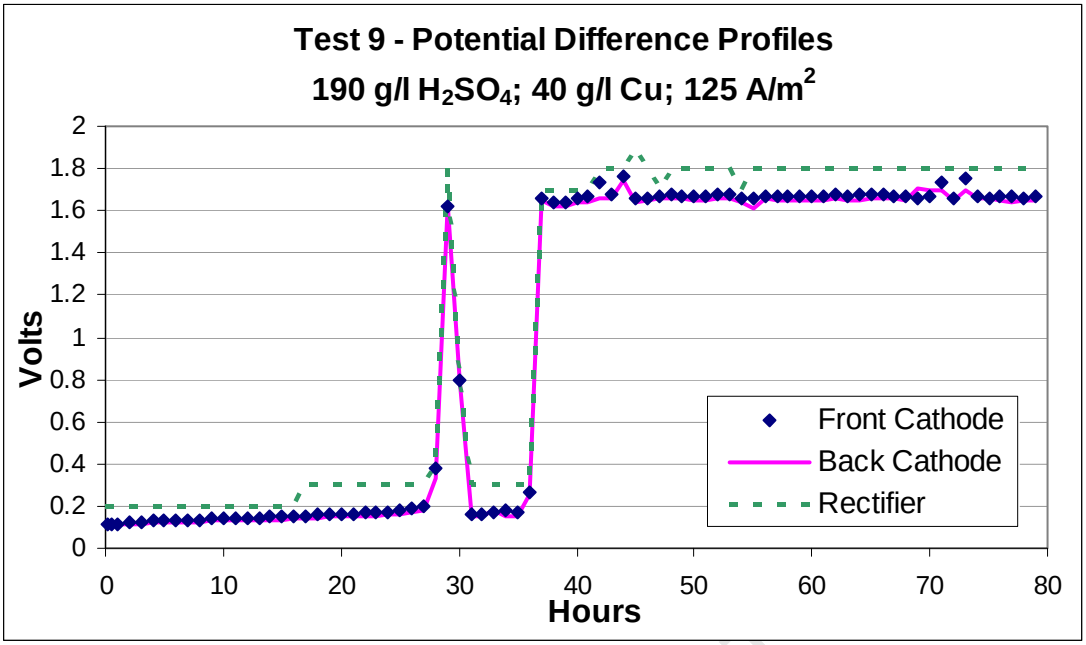

Figure D.25: Potential difference between back cathode and anode, front cathode and anode and the rectifier potential for test 9

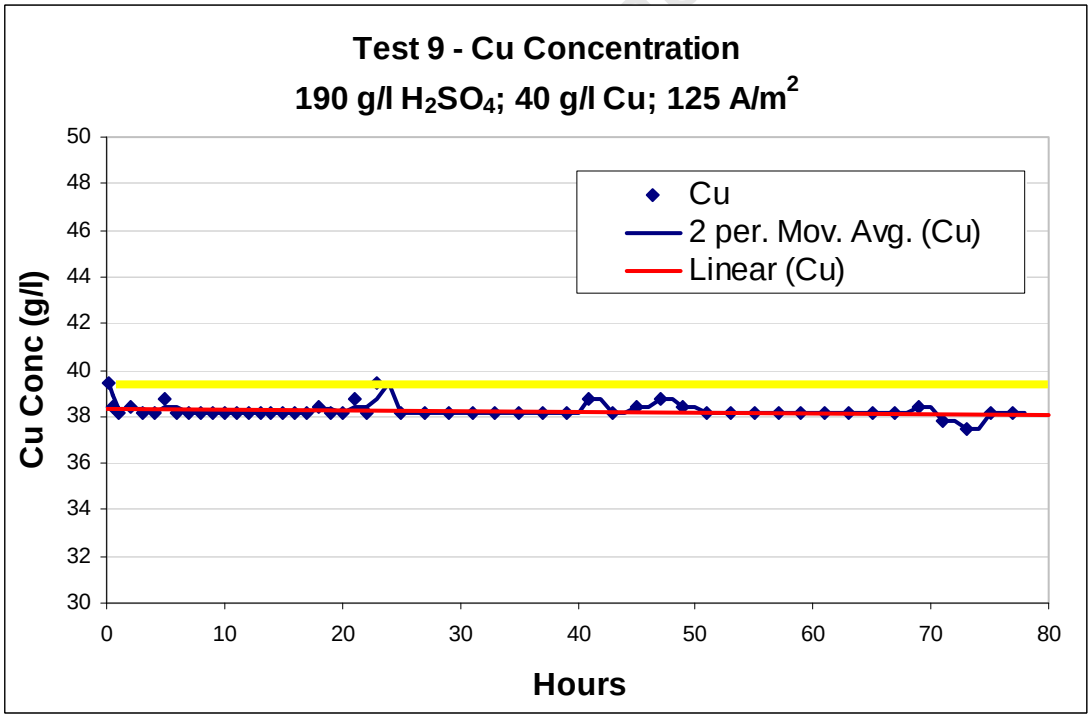

Figure D.26: Cu concentration profile during test 9 (190 g/l H_2SO_4)

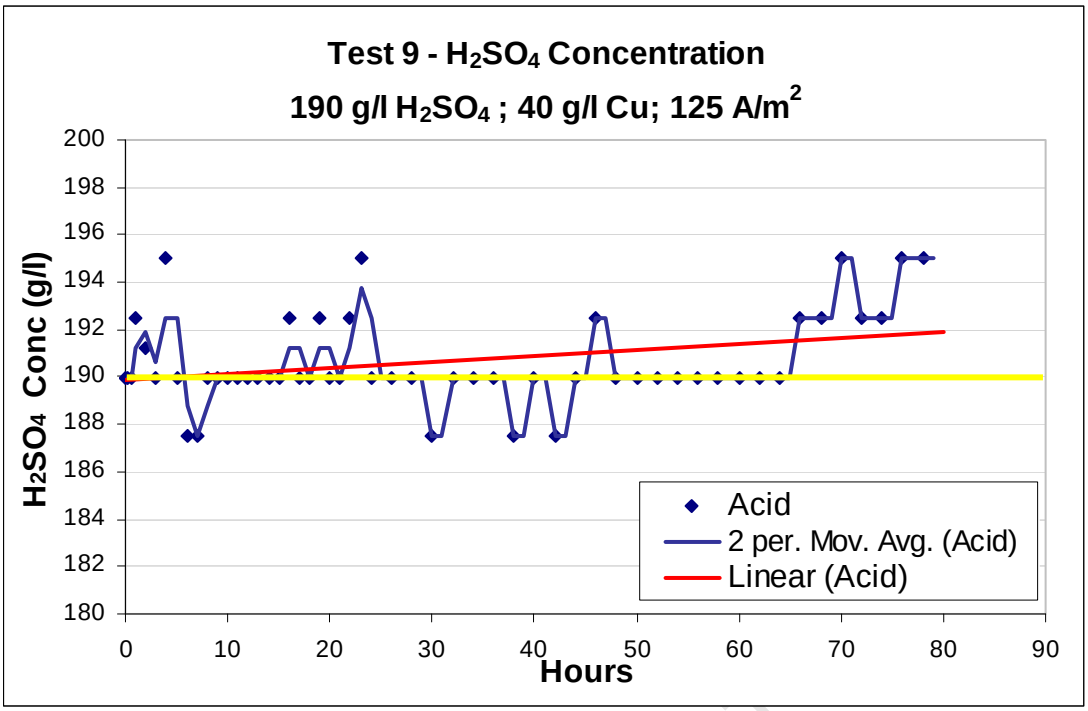

Figure D.27: H_2SO_4 Concentration profile during test 9 (190 g/l H_2SO_4)

Test 10

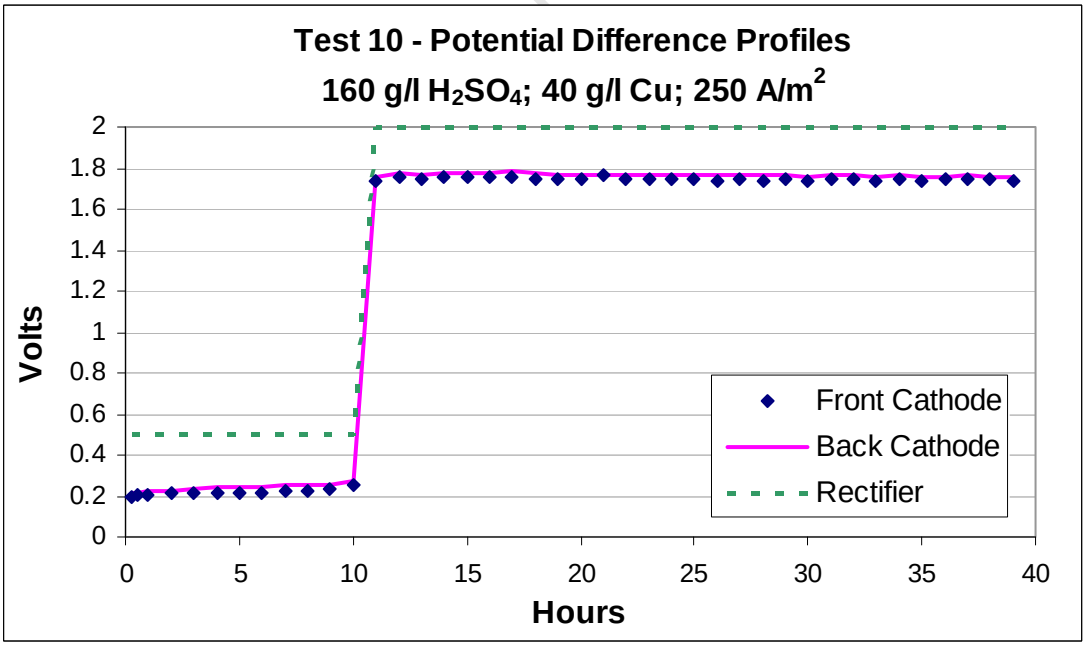

Figure D.28: Potential difference between back cathode and anode, front cathode and anode and the rectifier potential for test 10

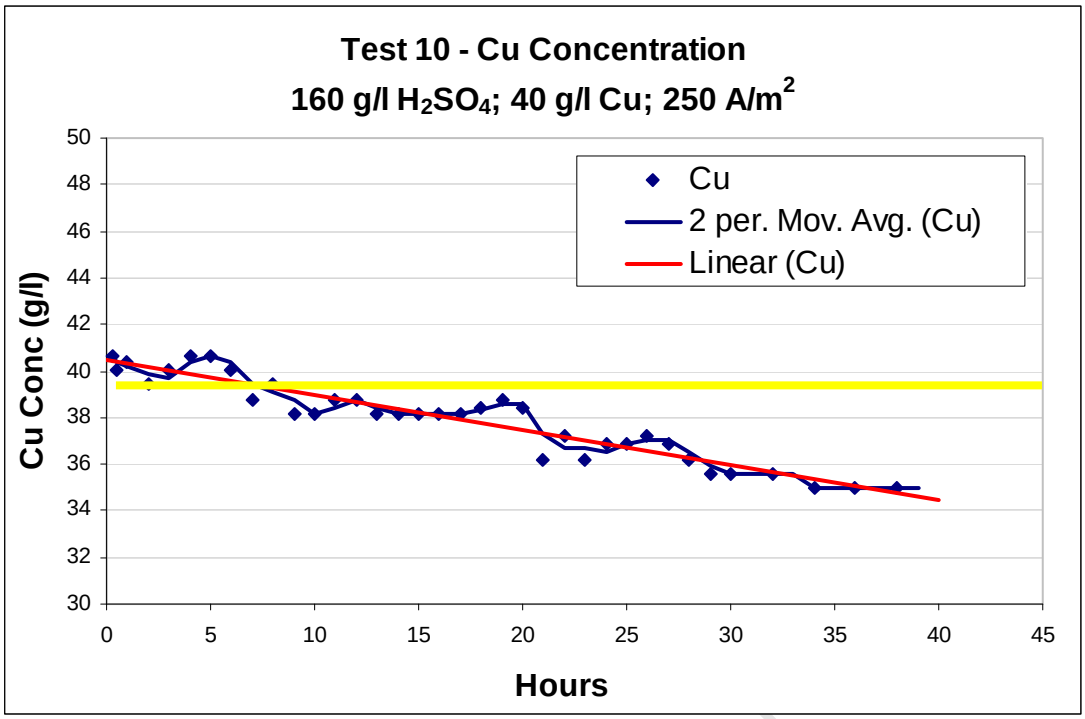

Figure D.29: Cu concentration profile during test 10 (250 A/m^2)

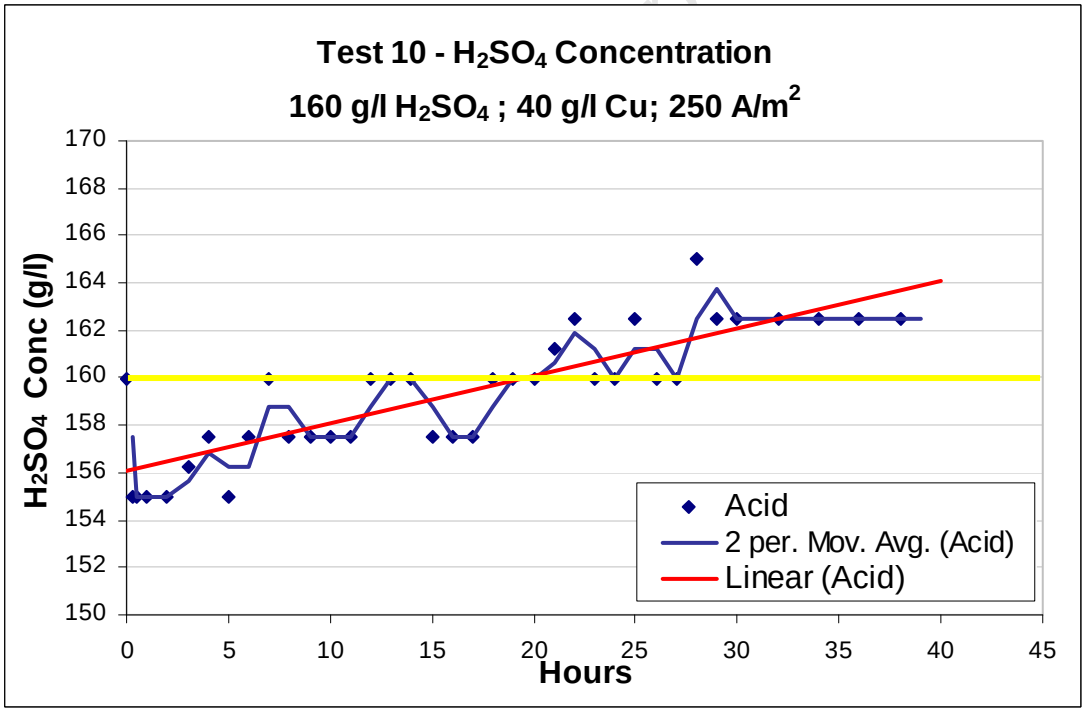

Figure D.30: H_2SO_4 Concentration profile during test 10 (250 A/m^2)

Test 11

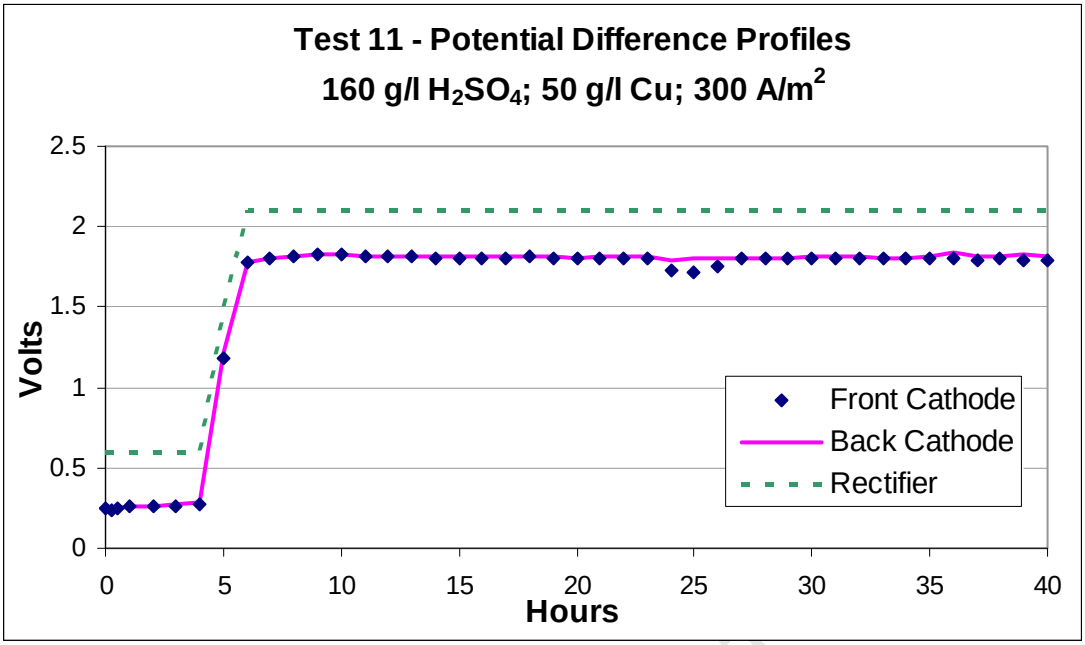

Figure D.31: Potential difference between back cathode and anode, front cathode and anode and the rectifier potential for test 11

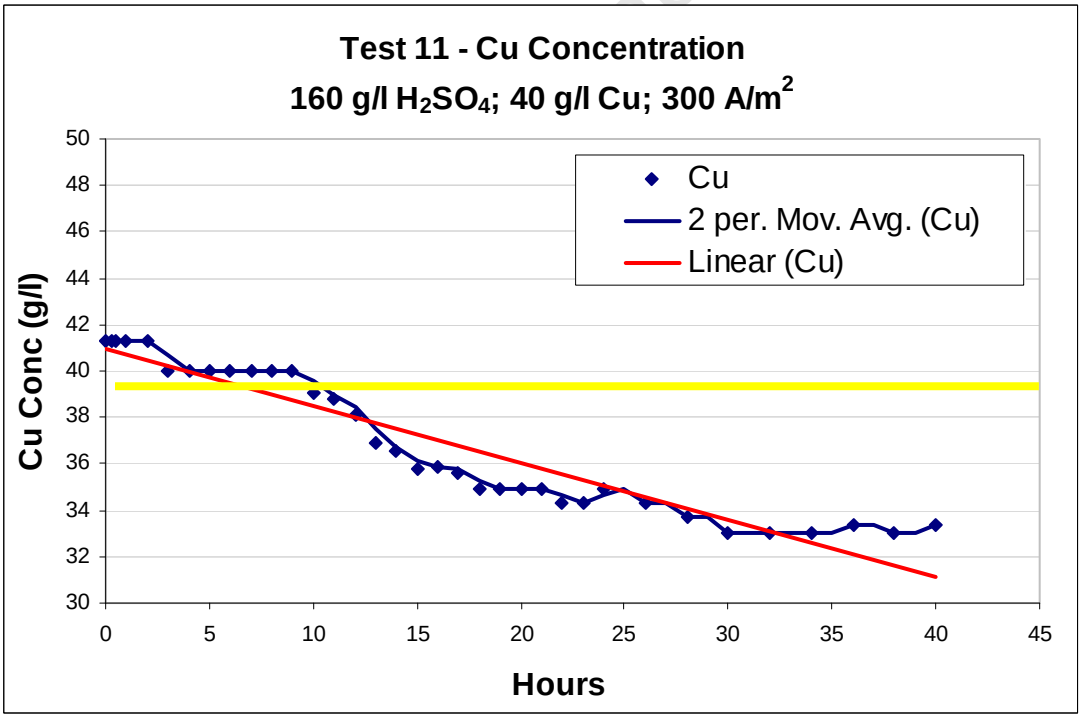

Figure D.32: Cu concentration profile during test 11 (300 A/m^2)

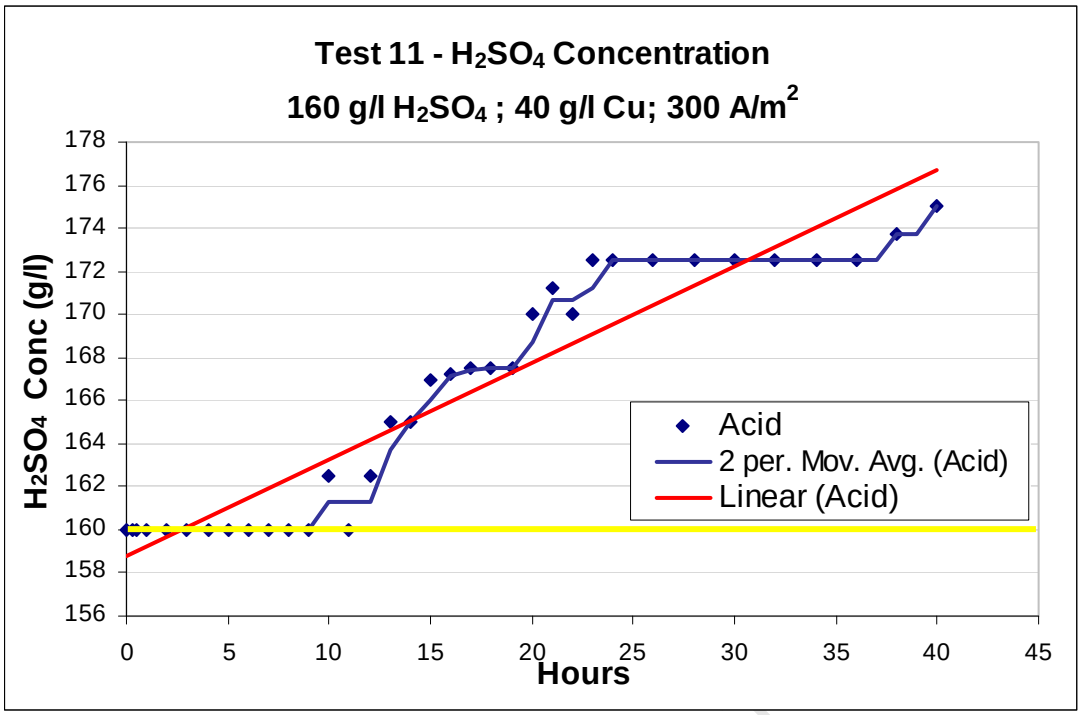

Figure D.33: H_2SO_4 Concentration profile during test 11 (300 A/m^2)

E. Element Deportment Results

Table E.1: Elemental input and output grades, concentrations and mass flows of test 1 (110 g/l H_2SO_4)

Element	Initial Anode	*Mass in Anode*	Electrolyte Feed	*Mass in Electrolyte Feed*	Total In	Cathode Front	Cathode Back	*Mass in Cathode*	Slimes	*Mass in Slimes*	Spent Electrolyte	*Mass in Spent Electrolyte*	Total Out
	(g/t)	*(g)*	(mg/l)	*(g)*	(g)	(g/t)	(g/t)	*(g)*	(g/t)	*(g)*	(mg/l)	*(g)*	(g)
Pt	886	*0.7*	<0.01	*0.0*	**0.7**	4.0	3.8	*0.0*	33500	*0.7*	<0.2	*0.0*	**0.7**
Pd	5110	*3.8*	<0.01	*0.0*	**3.8**	5.7	3.3	*0.0*	174300	*3.6*	<0.2	*0.0*	**3.6**
Rh	1152	*0.9*	2.8	*0.4*	**1.3**	2.8	1.5	*0.0*	47700	*1.0*	2.8	*0.4*	**1.4**
Ru	1025	*0.8*	16.0	*2.3*	**3.1**	0.0	0.0	*0.0*	34500	*0.7*	16.0	*2.2*	**3.0**
Ir	30.4	*0.0*	0.4	*0.1*	**0.1**	0.0	0.0	*0.0*	1200	*0.0*	0.4	*0.1*	**0.1**
Os	4.9	*0.0*	<0.02	*0.0*	**0.0**	0.0	0.0	*0.0*	230	*0.0*	<0.2	*0.0*	**0.0**
Au	421	*0.3*	<0.01	*0.0*	**0.3**	7.5	2.2	*0.0*	13800	*0.3*	<0.2	*0.0*	**0.3**
Ag	1500	*1.1*	0.1	*0.0*	**1.1**	0.0	0.0	*0.0*	7330	*0.2*	0.1	*0.0*	**0.2**
Cu	807300	*605.5*	40100	*5727.0*	**6332.5**	0.0	0.0	*775.1*	187500	*3.9*	41230	*5795.8*	**6574.9**
Ni	127100	*95.3*	56630	*8087.8*	**8183.2**	0.0	0.0	*0.0*	2800	*0.1*	56400	*7928.3*	**7928.4**
Fe	44600	*33.5*	2450	*349.9*	**383.4**	126.7	51.7	*0.1*	10500	*0.2*	2650	*372.5*	**372.8**
Co	1700	*1.3*	869.0	*124.1*	**125.4**	0.0	0.0	*0.0*	<500	*0.0*	944.0	*132.7*	**132.7**
Pb	2750	*2.1*	7.2	*1.0*	**3.1**	8.3	8.3	*0.0*	52600	*1.1*	8.7	*1.2*	**2.3**
As	2030	*1.5*	73.0	*10.4*	**11.9**	6.7	2.5	*0.0*	63000	*1.3*	74.0	*10.4*	**11.7**
S	1700	*1.3*	95330	*13614.9*	**13616.2**	0.0	0.0	*0.0*	95500	*2.0*	98340	*13824.0*	**13826.0**
Si	<1000	*0.4*	91.3	*13.0*	**13.4**	63.3	<0.833	*0.0*	<3000	*0.0*	112.0	*15.7*	**15.8**
Te	665	*0.5*	40.0	*5.7*	**6.2**	7.8	7.8	*0.0*	61200	*1.3*	33.0	*4.6*	**5.9**
Sb	990	*0.7*	9.1	*1.3*	**2.0**	0.0	0.0	*0.0*	20000	*0.4*	10.0	*1.4*	**1.8**
Bi	410	*0.3*	1.0	*0.1*	**0.5**	0.0	0.0	*0.0*	3400	*0.1*	2.5	*0.4*	**0.4**
Sn	161	*0.1*	<0.2	*0.0*	**0.1**	0.0	0.0	*0.0*	155	*0.0*	0.9	*0.1*	**0.1**
Se	68.6	*0.1*	11.0	*1.6*	**1.6**	4.0	1.8	*0.0*	7050	*0.1*	10.0	*1.4*	**1.6**
Zn	26	*0.0*	24.9	*3.6*	**3.6**	4.2	4.8	*0.0*	9.3	*0.0*	26.1	*3.7*	**3.7**

Table E.2: Elemental input and output grades, concentrations and mass flows of test 2 (Base-case)

Element	Initial Anode	*Mass in Anode*	Electrolyte Feed	*Mass in Electrolyte Feed*	Total In	Cathode Front	Cathode Back	*Mass in Cathode*	Slimes	*Mass in Slimes*	Spent Electrolyte	*Mass in Spent Electrolyte*	Total Out
	(g/t)	*(g)*	(mg/l)	*(g)*	**(g)**	(g/t)	(g/t)	*(g)*	(g/t)	*(g)*	(mg/l)	*(g)*	**(g)**
Pt	954	*0.7*	<0.01	*0.0*	**0.7**	0.2	<0.167	*0.0*	25700	*0.6*	<0.2	*0.0*	**0.6**
Pd	4950	*3.8*	<0.01	*0.0*	**3.8**	6.8	6.3	*0.0*	137600	*3.3*	<0.2	*0.0*	**3.3**
Rh	1312	*1.0*	2.8	*0.4*	**1.4**	7.7	8.2	*0.0*	38700	*0.9*	2.6	*0.3*	**1.3**
Ru	1269	*1.0*	16.0	*2.1*	**3.1**	13.0	14.3	*0.0*	38800	*0.9*	17.0	*2.2*	**3.1**
Ir	40	*0.0*	0.4	*0.1*	**0.1**	<0.167	<0.167	*0.0*	1100	*0.0*	0.4	*0.1*	**0.1**
Os	8	*0.0*	<0.2	*0.0*	**0.0**	<0.167	<0.167	*0.0*	220	*0.0*	<0.2	*0.0*	**0.0**
Au	404	*0.3*	<0.01	*0.0*	**0.3**	0.2	<0.167	*0.0*	10900	*0.3*	<0.2	*0.0*	**0.3**
Ag	1358	*1.0*	<0.2	*0.0*	**1.0**	0.3	<0.167	*0.0*	3420	*0.1*	0.9	*0.1*	**0.2**
Cu	795200	*608.0*	40400	*5314*	**5922**	0.0	0.0	*723.1*	281600	*6.7*	40100	*5193.8*	**5923.7**
Ni	139100	*106.4*	53660	*7058.2*	**7164.5**	85.2	83.5	*0.1*	6400	*0.2*	58280	*7548.6*	**7548.8**
Fe	48600	*37.2*	2330	*306.5*	**343.6**	266.7	50.0	*0.1*	6100	*0.1*	2730	*353.6*	**353.8**
Co	1900	*1.5*	841	*110.6*	**112.1**	5.3	5.8	*0.0*	<500	*0.0*	931	*120.6*	**120.6**
Pb	2480	*1.9*	8.2	*1.1*	**3.0**	<0.167	<0.167	*0.0*	49800	*1.2*	5.7	*0.7*	**1.9**
As	1902	*1.5*	73.0	*9.6*	**11.1**	7.8	5.0	*0.0*	57900	*1.4*	74.0	*9.6*	**11.0**
S	1600	*1.2*	112500	*14797.7*	**14798.9**	0.0	0.0	*0.0*	86500	*2.1*	118800	*15387.2*	**15389.3**
Si	<1000	*0.4*	36.7	*4.8*	**5.2**	65.0	85.0	*0.1*	4800	*0.1*	30.9	*4.0*	**4.2**
Te	592	*0.5*	41.0	*5.4*	**5.8**	123.3	118.8	*0.1*	46300	*1.1*	33.0	*4.3*	**5.5**
Sb	919	*0.7*	7.9	*1.0*	**1.7**	4.3	2.7	*0.0*	19300	*0.5*	8.6	*1.1*	**1.6**
Bi	373	*0.3*	1.0	*0.1*	**0.4**	2.3	0.2	*0.0*	2900	*0.1*	2.6	*0.3*	**0.4**
Sn	151	*0.1*	<0.2	*0.0*	**0.1**	<0.167	<0.167	*0.0*	53	*0.0*	1.0	*0.1*	**0.1**
Se	64	*0.0*	11.0	*1.4*	**1.5**	1.7	3.0	*0.0*	7820	*0.2*	9.2	*1.2*	**1.4**
Zn	20.9	*0.0*	25.3	*3.3*	**3.3**	<0.167	<0.167	*0.0*	12.3	*0.0*	27.6	*3.6*	**3.6**

Table E.3: Elemental input and output grades, concentrations and mass flows of test 3 (Base-case with additives)

Element	Initial Anode	*Mass in Anode*	Electrolyte Feed	*Mass in Electrolyte Feed*	Total In	Cathode Front	Cathode Back	*Mass in Cathode*	Slimes	*Mass in Slimes*	Spent Electrolyte	*Mass in Spent Electrolyte*	Total Out
	(g/t)	*(g)*	(mg/l)	*(g)*	**(g)**	(g/t)	(g/t)	*(g)*	(g/t)	*(g)*	(mg/l)	*(g)*	**(g)**
Pt	828	*0.6*	<0.01	*0.0*	**0.6**	<0.167	<0.167	*0.0*	27300	*0.6*	0.0	*0.0*	**0.6**
Pd	4920	*3.4*	<0.01	*0.0*	**3.4**	1.3	2.3	*0.0*	146200	*3.2*	0.1	*0.0*	**3.2**
Rh	1089	*0.8*	2.9	*0.4*	**1.1**	1.3	1.7	*0.0*	37800	*0.8*	2.6	*0.3*	**1.2**
Ru	1143	*0.8*	16.0	*2.0*	**2.8**	1.0	0.8	*0.0*	42100	*0.9*	16.0	*2.1*	**3.1**
Ir	34	*0.0*	0.4	*0.0*	**0.1**	<0.167	<0.167	*0.0*	1300	*0.0*	0.4	*0.1*	**0.1**
Os	5	*0.0*	<0.2	*0.0*	**0.0**	<0.167	<0.167	*0.0*	260	*0.0*	<0.2	*0.0*	**0.0**
Au	418	*0.3*	<0.01	*0.0*	**0.3**	0.2	0.2	*0.0*	11900	*0.3*	<0.01	*0.0*	**0.3**
Ag	1797	*1.3*	<0.2	*0.0*	**1.3**	1.2	1.8	*0.0*	10400	*0.2*	<0.2	*0.0*	**0.2**
Cu	827200	*579.4*	36200	*4501*	**5081**	0.0	0.0	*775.1*	155200	*3.4*	36900	*4941.4*	**5720.0**
Ni	122100	*85.5*	56120	*6978.0*	**7063.5**	24.0	24.3	*0.0*	6000	*0.1*	55860	*7480.5*	**7480.6**
Fe	30700	*21.5*	2370	*294.7*	**316.2**	111.7	10.8	*0.1*	6700	*0.1*	2560	*342.8*	**343.1**
Co	1600	*1.1*	852	*105.9*	**107.1**	13.7	1.5	*0.0*	630	*0.0*	877	*117.4*	**117.5**
Pb	3040	*2.1*	6.4	*0.8*	**2.9**	1.0	0.7	*0.0*	57700	*1.3*	8.4	*1.1*	**2.4**
As	2630	*1.8*	79.0	*9.8*	**11.7**	0.8	0.8	*0.0*	59300	*1.3*	74.0	*9.9*	**11.2**
S	1900	*1.3*	116800	*14522.9*	**14524.2**	0.0	0.0	*0.0*	93700	*2.0*	114400	*15319.8*	**15321.9**
Si	2600	*1.8*	44.3	*5.5*	**7.3**	8.0	16.7	*0.0*	14200	*0.3*	34.8	*4.7*	**5.0**
Te	865	*0.6*	43.0	*5.3*	**6.0**	11.8	7.3	*0.0*	48300	*1.1*	33.0	*4.4*	**5.5**
Sb	1110	*0.8*	8.3	*1.0*	**1.8**	0.3	0.8	*0.0*	10900	*0.2*	11.0	*1.5*	**1.7**
Bi	488	*0.3*	0.7	*0.1*	**0.4**	0.5	<0.167	*0.0*	3950	*0.1*	2.6	*0.3*	**0.4**
Sn	183	*0.1*	0.0	*0.0*	**0.1**	0.3	<0.167	*0.0*	69	*0.0*	1.0	*0.1*	**0.1**
Se	84	*0.1*	11.0	*1.4*	**1.4**	5.8	5.5	*0.0*	7460	*0.2*	9.2	*1.2*	**1.4**
Zn	72.7	*0.1*	26.5	*3.3*	**3.3**	8.2	14.7	*0.0*	8.9	*0.0*	27.7	*3.7*	**3.7**

Table E.4: Elemental input and output grades, concentrations and mass flows of test 4 (100 A/m^2)

Element	Initial Anode	*Mass in Anode*	Electrolyte Feed	*Mass in Electrolyte Feed*	Total In	Cathode Front	Cathode Back	*Mass in Cathode*	Slimes	*Mass in Slimes*	Spent Electrolyte	*Mass in Spent Electrolyte*	Total Out
	(g/t)	*(g)*	(mg/l)	*(g)*	**(g)**	(g/t)	(g/t)	*(g)*	(g/t)	*(g)*	(mg/l)	*(g)*	**(g)**
Pt	837	*0.6*	<0.01	*0.0*	**0.6**	<0.167	<0.167	*0.0*	25100	*0.5*	0.0	*0.0*	**0.5**
Pd	4740	*3.2*	<0.01	*0.0*	**3.2**	1.7	2.8	*0.0*	140100	*2.9*	0.1	*0.0*	**2.9**
Rh	1109	*0.8*	3.6	*0.5*	**1.3**	1.3	1.5	*0.0*	36200	*0.8*	2.5	*0.4*	**1.1**
Ru	1157	*0.8*	16.0	*2.4*	**3.1**	1.0	1.2	*0.0*	41500	*0.9*	15.0	*2.3*	**3.1**
Ir	35	*0.0*	0.4	*0.1*	**0.1**	<0.167	<0.167	*0.0*	1200	*0.0*	0.4	*0.1*	**0.1**
Os	5	*0.0*	<0.2	*0.0*	**0.0**	<0.167	<0.167	*0.0*	240	*0.0*	<0.2	*0.0*	**0.0**
Au	426	*0.3*	<0.01	*0.0*	**0.3**	<0.167	0.2	*0.0*	11300	*0.2*	<0.2	*0.0*	**0.2**
Ag	1693	*1.1*	<0.2	*0.0*	**1.1**	1.0	1.3	*0.0*	9080	*0.2*	2.2	*0.3*	**0.5**
Cu	827800	*560.4*	41050	*6065*	**6626**	0.0	0.0	*633.6*	270600	*5.6*	38400	*5856.0*	**6495.3**
Ni	121400	*82.2*	56800	*8392.2*	**8474.4**	28.3	33.5	*0.0*	10800	*0.2*	52820	*8055.1*	**8055.4**
Fe	31500	*21.3*	2365	*349.4*	**370.8**	6.3	7.5	*0.0*	8100	*0.2*	2450	*373.6*	**373.8**
Co	1600	*1.1*	854	*126.1*	**127.2**	2.8	3.2	*0.0*	770	*0.0*	868	*132.4*	**132.4**
Pb	2790	*1.9*	6.0	*0.9*	**2.8**	<0.167	0.8	*0.0*	53400	*1.1*	8.3	*1.3*	**2.4**
As	2650	*1.8*	80.0	*11.8*	**13.6**	0.8	0.8	*0.0*	63400	*1.3*	74.0	*11.3*	**12.6**
S	1900	*1.3*	130500	*19281.4*	**19282.7**	0.0	0.0	*0.0*	78700	*1.6*	110300	*16820.9*	**16822.5**
Si	2700	*1.8*	28.9	*4.3*	**6.1**	43.3	10.8	*0.0*	8000	*0.2*	48.4	*7.4*	**7.6**
Te	804	*0.5*	46.0	*6.8*	**7.3**	7.5	9.2	*0.0*	53900	*1.1*	33.0	*5.0*	**6.2**
Sb	1045	*0.7*	8.8	*1.3*	**2.0**	0.8	0.7	*0.0*	10500	*0.2*	10.0	*1.5*	**1.7**
Bi	456	*0.3*	1.1	*0.2*	**0.5**	<0.167	<0.167	*0.0*	3910	*0.1*	2.3	*0.4*	**0.4**
Sn	172	*0.1*	0.1	*0.0*	**0.1**	<0.167	<0.167	*0.0*	67	*0.0*	0.8	*0.1*	**0.1**
Se	74	*0.1*	11.0	*1.6*	**1.7**	4.3	4.8	*0.0*	7820	*0.2*	9.1	*1.4*	**1.6**
Zn	73.6	*0.0*	27.8	*4.1*	**4.2**	8.2	9.2	*0.0*	15.7	*0.0*	26.0	*4.0*	**4.0**

Table E.5: Elemental input and output grades, concentrations and mass flows of test 5 (150 A/m^2)

Element	Initial Anode	*Mass in Anode*	Electrolyte Feed	*Mass in Electrolyte Feed*	Total In	Cathode Front	Cathode Back	*Mass in Cathode*	Slimes	*Mass in Slimes*	Spent Electrolyte	*Mass in Spent Electrolyte*	Total Out
	(g/t)	*(g)*	(mg/l)	*(g)*	**(g)**	(g/t)	(g/t)	*(g)*	(g/t)	*(g)*	(mg/l)	*(g)*	**(g)**
Pt	860	*0.6*	<0.01	*0.0*	**0.6**	<0.167	<0.167	*0.0*	24100	*0.6*	<0.2	*0.0*	**0.6**
Pd	4730	*3.3*	<0.01	*0.0*	**3.3**	2.8	2.0	*0.0*	130400	*3.0*	<0.2	*0.0*	**3.0**
Rh	1135	*0.8*	2.7	*0.3*	**1.1**	3.5	7.3	*0.0*	34300	*0.8*	2.5	*0.3*	**1.1**
Ru	1179	*0.8*	15.0	*1.6*	**2.4**	14.5	14.2	*0.0*	36300	*0.8*	15.0	*1.6*	**2.5**
Ir	35	*0.0*	0.4	*0.0*	**0.1**	<0.167	<0.167	*0.0*	1100	*0.0*	0.4	*0.0*	**0.1**
Os	5	*0.0*	<0.2	*0.0*	**0.0**	<0.167	<0.167	*0.0*	220	*0.0*	<0.2	*0.0*	**0.0**
Au	403	*0.3*	<0.01	*0.0*	**0.3**	<0.167	<0.167	*0.0*	10400	*0.2*	<0.2	*0.0*	**0.2**
Ag	1593	*1.1*	<0.2	*0.0*	**1.1**	1.0	1.2	*0.0*	9600	*0.2*	<0.2	*0.0*	**0.2**
Cu	824000	*578.7*	37400	*3874*	**4453**	0.0	0.0	*655.0*	272400	*6.4*	38200	*4074.7*	**4736.0**
Ni	126900	*89.1*	56380	*5840.1*	**5929.2**	101.7	112.7	*0.1*	15500	*0.4*	55060	*5873.1*	**5873.5**
Fe	35000	*24.6*	2370	*245.5*	**270.1**	6.5	4.2	*0.0*	12300	*0.3*	2580	*275.2*	**275.5**
Co	1700	*1.2*	898	*93.0*	**94.2**	7.3	7.0	*0.0*	600	*0.0*	898	*95.8*	**95.8**
Pb	2800	*2.0*	6.6	*0.7*	**2.7**	1.0	0.3	*0.0*	45100	*1.1*	4.4	*0.5*	**1.5**
As	2310	*1.6*	76.0	*7.9*	**9.5**	0.8	0.8	*0.0*	60000	*1.4*	73.0	*7.8*	**9.2**
S	1700	*1.2*	114500	*11860.5*	**11861.7**	0.0	0.0	*0.0*	78300	*1.8*	111600	*11904.0*	**11905.8**
Si	<1000	*0.4*	62.5	*6.5*	**6.8**	41.7	38.3	*0.0*	3800	*0.1*	66.6	*7.1*	**7.2**
Te	711	*0.5*	42.0	*4.4*	**4.8**	138.7	139.8	*0.1*	39100	*0.9*	33.0	*3.5*	**4.5**
Sb	1014	*0.7*	8.4	*0.9*	**1.6**	1.0	0.8	*0.0*	15900	*0.4*	10.0	*1.1*	**1.4**
Bi	439	*0.3*	1.1	*0.1*	**0.4**	<0.167	<0.167	*0.0*	3440	*0.1*	2.9	*0.3*	**0.4**
Sn	167	*0.1*	<0.2	*0.0*	**0.1**	<0.167	<0.167	*0.0*	65	*0.0*	1.2	*0.1*	**0.1**
Se	74	*0.1*	11.0	*1.1*	**1.2**	8.2	9.0	*0.0*	6610	*0.2*	9.0	*1.0*	**1.1**
Zn	80.0	*0.1*	26.4	*2.7*	**2.8**	9.2	8.8	*0.0*	10.8	*0.0*	25.7	*2.7*	**2.7**

Table E.6: Elemental input and output grades, concentrations and mass flows of test 6 (30 g/l Cu)

Element	Initial Anode	*Mass in Anode*	Electrolyte Feed	*Mass in Electrolyte Feed*	Total In	Cathode Front	Cathode Back	*Mass in Cathode*	Slimes	*Mass in Slimes*	Spent Electrolyte	*Mass in Spent Electrolyte*	Total Out
	(g/t)	*(g)*	(mg/l)	*(g)*	**(g)**	(g/t)	(g/t)	*(g)*	(g/t)	*(g)*	(mg/l)	*(g)*	**(g)**
Pt	851	*0.6*	<0.01	*0.0*	**0.6**	<0.167	<0.167	*0.0*	22200	*0.6*	<0.2	*0.0*	**0.6**
Pd	4910	*3.4*	0.0	*0.0*	**3.4**	1.7	1.0	*0.0*	114200	*3.1*	<0.2	*0.0*	**3.1**
Rh	1134	*0.8*	1.9	*0.2*	**1.0**	9.7	8.2	*0.0*	30200	*0.8*	1.7	*0.2*	**1.0**
Ru	1177	*0.8*	11.0	*1.4*	**2.2**	15.5	13.5	*0.0*	33500	*0.9*	11.0	*1.4*	**2.3**
Ir	35	*0.0*	0.3	*0.0*	**0.1**	<0.167	<0.167	*0.0*	960	*0.0*	0.3	*0.0*	**0.1**
Os	7	*0.0*	<0.2	*0.0*	**0.0**	<0.167	<0.167	*0.0*	230	*0.0*	<0.2	*0.0*	**0.0**
Au	402	*0.3*	<0.01	*0.0*	**0.3**	<0.167	0.2	*0.0*	8900	*0.2*	<0.2	*0.0*	**0.2**
Ag	1609	*1.1*	0.1	*0.0*	**1.1**	1.5	2.2	*0.0*	17700	*0.5*	0.4	*0.0*	**0.5**
Cu	810700	*567.2*	28350	*3490*	**4058**	0.0	0.0	*671.6*	266500	*7.2*	28200	*3560.0*	**4238.8**
Ni	124100	*86.8*	39830	*4903.9*	**4990.7**	88.5	86.3	*0.1*	23800	*0.6*	40950	*5169.5*	**5170.2**
Fe	40100	*28.1*	1745	*214.8*	**242.9**	6.8	3.8	*0.0*	32200	*0.9*	1972	*248.9*	**249.8**
Co	1600	*1.1*	633	*77.9*	**79.1**	6.2	2.7	*0.0*	1400	*0.0*	644	*81.3*	**81.3**
Pb	2510	*1.8*	5.2	*0.6*	**2.4**	2.0	0.5	*0.0*	37800	*1.0*	6.5	*0.8*	**1.8**
As	2340	*1.6*	43.0	*5.3*	**6.9**	0.8	0.8	*0.0*	46300	*1.3*	54.0	*6.8*	**8.1**
S	1900	*1.3*	91550	*11271.6*	**11273.0**	0.0	0.0	*0.0*	56100	*1.5*	98950	*12491.4*	**12492.9**
Si	4500	*3.1*	62.5	*7.7*	**10.8**	66.7	68.3	*0.0*	42800	*1.2*	74.0	*9.3*	**10.5**
Te	745	*0.5*	30.0	*3.7*	**4.2**	148.5	168.3	*0.1*	32400	*0.9*	22.0	*2.8*	**3.8**
Sb	1021	*0.7*	6.7	*0.8*	**1.5**	1.8	2.3	*0.0*	11100	*0.3*	8.9	*1.1*	**1.4**
Bi	410	*0.3*	0.7	*0.1*	**0.4**	<0.167	<0.167	*0.0*	2870	*0.1*	1.9	*0.2*	**0.3**
Sn	165	*0.1*	0.1	*0.0*	**0.1**	<0.167	0.3	*0.0*	63	*0.0*	1.0	*0.1*	**0.1**
Se	70	*0.0*	8.7	*1.1*	**1.1**	9.5	9.8	*0.0*	5260	*0.1*	6.6	*0.8*	**1.0**
Zn	120.0	*0.1*	20.6	*2.5*	**2.6**	92.5	96.3	*0.1*	37.2	*0.0*	21.9	*2.8*	**2.8**

Table E.7: Elemental input and output grades, concentrations and mass flows of test 7 (50 g/l Cu)

Element	Initial Anode	*Mass in Anode*	Electrolyte Feed	*Mass in Electrolyte Feed*	Total In	Cathode Front	Cathode Back	*Mass in Cathode*	Slimes	*Mass in Slimes*	Spent Electrolyte	*Mass in Spent Electrolyte*	Total Out
	(g/t)	*(g)*	(mg/l)	*(g)*	**(g)**	(g/t)	(g/t)	*(g)*	(g/t)	*(g)*	(mg/l)	*(g)*	**(g)**
Pt	851	*0.6*	<0.01	*0.0*	**0.6**	<0.167	<0.167	*0.0*	19500	*0.6*	<0.2	*0.0*	**0.6**
Pd	4840	*3.4*	<0.01	*0.0*	**3.4**	<0.167	<0.167	*0.0*	106600	*3.2*	<0.2	*0.0*	**3.2**
Rh	1101	*0.8*	2.6	*0.3*	**1.1**	1.0	0.8	*0.0*	28100	*0.8*	2.5	*0.3*	**1.1**
Ru	1177	*0.8*	15.0	*1.6*	**2.4**	1.2	0.8	*0.0*	30000	*0.9*	15.0	*1.7*	**2.6**
Ir	35	*0.0*	0.4	*0.0*	**0.1**	<0.167	<0.167	*0.0*	850	*0.0*	0.4	*0.0*	**0.1**
Os	6	*0.0*	<0.2	*0.0*	**0.0**	<0.167	<0.167	*0.0*	200	*0.0*	<0.2	*0.0*	**0.0**
Au	403	*0.3*	<0.01	*0.0*	**0.3**	<0.167	<0.167	*0.0*	8300	*0.2*	<0.2	*0.0*	**0.2**
Ag	1589	*1.1*	<0.2	*0.0*	**1.1**	1.8	1.3	*0.0*	17000	*0.5*	<0.2	*0.0*	**0.5**
Cu	819800	*575.1*	37500	*4039*	**4614**	0.0	0.0	*672.0*	84700	*2.5*	40500	*4526.0*	**5200.5**
Ni	122000	*85.6*	54140	*5830.9*	**5916.5**	14.7	8.3	*0.0*	14400	*0.4*	52390	*5854.8*	**5855.2**
Fe	40100	*28.1*	2300	*247.7*	**275.8**	416.7	<0.833	*0.1*	21800	*0.7*	2520	*281.6*	**282.4**
Co	1600	*1.1*	835	*89.9*	**91.1**	0.5	0.3	*0.0*	930	*0.0*	838	*93.6*	**93.7**
Pb	2540	*1.8*	7.9	*0.9*	**2.6**	74.3	95.0	*0.1*	37600	*1.1*	5.1	*0.6*	**1.7**
As	2340	*1.6*	73.0	*7.9*	**9.5**	<0.167	<0.167	*0.0*	38300	*1.1*	71.0	*7.9*	**9.1**
S	1700	*1.2*	114100	*12288.6*	**12289.8**	0.0	0.0	*0.0*	84700	*2.5*	113200	*12650.5*	**12653.**
Si	5300	*3.7*	69.9	*7.5*	**11.2**	45.0	233.3	*0.1*	96800	*2.9*	66.7	*7.5*	**10.4**
Te	743	*0.5*	42.0	*4.5*	**5.0**	5.7	3.7	*0.0*	27800	*0.8*	34.0	*3.8*	**4.6**
Sb	1023	*0.7*	8.5	*0.9*	**1.6**	0.5	0.3	*0.0*	8020	*0.2*	11.0	*1.2*	**1.5**
Bi	412	*0.3*	1.0	*0.1*	**0.4**	<0.167	<0.167	*0.0*	2430	*0.1*	2.4	*0.3*	**0.3**
Sn	167	*0.1*	0.0	*0.0*	**0.1**	1.3	1.2	*0.0*	291	*0.0*	2.2	*0.2*	**0.3**
Se	72	*0.1*	11.0	*1.2*	**1.2**	9.2	12.7	*0.0*	4580	*0.1*	8.6	*1.0*	**1.1**
Zn	114.0	*0.1*	28.4	*3.1*	**3.1**	6.8	12.5	*0.0*	23.9	*0.0*	25.1	*2.8*	**2.8**

Table E.8: Elemental accountability and deportment for test 1 (110 g/l H_2SO_4)

Element	Accountability	Recovery From Anode + Electrolyte			Mass in Slimes / Mass from Anode
		To slimes	To Electrolyte	To Cathodes	
	%	%	%	%	Fraction
Pt	105.7%	99.6%	0.0%	0.4%	0.996
Pd	95.0%	99.9%	0.0%	0.1%	0.999
Rh	110.1%	71.6%	28.3%	0.1%	1.047
Ru	97.2%	24.2%	75.8%	0.0%	0.963
Ir	101.7%	30.8%	69.2%	0.0%	1.080
Os	130.9%	100.0%	0.0%	0.0%	1.000
Au	92.8%	98.3%	0.0%	1.7%	0.983
Ag	14.6%	91.6%	8.4%	0.0%	0.929
Cu	103.8%	0.1%	88.2%	11.8%	0.006
Ni	96.9%	0.0%	100.0%	0.0%	0.001
Fe	97.3%	0.1%	99.9%	0.0%	0.007
Co	105.8%	0.0%	100.0%	0.0%	0.000
Pb	75.3%	47.2%	52.6%	0.3%	0.707
As	98.1%	11.2%	88.7%	0.0%	0.880
S	101.5%	0.0%	100.0%	0.0%	1.539
Si	117.6%	0.0%	99.8%	0.2%	0.000
Te	95.3%	21.6%	78.3%	0.1%	2.686
Sb	89.3%	22.9%	77.1%	0.0%	0.630
Bi	93.8%	16.8%	83.2%	0.0%	0.246
Sn	107.5%	2.5%	97.5%	0.0%	0.025
Se	95.9%	9.5%	90.4%	0.2%	2.983
Zn	102.8%	0.0%	99.9%	0.1%	0.010

Table E.9: Elemental accountability and deportment for test 2 (Base-case)

Element	Accountability	Recovery From Anode + Electrolyte			Mass in Slimes / Mass from Anode
		To slimes	To Electrolyte	To Cathodes	
	%	%	%	%	Fraction
Pt	84.0%	100.0%	0.0%	0.0%	1.000
Pd	86.8%	99.9%	0.0%	0.1%	0.999
Rh	92.2%	72.9%	26.6%	0.5%	0.997
Ru	102.0%	29.5%	70.2%	0.3%	0.934
Ir	93.6%	33.6%	66.4%	0.0%	0.911
Os	90.9%	100.0%	0.0%	0.0%	1.000
Au	84.1%	100.0%	0.0%	0.0%	1.000
Ag	18.5%	42.5%	57.4%	0.1%	0.425
Cu	100.0%	0.1%	87.7%	12.2%	0.011
Ni	105.4%	0.0%	100.0%	0.0%	0.001
Fe	103.0%	0.0%	99.9%	0.0%	0.004
Co	107.6%	0.0%	100.0%	0.0%	0.000
Pb	64.7%	61.7%	38.3%	0.0%	0.967

Element	Accountability	Recovery From Anode + Electrolyte			Mass in Slimes / Mass from Anode
		To slimes	To Electrolyte	To Cathodes	
As	99.2%	12.6%	87.4%	0.0%	0.957
S	104.0%	0.0%	100.0%	0.0%	1.621
Si	80.0%	2.7%	95.9%	1.3%	0.374
Te	93.5%	20.2%	78.2%	1.6%	2.608
Sb	90.5%	29.2%	70.7%	0.2%	0.723
Bi	97.6%	17.0%	82.8%	0.2%	0.248
Sn	113.3%	1.0%	99.0%	0.0%	0.010
Se	92.2%	13.5%	86.4%	0.1%	4.130
Zn	107.0%	0.0%	100.0%	0.0%	0.017

Table E.10: Elemental accountability and deportment for test 3 (With additives)

Element	Accountability	Recovery From Anode + Electrolyte			Mass in Slimes / Mass from Anode
		To slimes	To Electrolyte	To Cathodes	
	%	%	%	%	Fraction
Pt	92.1%	99.7%	0.3%	0.0%	0.996
Pd	90.9%	99.6%	0.3%	0.0%	0.999
Rh	87.9%	66.3%	33.7%	0.1%	1.047
Ru	100.1%	27.3%	72.6%	0.0%	0.963
Ir	103.7%	29.0%	71.0%	0.0%	1.080
Os	139.3%	100.0%	0.0%	0.0%	1.000
Au	81.3%	100.0%	0.0%	0.0%	0.983
Ag	46.0%	35.7%	64.2%	0.1%	0.929
Cu	98.0%	0.1%	90.2%	9.8%	0.006
Ni	95.1%	0.0%	100.0%	0.0%	0.001
Fe	100.8%	0.0%	100.0%	0.0%	0.007
Co	104.1%	0.0%	100.0%	0.0%	0.000
Pb	85.5%	46.7%	53.3%	0.0%	0.707
As	92.6%	10.4%	89.6%	0.0%	0.880
S	87.2%	0.0%	100.0%	0.0%	1.539
Si	124.0%	2.2%	97.6%	0.2%	0.000
Te	83.9%	18.2%	81.8%	0.1%	2.686
Sb	86.8%	12.5%	87.5%	0.0%	0.630
Bi	91.6%	18.8%	81.2%	0.0%	0.246
Sn	90.0%	1.1%	98.9%	0.0%	0.025
Se	92.7%	10.4%	89.4%	0.2%	2.983
Zn	95.5%	0.0%	99.9%	0.1%	0.010

Table E.11: Elemental accountability and deportment for test 4 (100 A/m^2)

Element	Accountability	Recovery From Anode + Electrolyte			Mass in Slimes / Mass from Anode
		To slimes	To Electrolyte	To Cathodes	
	%	%	%	%	Fraction
Pt	92.1%	99.7%	0.3%	0.0%	0.997
Pd	90.9%	99.6%	0.3%	0.0%	0.996

Element	Accountability	Recovery From Anode + Electrolyte			Mass in Slimes / Mass from Anode
		To slimes	To Electrolyte	To Cathodes	
Rh	87.9%	66.3%	33.7%	0.1%	1.138
Ru	100.1%	27.3%	72.6%	0.0%	1.098
Ir	103.7%	29.0%	71.0%	0.0%	1.013
Os	139.3%	100.0%	0.0%	0.0%	1.000
Au	81.3%	100.0%	0.0%	0.0%	1.000
Ag	46.0%	35.7%	64.2%	0.1%	0.357
Cu	98.0%	0.1%	90.2%	9.8%	0.010
Ni	95.1%	0.0%	100.0%	0.0%	0.003
Fe	100.8%	0.0%	100.0%	0.0%	0.008
Co	104.1%	0.0%	100.0%	0.0%	0.014
Pb	85.5%	46.7%	53.3%	0.0%	0.686
As	92.6%	10.4%	89.6%	0.0%	0.792
S	87.2%	0.0%	100.0%	0.0%	1.455
Si	124.0%	2.2%	97.6%	0.2%	0.073
Te	83.9%	18.2%	81.8%	0.1%	2.449
Sb	86.8%	12.5%	87.5%	0.0%	0.355
Bi	91.6%	18.8%	81.2%	0.0%	0.287
Sn	90.0%	1.1%	98.9%	0.0%	0.013
Se	92.7%	10.4%	89.4%	0.2%	3.488
Zn	95.5%	0.0%	99.9%	0.1%	0.007

Table E.12: Elemental accountability and deportment for test 5 (150 A/m^2)

Element	Accountability	Recovery From Anode + Electrolyte			Mass in Slimes / Mass from Anode
		To slimes	To Electrolyte	To Cathodes	
	%	%	%	%	Fraction
Pt	93.2%	100.0%	0.0%	0.0%	1.000
Pd	91.7%	99.9%	0.0%	0.1%	0.999
Rh	99.5%	74.8%	24.9%	0.3%	1.010
Ru	103.2%	34.5%	65.1%	0.4%	0.993
Ir	103.6%	37.6%	62.4%	0.0%	1.009
Os	140.5%	100.0%	0.0%	0.0%	1.000
Au	85.8%	100.0%	0.0%	0.0%	1.000
Ag	20.1%	99.7%	0.0%	0.3%	0.997
Cu	106.4%	0.1%	86.0%	13.8%	0.010
Ni	99.1%	0.0%	100.0%	0.0%	0.004
Fe	102.0%	0.1%	99.9%	0.0%	0.011
Co	101.7%	0.0%	100.0%	0.0%	0.012
Pb	57.5%	69.2%	30.8%	0.0%	0.932
As	96.8%	15.3%	84.7%	0.0%	0.893
S	100.4%	0.0%	100.0%	0.0%	1.526
Si	105.8%	1.2%	98.4%	0.4%	0.239
Te	93.3%	20.2%	77.8%	2.0%	1.961
Sb	90.9%	25.8%	74.1%	0.0%	0.574
Bi	92.3%	20.6%	79.4%	0.0%	0.282
Sn	110.4%	1.2%	98.8%	0.0%	0.012
Se	94.0%	13.8%	85.7%	0.5%	3.181
Zn	98.4%	0.0%	99.8%	0.2%	0.005

Table E.13: Elemental accountability and deportment for test 6 (30 g/l Cu)

Element	Accountability	Recovery From Anode + Electrolyte			Mass in Slimes / Mass from Anode
		To slimes	To Electrolyte	To Cathodes	
	%	%	%	%	Fraction
Pt	101.3%	100.0%	0.0%	0.0%	1.000
Pd	90.3%	100.0%	0.0%	0.0%	1.000
Rh	101.3%	78.8%	20.6%	0.6%	1.020
Ru	106.0%	39.4%	60.2%	0.4%	1.042
Ir	110.5%	40.8%	59.2%	0.0%	0.958
Os	132.7%	100.0%	0.0%	0.0%	1.000
Au	86.0%	100.0%	0.0%	0.0%	1.000
Ag	46.4%	90.9%	8.8%	0.2%	0.920
Cu	104.5%	0.2%	84.0%	15.8%	0.012
Ni	103.6%	0.0%	100.0%	0.0%	0.007
Fe	102.9%	0.4%	99.6%	0.0%	0.030
Co	102.9%	0.0%	99.9%	0.0%	0.033
Pb	77.1%	55.6%	44.4%	0.0%	0.758
As	116.5%	15.6%	84.4%	0.0%	0.659
S	110.8%	0.0%	100.0%	0.0%	1.034
Si	97.3%	11.0%	88.6%	0.4%	0.380
Te	89.3%	23.4%	73.8%	2.8%	1.891
Sb	92.7%	21.1%	78.8%	0.1%	0.455
Bi	85.2%	24.5%	75.5%	0.0%	0.319
Sn	104.3%	1.3%	98.6%	0.1%	0.014
Se	87.7%	14.5%	84.8%	0.7%	3.326
Zn	108.1%	0.0%	97.7%	2.2%	0.011

Table E.14: Elemental accountability and deportment for test 7 (50 g/l Cu)

Element	Accountability	Recovery From Anode + Electrolyte			Mass in Slimes / Mass from Anode
		To slimes	To Electrolyte	To Cathodes	
	%	%	%	%	Fraction
Pt	97.4%	100.0%	0.0%	0.0%	1.000
Pd	93.6%	100.0%	0.0%	0.0%	1.000
Rh	106.2%	75.0%	25.0%	0.1%	1.021
Ru	105.3%	34.8%	65.2%	0.0%	1.029
Ir	103.5%	36.2%	63.8%	0.0%	0.995
Os	146.6%	100.0%	0.0%	0.0%	1.000
Au	87.5%	100.0%	0.0%	0.0%	1.000
Ag	45.6%	99.8%	0.0%	0.2%	0.998
Cu	112.7%	0.0%	87.0%	12.9%	0.004
Ni	99.0%	0.0%	100.0%	0.0%	0.005
Fe	102.4%	0.2%	99.7%	0.0%	0.023
Co	102.9%	0.0%	100.0%	0.0%	0.024
Pb	66.4%	64.1%	32.6%	3.3%	0.947
As	95.5%	12.6%	87.4%	0.0%	0.728

Element	Accountability	Recovery From Anode + Electrolyte			Mass in Slimes / Mass from Anode
		To slimes	To Electrolyte	To Cathodes	
S	103.0%	0.0%	100.0%	0.0%	2.057
Si	92.9%	27.6%	71.4%	1.0%	0.836
Te	91.8%	17.9%	82.0%	0.1%	1.732
Sb	89.9%	16.3%	83.7%	0.0%	0.371
Bi	85.9%	21.3%	78.7%	0.0%	0.292
Sn	218.0%	3.4%	96.3%	0.3%	0.034
Se	89.5%	12.4%	87.0%	0.7%	3.022
Zn	89.4%	0.0%	99.7%	0.2%	0.010

F. Product Characterisation Results

Anode Slimes Composition

Table F.1: Element group composition of anode slimes

Special Condition	PGMs	BMs	Ag, As, Te, Se & Pb	Al, Si, Sb, Bi, Sn & Zn	S
110 g/l Acid	30.52%	20.08%	19.12%	2.56%	9.55%
Base-case	25.30%	29.41%	16.52%	2.89%	8.65%
With Additives	26.69%	16.85%	18.32%	2.91%	9.37%
100 CD	25.56%	29.03%	18.76%	2.25%	7.87%
150 CD	23.68%	30.08%	16.04%	2.32%	7.83%
30 g/l Cu	21.02%	32.39%	13.95%	5.69%	5.61%
50 g/l Cu	19.36%	12.18%	12.53%	10.76%	8.47%
130 g/l Acid	3.92%	62.53%	1.81%	18.44%	1.05%
190 g/l Acid	2.79%	31.87%	1.78%	18.99%	4.61%
250 CD	3.17%	59.60%	1.40%	15.99%	2.02%
300 CD	3.36%	60.92%	8.18%	16.96%	1.92%
PMR	0.5847	0.172	4.28%	0.43%	0.02

Table F.2: Impurity grade in PMR feed and slimes produced by altered anode material

Element	130 g/l H_2SO_4	190 g/l H_2SO_4	250 A/m^2	300 A/m^2	PMR Feed
Ag (g/t)	4270	2960	3340	3510	300000
Cu (g/t)	21700	17500	18800	20400	170000
Ni (g/t)	5220	2900	3800	3900	35000
Fe (g/t)	5750	2980	3980	3970	46000
Co (g/t)	142	72	100	105	14000
Pb (g/t)	2110	1529	1700	1751	13000
As (g/t)	8200	6950	7300	75100	4700
Al (g/t)	75700	39500	81500	84500	50000
S (g/t)	391400	191300	346800	354500	90000
Cr (g/t)	152600	85200	162900	165400	30000
Mg (g/t)	5600	2700	4800	4800	2000

Element	130 g/l H_2SO_4	190 g/l H_2SO_4	250 A/m^2	300 A/m^2	PMR Feed
Si (g/t)	<1000	<1000	<1000	<1000	
Te (g/t)	4770	5490	2890	2880	9000
Sb (g/t)	3060	1890	2150	2130	8400
Bi (g/t)	1400	1900	<1000	<1000	
Sn (g/t)	10500	46100	20200	19200	20000
Se (g/t)	<1000	<1000	<1000	<1000	2000
Zn (g/t)	<1000	<1000	<1000	<1000	
Ag (g/t)	182400	187200	159400	169000	
Cu (g/t)	1440	2500	1248	1284	5000
Ni (g/t)	468	713	438	487	2000
Fe (g/t)	102	75	75	68	1400
Co (g/t)	43	16	17	17	500
Ca (g/t)	626	1005	366	386	15900
Pb (g/t)	14	8	5		400

G. Effect of Blended Feed on PMR Feed Composition

Table G.1: Monthly throughput of typical PMR feed, slimes and new blended feed with the change in average composition (Test1 Test 2)

Anodes t/month:		110	Test 1					Test 2				
	FC		Slimes % Slimes/Anode	2.78%	New Total		Over initial mean	Slimes % Slimes/Anode	3.12%	New Total		Over initial mean
	kg/month	%	kg/month	%	kg/month	%		kg/month	%	kg/month	%	
Total	22078.54	91.72%	3058.00	82.18%	25136.54	90.56%		3432.00	82.82%	25510.54	90.52%	
Pt	7134.94	32.32%	102.44	3.35%	7237.39	28.79%	-3.52%	88.20	2.57%	7223.15	28.31%	-4.00%
Pd	3831.67	17.35%	533.01	17.43%	4364.68	17.36%	0.01%	472.24	13.76%	4303.91	16.87%	-0.48%
Au	215.77	0.98%	42.20	1.38%	257.97	1.03%	0.05%	37.41	1.09%	253.18	0.99%	0.02%
Rh	935.39	4.24%	145.87	4.77%	1081.26	4.30%	0.06%	132.82	3.87%	1068.21	4.19%	-0.05%
Ir	364.01	1.65%	3.67	0.12%	367.68	1.46%	-0.19%	3.78	0.11%	367.79	1.44%	-0.21%
Ru	1235.27	5.59%	105.50	3.45%	1340.77	5.33%	-0.26%	133.16	3.88%	1368.43	5.36%	-0.23%
Os	129.99	0.59%	0.70	0.02%	130.69	0.52%	-0.07%	0.76	0.02%	130.74	0.51%	-0.08%
Ag	50.24	0.23%	22.42	0.73%	72.66	0.29%	0.06%	11.74	0.34%	61.98	0.24%	0.02%
Fe	1050.03	4.76%	32.11	1.05%	1082.14	4.31%	-0.45%	20.94	0.61%	1070.97	4.20%	-0.56%
Ni	2880.86	13.05%	8.56	0.28%	2889.42	11.49%	-1.55%	21.96	0.64%	2902.83	11.38%	-1.67%
Cu	1026.47	4.65%	573.38	18.75%	1599.84	6.36%	1.72%	966.45	28.16%	1992.92	7.81%	3.16%
S	441.57	2.00%	292.04	9.55%	733.61	2.92%	0.92%	296.87	8.65%	738.44	2.89%	0.89%
Co	39.06	0.18%	1.53	0.05%	40.59	0.16%	-0.02%	1.72	0.05%	40.77	0.16%	-0.02%
Te	81.30	0.37%	187.15	6.12%	268.45	1.07%	0.70%	158.90	4.63%	240.20	0.94%	0.57%
Se	202.52	0.92%	21.56	0.71%	224.08	0.89%	-0.03%	26.84	0.78%	229.36	0.90%	-0.02%
Pb	273.68	1.24%	160.85	5.26%	434.53	1.73%	0.49%	170.91	4.98%	444.59	1.74%	0.50%
Zn	17.66	0.08%	0.03	0.00%	17.69	0.07%	-0.01%	0.04	0.00%	17.70	0.07%	-0.01%
Sb	32.22	0.15%	61.16	2.00%	93.38	0.37%	0.23%	66.24	1.93%	98.46	0.39%	0.24%
As	228.99	1.04%	192.65	6.30%	421.65	1.68%	0.64%	198.71	5.79%	427.71	1.68%	0.64%
Bi	55.96	0.25%	10.40	0.34%	66.36	0.26%	0.01%	9.95	0.29%	65.91	0.26%	0.00%
Sn	6.32	0.03%	0.47	0.02%	6.80	0.03%	0.00%	0.18	0.01%	6.50	0.03%	0.00%
Al	16.33	0.07%	6.12	0.20%	22.45	0.09%	0.02%	6.18	0.18%	22.51	0.09%	0.01%
Si			9.17	0.30%	9.17	0.04%	0.04%	16.47	0.48%	16.47	0.06%	0.06%

Table G.2: Monthly throughput of typical PMR feed, slimes and new blended feed with the change in average composition (Test3 Test 4)

	Test 3					Test 4				
	Slimes		New Total		Over initial mean	Slimes		New Total		Over initial mean
	% Slimes/Anode	3.11%				% Slimes/Anode	3.08%			
	kg/month	%	kg/month	%		kg/month	%	kg/month	%	
Total	3421.00	74.24%	25499.54	89.37%		3388.00	83.57%	25466.54	90.64%	
Pt	93.39	2.73%	7228.34	28.35%	-3.97%	85.04	2.51%	7219.98	28.35%	-3.97%
Pd	500.15	14.62%	4331.82	16.99%	-0.37%	474.66	14.01%	4306.33	16.91%	-0.44%
Au	40.71	1.19%	256.48	1.01%	0.03%	38.28	1.13%	254.06	1.00%	0.02%
Rh	129.31	3.78%	1064.70	4.18%	-0.06%	122.65	3.62%	1058.04	4.15%	-0.08%
Ir	4.45	0.13%	368.46	1.44%	-0.20%	4.07	0.12%	368.08	1.45%	-0.20%
Ru	144.02	4.21%	1379.29	5.41%	-0.19%	140.60	4.15%	1375.87	5.40%	-0.19%
Os	0.96	0.03%	130.94	0.51%	-0.08%	0.85	0.03%	130.83	0.51%	-0.07%
Ag	35.58	1.04%	85.82	0.34%	0.11%	30.76	0.91%	81.01	0.32%	0.09%
Fe	22.92	0.67%	1072.95	4.21%	-0.55%	27.44	0.81%	1077.48	4.23%	-0.52%
Ni	20.53	0.60%	2901.39	11.38%	-1.67%	36.59	1.08%	2917.45	11.46%	-1.59%
Cu	530.94	15.52%	1557.41	6.11%	1.46%	916.79	27.06%	1943.26	7.63%	2.98%
S	320.55	9.37%	762.12	2.99%	0.99%	266.64	7.87%	708.21	2.78%	0.78%
Co	2.16	0.06%	41.21	0.16%	-0.02%	2.61	0.08%	41.67	0.16%	-0.01%
Te	165.23	4.83%	246.54	0.97%	0.60%	182.61	5.39%	263.91	1.04%	0.67%
Se	25.52	0.75%	228.04	0.89%	-0.02%	26.49	0.78%	229.02	0.90%	-0.02%
Pb	197.39	5.77%	471.07	1.85%	0.61%	180.92	5.34%	454.60	1.79%	0.55%
Zn	0.03	0.00%	17.69	0.07%	-0.01%	0.05	0.00%	17.72	0.07%	-0.01%
Sb	37.29	1.09%	69.51	0.27%	0.13%	35.57	1.05%	67.80	0.27%	0.12%
As	202.87	5.93%	431.86	1.69%	0.66%	214.80	6.34%	443.79	1.74%	0.71%
Bi	13.51	0.40%	69.47	0.27%	0.02%	13.25	0.39%	69.21	0.27%	0.02%
Sn	0.24	0.01%	6.56	0.03%	0.00%	0.23	0.01%	6.55	0.03%	0.00%
Al	3.42	0.10%	19.75	0.08%	0.00%	3.39	0.10%	19.72	0.08%	0.00%
Si	48.58	1.42%	48.58	0.19%	0.19%	27.10	0.80%	27.10	0.11%	0.11%

Table G.3: Monthly throughput of typical PMR feed, slimes and new blended feed with the change in average composition (Test5 Test 6)

	Test 5					Test 6				
	Slimes		New Total		Over initial mean	Slimes		New Total		Over initial mean
	% Slimes/Anode	3.33%				% Slimes/Anode	3.88%			
	kg/month	%	kg/month	%		kg/month	%	kg/month	%	
Total	3663.00	80.06%	25741.54	90.06%		4268.00	78.75%	26346.54	89.62%	
Pt	88.28	2.41%	7223.22	28.06%	-4.26%	94.75	2.22%	7229.69	27.44%	-4.88%
Pd	477.66	13.04%	4309.33	16.74%	-0.61%	487.41	11.42%	4319.08	16.39%	-0.96%
Au	38.10	1.04%	253.87	0.99%	0.01%	37.99	0.89%	253.76	0.96%	-0.01%
Rh	125.64	3.43%	1061.03	4.12%	-0.11%	128.89	3.02%	1064.28	4.04%	-0.20%
Ir	4.03	0.11%	368.04	1.43%	-0.22%	4.10	0.10%	368.11	1.40%	-0.25%
Ru	132.97	3.63%	1368.24	5.32%	-0.28%	142.98	3.35%	1378.25	5.23%	-0.36%
Os	0.84	0.02%	130.83	0.51%	-0.08%	0.98	0.02%	130.97	0.50%	-0.09%
Ag	35.16	0.96%	85.41	0.33%	0.10%	75.54	1.77%	125.79	0.48%	0.25%
Fe	45.05	1.23%	1095.09	4.25%	-0.50%	137.43	3.22%	1187.46	4.51%	-0.25%
Ni	56.78	1.55%	2937.64	11.41%	-1.64%	101.58	2.38%	2982.44	11.32%	-1.73%
Cu	997.80	27.24%	2024.27	7.86%	3.21%	1137.42	26.65%	2163.89	8.21%	3.56%
S	286.81	7.83%	728.38	2.83%	0.83%	239.43	5.61%	681.01	2.58%	0.58%
Co	2.20	0.06%	41.25	0.16%	-0.02%	5.98	0.14%	45.03	0.17%	-0.01%
Te	143.22	3.91%	224.52	0.87%	0.50%	138.28	3.24%	219.58	0.83%	0.47%
Se	24.21	0.66%	226.74	0.88%	-0.04%	22.45	0.53%	224.97	0.85%	-0.06%
Pb	165.20	4.51%	438.88	1.70%	0.47%	161.33	3.78%	435.01	1.65%	0.41%
Zn	0.04	0.00%	17.70	0.07%	-0.01%	0.16	0.00%	17.82	0.07%	-0.01%
Sb	58.24	1.59%	90.46	0.35%	0.21%	47.37	1.11%	79.60	0.30%	0.16%
As	219.78	6.00%	448.77	1.74%	0.71%	197.61	4.63%	426.60	1.62%	0.58%
Bi	12.60	0.34%	68.56	0.27%	0.01%	12.25	0.29%	68.21	0.26%	0.01%
Sn	0.24	0.01%	6.56	0.03%	0.00%	0.27	0.01%	6.59	0.03%	0.00%
Al	3.66	0.10%	20.00	0.08%	0.00%	4.27	0.10%	20.60	0.08%	0.00%
Si	13.92	0.38%	13.92	0.05%	0.05%	182.67	4.28%	182.67	0.69%	0.69%

Table G.4: Monthly throughput of typical PMR feed, slimes and new blended feed with the change in average composition (Test7)

	Test 7				
	Slimes		New Total		Over initial mean
	% Slimes/Anode	4.25%			
	kg/month	%	kg/month	%	
Total	4675.00	63.39%	26753.54	86.77%	
Pt	91.16	1.95%	7226.11	27.01%	-5.31%
Pd	498.36	10.66%	4330.03	16.18%	-1.17%
Au	38.80	0.83%	254.57	0.95%	-0.03%
Rh	131.37	2.81%	1066.76	3.99%	-0.25%
Ir	3.97	0.09%	367.99	1.38%	-0.27%
Ru	140.25	3.00%	1375.52	5.14%	-0.45%
Os	0.94	0.02%	130.92	0.49%	-0.10%
Ag	79.48	1.70%	129.72	0.48%	0.26%
Fe	101.92	2.18%	1151.95	4.31%	-0.45%
Ni	67.32	1.44%	2948.18	11.02%	-2.03%
Cu	395.97	8.47%	1422.44	5.32%	0.67%
S	395.97	8.47%	837.54	3.13%	1.13%
Co	4.35	0.09%	43.40	0.16%	-0.01%
Te	129.97	2.78%	211.27	0.79%	0.42%
Se	21.41	0.46%	223.93	0.84%	-0.08%
Pb	175.78	3.76%	449.46	1.68%	0.44%
Zn	0.11	0.00%	17.77	0.07%	-0.01%
Sb	37.49	0.80%	69.71	0.26%	0.11%
As	179.05	3.83%	408.04	1.53%	0.49%
Bi	11.36	0.24%	67.32	0.25%	0.00%
Sn	1.36	0.03%	7.68	0.03%	0.00%
Al	4.68	0.10%	21.01	0.08%	0.00%
Si	452.54	9.68%	452.54	1.69%	1.69%

H. Mineralogical Results for Initial Anodes

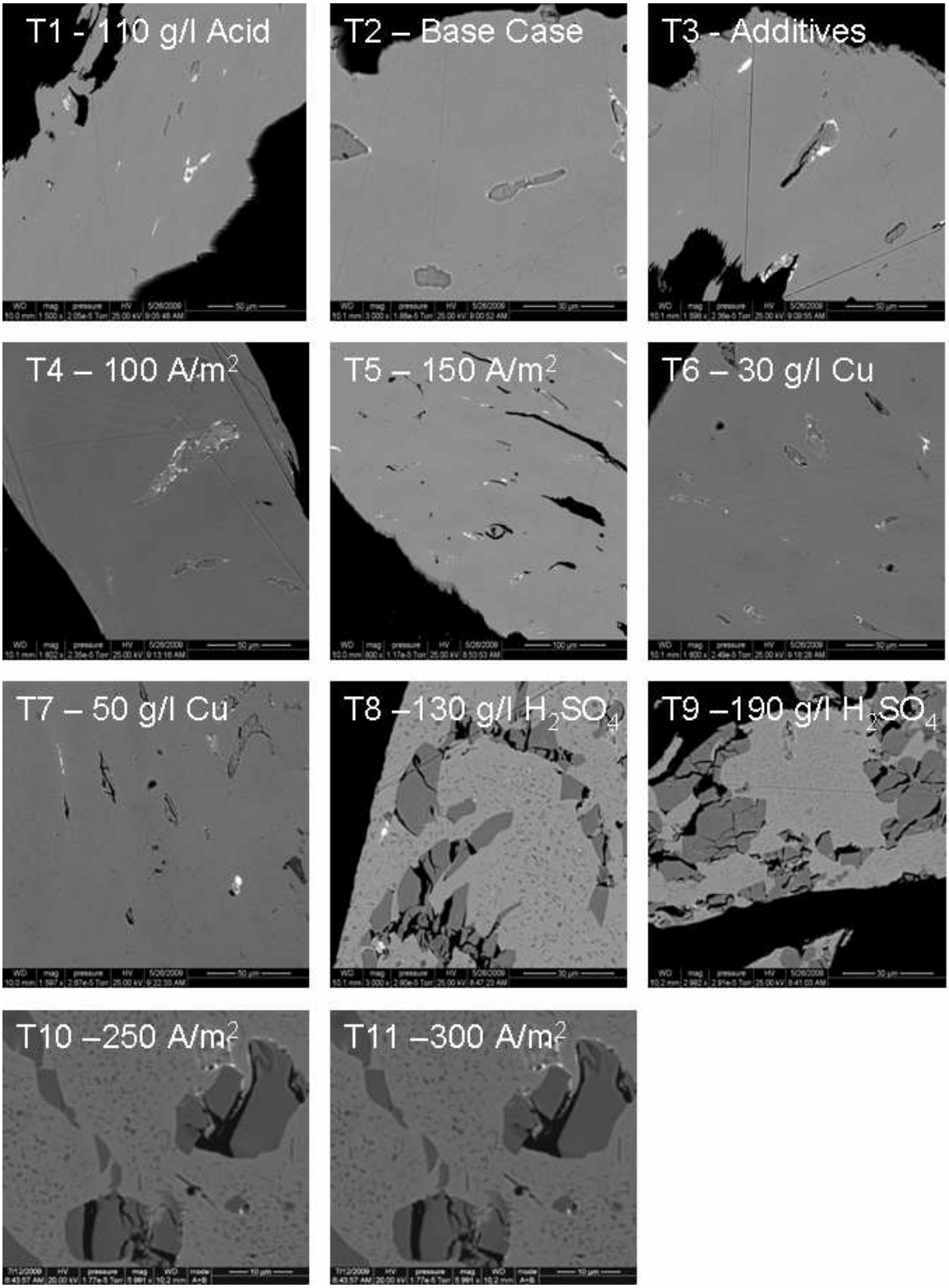

Figure H.1: MLA Backscattered Electron images for initial anodes

Table H.1: Phases in anode material and their compositions at different operating parameters

Phase	*Element*	*Test 1*	*Test 2*	*Test 3*	*Test 4*	*Test 5*	*Test 6*	*Test 7*	*Test 8*	*Test 9*	*Test 10*	*Test 11*
Light Grey Matrix	Cu	78.4	78.3	84.5	82.0	83.2	83.9	81.2	92.5	90.2	93.8	93.8
	Pd	*0.0*	*1.2*	*0.6*	*0.0*	*1.1*	*0.0*	*0.3*	*0.7*	*1.2*	*0.5*	*0.5*
	Ru	*0.0*	*1.0*	*0.0*	*0.0*	*0.0*	*0.0*	*0.0*	*0.0*	*0.0*	*0.0*	*0.0*
	Ni	16.2	14.6	11.8	13.7	12.5	11.8	13.8	4.3	5.0	3.6	3.6
	Fe	5.4	4.8	2.7	3.2	2.8	3.3	3.8	1.9	2.3	1.5	1.5
	Si	*0.0*	*0.0*	*0.3*	*0.7*	*0.0*	*0.6*	*0.6*	*0.7*	*1.3*	*0.6*	*0.6*
	Co	*0.0*	*0.0*	*0.1*	*0.5*	*0.4*	*0.4*	*0.2*	*0.0*	*0.0*	*0.0*	*0.0*
Dark Grey Blebs	Cu	64.7	65.3	68.8	69.5		68.8	62.2	67.3		77.5	77.5
	Ni	*1.1*	*1.0*	*0.4*	*0.8*		*0.8*	*1.1*	*1.5*		*0.7*	*0.7*
	Fe	6.5	5.9	4.7	3.4		3.5	3.9	5.4		5.4	5.4
	S	21.2	20.3	20.1	19.8		19.1	18.2	20.0		9.5	9.5
	Te	6.0	5.2	5.8	6.5		7.8	6.5	3.6		5.9	5.9
	Co	*0.2*	*0.0*	*0.0*	*0.0*		*0.0*	*0.0*	*0.0*		*0.0*	*0.0*
	Se	*0.3*	*0.7*	*0.2*	*0.0*		*0.0*	*8.1*	*0.5*		*0.5*	*0.5*
	Pb	*0.0*	*3.9*	*0.0*	*0.0*		*0.0*	*0.0*	*1.7*		*0.0*	*0.0*
Bright Dots	Pb							42.7			32.7	
	Bi							23.7			7.0	
	Ag							18.9				
	cu							8.0			28.0	
	Ni							7.5			3.7	
	Fe										18.0	
	Te										9.2	
Nested Needles	Cu							15.0	11.0	15.0	12.3	12.3
	Pd							*0.3*	*0.2*	*1.0*	*0.4*	*0.4*
	Rh							*1.5*	*1.1*	*0.9*	*0.2*	*0.2*
	Ru							*4.6*	*1.1*	*1.1*	*1.7*	*1.7*
	Ni							43.5	51.2	46.8	36.2	36.2
	Fe							25.7	18.3	19.4	33.2	33.2
	Si							7.7	16.2	15.5	15.1	15.1
	Co							*1.6*	*0.9*	*0.3*	*1.0*	*1.0*

I. Mineralogical Results for Anode Slimes

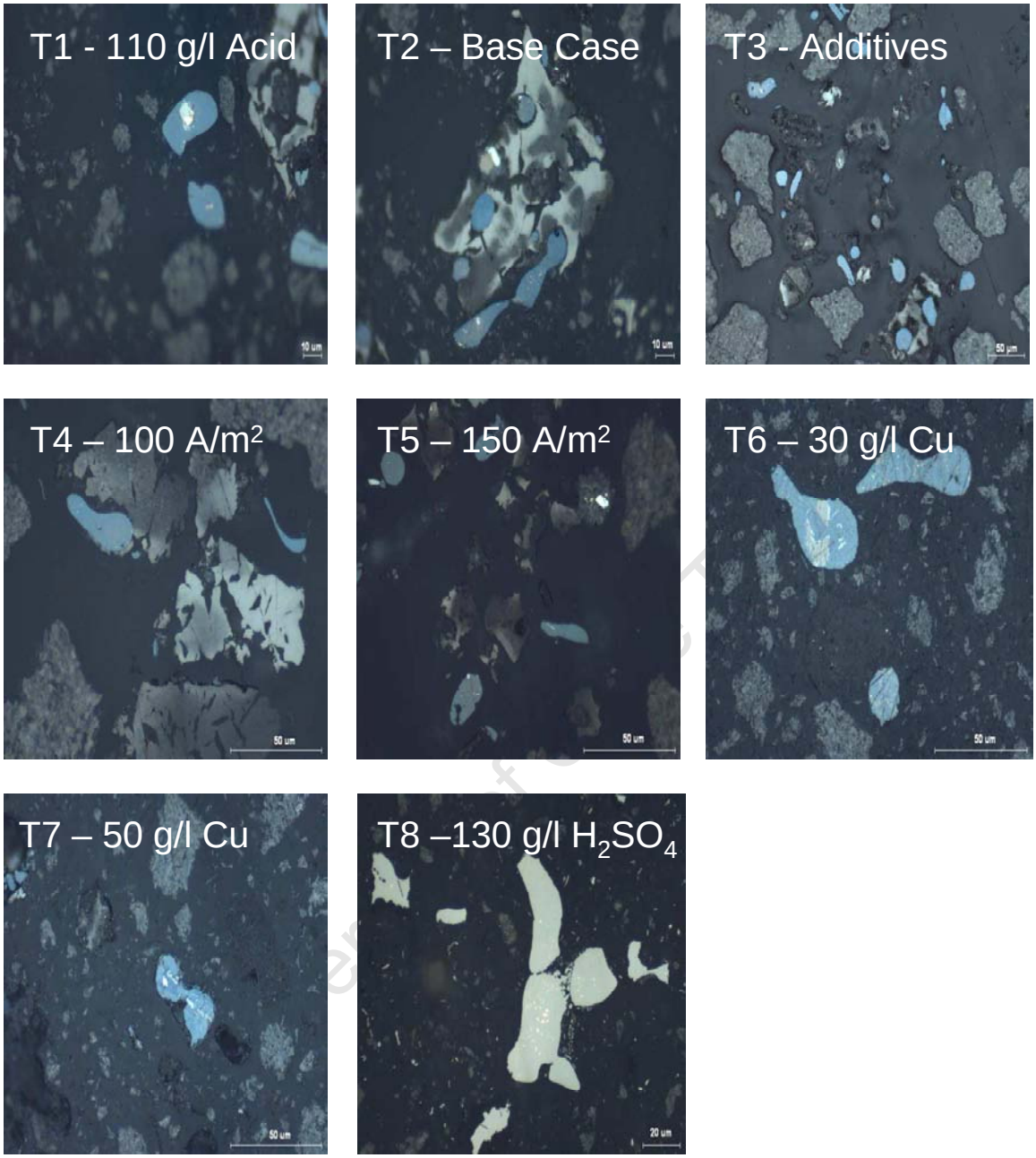

Figure I.1: Reflected Light Microscope Pictures for Anode Slimes

Blue blebs: Cu sulphide

Massive vague zone: Pd-Te-As

Bright phase: Alloys of Pb-Bi-Pd-Ag-Pt

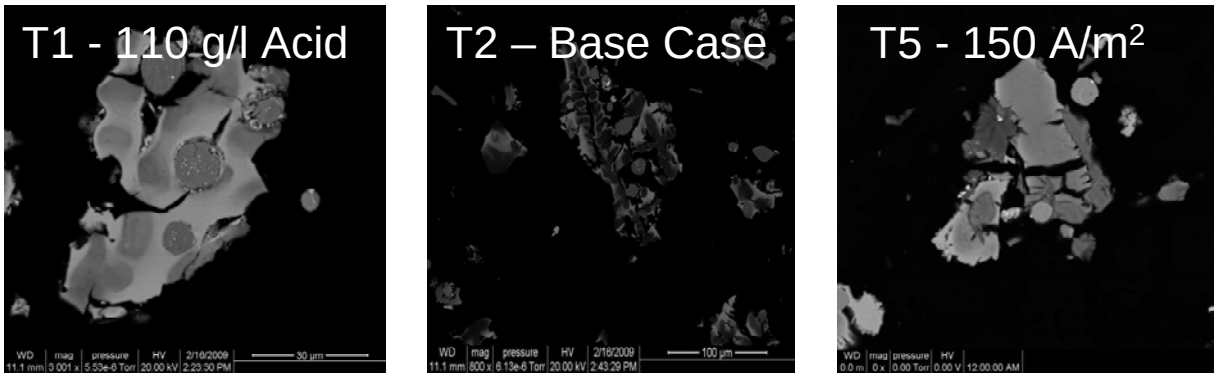

Figure I.2: MLA Backscattered Electron images for anodes slimes

J. Mineralogy Procedures

X-RAY POWDER DIFFRACTION METHODOLOGY

Mineralogical investigation of the anode slimes was performed by Petra Dinham & Anelda van Staden. The methodology that was used during the XRD Diffraction investigation has been supplied in report form and is quoted underneath for reference:

Ten percent corundum was added as an internal standard to all samples and in combination with the sample material was micronized in a McCrone micronizing mill for 4 minutes with methanol and then air-dried.

X-ray powder diffraction (XRD) (Bish and Post, 1989) patterns were collected using powder pellets, produced by front-loading. The instrument used to acquire the XRD data is a Bruker D8 Advance diffractometer employing the settings depicted in Table .

A search-match routine based on profile and peak data in association with the Powder Diffraction (PDF) 2 database was used to identify the best-fitting phases in the database. Amorphous material present below 10 volume percent will not be detected and the detection limit of XRD is approximately 5 volume percent.

Table J.1: Difractometer settings

Detector type	LynxEye
Start Position [°2Th.]	15
End Position [°2Th.]	70
Step Size [°2Th.]	0.02
Scan Step Time [s]	2.5
No. of steps	2784
Scan time (hh:mm:ss)	0:09:52
Anode Material	Cu
Generator Settings	40 mA, 40 kV

Due to the amorphous nature of Tests 1 to 7, as observed through a large amorphous hump as part of the background (see appended XRD traces, Figure to Figure) and the absence of representative structures in the Inorganic Crystal Structure Database (ICSD) for phases in Tests 8 to 12, it was not possible to determine the absolute quantities of the phases present. An attempt was nonetheless made to determine an approximate amount of amorphous material present by modelling the amorphous hump and taking into account the crystal structure data related to the best-fitting phases from the ICSD with the TOPAS 4 software. The TOPAS 4 software employs the Rietveld method (Young, 2002) and the fundamental parameters approach was used. The amount of internal standard, corundum, was used as reference and Rietveld parameters were subsequently refined to a point where optimal agreement was reached between the calculated pattern and the observed pattern.

The relative phase abundances of Tests 1 to 7 were determined with the Reference Intensity Ratio (RIR) method. The RIR method is based on the inclusion of corundum as an internal standard, as referenced in the International Centre for Diffraction Database (ICDD). The RIR technique allows for concentration comparison between the same species within different samples but not between different mineral species in the same sample.

X-ray powder diffraction patterns are given in Figure to Figure . Please note that some samples were re-run with a different instrument set-up so as to standardise all the patterns and corundum is therefore absent in some of the traces.

Anode slimes Tests 1-7

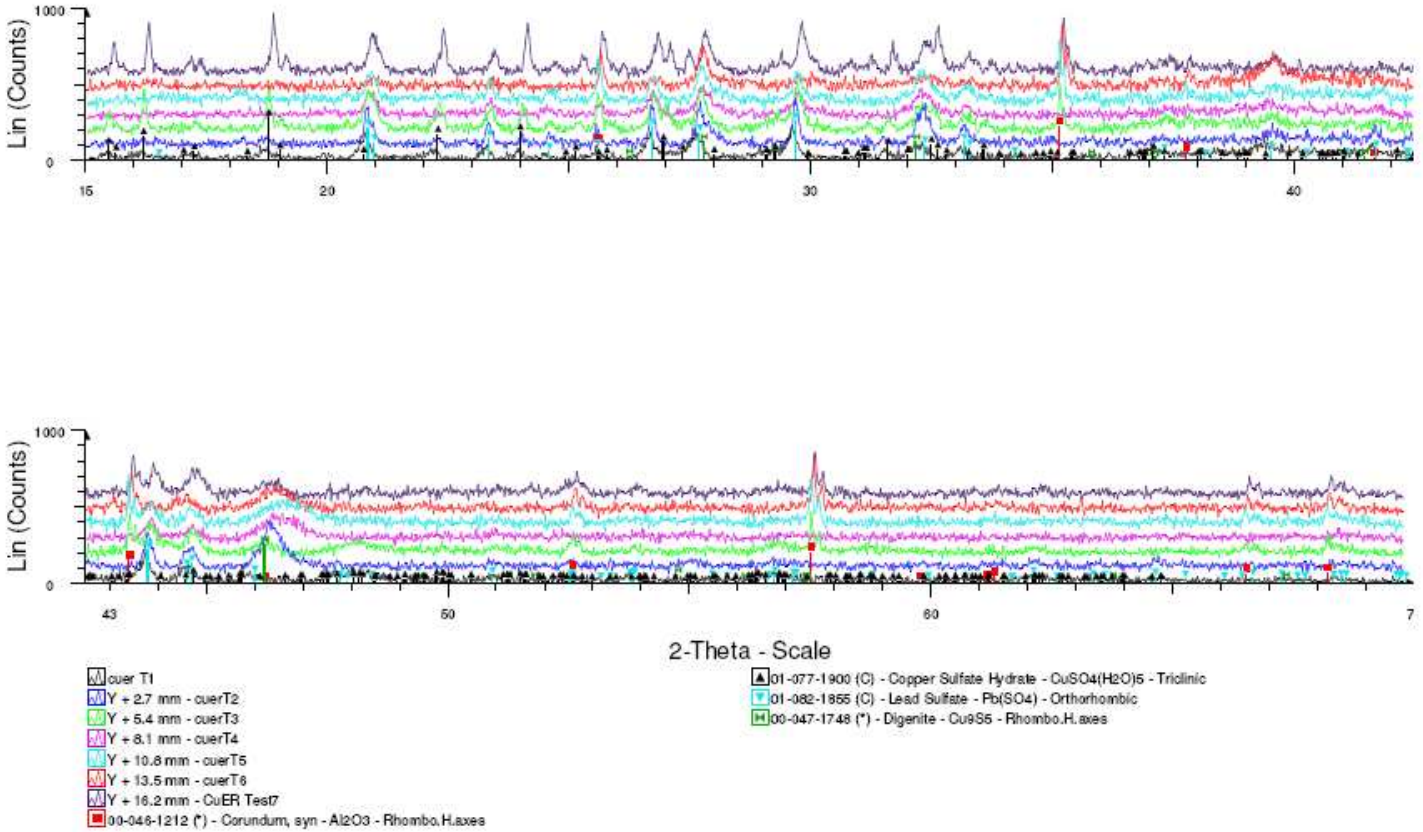

Figure J.1: XRD traces of anode slimes samples of test 1 - 7

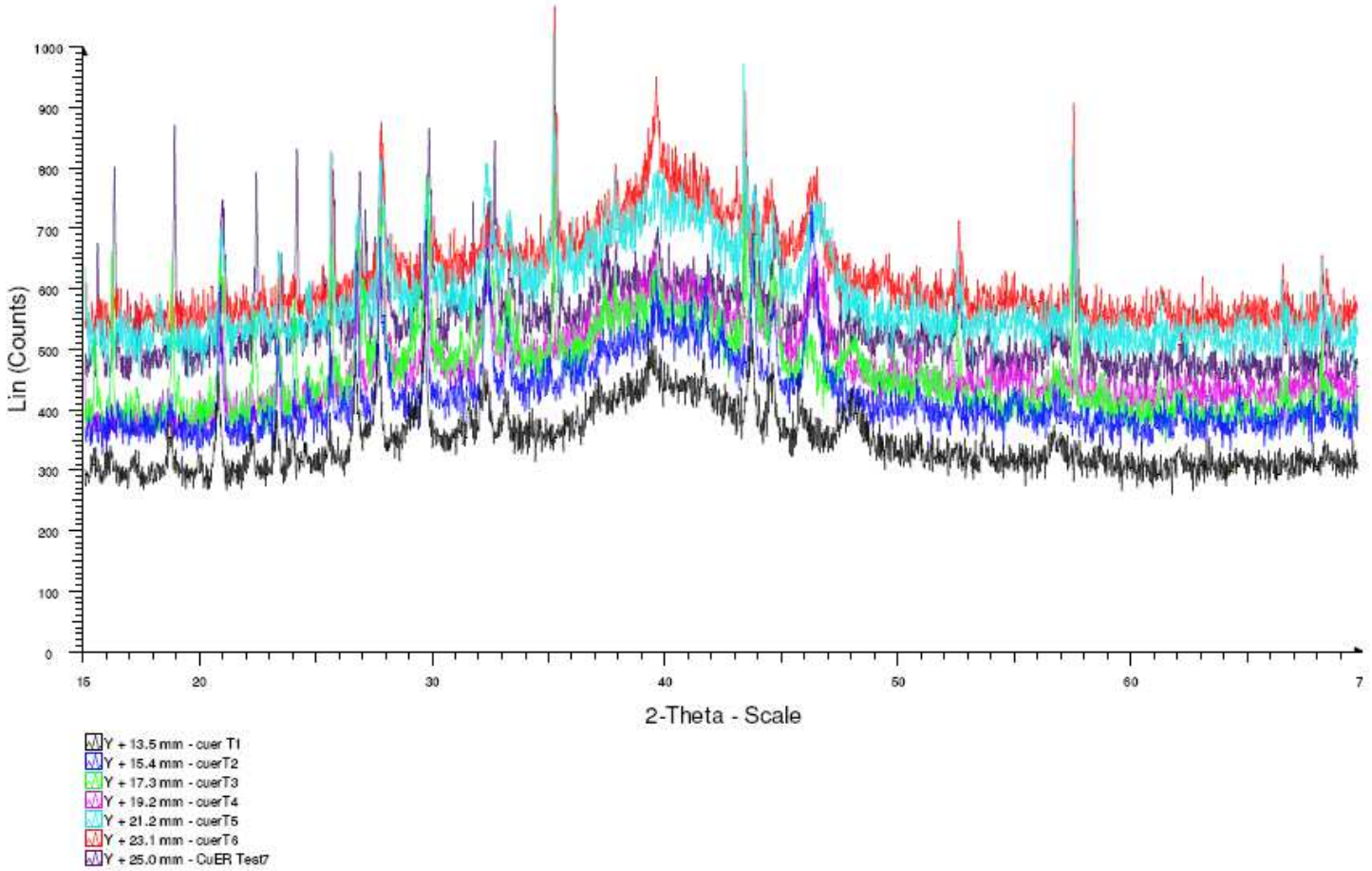

Figure J.2: XRD traces of anode slimes samples of test 1 – 7 showing amorphous phase

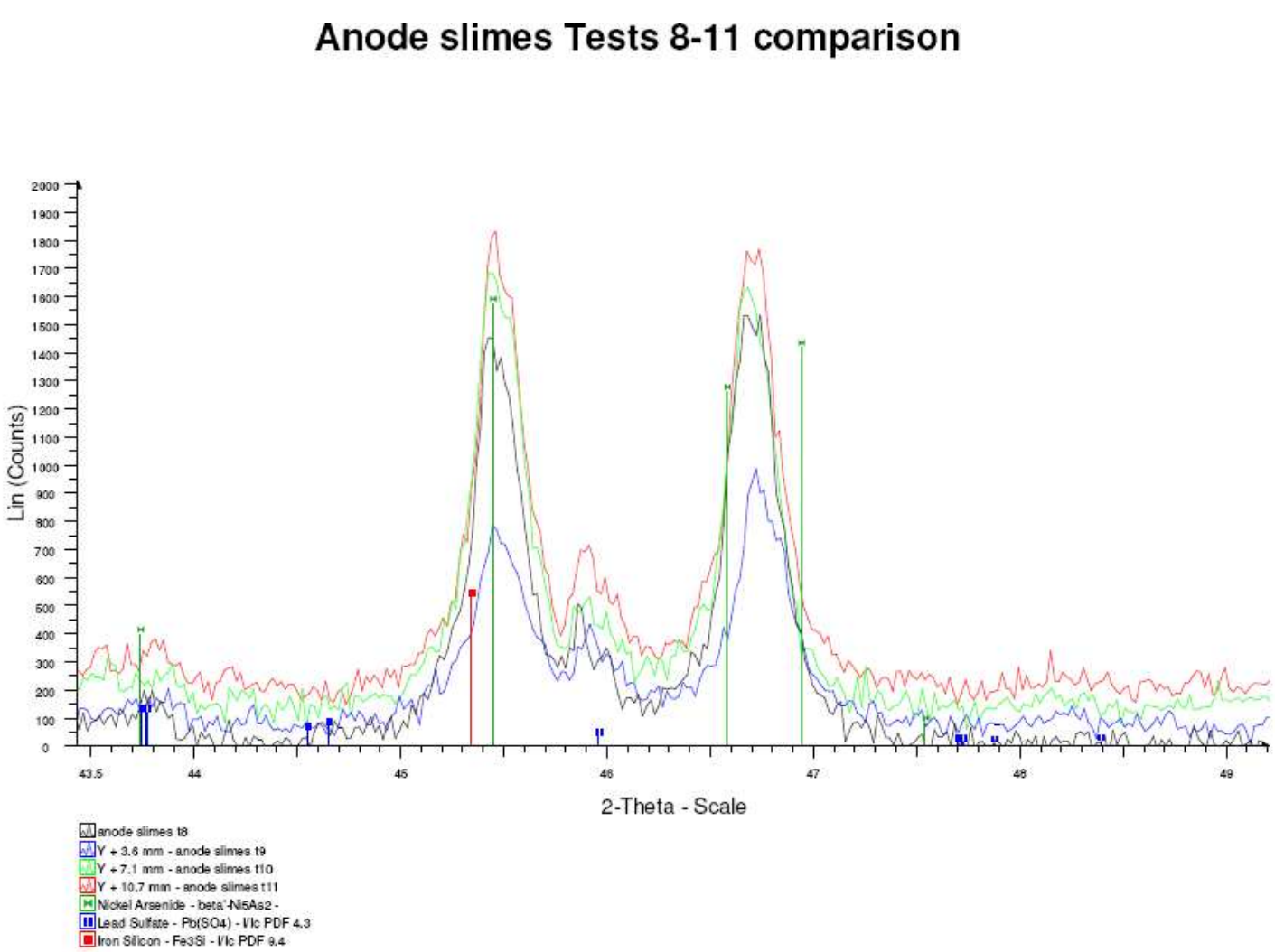

Figure J.3: XRD traces of anode slimes samples of test 8 – 11 (1)

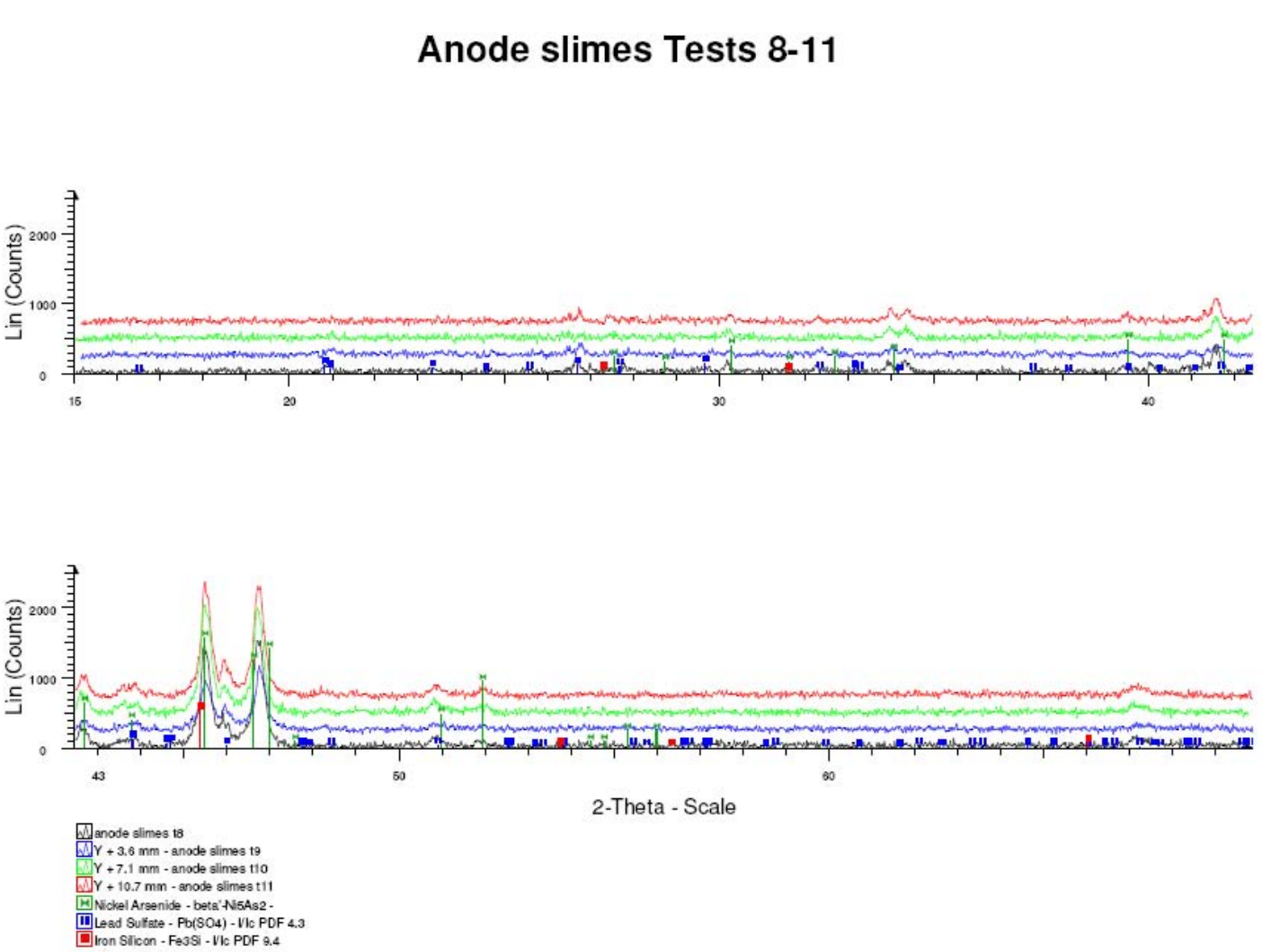

Figure J.4: XRD traces of anode slimes samples of test 8 – 11 (2)

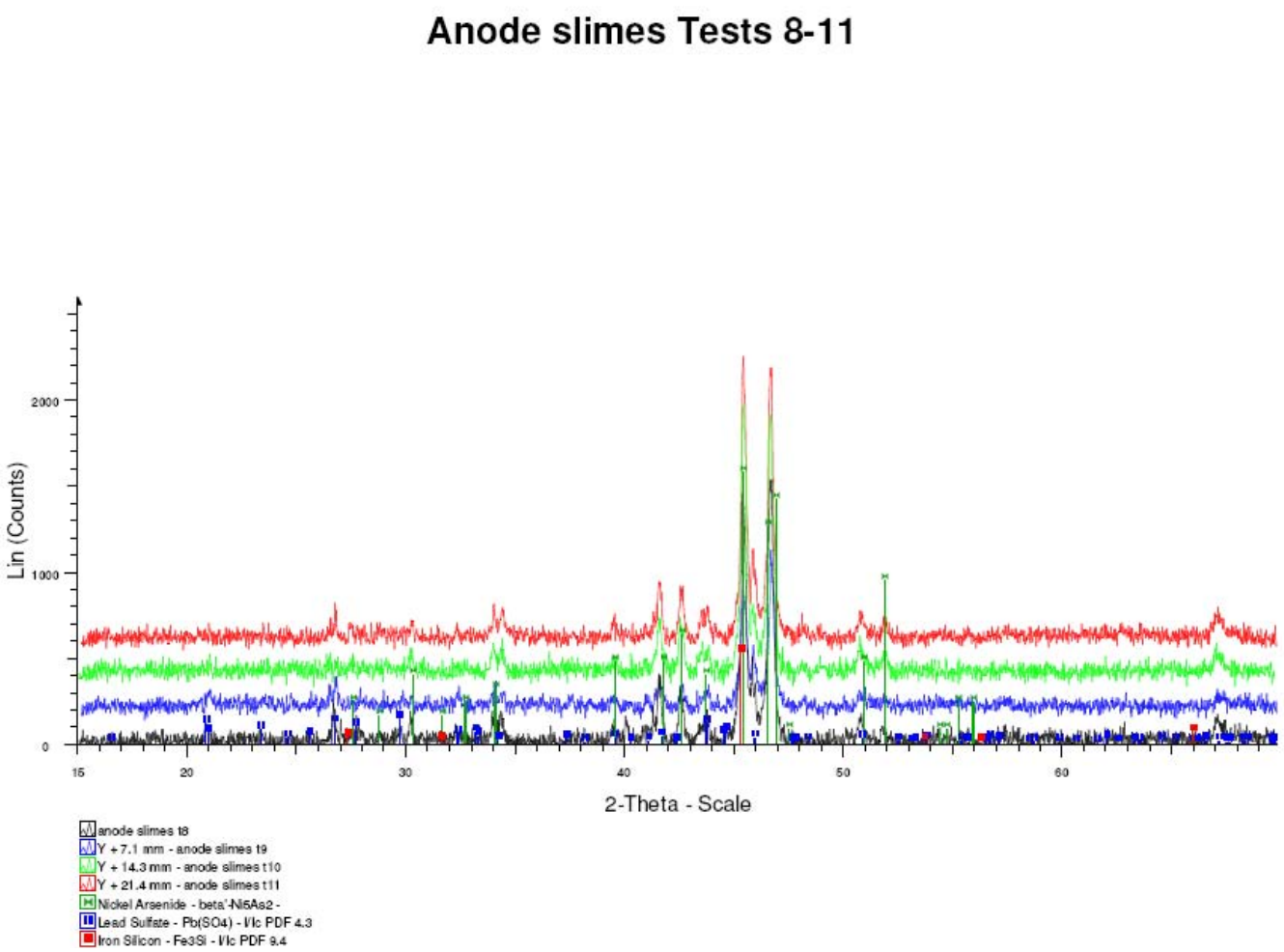

Figure J.5: XRD traces of anode slimes samples of test 8 – 11 (3)

Appendix II

II. APPENDIX II

MINTEK

Specialists in mineral and metallurgical technology

EXTERNAL REPORT

[enter report number]

MELTING AND CASTING OF COPPER BULLION TO PRODUCE ANODES FOR ELECTROREFINING PROCESS

by

Joseph Moema, Tiyani Khoza, Sibusiso Kantwela, Tutu Madiba, Given Maruma, Chris Fletcher and Clement Dhlamini

CONFIDENTIAL

06 July 2009

Specialists in mineral and metallurgical technology

Confidential

Mintek
200 Malibongwe Drive, (Formerly Hans Strijdom)
Randburg, South Africa
Private Bag X3015, Randburg 2125, South Africa
Tel : +27-11-709-4111
Fax : +27-11-709-2413
Website : http://www.mintek.co.za

EXTERNAL REPORT : xxxx		
TITLE: MELTING AND CASTING OF COPPER BULLION TO PRODUCE ANODES FOR ELECTROREFINING PROCESS		
CLIENT: Hydro Metallurgy Division		
DIVISION: Advanced Materials		PROJECT NO : HMC-100
AUTHOR: J.S Moema, T Khoza, S Kantwela, T Madiba G Maruma, C Fletcher and C Dhlamini		COMPACT NO : 2010-18
DATE: 28 July 2009	NUMBER PAGES: 40	COPY NO: 01 of 10 Issued

QUALITY CONTROL:

SUBMITTED BY	CHECKED BY	APPROVED BY
[SIGNATURE]	[SIGNATURE]	[SIGNATURE]
Joseph S Moema **Chief Investigator**	**M . Jones Papo** **Head: Physical Metallurgy**	**Elma van der Lingen** **Manager: Advanced Materials**
E-Mail:JosephM@mintek.co.za	**E-Mail:JonesP@mintek.co.za**	**E-Mail:ElmavdL@mintek.co.za**

QUALITY ASSURANCE:

Mintek's quality, environmental, safety, and health management systems are certified compliant to ISO 9001: 2000, ISO 14001: 2004, and OHSAS 18001: 1999. The quality systems of Mintek's Analytical Services Division are accredited to ISO 17025:2005.

SUMMARY

This report summarises the work undertaken in the development of method to melt and cast the copper nickel alloy. This report detailed the laboratory production of ten anodes and problems encountered during the project.

TABLE OF CONTENTS

1. INTRODUCTION 5

1.1. Cast Copper Alloys 6

2. EXPERIMENTAL PROCEDURES 7

2.1. Anode Casting 8

2.1.1. Pattern Design 8

2.1.2. Pattern Preparation 9

2.1.3. Mould Preparation 10

2.1.4. Melting and Casting 12

2.1.5. Casting Knockout and Fettling 13

3. RESULTS AND DISCUSSION 13

3.1. Integrity of Cast Anodes 13

3.2. Visual Examination 16

3.3. Chemical Analysis 19

3.4. Weight of Copper Bullion and Anodes 21

4. CONCLUSION 22

5. REFERENCES 22

APPENDIX 1 24

CALCULATION OF THE SIZE OF THE FEEDER/RISER *24*

DISTRIBUTION 26

LIST OF FIGURES

Figure 1.1. A schematic phase diagram of the Cu – Ni system 7

Figure 2. 1. Photograph of the as received copper matte (copper Bullion) 7

Figure 2. 2. Photograph of the pattern used in mould preparation of anodes (first design) 9

Figure 2. 3. Photograph of the modified pattern used in mould preparation of anodes (second design)10

Figure 2. 4.Photograph of the bottom mould (drag) used for sand casting anodes (first design).....11

Figure 2. 5.Photograph of the top mould (cope) used for sand casting anodes.....11

Figure 2. 6. Photograph of the modified mould used for sand casting anodes (third design).....12

LIST OF TABLES

Table 2 1. Typical chemical composition 13

Table 3 1. The composition of Copper Bullion (wt.-%) 20

Table 3 2. The weights of copper bullion anodes (grams) 21

GLOSSARY

Cope: Top half of the mould box.

Drag: Bottom half of the mould box.

Ingate: The channel though which the metal leaves the runner to enter either the mould cavity or risers adjacent to the cavity.

Mould: Compacted sand enclosed in the mould box containing the cavity in which has to be moulded.

Pattern: Casting replica around which moulding sand is compacted

Ramming: Compacting of foundry sand in the mould box or core box.

Riser: A reservoir connected to the casting so as to provide liquid metal to the casting during solidification to offset the shrinkage which takes place when casting solidifies.

Runner: Horizontal channel through which the metal flows towards or distributed around the mould cavity.

Shrinkage Porosity: This is porosity in a casting caused by insufficient feed metal.

Sprue: The opening into which the metal is poured first.

Vent: A small channel from the top of the mould cavity through for allowing air to escape as the metal fills the mould.

1. INTRODUCTION

Copper alloys are extremely difficult to cast as well as being prone to surface cracking, porosity problems, and to the formation of internal cavities. The copper-base casting alloy family is subdivided into three groups according to solidification (freezing range). Unlike pure metals, alloys solidify over a range of temperatures. Solidification begins when the temperature drops below the liquidus; it is completed when the temperature reaches the solidus. The liquidus is the temperature at which the metal begins to freeze, and the solidus is the temperature at which the metal is completely frozen. The copper nickel alloys are Group II alloys that have an intermediate freezing range, that is, a freezing range of 50 to 110°C between the liquidus and the solidus. Casting is a multiple step process that includes melting the metal into molten, pouring the molten into a mould and cooling it back to a solid. Casting has both artistic and industrial uses, and is a preferred method for fabricating custom pieces.

The Hydrometallurgy Division (HMD) approached the Advanced Materials Division (AMD) at Mintek to develop a melting and casting technique for a copper matte[1] (referred to as Copper Bullion). The objective of this work was to melt the copper matte produced from SLC in a two stage process in an Ausmelt TSL Furnace and cast[2] into the moulds to produce anodes that will later be used in an electro-refining process. It was also requested to compare the chemical composition and the colour of the supplied material with the produced anodes in order to gauge any significant differences. A total of ten anodes were requested to be produced. A sand casting route was chosen for this project because it is a commonly used process used in the foundry industry, relatively cheap and can be employed economically to a small scale producer. The sand casting process involves different steps as listed below and each step is discussed in detail in the experimental technique section of this report:

- Pattern manufacture
- Core manufacture
- Manufacture of the casting mould
- Melting and pouring
- Cleaning and finishing

[1] Copper Matte – This was described as a copper-nickel (Cu-Ni) alloy with some trace amounts of PGMs (i.e. Platinum Group Metals)

The client requested a T-shaped anode with the following dimensions:

- 20mm thick
- 150mm width
- 240mm long

The width on the T slots was supposed to be 250mm. About 156kg of the copper matte was supplied for use in the production of the anodes. AMD's task was to design a pattern that would result into an anode with the dimensions as indicated above. The anodes were to be supplied to HMD in the machined condition for further processing.

1.1. Cast Copper Alloys

Cast copper alloys are often selected for their excellent corrosion resistance, favourable mechanical properties, good friction and wear properties, high electrical and thermal conductivity, good castability and excellent machinability and fabricability.

Like other cast materials, solidification of copper-based alloys usually takes place by nucleation and growth of dendrites of a copper-rich face centered cubic (FCC) solid solution in which all of the problems associated with dendritic growth can and will occur. These problems include micro-segregation of alloying elements within the dendrites producing cored structures, entrapment of solidification shrinkage and gas porosity in between dendrite arms, and the presence of complex interdendritic phases [1].

In addition, like the transformations that occur in aluminium and ferrous alloys, solid state phase transformations such as eutectoid transformations, martensitic transformations and precipitation hardening are all possible in these materials. The appropriate phase diagram is a ternary in which the Ni is completely soluble in the Cu in the solid state. A schematic phase diagram of the Cu – Ni system is given below in Figure 1.1.

[2] Casting – This is a process whereby a molten liquid is poured into a mould which resembles the final shape of the component.

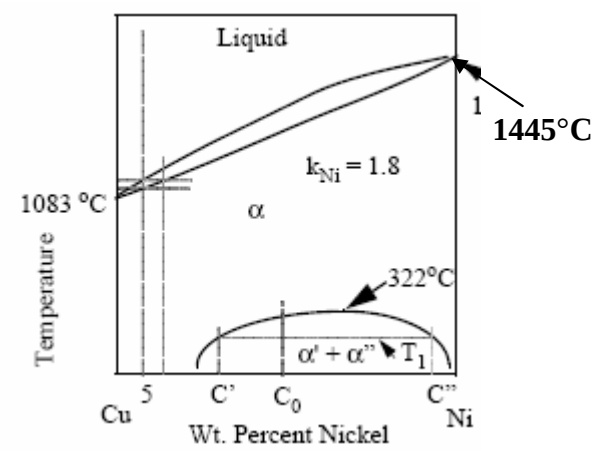

Figure 1.1. A schematic phase diagram of the Cu – Ni system

2. EXPERIMENTAL PROCEDURES

The as received copper nickel alloys were visually examined, broken into small pieces and sorted out into equal weights in preparation for melting. Two pieces of the supplied copper nickel metals were randomly selected, and prepared for chemical analysis prior melting. The supplied broken pieces of copper nickel alloy are shown in Figures 2.1(a) and (b). It consisted of slag (black in colour) on the surface that formed when it was being processed at the supplier's premises.

a ***b***

Figure 2. 2. Photograph of the as received copper matte (copper Bullion)

2.1. Anode Casting

There are three broad stages that need to the completed in order to obtain a desired casting. The stages are, namely; pre-casting, casting and post-casting. The pre-casting stage involves the design of pattern, sand preparation, mould making and lastly putting together the mould. The casting process involves charging the furnace, melting and pouring into the melt into the mould. The post casting stage involves removing casting from mould, cleaning, fettling and inspection. These stages are described in detail as follows.

2.1.1. Pattern Design

A pattern is used to produce a casting with the desired dimensions. However, it is rarely dimensionally identical to the final casting. The pattern used in this project was mainly manufactured from wood due to its affordability and easy to process. The design of patterns must include the following components:

- An allowance for the solid state shrinkage that will always accompany a casting as it cools from the melting temperature to room temperature. This depends upon the metal being cast, given that each metal has its own unique coefficient of thermal expansion (α). For example, α for copper is 16.5 x 10^{-6} in/in °C. Thus, the linear dimensions of a pattern will always be larger than the casting by an amount determined by the linear expansion coefficient.

- Inclusion of a draft angle so that the pattern can be removed from the mould after the moulding sand has been rammed around the pattern. These draft angles can vary from one casting to another but angles in the range 1 - 2° are quite common.

During solidification, casting defects can form due to shrinkage, presence of dissolved gases and dendrite formation. The primary objective of a mould design is to prevent these phenomena. The following parts are very important in the mould design:

- Risers
- Gating system
- Runners

The method for calculating the sizes of these mould parts is shown in Appendix 1.

2.1.2. Pattern Preparation

Before moulding, the pattern was painted with a release agent to prevent the moulding sand from adhering to it. Exothermic cored sleeves were placed on the top of each anode-pattern to act as feeders to the cast anode. The types of the patterns used in this project are shown in Figures 2.2 and 2.3 below.

For each sleeve, a 6mm diameter ventilation hole was pierced on the surface of the mould, to allow gas to escape during casting. When the pattern was removed from the completed mould, the sleeves remained in the mould.

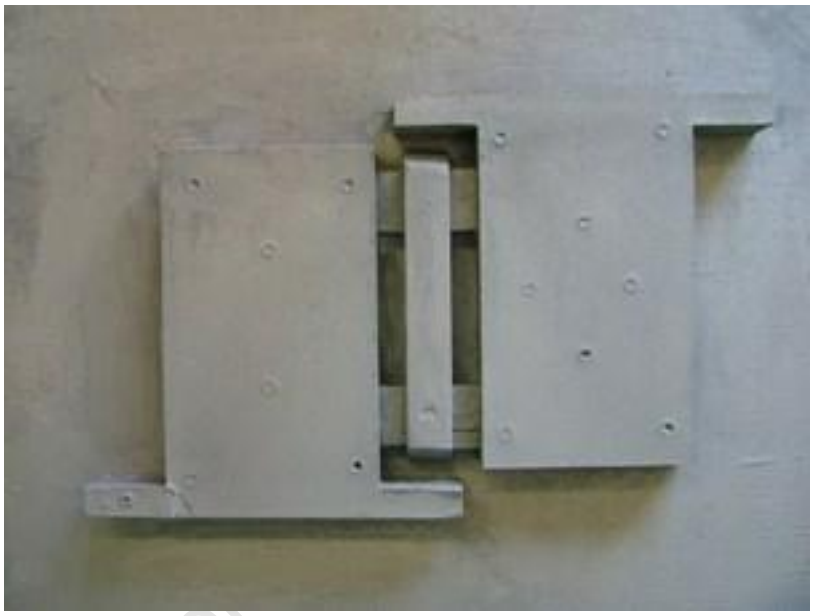

Figure 2. 3. Photograph of the pattern used in mould preparation of anodes (first design)

Figure 2. 4. Photograph of the modified pattern used in mould preparation of anodes (second design)

2.1.3. Mould Preparation

Cast iron mould boxes (0.5m length, 0.38m width and 0.14m depth) were used to accommodate both the drag (bottom) and cope (top) parts of the pattern. Approximately 50kg of silica (SiO_2) sand with a particle size range of 0.075 to 0.65mm was mixed with 1000ml of sodium silicate (Na_2SiO_3) binding agent. The mould box with the pattern in place was then filled with moist sand, with the sand being pushed firmly into recessed areas. More sand was gradually added and rammed until the mould was completely filled. This was done in order to allow the mould to be gassed with carbon dioxide (CO_2) which was introduced through the holes. This results in the hardening of the mould through the reaction of CO_2 with Na_2SiO_3, which produces silica gel ($SiO_2.xH_2O$ or H_2O_3Si). The mould was then lifted from the pattern and loose sand was removed by blowing with compressed air. The mould was coated with an alcohol-based ceramic mould wax that helps to prevent sand burn-on during casting, and improves the surface finish. The moulds were ignited in order to burn off excess alcohol and all remnant moisture that may cause gas porosity in the casting. The drag and cope were glued and clamped tightly in order to prevent any leakages. Photographs of the moulds used can be seen in Figures 2.4 to 2.6.

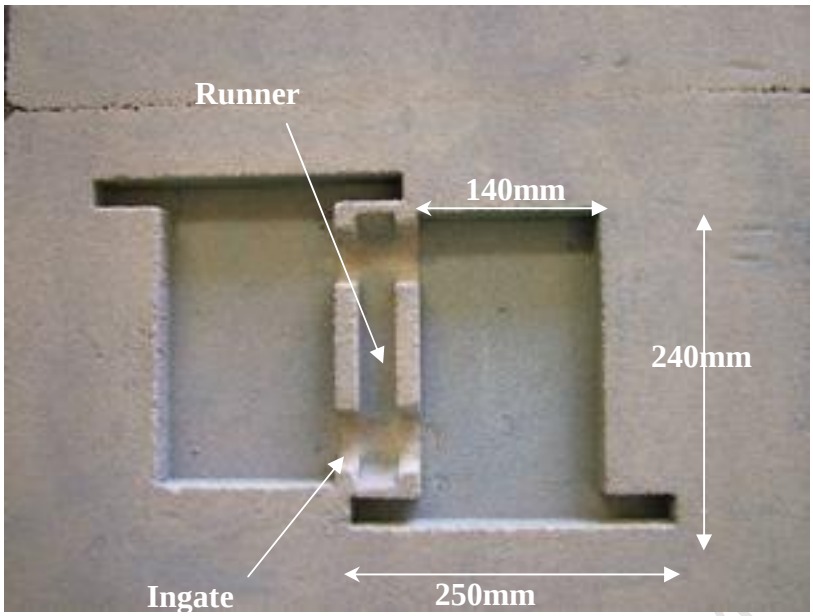

Figure 2. 5.Photograph of the bottom mould (drag) used for sand casting anodes (first design)

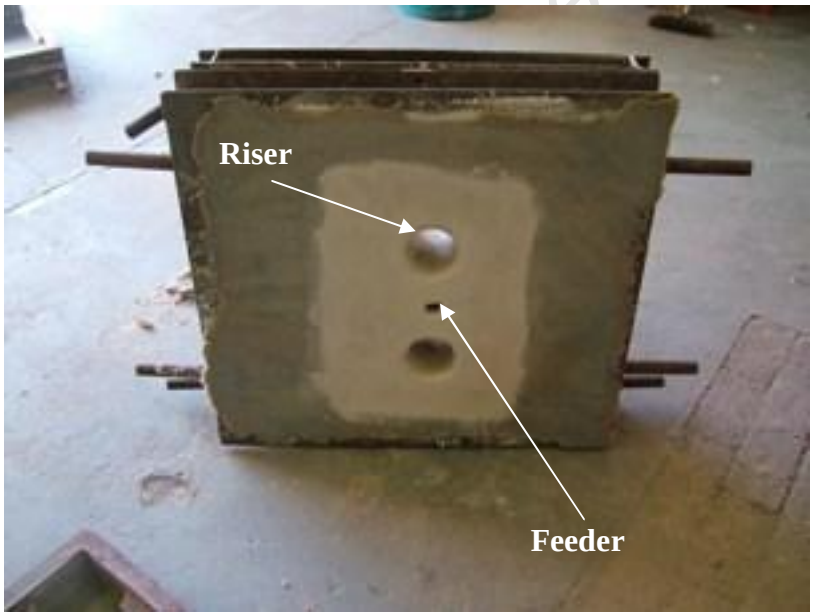

Figure 2. 6.Photograph of the top mould (cope) used for sand casting anodes

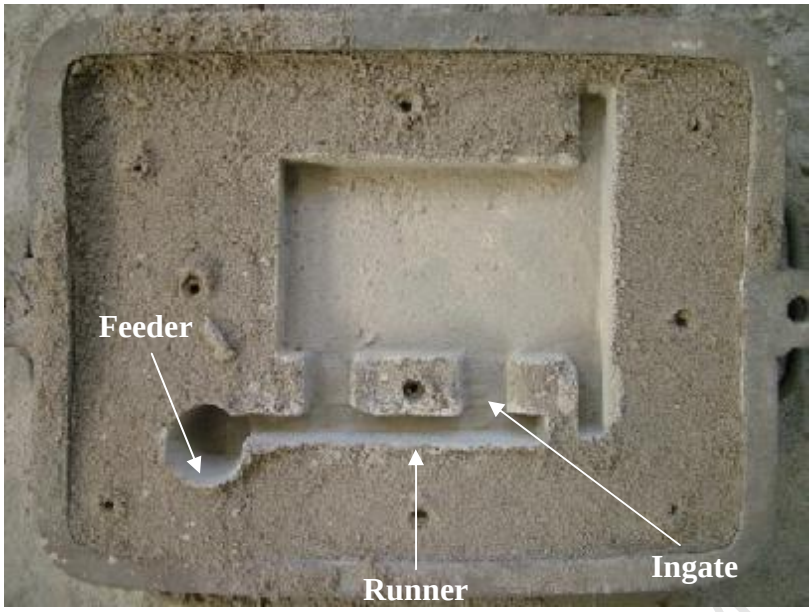

Figure 2. 7. Photograph of the modified mould used for sand casting anodes (third design)

In some case, however, an open mould is used for casting purposes. A typical design of such a mould is shown in Figure 2.6. In this type of casting technique, no cope is required.

2.1.4. Melting and Casting

Melting was done in a medium frequency induction furnace open to the atmosphere and with a capacity of about 150kg. A 50kg Silicon Carbide Cast crucible with the dimensions, Height (H) = 318mm, Outside Diameter (OD) at the top = 232mm and at the bottom = 160mm, was fitted in this furnace for melting of the alloy.

When the charge was completely molten, the slag coagulant, SLAX 30, was poured over the molten metal surface so as to grip the slag[3]. At the molten metal temperatures, the SLAX 30 granules expand and form a low density, high volume crust which mops up the slag. The slag can then easily be lifted off the metal with ease leaving the metal surface clean. A typical chemical composition of the SLAX 30 slag coagulant is shown in Table 2.1. The slag coagulant does not trap the metal nor not contaminate the melt in any way. After leaving the coagulant for a few seconds on the melt surface, the slag was skimmed out of the furnace.

[3] Slag - unwanted impurities within the molten metal.

Table 2. 1. Typical chemical composition of SLAX 30 slag coagulant

Chemical	Percentage (%)
SiO_2	73 – 75
Al_2O_3	12 – 14
Fe_2O_3	0.61
TiO_2	0.29
CaO	0.83 – 1.0
MgO	0.16
Na_2O	3.08
K_2O	4.65

The temperature was measured with a disposable-tip immersion thermocouple, and then adjusted to ≈ 1640°C. Upon reaching the desired temperature, the melt was tapped into a pre-heated insulated magnesia-lined hand ladle. The slag grip was again added into the ladle to ensure that all unwanted impurities are removed. The molten metal was subsequently poured into the mould while at the same care was taken to ensure that the pouring rate was such that the sprue was always full with molten metal.

2.1.5. Casting Knockout and Fettling

The castings were removed from the mould 3 hours after pouring, and allowed to cool on their trees, on a sand floor. Thereafter, the runners and risers were removed by nicking with an angle grinder. The remains of the feeding system were flash removed by light grinding. Before proceeding with any machining of the cast anodes, it was deemed critical to ascertain their integrity. Several cast anodes were sent to Engineering Support Division (ESD) to be machined and visually examined for any casting defects, such shrinkage porosity, etc.

3. RESULTS AND DISCUSSION

3.1. Integrity of Cast Anodes

All the anodes produced were checked for surface defects such as burnt-on sand, flashes, etc. Photographs of the sand cast anodes showing, feeder, runner and riser system can be seen in Figures 3.2 to 3.4. It can be seen that some of the foundry sand is adhered to the casting and referred to as sand burnt-on.

Silica (SiO_2) sand and Silchem (sodium silicate – Na_2SiO_3) is used in foundries to produce moulds for casting as a standard practice. Before melting the sand on these risers, feeders and runners is removed to a degree and there will be no elemental silicon (Si) pick up into the metal as any remaining sand attached to the metal would go into the slag. Quartz consists of a three network of SiO_4^{4-} tetrahedral with a hexagonal crystal structure. When heated, quartz undergoes structural changes coupled with volume expansion. The conversion of $SiO_2 \rightarrow Si$ is not a simple reaction and it cannot happen under these normal casting conditions. The transformation of silica (SiO_2) sand or quartz occurs as follow:

$$\alpha\text{-quartz} \xrightarrow{540°C} \beta\text{-quartz} \xrightarrow{879°C} \text{tridymite} \xrightarrow{1470°C} \text{cristobalite}$$

The transformation $\alpha \rightarrow \beta$ occurs very rapidly, coupled with a large volume expansion. While the $\beta \rightarrow$ tridymite transformation is very slow and would normally not occur during heating with pouring. The rapid volume change during the $\alpha \rightarrow \beta$ transformation can cause fragmentation of the mould during pouring. Slow heating of moulds to 600°C before pouring reduces this risk.

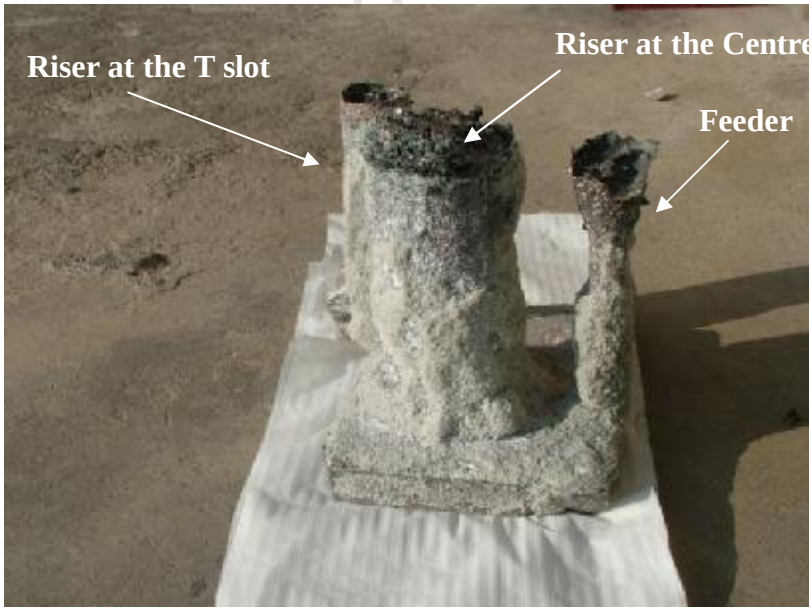

Figure 3.1. As-cast anode on a tree showing a feeder, runner and risers (second design)

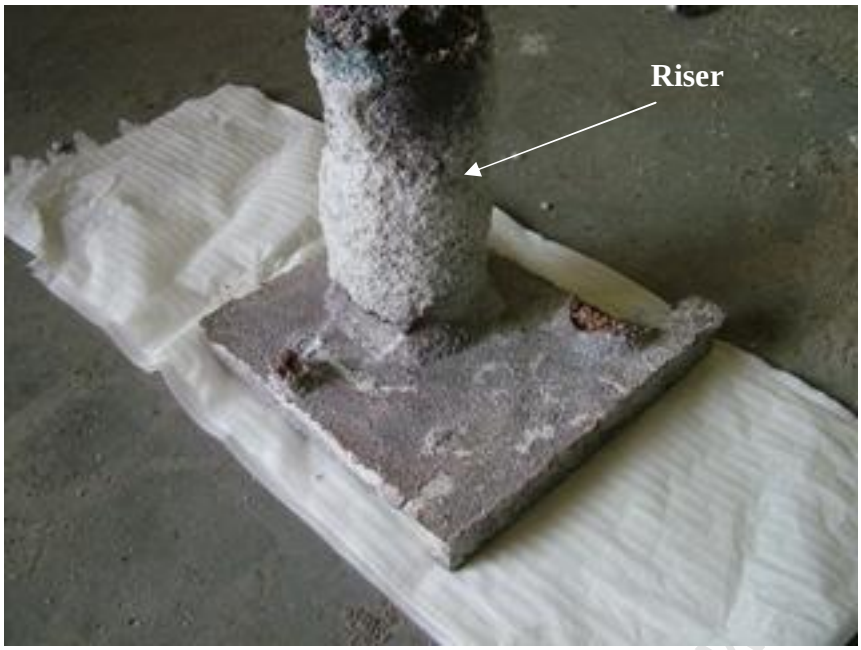

Figure 3.2. As-cast anode showing a removed feeder and one of the risers

Figure 3.3. As-cast anode produced using a third design

A high prevalence of shrinkage porosity was observed in the first batch of castings, this necessitated a redesign of the entire feeding system. The calculation of the gating and feeding system is shown in section 2.1.1. Risers are used in the production of castings for the purpose of providing molten metal for the solidifying and shrinking casting. Riser design in sand castings requires, at a minimum, that the riser solidify after the casting. A casting and riser are shown schematically in a sand mould below. The desired situation after solidification would result in all the shrinkage within the riser as illustrated in Figure 3.5.

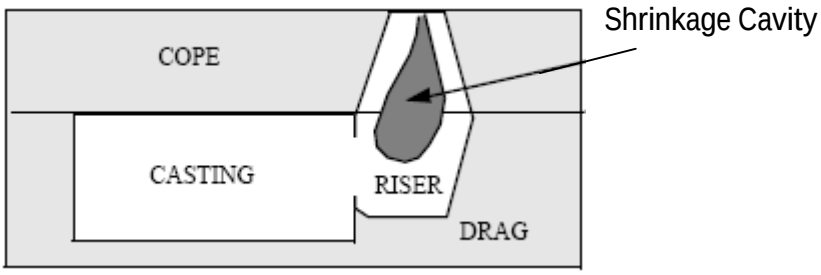

Figure 3.4. Schematic casting set-up showing shrinkage in a riser [2-4]

Therefore, feeders with a geometric modulus of 1.2 times that of the cast were incorporated on the pattern and positioned at the centre of each anode to ensure an effective feed path (shown in Figure 3.6 of Section 3.2). This ensured that the feeders solidified after the anodes had already solidified. The feeders proved effective in eliminating shrinkage cavities in all the subsequent casts.

3.2. Visual Examination

Visual examination of the first set of anodes showed large cavities close to the centre and at the T slot of the anodes (Figure 3.6). Further examination with the aid of a magnifying glass showed the inside of these cavities to be rough and dendritic - the tell-tale signs of shrinkage porosity as opposed to gas-related porosity, which is smooth. The redesigning of the entire feeding system, whereof feeders with a modulus 1.2 times that of the anodes was incorporated on to the pattern. This ensured that the feeders solidified after the anodes had already solidified. Figures 3.7 and 3.8 show the machined as cast anodes before and after modification of the feeding system respectively. The feeders proved effective in eliminating shrinkage cavities in all the subsequent casts. The colour of the anode also changed from a silvery colour to a reddish-brown colour.

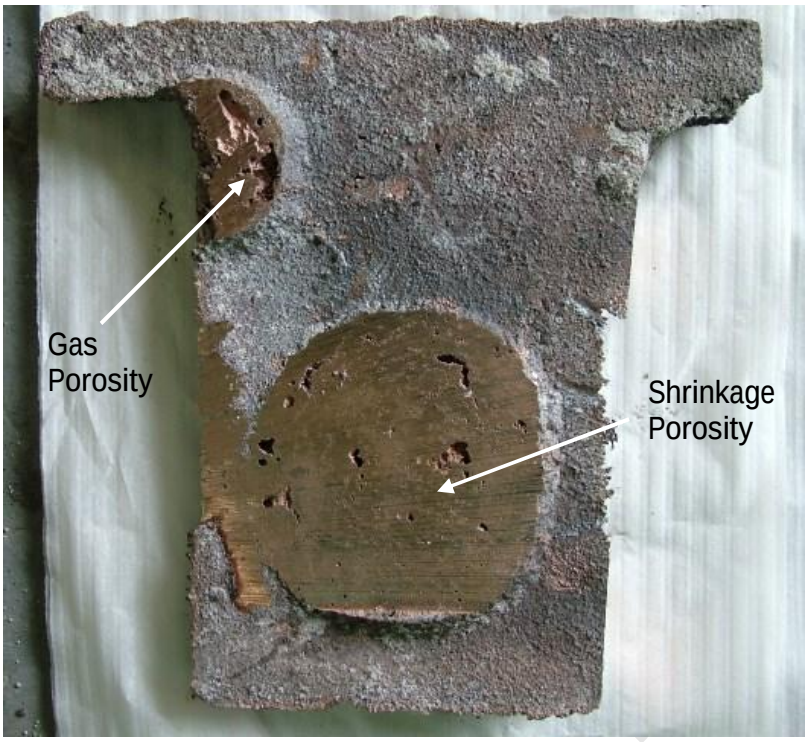

Figure 3.5. As-cast anode prior to machining showing shrinkage and gas porosities

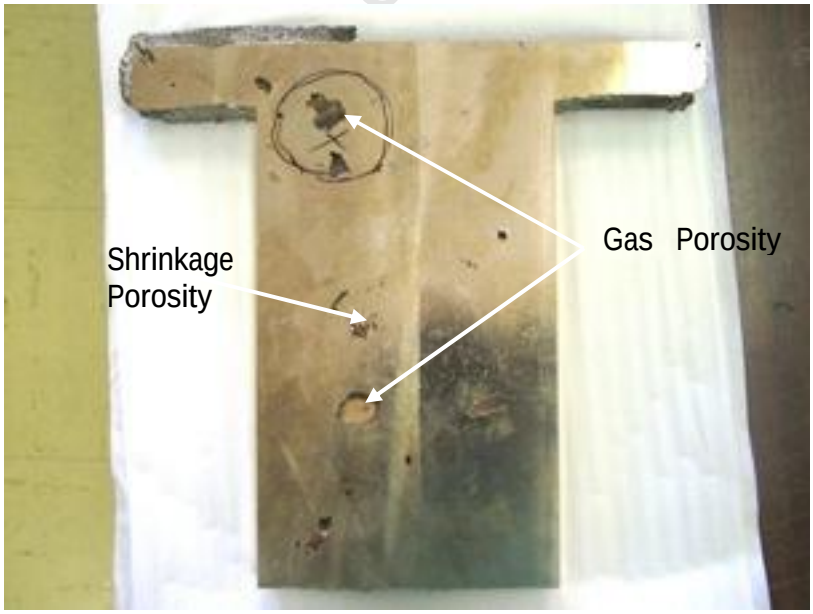

Figure 3.6. Machined as-cast anode showing shrinkage and gas porosities

Figure 3.7. As-cast anode after machining showing no casting defects (with a modified feeding system)

The gas porosity results from the gases entrapped in the mould or gases that dissolved during melting of the alloys which then try to escape during the cooling and solidification inside the mould. These gases get trapped into the casting and results into blow holes (i.e. internal and surface blow holes). Shrinkage porosity is caused by the volume contraction of the liquid state during the solidification.

The shrinkage that occurs during solidification of metals (that ideally all ends up in the shrinkage cavity in the riser shown in Figure 3.5) results from three distinct contributions which are:

- Thermal Contraction of Liquid from pouring temperature (T_P) to liquid temperature (T_L)
- Thermal Contraction of Liquid and Solid from T_L and solid temperature (T_S)
- Change in State from Liquid to Solid from T_L to T_S and at T_S

The type of shrinkage observed in these castings can be classified as macro-shrinkage porosity. Macro-shrinkage defects can be seen by the unaided eye. Two types of shrinkage were observed, shrinkage which can be observed externally on the casting surface and shrinkage which is observed internally after sectioning. Poor riser design (riser solidifies before casting) was found to be the main factor that led to these defects in the first casting.

3.3. Chemical Analysis

No specifications were supplied for the Copper Bullion, however, the analysis performed by the client were received for comparison purposes. The chemical composition of the copper bullion before and after casting is shown in Table 3.1 below. It can be seen that there is a compositional change on anode number 10 as compared to anodes 1 to 3 which have similar composition to that of the as received metal. The silicon content for anode number 10 is 10 times more than that of the as received copper matte. This silicon pickup might be from the shavings that were used as a top up during melting of the anodes. It is envisaged that the shaving were contaminated and could possibly be the source of silicon pick up. Unfortunately, the spectrometer in AMD is not equipped to analyze the precious metals and only four anodes were analyzed. A copper program was used to analyze the anodes.

The client requested 10 anodes and the supplied material was not enough to make these anodes. Therefore, it was necessary to start recycling shavings that were machined off the previous material or produced and tested anodes. The shavings that were gathered from the machine that was used to clean the anodes also poses another possibility of contamination because it was not guaranteed that the area from the shavings were collected was 100% free of other metals.

During the casting process, the anode composition changed (see anode 10), it had a slightly different composition to that of anodes 1 to 3 (as shown in Table 3.1). The main difference was the silicon content and the other elements were within the initial analysis. The copper and nickel content also decreased and this might have led to colour change of the anode. The primary cause of the change in anode composition has not been confirmed but the multiple re-casting could have contributed to an extent. This needs to be investigated to find the source of the silicon that was picked up in Anodes number 10. Another possible cause could be the use of anode shavings collected from the milling machine. It is envisaged that the shavings could have also contained some silicon or other contaminant; however the latter was not confirmed.

Table 3. 1. The composition of Copper Bullion (wt.-%)

Elements	Copper Matte (supplied)	Anode 1	Anode 2	Anode 3	Anode 10
Pt	0.0912	-	-	-	-
Pd	0.5464	-	-	-	-
Au	0.0443	-	-	-	-
Rh	0.1374	-	-	-	-
Ir	0.0041	-	-	-	-
Ru	0.1579	-	-	-	-
Os	0.0007	-	-	-	-
Ag	0.1484	-	-	-	-
As	0.3040	-	-	-	-
Bi	0.0447	0.045	0.036	0.051	0.014
Cd	<0.0005	-	-	-	-
Mn	0.0017	<0.0008	<0.0008	<0.0008	0.023
Mo	<0.0008	-	-	-	-
Pb	0.2460	>0.114	>0.114	>0.114	0.093
Sb	0.0994	-	-	-	-
Se	0.0148	-	-	-	-
Sn	0.0194	0.020	0.018	0.024	0.014
Te	0.1051	-	-	-	-
Ti	0.0026	0.0080	0.0083	0.0085	0.013
Zr	<0.0010	-	-	-	-
Cu	79.16	83.0	82.0	83.9	61.8
Ni	12.49	12.62	13.66	12.21	10.11
Fe	5.39	>3.12	>3.12	2.44	>3.12
Cr	<0.23	-	-	-	-
Co	0.123	0.144	0.161	0.149	0.102
Si	<0.3000	0.0026	0.0034	0.253	>1.08
Al	0.1880	-	-	-	-
Ca	<0.2500	-	-	-	-
Mg	<0.2000	<0.0002	<0.0002	0.0002	0.005
S	0.2600	>0.144	0.140	>0.144	>0.144
Zn	-	<0.002	<0.002	0.0023	0.0150
P	-	0.0025	0.0027	0.0030	0.0017
Cr	-	<0.005	<0.005	<0.005	0.042
C	-	0.003	0.011	0.041	0.014

3.4. Weight of Copper Bullion and Anodes

The as-received material was unfortunately not weighed by AMD; therefore it is difficult to determine an overall casting yield. The casting yield is defined as the ratio:

$$\text{Casting Yield (CY)} = \frac{\text{Weight of Castings Shipped}}{\text{Weight of Metal Poured}} \times 100\%$$

It is obvious that the goal for a metal casting plant would be to make casting yield as high as possible. It is also obvious that the riser size and number of risers has a big impact on the casting yield. It is common practice for metal casting plants to have overall casting yields of between 40 and 80%. Maximization of the yield will involve reducing the number and size of the risers as an important contributor. Of course, reducing the size of the gating system will also have a significant effect on casting yield.

Also, it is impossible to confirm the initial weight which will be used to estimate the material loss during casting trials. It is however a norm that in the foundry you will definitely lose some material during melting and casting but not as high as 60 kg. Of the 160 kg that were provided to be re-melted and cast into anodes – only 90-100 kg can be accounted for. The supplied material before and during melting trials was kept in the material storage area of Bay 7 which is locked every night. The likelihood that the material could have been stolen is unlikely. All the anodes produced were weighed after machining prior to sending for electro-refining test as summarised in Table 3.2 below.

Table 3 2. The weights of copper bullion anodes (grams)

Anode Number	Weight after Machining (grams)
1	7750
2	5120
3	5622
4	5443
5	5766
6	5594
7	5838
8	4039
9	2160
10	6177

4. CONCLUSION

- Casting is a multiple step process that includes melting the metal into molten, pouring the molten into a mould and cooling it back to a solid.
- A pattern to be used in the making of mould for producing of the copper nickel alloy anodes have been successfully designed and made.
- Calculations were made to make sure that the pattern can be removed easily from the casting cavity without damaging the mould. The modified feeders proved effective in eliminating shrinkage cavities in all the casts.
- It has been found that Copper-Nickel Alloys must be melted carefully because the presence of nickel in high percentages raises not only the melting point but also the susceptibility to hydrogen pickup.
- The copper nickel alloys were melted in coreless electric induction furnaces, because the melting rate is much faster than it is with other furnace. It has been found that when ingot is melted in this manner, the metal should be quickly heated to a temperature slightly above the pouring temperature and deoxidized either by the use of one of the proprietary degasifiers used with nickel bronzes or, better yet, by plunging 0.1% Mg stick to the bottom of the transfer ladle. The purpose of this is to remove all the oxygen and to prevent any possibility of steam-reaction porosity from occurring.
- It has been found out that there is little need to use cover fluxes especially if the material melted is cleaned prior to melting.
- During the melting and casting process, the anode composition and colour changed, the main difference was the silicon, copper and nickel contents. It is envisaged that this might have also led to a change in colour. This needs to be investigated to find the source of the silicon that was picked up.

5. REFERENCES

[1] Rundman, K.B, *Metal Casting*, Dept. of Materials Science and Engineering Michigan Tech. University,

[2] Clegg, A.J, *Precision Casting Processes*, 1st Edition, Pergamon Press. 1991

[3] Heine, R and Rosenthal, P, *Principle of Metal Casting*, International Student Edition, Mcgraw-Hill Book Company, Inc. 1955

[4] Flinn R.A, *Fundamentals of Metal Casting*, Addison-Wesley Publishing Company, Inc, United States of America. 1963

5.1.1. SHE Risks

"Kindly note that all safety, health and environmental ("SHE") risk information are given for information purposes only and does not constitute a risk assessment for any SHE purposes, nor does it substitute any statutory risk assessment that the client is required to undertake. Mintek assumes no risk or liability on behalf of the client or any of its officers or employees in respect of SHE legislative requirements."

APPENDIX 1

CALCULATION OF THE SIZE OF THE FEEDER/RISER

Risers are used to feed molten metal into the mould cavity during solidification in order to compensate for shrinkage. Riser design in sand mould castings requires, as a minimum, that the riser solidify after the casting, i.e.:

$$t_S(\text{riser}) > t_S(\text{casting})$$

where t_s refers to solidification time. The shape, size and positioning of risers is very important. The size of the riser/feeder is calculated according to the Chvorinov's Rule [2-4] which is given below as:

$$t = B.\,(V/A)^2$$

where:
t is the solidification time,
V is the volume of the metal,
A is the area of the casting, and
B is a constant which is dependent on the type of mould material.

According to the Wlodawer [1-3], the modulus[1] of the feeder/riser should be at least 20% greater than the modulus of the casting according to the formula below:

$$M_f = 1.2M_c$$

where:

M_f is the modulus of the feeder which is equivalent to $\left(\frac{V_f}{A_f}\right)$ and M_c is the modulus of the casting which is equivalent to $\left(\frac{V_c}{A_c}\right)$. V_f, V_c, A_c and A_f refere to the volume of the feeder, the volume of the casting, the area of the casting and the area of the feeder, respectively.

The following information on the requested anodes was obtained and this helped in the design of the pattern:

[1] Modulus – This is

For a plate-like casting with the dimensions, Length = 220mm, Width = 140mm and Thickness = 20mm, the volume and area were calculated as follows:

$$M_c = \left(\frac{V_c}{A_c}\right)$$

V_c= L x W x T = 22cm x 14cm x 2cm = 616cm^3

A_c = 2(L x B) + 2(L x T) + 2(B X T) = 760cm^2

M_c = (616/760) = 0.81 cm

M_f =1. 2M_c = 1.2(0.81) = 0.97 cm

$$0.97=\left(\frac{V_f}{A_f}\right)$$

Using a cylindrical feeder/riser:

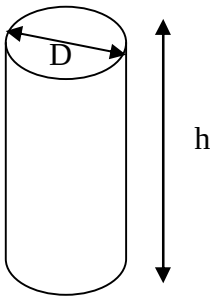

Volume of the feeder = πr^{2}h

h = 2D = 4r

Therefore,

V = πr^{2}x4r = 4πr^3

The area of the feeder = A = 2πrh = 8πr^2

$$0.97 = \left(\frac{V_f}{A_f}\right) = \left(\frac{4pr^3}{8pr^2}\right) = \frac{r}{2}$$

r = 1.94cm

h = 7.78cm

The size of the riser of the anode was made such that both the solidification and shrinkage criterion are met simultaneously. For the above criterion to be met the solidification time of the riser should be longer than the solidification time of the casting, i.e. $t_r > t_c$. This will be met if $\left(\frac{V}{A}\right)_r > \left(\frac{V}{A}\right)_c$.

DISTRIBUTION

Copy Number	Issued to
1-6	Ms T Thulare
7	Mr A Mngomezulu
8	Dr RL Paul
9	Dr M Motuku
10	Dr D Hulbert
11	Dr E van der Lingen
12	Dr MJ Papo
13	Mr SJ Moema
14	Mr C Fletcher
15	Mr S Kantwela
16	Mr T Madiba
17	Mr T Khoza
18	File

Draft Electronic copies of the report were issued to the following by e-mail:

Ms Thembi Thulare

Ms Ndina Mulaudzi